Thèse **2019** **Open Access**

- -

Micropearls: a newly discovered biomineralization process in eukaryotes

- -

Martignier, Agathe

UNIVERSITÉ DE GENÈVE
Département des Sciences de la Terre

FACULTÉ DES SCIENCES
Directeur Prof. Daniel Ariztegui
Co-directeur Dr Jean-Michel Jaquet

Micropearls:
a newly discovered biomineralization process in eukaryotes

THÈSE

présentée à la Faculté des sciences de l'Université de Genève
pour obtenir le grade de Docteur ès Sciences, mention sciences de la Terre

par

Agathe Martignier

de

Genève (Suisse)

Thèse N° 5407

GENÈVE
Atelier de reprographie ReproMail
2019

DOCTORAT ÈS SCIENCES, MENTION SCIENCES DE LA TERRE

Thèse de Madame Agathe MARTIGNIER

intitulée :

«Micropearls: a New Biomineralization Process in Eukaryotes»

La Faculté des sciences, sur le préavis de Monsieur D. ARIZTEGUI, professeur associé et directeur de thèse (Département des sciences de la Terre), Monsieur J.-M. JAQUET, docteur et codirecteur de thèse (Département des sciences de la Terre), Madame M. FILELLA, docteure (Département F.-A. Forel des sciences de l'environnement et de l'eau), Monsieur F. BARJA, docteur (Département de botanique et biologie végétale), Monsieur A. IMMENHAUSER, professeur (Department of geology, mineralogy and geophysics, Ruhr-Universität Bochum, Germany), autorise l'impression de la présente thèse, sans exprimer d'opinion sur les propositions qui y sont énoncées.

Genève, le 1er novembre 2019

> **Thèse - 5407 -**

Le Doyen

Thesis director :

Prof. Daniel Ariztegui
Department of Earth sciences,
University of Geneva, Swizterland

Thesis co-director :

Dr. Jean-Michel Jaquet
Department of Earth sciences,
University of Geneva, Swizterland

Jury members :

Dr. Montserrat Filella
Department F.A. Forel for Environmental
and Aquatic sciences,
University of Geneva, Swizterland

Dr. François Barja
Microbiology unit,
University of Geneva, Swizterland

Prof. Adrian Immenhauser
Institute for Geology, Mineralogy and
Geophysics,
Ruhr-Universität Bochum, Germany

Abstract

_____

Calcium carbonates are the most abundant biogenic minerals, but intracellular inclusions of this same composition in unicellular organisms were generally thought to be rare. The present work uncovers a potentially ancient but yet undiscribed biomineralization process, in which unicellular planktonic eukaryotes produce multiple intracellular inclusions of near-amorphous calcium carbonate (ACC), called micropearls. The process is not related to a specific habitat and occurs in marine, brackish and freshwater environments. Micropearls have been identified in the water column of seven different lakes in Switzerland, France, Greece and Bolivia and literature mentions occurrences of the marine species producing them in multiple areas around the world. This phenomenon is therefore widespread geographically.

The micropearls can be highly enriched in alkaline-earth elements such as strontium and barium, compared to the surrounding water: Sr/Ca ratio can be up to 87x higher in the micropearls and Ba/Ca ratio up to 800 000 times higher. In that case, these microspheres typically present nanometer-scale internal concentric zonation, expressing oscillatory variations of their chemical composition (Sr/Ca or Ba/Ca ratio). The process seems biologically controlled and the composition of the micropearls is characteristic for a given species: in the same culture medium, some will metabolize only Ca, some Ca and Sr, and others Ca, Sr and Ba.

This unsuspected biomineralization capacity was discovered to be common in the *Tetraselmis* genus (Chlorodendrophyceae, Chlorophyta) and potentially in the whole class Chlorodendrophyceae, as micropearls were also observed in a species of the genus *Scherffelia (S. dubia)*. The micropearls of Chlorodendrophyceae are mostly composed of pure calcium carbonate or enriched in strontium. The micropearls are not randomly scattered throughout the cell and their arrangement often forms a pattern (e.g. longitudinal alignments), which is characteristic for a given species. This arrangement pattern is linked to the chloroplast shape, as the mineral inclusions align themselves along the incisions between chloroplast lobes. Moreover, ITS and rbcL phylogenies suggest that this pattern may constitute a valid criterion

to distinguish different phylogenetic groups in the genus *Tetraselmis*: the species belonging to a given phylogenetic clade all seem to present similar micropearl arrangement patterns.

In Lake Geneva (Switzerland), a different organism was discovered to produce near-amorphous micropearls with composition ranging from calcium carbonate highly enriched in barium to barium carbonate (up to > 90 Ba/Ca mol%). Although it is still unidentified, our results show that this organism is not a close relative of the Chlorodendrophyceae and even suggest that it might belong to the zooplankton or the mixotroph eukaryotes.

Micropearls represent a new physiological feature for eukaryotes. It may seem puzzling that this had gone unnoticed, especially as they are widespread in the class Chlorodendrophyceae, which includes many well-studied organisms. In fact, early microscopists had spotted alignments of "refractive granules" in some *Tetraselmis* species, but without identifying their mineral nature. Later, micropearls have not been detected despite multiple electronic imagery observations of the organisms producing them, because they are easily dissolved by most sample preparation techniques used to fix the organic matter. The discovery and study of micropearls, in the present research, was due to an uncommon sample preparation technique originally meant for the observation of diatom frustules in the natural environment. It seems possible that calcium carbonate inclusions might have been dissolved by traditional sample preparation for electronic imagery in other samples too: other well-studied organisms may therefore also have unsuspected biomineralization capacities to produce micropearls or similar ACC inclusions.

Résumé

_____

Les carbonates de calcium sont les minéraux biogéniques les plus abondants. Cependant, jusqu'à récemment, les inclusions intracellulaires de cette composition étaient considérées comme rares dans les organismes unicellulaires. Le travail présenté dans ce manuscrit met au jour un processus de biominéralisation, potentiellement très ancien, qui n'avait pas encore été décrit: des organismes unicellulaires appartenant aux eucaryotes forment de multiples inclusions minérales intracellulaires, appelées microperles, qui sont constituées de carbonate de calcium amorphe (ACC) ou quasi amorphe. Ce processus ne semble pas être lié à un habitat spécifique et peut avoir lieu dans des environnements aussi bien marin que saumâtre ou encore d'eau douce. Jusqu'à présent, les microperles ont été détectées dans sept lacs différents en Suisse, France, Grèce et Bolivie. De plus, la littérature décrit que les organismes marins qui produisent des microperles ont été observés en de nombreux points du globe. Ce phénomène est donc largement répandu du point de vue géographique.

Les microperles peuvent être fortement enrichies en éléments alcalino-terreux tels que le strontium et le baryum : le rapport Sr/Ca peut être 87 fois plus élevé dans les microperles que dans l'eau environnante et le rapport Ba/Ca jusqu'à 800 000 fois plus. Dans ce cas, les microsphères présentent typiquement des zonations internes concentriques de l'échelle du nanomètre qui expriment des variations de composition chimique (ratio Sr/Ca ou Ba/Ca). Le processus semble être contrôlé biologiquement et la composition des microperles apparaît être caractéristique pour une espèce donnée. Ainsi, dans un même milieu de culture, certaines espèces métabolisent-elles seulement du Ca, d'autres du Ca et du Sr et d'autres encore du Ca, du Sr et du Ba.

Il a été découvert que cette capacité de biominéralisation, insoupçonnée jusque-là, est fréquente parmi les espèces du genre _Tetraselmis_ (Chlorodendrophyceae, Chlorophyta) et potentiellement dans toute la classe Chlorodendophyceae, puisque des microperles ont également été observées dans une espèce du genre _Scherffelia_ (_S. dubia_). Les microperles produites par les Chlorodendrophyceae sont généralement composées d'ACC pur ou enrichi

en strontium. Les microperles ne sont pas éparpillées aléatoirement : leur distribution forme généralement un motif à l'intérieur de la cellule (p. ex. des alignements longitudinaux). Ce motif est caractéristique pour une espèce donnée et dépend de la forme du chloroplaste, puisque les microperles s'alignent le long des incisions présentes entre les lobes de celui-ci. D'autre part, la phylogénie basée sur les séquences ITS et rbcL suggère que ce motif pourrait constituer un critère valable pour distinguer différents groupes phylogénétiques au sein du genre *Tetraselmis*. En effet, les espèces appartenant à un même clade semblent toutes présenter un motif similaire.

Dans le Léman (Suisse), un autre organisme forme également des microperles, mais de composition différente: elle va du carbonate de calcium enrichi en baryum jusqu'au carbonate de baryum (ratio Ba/Ca > 90 mol%). Bien qu'il ne soit pas encore identifié, nos résultats démontrent que cet organisme ne semble pas être un proche parent des Chlorodendrophycées et suggèrent même qu'il pourrait être mixotrophe ou faire partie du zooplancton.

Les microperles représentent un nouveau composant physiologique chez les eucaryotes. Il peut sembler étrange que ces inclusions minérales aient pu passer inaperçues alors qu'elles sont très répandues parmi les Chlorodendrophycées, dont font partie des organismes très bien étudiés. En réalité, des alignements de "granules réfractives" avaient bien été repérées par d'anciens microscopistes dans certaines espèces de *Tetraselmis*, sans qu'ils aient toutefois identifié leur nature minérale. Par la suite, malgré de multiples observations de Chlorodendrophycées par microscopie électronique, les microperles ont échappé à la détection parce qu'elles sont dissoutes par la plupart des préparations d'échantillons utilisées pour fixer la matière organique. La découverte et l'étude des microperles présentée ici résulte d'une méthode de préparation d'échantillon originale, utilisée au départ pour l'observation de frustules de diatomées prélevées dans un environnement naturel. Il semble possible que des artefacts similaires aient pu survenir dans d'autres échantillons fixés pour préserver la matière organique. Cela signifie que d'autres organismes connus et bien étudiés pourraient également posséder la capacité de produire des microperles ou des inclusions d'ACC similaires sans que personne ne le suspecte.

Contributions

_____

The pluridisciplinary nature of this project favoured multiple collaborations because different knowledges and competences were required to complete a wider picture of the micropearls' nature and origin. This part describes the respective contributions of the people who collaborated to this project. All are co-authors of at least one of the articles included in this PhD. Each reviewed the paper(s) which they co-authored.

Agathe Martignier _(University of Geneva, Department of Earth sciences)_ discovered the micropearls with Jean-Michel Jaquet. AM characterized and identified the different types of micropearls, linked their respective origin to different species of organisms, made all the SEM images and EDS analyses which are the basis of the present research and produced the epifluorescence analyses. AM also developed with Jean-Michel Jaquet the different methods of sample preparation used in this paper. She suggested the idea of studying the marine strains of _Tetraselmis_ and spotted the arrangement of micropearls in the _Tetraselmis_ cells. AM raised part of the funds necessary to finance the analyses as well as her participation to meetings and congresses to share the present results. AM also managed, throughout the PhD, the contact with the different research groups which collaborated to this project. She discussed and helped to design the different analyses lead on the micropearls, travelled to the different labs and was present and participated to nearly all of the analyses, compiled the information issued from the various analytical methods and wrote the papers which constitute this manuscript (apart from the appendices).

Jean-Michel Jaquet _(University of Geneva, Department of Earth sciences)_ allowed the discovery of micropearls by bringing a sample of Lake Geneva water to the SEM. JMJ supervised the whole research, which he launched by writing a first descriptive article on the subject in 2013 (see Appendices 1). He initiated the ideas to order algal strains from Algal Culture Collections and to study the inner structure of the micropearls. JMJ carried out sample preparations and processed EDXS data. He established and maintained the collaboration with the SECOE (Service de l'Ecologie de l'Eau, Geneva State) who provided monthly samples from

Lake Geneva and initiated the contact with several of the research groups, which then collaborated to the project.

Daniel Ariztegui *(University of Geneva, Department of Earth sciences)* supervised the whole PhD and funded part of the project as well as the participation to some congresses. He helped design the research and provided the framework and guidelines driving the positive development of the project. DA also provided important contacts and key expertise.

Montserrat Filella *(University of Geneva, Department F.A. Forel for Environmental and Aquatic sciences)* was a major collaborator for the writing of the articles, provided expertise regarding environmental chemistry all along the project and initiated contacts allowing key collaborations.

François Barja *(University of Geneva, microbiology unit)* provided biological expertise in general and support for sample preparation for SEM observation, introducing us to biological fixation of organic matter. The collaboration with the SUPSI (Bellinzona) started thanks to his support.

Michael Melkonian (University of Cologne, Cologne biocenter, botany department) provided phycological expertise, especially for class Chorodendrophyceae, and selected strains from the CCAC for further study. MM also revised the manuscript and placed results into a biological context. **Kerstin Hoef-Emden** made her unpublished Master thesis on light microscopy of Chlorodendrophyceae available and provided important information on light microscopy of chloroplasts; **Birger Marin** performed phylogenetic analyses and constructed phylogenetic trees on Chlorodendrophyceae; **Gerd Günther** provided DIC optical microscope images of *Tetraselmis* and *Scherffelia* spp. showing micropearls, and **Barbara Melkonian**, curator of the CCAC (Central Collection of Algal Cultures, now at the University of Duisburg-Essen), provided strains of *Tetraselmis* and *Scherffelia* spp. and gave advice concerning cultivation and preservation of strains.

Falko Langenhorst *(Friedrich Schiller University Jena, Institute of Geosciences)* collaborated with our research and allowed us access to his laboratory to make a FIB-TEM study of the micropearls. He also produced the EELS analyses of micropearls. **Kilian Pollok** produced the FIB sections shown in several articles of this manuscript, conducted the TEM analyses, processed the results and helped for their interpretation. Both contributed to chapter II.

Mauro Tonolla *(SUPSI (Bellinzona), laboratory of applied microbiology)* supported our project and allowed a close collaboration with his associate **Sophie De Respinis** who conducted the

DNA extractions and analyses providing the phylogenetic data detailed in chapter IV and contributed to the writing of this same chapter.

Pascale Nirel *(SECOE, Service de l'Ecologie de l'eau, state of Geneva)* supported our project, allowed us to have access to water composition data and to obtain monthly water samples from their campaign on Lake Geneva while permitting the development of a research collaboration with **Sophie Lavigne** who provided statistical data related to the monthly phytoplankton composition of Lake Geneva, produced beautiful images of live phytoplankton in these same samples and helped us to identify *Tetraselmis cordiformis* as the organism producing Sr-rich micropearls.

Rossana Martini *(University of Geneva, Department of Earth sciences)* collaborated to the project and, as the director of the SEM lab of our department, allowed access to the machine during the whole PhD. **Camille Thomas** *(University of Geneva, Department of Earth sciences)* also collaborated to the project at its beginning, provided useful advice regarding the use of fluorescence techniques and contributed to the identification of *Tetraselmis cordiformis*.

Muriel Pacton *(University of Lyon 1, Laboratory of Geology of Lyon)* was a key collaborator for the research leading to the publication of the first article of this PhD, to which she contributed (see chapter II). She participated to our understanding of the organic origin of the micropearls and was the founder of the term "micropearls". She also introduced our subject to **Paul Guagliardo** and **Matt R. Kilburn** *(The University of Western Australia, Center for Microscopy, Characterisation and Analysis)* who produced NanoSIMS analyses of some micropearls.

Ines Segovia *(University of Geneva, Department of Earth sciences)* recently started a PhD in the wake of the research presented in this manuscript. She produced SEM images of cultured samples, which are presented in Chapter IV.

Stephan Jacquet *(INRA, CARRTEL of Thonon-les-Bains)* collaborated to the project, allowing the use of flux cytometry technology on our samples. He will be co-author to the publication of Chapter V.

Laure Apothéloz-Perret-Gentil *(INRA, CARRTEL of Thonon-les-Bains)* produced meta-genomic data aiming to identify the organism producing Ba-rich micropearls and will be co-author to the publication of Chapter V.

Michael Bensimon *(EPFL, IsoTraceLab)* led the ICP-MS analyses of the growth media for the second paper of this PhD (see Chapter III).

Table of contents

- **Jaquet J.M., Nirel P. and Martignier A. (2013)**
  Preliminary investigations on picoplankton-related precipitation of alkaline-earth metal carbonates in meso-oligotrophic lake Geneva (Switzerland). *J. Limnol*. 72, 592–605.

- **Thien B., Martignier A., Jaquet J.-M. and Filella M. (2017)**
  Linking environmental observations and solid solution thermodynamic modeling: the case of Ba- and Sr-rich micropearls in Lake Geneva. *Pure Appl. Chem.* 89 (5), 645-652.

Introduction

_____

1.1 Biomineralization

Biomineralization is the process by which living organisms produce minerals. This capacity is shared by species belonging to all taxonomic kingdoms, from single cells to complex organisms (Veis, 2008). Biomineralization mostly serves to provide a structure (skeleton) or a protection (shell) to the organisms' soft tissues, but multiple other applications can be listed. For example, the otoliths are small structures including calcium carbonate crystals, which are essential to all vertebrates' balance capacities through the estimation of horizontal and vertical acceleration (Purves et al., 2002); the green algae *Chara* developed a system of graviperception involving microcrystals of $BaSO_4$, allowing to orientate the direction of their rhizoids' growth (Gilroy and Masson, 2008); and small magnetic minerals are used by numerous organisms for orientation by perceiving the geomagnetic field, including sea turtles (Brothers and Lohmann, 2015), pigeons (Mora et al., 2004), bats (Holland et al., 2006) and magnetotactic bacteria (Faivre and Schüler 2008). Biomineralization can also serve chemical needs of the metabolism such as detoxification processes: for example, several organisms were discovered to have a similar ability to store Cd^{++} in sulphide minerals when it reaches harmful concentrations in their environment, such as plants, yeasts, fungi and sulfite-reducing bacteria (Carney et al., 2007).

At the micro-scale, part of the biomineralization processes occurs as an indirect consequence induced by the metabolic functioning of the organisms (Konhauser, 2007; Lowenstam, 1981). For example, cyanobacteria induce the precipitation of calcium carbonates in their close surrounding through their photosynthetic activity (Kamennaya et al., 2012). But other species completely control the mineralization process (Konhauser, 2007) and model the minerals for specific uses. The controlled production of biominerals often takes place inside the cells, allowing the selective extraction and uptake of elements from the surrounding environment (Mann, 2004) to compose the biomineral. In that case, the prefix " "bio" in the term biomineral implies that the high activation energy, and thus stringent or extreme temperature, pressure and concentration conditions required to produce the mineral by strictly inorganic chemical means, is bypassed by the intervention of biopolymers which alter the crystallization reaction pathways" (Veis, 2008). Most of the time, these biominerals differ greatly from minerals of the same composition precipitated inorganically, by their morphology and/or their mineralogical state (Weiner and Dove, 2003). The composition of biominerals generally include organic molecules (e.g. proteins) in addition to the core chemical elements (Polowczyk et al., 2016).
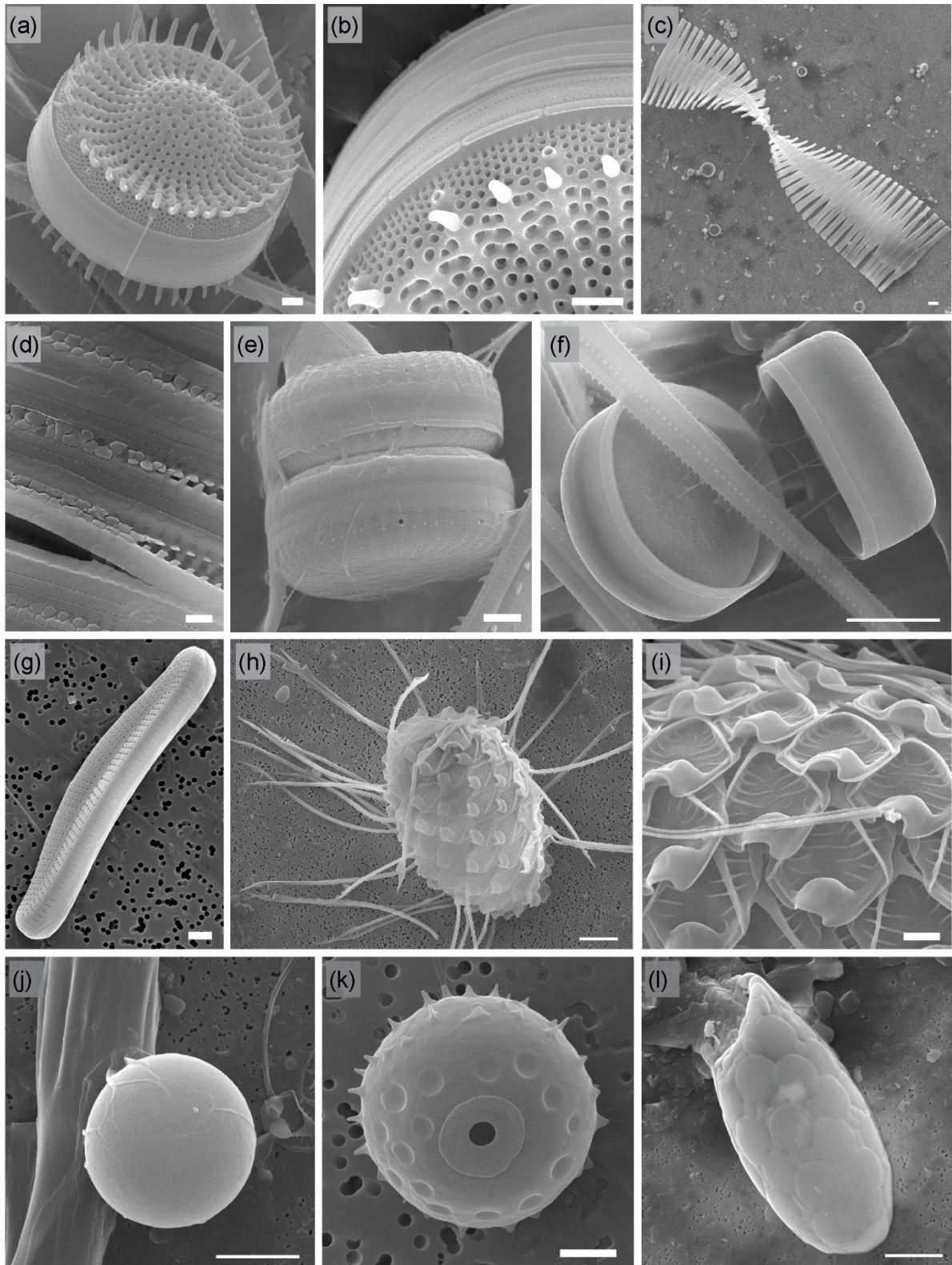
Figure 1 (preceding page) – Examples of silica biomineralization observed in Lake Geneva

SEM images of dried samples, taken from the water column of Lake Geneva. (a) to (f) Frustules of diatoms (unicellular algae). Note the detail of (c) imaged in (d): in these colonies, the individual diatoms of this species are attached together by a system similar to a zipper. (f) shows two separate halves of a frustule. (h) and (i): amorphous silica scales and bristles produced by the unicellular alga *Mallomonas* (Siver, 2012). (j) and (k): siliceous cysts formed by Chrysophyceae. (l): siliceous autogenic test produced by a testate amoeba (probably a member of the order Euglyphida) (Chatelain et al., 2013).The black dots at the back of (g), (h), (j) and (k) are filter pores. Scale bars: thin= 5 µm; thick = 1 µm.

For example, amorphous silica can precipitate chemically under ambient conditions (temperature and pressure), but only from waters with high silica concentrations (Nichols, 2009, Buckley et al., 2018). If we consider the example of Lake Geneva, where most of the present research was carried out, the water contains very insufficient amounts of silica (~1.03 $mgSiO_2 \cdot L^{-1}$) (Barbier et al., 2017 ;Morey et al., 1964) for natural precipitation. Nevertheless, many organisms succeed to produce amorphous silica to form tests, scales or frustules of delicate shapes (Fig. 1). These complex structures result of the biomineralization taking place in shaped biological compartments (e.g. vesicles) (Mann, 2004), mostly inside the cells.

Calcium carbonate is the most widespread composition of biominerals (Weiner and Dove, 2003). For this single composition, six different minerals (polymorphs) exist, distinguished by their atomic structure: calcite, aragonite, vaterite, calcium carbonate monohydrate, calcium carbonate hexahydrate and amorphous calcium carbonate (Feng, 2011). The two first ones are the most frequently used by organisms, as they are stable at ambient temperature and pressure. For example, the exoskeleton of corals, the shell of foraminifera and the plates of coccolithophores are made of calcite, while the vast majority of mollusc shells is composed of both calcite and aragonite (Mann, 2004).

Amorphous calcium carbonate (without overall periodic arrangement of its atoms), also called ACC, is unstable and normally soon crystallizes into calcite or aragonite under ambient conditions (Addadi et al., 2003; Weiner and Addadi, 2011; Bots et al., 2012).Nevertheless, ACC has been recognized as being of major importance as many organisms of various phyla use it as a biomineralization precursor (Ihli et al., 2014; Alberic et al., 2018). This "transient ACC" will then crystallize into calcite or aragonite, but only once it is dispatched in its dedicated place by the organism (e.g. on a growing urchin's spine).
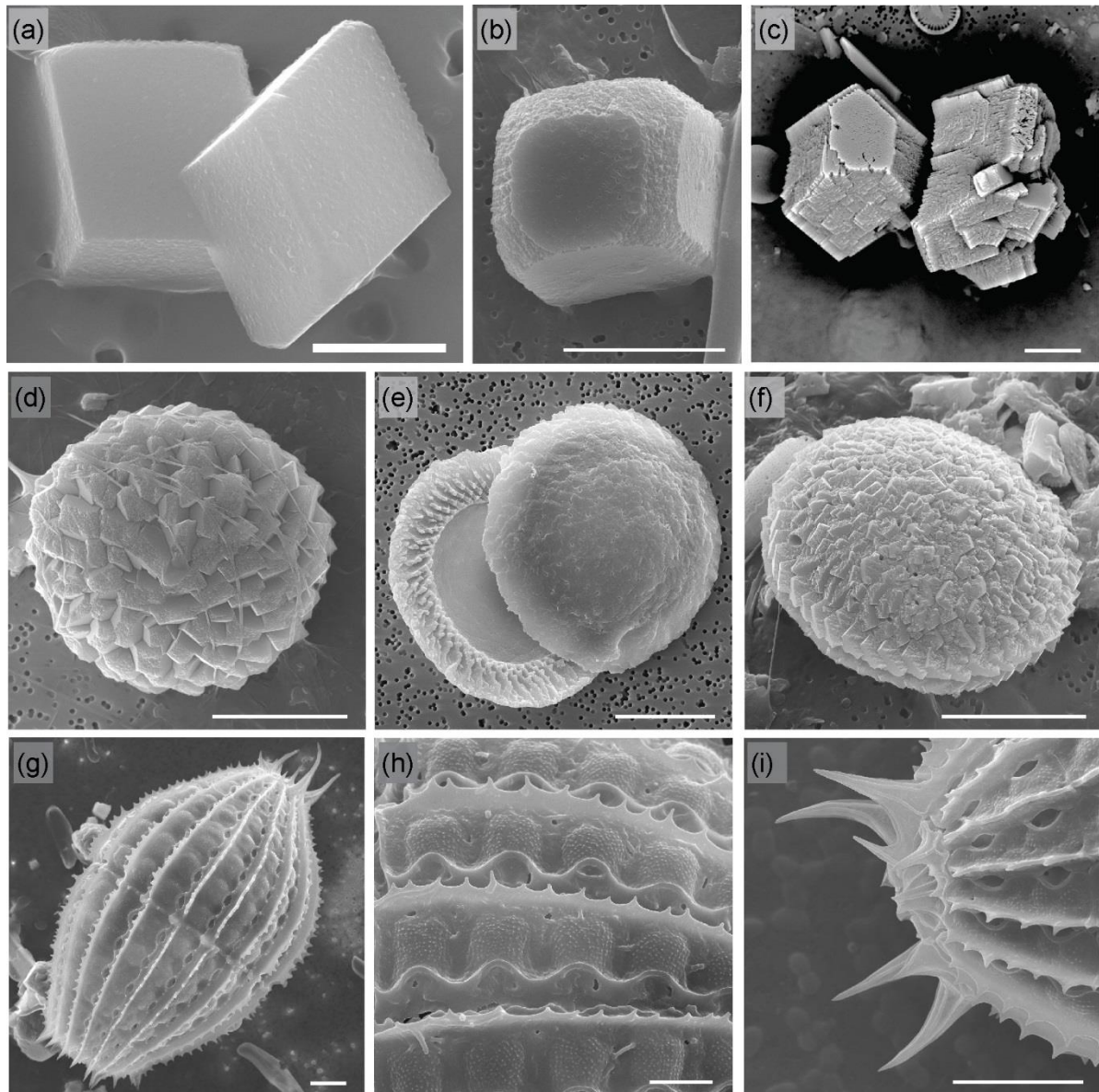
Figure 2 – Examples of calcium carbonate particles observed in the water column of Lake Geneva

SEM images of dried samples from Lake Geneva water column. (a) to (c) Newly formed or corroded calcium carbonate crystals, through purely chemical and inorganic processes. (d) to (i) biogenic calcium carbonate minerals. (d) to (f): shell of the unicellular alga *Phacotus lenticularis*, composed of calcite crystals. (g) to (h) Test of the unicellular ciliate *Coleps* cf. *hirtus*, made of plates mostly composed of ACC. Secondary Electron Images, except (c): Backscattered Electron Image. The black dots at the back are filter pores. Scale bars: thin= 5 µm; thick = 1 µm.

Organisms can also produce "stable ACC" (like the micropearls, which are the subject of this study). This stable ACC can remain in its amorphous state, even, in some cases, long after the organism's death (Addadi et al., 2003; Martignier et al., 2017). In fact, as it is not proved that this amorphous state can last forever, the term "metastable ACC" (theoretically unstable but so long-lived as to be stable for practical purposes) would be more accurate. Research is still ongoing as to how the organisms succeed to maintain the amorphous state of ACC for so long. It seems to result of a combined addition of organic compounds (e.g. proteins or

polysaccharides), of inorganic elements (e.g. Mg or P) or of the confinement in a closed space (e.g. vacuole or vesicle). Indeed, *in vitro* experiments succeeded to maintain inorganically formed calcium carbonate in its amorphous state for long lengths of time, by playing with one or several of these parameters (Mavromatis et al., 2017; Alberic et al., 2018). Figure 2 illustrates the difference between the angular shapes of chemically formed calcium carbonate minerals (Fig. 2a to 2c) and the complex forms of biominerals through examples observed in Lake Geneva. Indeed, if the phytoflagellate *Phacotus lenticularis* produces a shell made of calcite crystals (Fig. 2d to 2f) (Gruenert and Raeder, 2014) the ciliate *Coleps cf. hirtus* synthesizes plates mostly composed of ACC (Fig. 2g to 2i) (Lemloh et al., 2013).

1.2   A multidisciplinary subject

Biomineralization is by essence a multidisciplinary subject, which is at the same time one of the major challenges and one of the main interests of this field.

Mineralogy

The particularities of biominerals are of great interest to mineralogy and are studied either "in vivo", at different development stages of the organisms (e.g. Beniash et al., 1997; Mahamid et al., 2008; Politi et al., 2004; Weiss et al., 2002, Lemloh et al., 2013; Gruenert and Raeder, 2014), or by lab experiments aiming to evaluate the influence of different parameters (additives, temperature, etc.) on the nucleation and growth of the crystal (morphology, size, phase, etc.) (e.g. Sondi et al., 2003; Polowczyk et al., 2016; Nudelman et al., 2010; Cam et al., 2015 ; Ihli et al., 2014, Jaquet et al., 2013 – annexe 1).

Biology

Biologists study for example the role of biominerals for the organisms (skeleton, protection, graviperception, buoyancy, chemical storage, etc.) (e.g. Gray, 2006; Raven and Knoll, 2010) and try to comprehend through which biological means the organisms succeed controlling and achieving biomineralization (e.g. Kröger and Poulsen, 2005; Müller et al., 2008; Brownlee et al., 2015).

Environmental chemistry - Biogeochemistry

Biomineralization processes imply that the organisms extract specific elements from the environment. Multiplied by the number of organisms, this micro-scale phenomenon can have
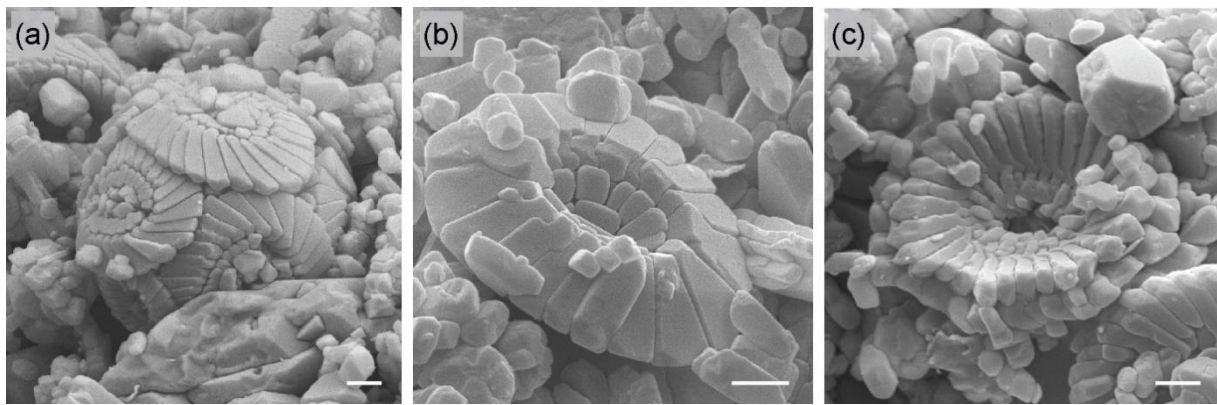
Figure 3 – Coccoliths in chalk deposits.

SEM (secondary electron) images of chalk sample. Coccoliths (ornamented calcite plates produced by the unicellular green algae Coccolithophores). (a) Preserved coccosphere: living cells arrange the coccoliths around themselves as coccospheres for protection. Generally, the coccoliths are scattered after the organism's death. (b) and (c) isolated coccoliths, surrounded by broken coccolith elements, main constituents of chalk. Scale bars: 1 μm.

large-scale impacts, particularly in an environment where these elements are present in low concentrations (for example, see Chapter II). Biomineralization plays an important role in the geochemical cycle of many elements (Van Cappellen, 2003). For example, the coccolithophores (small unicellular green algae) produce ornamented calcite plates for protection (Fig. 3) which are the major constituent of chalk. These organisms play an important role in the carbon cycle through both photosynthesis and biomineralization. Indeed, after the death of the organism, the carbonate plates sink and are deposited in sediments, thus removing carbon from the ocean surface (Meyer and Riebesell, 2015).

Materials - Biomimicry

Biominerals often possess characteristics surpassing those of chemically precipitated minerals (DiMasi and Gower, 2014; Rao and Cölfen, 2016). For example, the nacreous layer inside mollusk shells (also called mother-of-pearl) is composed of the alternating succession of aragonite sheets and layers of polysaccharide-protein matrix and it is 3000 times tougher than purely mineral aragonite (Feng, 2011). New materials for industrial production and other uses can be developed by mimicking the biomineralization process. For example, the controlled synthesis of mineral or organic/mineral materials at the micron or nanometer scale with given characteristics (size, orientation, shape, etc.) would have a wide field of applications in catalysis, electronics, medicine, nanomaterials, and many other fields (Cölfen and Antonietti, 2008; Polowczyk et al., 2016; Skeffington and Scheffel, 2018; Ihli et al., 2014).

Others

Several other disciplines are closely linked to biomineralization. For example, biominerals constitute a large part of the sediments, which are accumulated at the bottom of lakes, seas and oceans. Therefore, they play an important role in the fields of limnology and sedimentology (Jones and Bowser, 1978; Nichols, 2009). These fossils are also the focus of paleontology (micro- and macro) and are widely used for the relative dating of rocks (based on the principle of species evolution through time). Geochemistry analyses are also performed on fossils, allowing to obtain absolute dating or proxy measurements, which can help, for example, to reconstruct the paleoenvironment in which these organisms lived (e.g. Pigati et al., 2010; Pretet et al., 2016; Marshall and McCulloch, 2002; Wei et al., 2007).
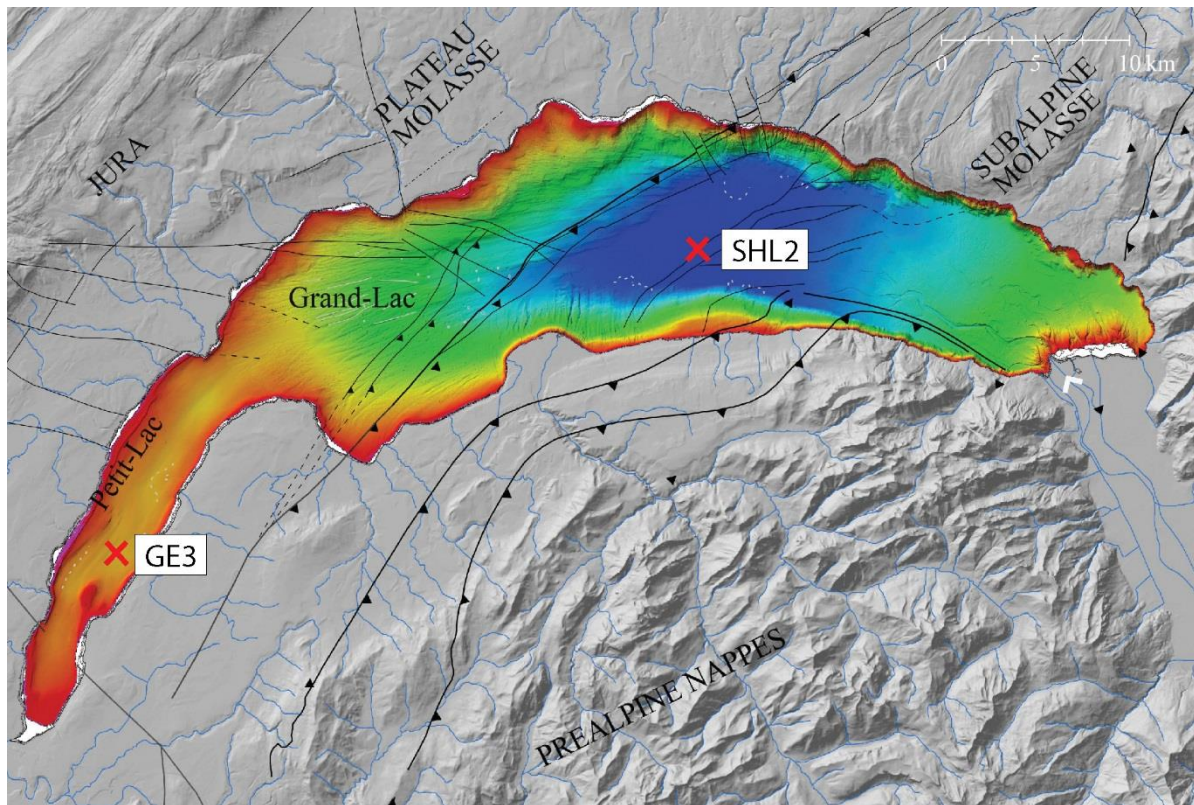
Figure 4 – Sampling locations in Lake Geneva.

GE3: 72 m water depth; SHL2: 309 m water depth. Bathymetry of Lake Geneva (from UniGE / UniBE – Data from Canton de Vaud) with surrounding topography (modified from Kremer et al., 2014 – Data from Swisstopo).

1.3   Micropearls: the origin of the project

Micropearls were first observed with Scanning Electron Microscopy (SEM) in a sample taken from Lake Geneva (*GE3* location) in summer 2011 (Fig. 4), in the context of a study on diatom frustules, led by the SECOE (Water and Ecology Service of the Canton Geneva).   The appearance (Fig. 5) and the composition of these mineral particles aroused our interest, as they contained high proportions of barium and calcium, which appeared exotic compared to the composition of Lake Geneva waters.

In the following years, thanks to the collaboration of the SECOE, monthly study of water samples coming from the same location showed a repeated occurrence of these mineral microsphere aggregates and launched the present research. The biological origin of these minuscule precipitates quickly became obvious as they were systematically embedded in organic matter, but the responsible organism(s) persistently eluded identification.
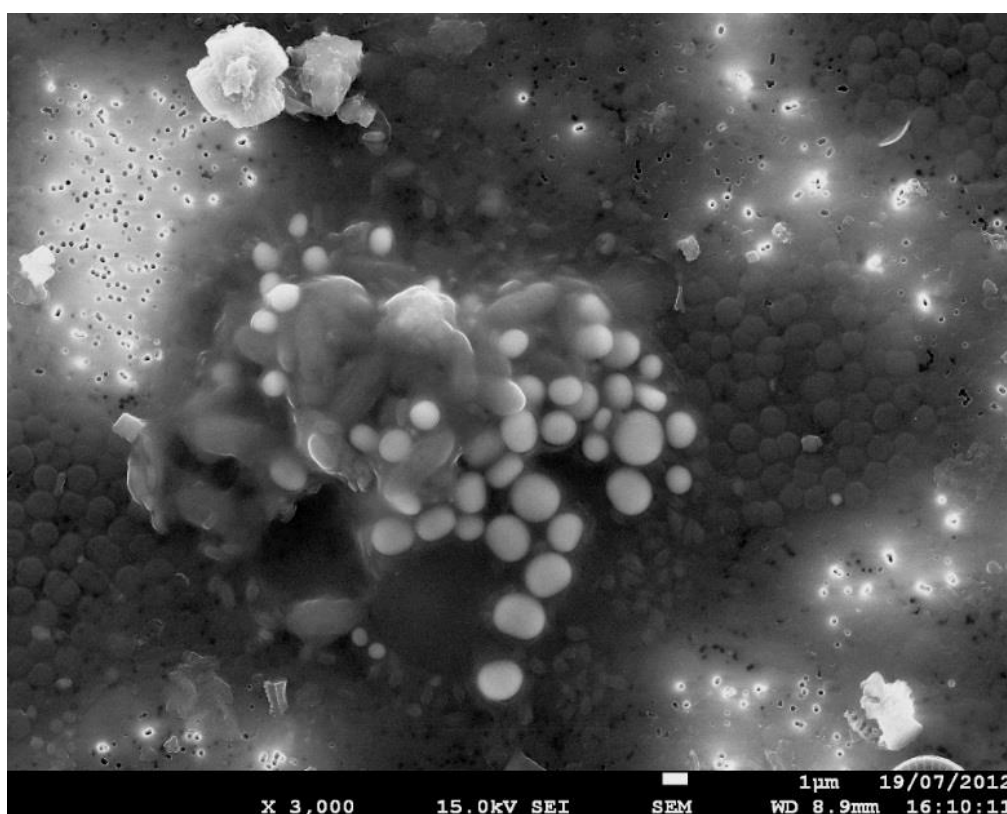
Figure 5 – Micropearl cluster as observed in summer 2012.

SEM secondary electron image. This is one of the very first images showing a micropearl cluster. The micropearls are highly enriched in barium. Due to sample preparation, several elements were superposed during filtration. Here we can identify a cyanobacteria colony (small round dark grey items embedded in a darker organic matrix) and, on top, an organism forming Ba-rich micropearls (the round white microspheres, embedded in grey organic matter).The black and white small spots appearing when no organic matter covers the filter are filter pores. Calcite minerals appear in the top-most part of the image.

A major interest of the subject was also to understand the process leading to the sequestration of alkaline-earth metals, the dominant cations present in the micropearls being calcium (Ca) and barium (Ba), with smaller amounts of magnesium (Mg) and strontium (Sr).

A first description of the phenomenon was published in 2013 by Jaquet et al. (see Annex 1). The only known similar mineral inclusions, at that time, were described in cyanobacteria (Couradeau et al., 2012). It was therefore supposed, that the micropearls probably had a prokaryotic origin and were embedded in extracellular polymeric substance (EPS).

1.4   Thesis overview

The aim of the present PhD thesis was to understand the origin of the biomineralization process that resulted in the formation of micropearls. Conscious of the multidisciplinary nature of the subject, a collaboration had been pre-established with Montserrat Filella (environmental chemist, teaching at the Department of environmental and aquatic sciences, University of Geneva). Additional collaborations then arose in the course of the project with specialists of (in the chronological order) mineralogy and TEM imagery (Institute of Geosciences, Friedrich Schiller University of Jena, Germany), NanoSIMS (Center for Microscopy, Characterization and Analysis, The University of Western Australia), microbiology (Microbiology Unit, University of Geneva, Switzerland), protein and DNA extraction (Laboratory of Applicated Microbiology, SUPSI, Switzerland), phycology (Botany Department, Cologne Biocenter, University of Cologne, Germany), ICPMS (Isotrace Lab, EPFL, Switzerland), phylogenetic analyses (Department of Genetics and Evolution, University of Geneva, Switzerland), flow cytometry (CARRTEL of Thonon-les-Bains, INRA, France) and plant imaging (Department of Botany and Plant biology, University of Geneva, Switzerland). A detailed description of the contribution of these different researchers have been previously described in the section *Contributions*.The following chapters present the result of this multidisciplinary work, each representing a diverse stage of the research and a different focus.

Chapter II: A new biomineralization process uncovered in Lake Geneva

Published in 2017 in *Geobiology*, this paper presents the mineralogical description of micropearls as well as the identification of the organism that produces micropearls enriched in strontium (*Tetraselmis cf. cordiformis* (Chlorophyta, Prasinophyceae)). The latter result was

obtained though the correlation of data issued from numerous different fields and techniques, involving:

- mineralogy: SEM with EDXS analyses; TEM with EDXS and EELS analyses; NanoSIMS analyses;
- biology: monthly phytoplankton counting, SEM observation of fixed organic samples;
- limnology: monthly analyses of the chemistry of the lake water;

These data also suggested the existence of a second undetermined organism producing Ba-rich micropearls (see Chapters V).   Overall, these results uncover a yet undescribed biomineralization process in unicellular eukaryotes.

Chapter III: A biomineralization process observed in both fresh- and marine water

Published in 2018 in *Biogeosciences*, this article confirmed that other species than *Tetraselmis cordiformis* had the capacity to produce micropearls. Cultured strains of 11 *Tetraselmis* species (mainly marine species) were studied with SEM, TEM and EDXS. The results revealed that, depending on the species, the arrangement of the micropearls in the cells varies. These mineral inclusions had never been identified before in these otherwise well studied species.

Chapter IV: Micropearl arrangement in the cell, a criterion to identify phylogenetic groups in the Tetraselmis genus

This article, which will be submitted to the journal *Protist*, shows that the arrangement of the micropearls in the cell differs between different *Tetraselmis* species because it depends of the shape of the chloroplast. SEM, light microscopy and fluorescence images confirm this hypothesis. Moreover, the phylogenetic analyses of *Tetraselmis* species reveals groups that are similar to those suggested by the arrangement of the micropearls in the cells.

Chapter V: Microorganisms producing barium-rich micropearls

Although it has been established that an unidentified organism living in Lake Geneva produces Ba-rich micropearls (see chapter II, Martignier et al., 2017). This chapter details the characteristics of this organism and displays SEM, light microscopy and fluorescence images. Several hypothesis are proposed regarding its identity.

1.5   References

Addadi, L., Raz, S., and Weiner, S.: Taking advantage of disorder: amorphous calcium carbonate and its role in biomineralization. *Adv. Mat.*, 15, 959–970, 2003.

Albéric, M., Bertinetti, L., Zou, Z., Fratzl, P., Habraken, W. and Politi, Y.: The crystallization of amorphous calcium carbonate is kinetically governed by ion impurities and water. Adv. Sci., 5, 1701000, doi:10.1002/advs.201701000, 2018.

Barbier, C., Quetin, P. and Anneville, O.: Physico-chemical changes in the waters of Lake Geneva (major elements) aand meteorological datas (2016). In: Rapp. Comm. int. prot. eaux Léman contre pollut. (Internal report for the protection of the waters of Lake Geneva against pollution), 17-62, 2017.

Beniash, E., Aizenberg, J., Addadi, L. and Weiner, S.: Amorphous calcium carbonate transforms into calcite during sea urchin larval spicule growth. *P. Roy. Soc. London B*, 264, pp. 461-465, 1997.

Bots, P., Benning, L.G., Rodriguez-Blanco, J.D., Roncal-Herrero, T. and Shaw, S.: Mechanistic insights into the crystallization of amorphous calcium carbonate (ACC). *Cryst. Growth Des*., 12, 3806–3814, 2012.

Brothers J.R. and Lohmann K.J.: Evidence for geomagnetic imprinting and magnetic navigation in the natal homing of sea turtles. *Curr. Biol*., 25, 392-396, 2015.

Brownlee, C., Wheller, G.L. and Taylor, A.R.: Coccolithophore biomineralization: New questions, new answers. *Semin. Cell Dev. Biol*., 46, 11-6, doi:10.1016/j.semcdb.2015.10.027, 2015.

Cam, N., Georgelin, T., Jaber, M., Lambert, JF. and Benzerara, K.: In vitro synthesis of amorphous Mg-, Ca-, Sr- and Ba-carbonates: what do we learn about intracellular calcification by cyanobacteria?, Geochim. Cosmochim. Ac., 161, 36-49, doi:10.1016/j.gca.2015.04.003, 2015.

Carney, C.K., Harry, S.R., Sewell, S.L. and Wright, D.W.: Detoxification Biominerals. *Top Curr. Chem*., 270, 155–185, 2007.

Chatelain, A.P., Meisterfeld, R., Roussel-Delif, L. and Lara, E.: Sphenoderiidae (fam. nov.), a new clade of Euglyphid testate amoebae characterized by small, round scales surrounding the aperture. *Protist*, 164(6), 782-792, 2013.

Cölfen, H. and Antonietti, M.: Polymer-controlled biomimetic mineralization of novel inorganic materials. *Met. Ions Life Sci*., 4, 607–643, 2008.

Couradeau, E., Benzerara, K., Gérard, E., Moreira, D., Bernard, S., Brown Jr., G. E., and López-García, P.: An early-branching microbialite cyanobacterium forms intracellular carbonates. *Science*, 336, 459–462, doi:10.1126/science.1216171, 2012.

DiMasi, E. and Gower, L.B.: Biomineralization Sourcebook : characterization of biominerals and biomimetic materials. Publ. CRC Press, 2014.

Faivre, D. and Schüler, D. : Magnetotactic bacteria and magnetosomes. *Chem. Rev*., 108, 4875–4898, 2008.

Feng, Q.L.: Principles of calcium-based biomineralization. In: Molecular biomineralization: Aquatic organisms forming extraordinary materials. Müller, W.E.G. ed., Springer, 2011.

Gilroy, S. and Masson, P.H.: Plant tropisms. Blackwell publ., 2008.

Gray, N.D.: The unique role of intracellular calcification in the genus *Achromatium*. *Microbiol. Monographs,* 1, 299-309, 2006.

Gruenert, U. and Raeder, U.: Growth responses of the calcite-loricated freshwater phytoflagellate *Phacotus lenticularis* (Chlorophyta) to the $CaCO_3$ saturation state and meteorological changes*. J. Plankton Res*., 36(3), 630–640, doi:10.1093/plankt/fbu006, 2014.

Holland, R.A., Thorup, K., Vonhof, M.J., Cochran, W.W. and Wikelski, M.: Navigation: Bat orientation using Earth's magnetic field. *Nature*, 444(702), 2006.

Ihli, J., Wong, W.C., Noel, E.H., Kim, Y.Y., Kulak, A.N., Christenson, H.K., Duer, M.J. and Meldrum, F.C.: Dehydration and crystallization of amorphous calcium carbonate in solution and in air. *Nat. Comm*., 5, 3169, doi:10.1038/ncomms4169, 2014.

Jaquet, J.M., Nirel, P. and Martignier, A.: Preliminary investigations on picoplankton-related precipitation of alkaline-earth metal carbonates in meso-oligotrophic lake Geneva (Switzerland). J. Limnol., 72, 592–605, 2013. (Appendix I of this manuscript).

Jones, B.F. and Bowser, C.J.: The mineralogy and related chemistry of lake sediments. In: Lakes: Chemistry, Geology, Physics. Lerman, A. ed., Springer-verlag publ., 1978.

Kamennaya, N.A., Ajo-Franklin, C.M., Northen, T. and Jansson, C.: Cyanobacteria as biocatalysts for carbonate mineralization. Minerals, 2, 338-364; doi:10.3390/min2040338, 2012.

Konhauser, K.: Introduction to Geomicrobiology. Blackwell publ., 2007.

Kremer, K., Marillier, F., Hilbe, M., Simpson, G., Dupuy, D., Yrro, B.J.F., Rachoud-Schneider, A.-M., Corboud, P., Bellwald, B., Wildi, W. and Girardclos, S.: Lake dwellers occupation gap in Lake Geneva (France–Switzerland) possibly explained by an earthquake–mass movement–tsunami event during Early Bronze Age. *Earth Planet. Sc. Lett.*, 385, 28-39, 2014.

Kröger, N. and Poulsen, N.: Biosilica nanofabrication in diatoms: the structures and properties of regulatory silaffins. *Mater. Res. Soc. Symp. Proc*., 873E, 2005.

Lemloh, M.L., Marin, F., Herbst, F., Plasseraud, L., Schweikert, M., Baier, J., Bill, J. amd Brümmer, F.: Genesis of amorphous calcium carbonate containing alveolar plates in the ciliate *Coleps hirtus* (Ciliophora, Prostomatea). *J. Struct. Biol*., 181, 155–161, doi:10.1016/j.jsb.2012.12.001, 2013.

Lowenstam, H.A.: Minerals formed by organisms. *Science*, 211, 1126-1131, 1981.

Mahamid, J., Sharir, A., Addadi, L. and Weiner, S.: Amorphous calcium phosphate is a major component of the forming fin bones of zebrafish: Indications for an amorphous precursor phase. *P. Natl. A. Sci. USA*, 105, 12748-12753, 2008.

Mann, S.: Bomineralization: Principles and concepts in bioinorganic materials chemistry. Oxford University Press publ., 2001.

Marshall, J.F. and McCulloch, M.T.: An assessment of the Sr/Ca ratio in shallow water hermatypic corals as a proxy for sea surface temperature. *Geochim. Cosmochim*., 66(18), 3263-3280, doi:10.1016/S0016-7037(02)00926-2, 2002.

Martignier A., Pacton M., Filella M., Jaquet J.-M., Barja F., Pollok K., Langenhorst F., Lavigne S., Guagliardo P., Kilburn M.R., Thomas C., Martini R. and Ariztegui D.: Intracellular amorphous carbonates uncover a new biomineralization process in eukaryotes. *Geobiology*, 15, 240-253, 2017. (Chapitre II of this manuscript).

Martignier A., Filella M., Pollok K., Melkonian M., Bensimon M., Barja F., Langenhorst F., Jaquet J.-M. and Ariztegui D.: Marine and freshwater micropearls: biomineralization producing strontium-rich amorphous calcium carbonate inclusions is widespread in the genus *Tetraselmis* (Chlorophyta). *Biogeosciences* 15, 6591-6605, 2018. (Chapter III of this manuscript).

Mavromatis V., Purgstaller B., Dietzel M., Buhl D., Immenhauser A. and Schott J.: Impact of amorphous precursor phases on magnesium isotope signatures of Mg-calcite. Earth Planet. Sc. Lett, 464, 227-236, doi: 10.1016/j.epsl.2017.01.031, 2017.

Meyer, J. and Riebesell, U.: Reviews and Syntheses: Responses of coccolithophores to ocean acidification: a meta-analysis. *Biogeosciences*, 12, 1671–1682, doi:10.5194/bg-12-1671-2015, 2015.

Mora, C. V., Davison, M., Wild, J.M. and Walker, M.M.: Magnetoreception and its trigeminal mediation in the homing pigeon. *Nature*, 432(508), 2004.

Morey, G.W., Fournier, R.O. and Rowe, J.J.: The Solubility of Amorphous Silica at 25°C. *J. Geophys. Res. Atm*., 69(10), 1995-2002, doi :10.1029/JZ069i010p01995, 1964.

Müller, W.E.G., Wang, X., Belikov, S.I., Tremel, W., Schloßmacher, U., Natoli, A., Brandt, D., Boreiko, A., Tahir, M.N., Müller, I.M. and Schröder, H.C.: Formation of siliceous spicules in demosponges: example *Suberites domuncula.* In: Handbook of Biomineralization: Biological Aspects and Structure Formation, p. 59-82. Bäuerlein, E., ed., Wiley publ., doi: 10.1002/9783527619443.ch4, 2008.

Nichols, G.: Sedimentology and stratigraphy. John Wiley & Sons eds, 2009.

Nudelman, F., Pieterse, K., George, A., Bomans, P.H., Friedrich, H., Brylka, L.J., Hilbers, P.A., de With, G. and Sommerdijk, N.A.: The role of collagen in bone apatite formation in the presence of hydroxyapatite nucleation inhibitors. *Nat. Mat*., 9, 1004-1009, 2010.

Pigati, J.S., Rech, J.A. and Nekola, J.C.: Radiocarbon dating small terrestrial gastropod shells in North America. *Quat. Geochronol*., 5(5), doi:519-532, 10.1016/j.quageo.2010.01.001, 2010.

Politi, Y., Arad, T., Klein, E., Weiner, S. and Addadi, L.: Sea urchin spine calcite forms via a transient amorphous calcium carbonate phase. *Science*, 306, pp. 1161-1164, 2004.

Polowczyk , I., Bastrzyk, A. and Fiedot, M.: Protein-mediated precipitation of calcium carbonate. *Materials*, 9, 944; doi:10.3390/ma9110944, 2016.

Pretet, C., Van Zuilen, K., Nägler, T.F., Reynaud, S., Böttcher, M.E. and Samankassou, E.: Constraints on barium isotope fractionation during aragonite precipitation by corals. *Dep. Rec*., 1(2), 118-129, doi:10.1002/dep2.8, 2016.

Purves, D., Augustine, G.J., Fitzpatrick, D., Hall, W., Lamantia, A.S., McNamara, J.O., White, L., Coquery, J.M., Gailly, P., Tajeddine, N., Jeannerod, M. and Volterra, A.: Neuroscience. Sinauer Associates eds, 2002.

Rao A., Cölfen H.: On the biophysical regulation of mineral growth: Standing out from the crowd. *J. Struct. Biol.*, 196(2),232-243, doi:10.1016/j.jsb.2016.03.021, 2016.

Raven, J. A. and Knoll, A. H.: Non-skeletal biomineralization by eukaryotes: Matters of moment and gravity. *Geomicrobiol. J.*, 27, 572–584, doi:10.1080/01490451003702990, 2010.

Siver , P.A.: The biology of Mallomonas: Morphology, Taxonomy and Ecology. Developments in Hydrobiology n°63, Springer Netherlands eds, 230 pp., 2012.

Skeffington, A.W. and Scheffel, A.: Exploiting algal mineralization for nanotechnology: bringing coccoliths to the fore. *Curr. Opin. Biotech*., 49, 57–63, doi:10.1016/j.copbio.2017.07.013, 2018.

Sondi, I. and Matjevic, E.: Homogeneous precipitation by enzyme-catalyzed reactions: 2. Strontium and barium carbonates. *Chem. Mater*., 15, 1322-1326, 2003.

Van Cappellen, P.: Biomineralization and global biogeochemical cycles. *Rev. Min. and Geochem*., 54, 357-381, 2003.

Veis, A.: Crystals and life: An introduction. *Met. Ions Life Sci*., 4, 1–35, 2008.

Wei, G., Deng, W., Liu, Y and Li, X.: High-resolution sea surface temperature records derived from foraminiferal Mg/Ca ratios during the last 260 ka in the northern South China Sea. *Palaeogeogr. Palaeocl*., 250, 126–138, 2007.

Weiner, S. and Addadi, L.: Crystallization pathways in biomineralization. *Ann. Rev. Mat. Res*., 41, 21–40, 2011.

Weiner, S., and Dove, P. M.: An overview of biomineralization processes and the problem of the vital effect. *Rev. Min. Geochem*., 54, 1–29, 2003.

Weiss, I.M., Tuross, N., Addadi, L. and Weiner, S.: Mollusc larval shell formation: Amorphous calcium carbonate is a precursor phase for aragonite. *J. Exp. Zool*., 293, 478-491, 2002.

Chapter II

Intracellular amorphous carbonates uncover a new biomineralization process in eukaryotes *

_____

Agathe Martignier, Muriel Pacton, Montserrat Filella, Jean-Michel Jaquet, François Barja, Kilian Pollok, Falko Langenhorst, Sophie Lavigne, Paul Guagliardo, Matt R. Kilburn, Camille Thomas, Rossana Martini and Daniel Ariztegui

2.1   Abstract

Until now, descriptions of intracellular biomineralization of amorphous inclusions involving alkaline-earth metal (AEM) carbonates other than calcium have been confined exclusively to cyanobacteria (Couradeau et al., 2012). Here, we report the first evidence of the presence of intracellular near-amorphous granules of AEM carbonates (calcium, strontium, and barium) in unicellular eukaryotes. These inclusions, which we have named micropearls, show concentric and oscillatory zoning on a nanometric scale. They are widespread in certain eukaryote phytoplankters of Lake Geneva (Switzerland) and represent a previously unknown type of non-skeletal biomineralization, revealing an unexpected pathway in the geochemical cycle of AEMs. We have identified *Tetraselmis cf. cordiformis* (Chlorophyta, Prasinophyceae) as being responsible for the formation of one micropearl type containing strontium ($[Ca,Sr]CO_3$), which we also found in a cultured strain of *Tetraselmis cordiformis*. A different flagellated eukaryotic cell forms barium-rich micropearls $[(Ca,Ba)CO_3]$. The strontium and barium concentrations of both micropearl types are extremely high compared with the undersaturated water of Lake Geneva (the Ba/Ca ratio of the micropearls is up to 800,000 times higher than in the water). This can only be explained by a high biological pre-concentration of these elements. The particular characteristics of the micropearls, along with the presence of organic sulfur-containing compounds—associated with and surrounding the micropearls—strongly suggest the existence of a potentially old but yet unreported intracellular biomineralization pathway in eukaryotic microorganisms.

2.2   Introduction

The purpose and mechanisms of intracellular biomineralization in unicellular organisms are varied, but can have great significance for applied sciences, environment, geology, or biology (Sigel, Sigel, & Sigel, 2008; Raven & Giordano, 2009; Weiner & Addadi, 2011). For example, the main constituents of chalk are the very precisely shaped calcite coccoliths, formed in intracellular vesicles of Haptophyte eukaryotes and used as an external structure for the organism after export to the cell surface (Young & Henriksen, 2003). While strontium and barium sulfate crystals formed in the terminal vacuole of *Closterium moniliferum* are of considerable interest in the remediation of ^{90}Sr from the environment and nuclear waste: indeed, as there is only a very small number of organisms that can selectively sequester

strontium or barium in biominerals and have the ability to concentrate strontium in the presence of an excess of calcium (Krejci et al., 2011).

In most cases, intracellular biominerals eventually become extracellular (Weiner & Dove, 2003), typically for the construction of an external solid structure or "skeleton" (e.g., coccoliths; or most foraminifera's calcification (Saraswati & Srinivasan, 2016)). However, in some cases, such as *Closterium moniliferum*, intracellular biominerals remain permanently within the cell (Weiner & Dove, 2003). These biominerals can either serve to the constitution of an intracellular skeletal structure (e.g., amorphous silica in radiolarians and diatoms) or stay as non-skeletal inclusions inside the cell (Konhauser, 2007).

The nature of non-skeletal intracellular inclusions reported so far in unicellular eukaryotes is limited to a few minerals only: magnetite, calcium oxalate, barite, barium and strontium sulfates, sulfur globules, and polyphosphates (for more details and references, see Table S1). Strontium and barium "salts" were also mentioned in the ciliate *Loxodes* (Rieder, Ott, Pfundstein, & Schoch, 1982), and calcium carbonate inclusions have been described in several ciliates by Fauré-Fremiet and Gauchery (1957); but further analysis would be needed to determine their exact nature and mineral state. Apart from sulfur globules and polyphosphates, these inclusions are uncommon (Raven & Knoll, 2010).

Thus, reports of non-skeletal intracellular calcium carbonate inclusions are scarce. Among unicellular organisms, notwithstanding the calcite inclusions in ciliates mentioned above, they have only been reported in bacteria. Originally, they were observed only in the giant sulfur proteobacterium *Achromatium* (Head et al., 2000; Gray, 2006), in which the calcite microspheres are interpreted to be composed of aggregated micro-crystals (Head et al., 2000; Salman et al., 2015). Recently, similar calcium carbonate microspheres have proved to be also widespread in cyanobacteria, but in an amorphous state (Couradeau et al., 2012; Benzerara et al., 2014; Ragon, Benzerara, Moreira, Tavera, & Lopez-Garcia, 2014). While it was previously thought to be essentially an extracellular process, the latter discovery showed that carbonate biomineralization in cyanobacteria could also occur intracellularly. No such amorphous inclusions have been reported in unicellular eukaryotes as yet.

The complexity of calcite biomineralization processes already described in eukaryotes (e.g., vacuole export) seems very far from the formation of simple intracellular spherical inclusions of amorphous calcium carbonate, which were recently described in cyanobacteria. The following results could help filling in this evolutionary gap and might be further sustained by revisiting last century observations of calcium carbonate inclusions in ciliates.

This paper describes the origin and structure of intriguing calcium-, strontium-, and barium-rich microspheres, embedded in an organic matrix, which were first observed in the water column of meso-oligotrophic Lake Geneva (Switzerland) during a routine lake water quality survey in 2012. Lake Geneva is a deep (309 m max. depth), monomictic subalpine lake (for details on the chemistry and environment of Lake Geneva see Jaquet, Nirel, and Martignier (2013) and CIPEL (2015)). The microspheres, hereafter referred to as "micropearls", have now been studied for 3 years through monthly water sampling, coupled with multiple analyses and observation techniques: water chemistry, phytoplankton identification and biomass measurements, scanning electron microscopy coupled with micro-analysis (SEM-EDXS) and, during a 9-month period, a systematic count of the micropearl clusters. The inner structure and chemistry of the micropearls were studied by transmission electron microscopy (EDXS, EELS, and diffraction) on focused ion beam (FIB)-cut sections and by NanoSIMS. Finally, biological fixations of the samples allowed the identification of certain organisms and a comparison with cultured strains.

2.3   Methods

2.3.1   Sampling and pre-treatment methods

Lake water samples were taken with a plastic sampling bottle lowered into the water from the "Mariane" research vessel. After the first observation of the micropearls in summer 2012, monthly sampling was conducted between May 2013 and November 2015 at two stations in Lake Geneva: *GE3* located at 6.2197 ° E/ 46.2994 ° N (water depth: 72 m) and *SHL2* located at 6.589 ° E / 46.452 ° N, in the deepest part of Lake Geneva (water depth: 309 m). *GE3* was the main site of this study; only a few samples from *SHL2* have been considered. Most samples were taken at the depth of maximum Chl *a* concentration, measured with a FLNTUB probe (WetLabs, Philomath, OR 97370, USA). Occasionally, water samples were collected at different depths from both locations. Samples for phytoplankton determination were collected with a depth-integrating sampler between 0 and 20 m at the *GE3* station.

Samples for microscopic observation were pre-filtered through a 64-µm mesh sieve to eliminate debris and most zooplankton before being filtered under moderate vacuum (−20 to−30 kPa) on pre-weighed, 45 mm diameter polycarbonate filter membranes with pore sizes of either 0.2 or 5 µm. Volumes filtered (100–400 ml depending on water turbidity) were

recorded. Membranes were dried in the dark at room temperature and weighed to calculate the amount of suspended matter.

Water samples intended for metal analysis were filtered through 0.45 μm pore-size membrane filters (Millipore Millex SLHV033NK), acidified to pH 1 with Suprapur nitric acid and kept at 2°C (±2) until analysis.

2.3.2   Water chemistry measurements

Elemental composition of lake water was measured by the Service de l'Ecologie de l'Eau (SECOE) of Canton Geneva. Barium and strontium were measured by inductively coupled plasma mass spectrometry (ICP-MS) using a ThermoFisher X7 II model, with detection limits of 8 μg/L for strontium and 0.05 μg/L for barium. The analytical accuracy was calibrated from replicated analysis of the certified standard SLRS-5 (NRC). Samples for metal analysis were systematically taken at the same time, location, and depth as those for the follow-up of micropearls.

2.3.3   Optical microscope images

The images of *Tetraselmis cf. cordiformis* (Figure 5a) were taken by the Service de l'Ecologie de l'Eau (SECOE) of Canton Geneva, using an inverted optical microscope (Axiovert 35 Zeiss), under phase-contrast illumination.

2.3.4   Phytoplankton biomass measurements

The detailed procedure is given in Druart and Rimet (2008). Briefly, water samples were fixed with Lugol's iodine; 50 ml subsamples were then left to sediment during 24 hr. Qualitative and quantitative analyses were made with an inverted microscope, following Utermohl's method, which is now normalized throughout Europe. Algal biomass results are given in mg/m^3. The identification of the taxa (down to genus or species) was performed by referring to a list of reported species in Lake Geneva (Druart, Pongratz, & Revaclier, 1983), which is typically used as a reference by researchers working on this subject.

2.3.5 Sample fixation

In a second phase of the study (during summer 2015), different fixation techniques were tested with the aim of identifying the organism(s) responsible for the micropearl formation. These tests were performed on fresh water samples collected the same day or the day before. Numerous different preparation techniques were tested (low-speed centrifugation, resuspension, decantation, etc.) as well as several fixation protocols (different fixation times, different fixatives with different exposition times, at low temperature or room temperature, optimal buffers, etc.). The fixatives tested include glutaraldehyde, formaldehyde, methanol, lugol, alkaline lugol, and mixtures of the pre-cited. For the clusters of micropearls containing strontium (i.e., *Tetraselmis cf. cordiformis*), the best results were obtained through pre-concentration by filtration (0.2-μm filter) and gentle resuspension in lake water, followed by 2.5% glutaraldehyde fixation during 5–10 min, and rinsing with 2% cacodylate buffer pH 8.2. For the Ba-micropearl cluster fixation, no real conclusive results have been reached so far.

In particular, the strontium-rich cluster presented in Figure 5b is issued from lake water which, after filtration and resuspension, was fixed with 2.5% glutaraldehyde during 10 min at room temperature and rinsed with 2% cacodylate buffer (pH 8.2). The images of barium-rich clusters shown in Figures 5d and 5e both come from lake water which, after filtration and resuspension, was fixed with 2% glutaraldehyde during 5 min at room temperature and then rinsed with 2% cacodylate buffer (pH 8.2).

2.3.6 Cultured strains of Tetraselmis cordiformis

A strain of *Tetraselmis cordiformis* was obtained in December 2015 from the culture collection of algae at the University of Göttingen (Germany) under the label "SAG 26.82 *Tetraselmis cordiformis*." This strain had been isolated from a sample taken in 1978 from a castle ditch near Münster (Germany) and cultured since then in SAG's Bacillariophycean medium ("Diat"). The same strain was also acquired from the University of Cologne in February 2016, labeled CCAC 0079B, and cultured in Waris-H medium. From the same source, we also obtained the strain CCAC 0051, coming from Lake Frühlinger and cultured in SFM medium. For additional information on the media, refer to Tables S2 and S3. Aliquots of strains CCAC 0079B and CCAC 0051 were immediately filtered and analyzed following the same procedure as the field samples, and the rest incubated for further studies. All images were taken from dried non-fixed samples, shortly after delivery from the provider, without any change to the medium.

2.3.7 *Scanning electron microscopy (SEM) and energy-dispersive X-ray spectroscopy (EDXS)*

Parts of the dried or fixed filters were mounted on a conductive support (i.e., aluminum stub) with double-sided conductive carbon tape. An ultra-thin coating (ca 10 nm) of gold was then deposited on most samples by low vacuum sputter coating (a few samples were carbon-coated (~15 nm) by carbon-thread evaporation). Imaging and EDXS measurements were performed with a JEOL JSM 7001F Scanning Electron Microscope (Department of Earth Sciences, University of Geneva, Switzerland), with an integrated EDXS detector (model EX-94300S4L1Q; JEOL). The ZAF correction method was used for semiquantitative results.

Samples were imaged using secondary and backscattered electrons. Backscattered electron imaging revealed the location of the micropearls inside the organisms due to the high mean atomic number of the micropearls compared with the surrounding organic matter. EDXS measurements were performed at 15 kV accelerating voltage, with a beam current of ~7 nA and acquisition times of 30 s. Each observed cluster was numbered. Two to three EDXS analyses were performed on the micropearls in each cluster (depending on the size of the cluster). Carbon, nitrogen, and oxygen were not taken into account for the semiquantitative EDXS calculation of the elemental concentrations. Altogether, about 1000 semiquantitative analyses were performed on various micropearl types, with 460 of them representing the Ba- and Sr-rich varieties retained for the present study (a provisional typology of micropearls is given in Jaquet et al. (2013)). Their chemical composition, normalized for the calcium, strontium, and barium cations, is plotted in a ternary diagram in Figure 1, as anhydrous carbonates. EDXS results were calculated as mol%. Examples of raw EDXS micropearl measurements are given in Table S4.

2.3.8 *Estimation of the quantity of Sr- and Ba-micropearl clusters during a 9 months survey*

For a period of 9 months (May 2013 to January 2014), the number of Sr-and Ba-micropearl clusters was estimated each month on filtered and dried lake water samples, taken at the *GE3* sampling station from depths between 2 and 27 m. Number estimation was performed in a systematic way: The number of clusters were counted by SEM observation of 60 different views of the same sample at 600x (corresponding approximately to a surface of 1,4 mm^2). The resulting number was then scaled up to be comparable to a 0.5 L water sample (e.g., values obtained for a 0.25 L water sample would be doubled).

2.3.9   Focused Ion Beam (FIB) preparation

Focused ion beam preparation of electron-transparent lamellae for TEM was performed with a FEI Quanta 3D FEG at the Institute of Geosciences, Friedrich Schiller University Jena (Germany).

Grains of interest were selected based on SEM imaging. A platinum strap of 10 to 20 μm length, ~2 μm width, and ~2 μm high was deposited on the micropearl cluster via ion beam-induced deposition using the gas injection system (GIS) to protect them during lamella preparation. Stepped trenches on both sides of the Pt straps were formed by sputtering material ("milling") with the Ga^+ ion beam operated at 30 keV energy and 5 to 30 nA beam current.

The remaining lamellae were then thinned to approximately 1 μm thickness at 30 keV energy using sequentially lower beam currents, starting at 5 nA and ending at 0.5 or 0.3 nA. The exact position of the lamellae was chosen to obtain maximum diameter for the largest micropearls. The lamellae were partially released from the trenches by undercutting and removal of material at the walls of the trenches. The still thick lamellae were connected with the tungsten needle of the micromanipulator by Pt deposition. They were then cut off the last contact point to the bulk material by sputtering.

After lift-out from the sample, the lamellae were transferred to a post-type copper TEM grid and attached there by Pt deposition.

Final thinning to electron transparency (~100 to 200 nm) was carried out on both sides of the lamellae using sequentially lower beam currents of 0.5 to 0.1 nA at 30 keV energy. At this step of the preparation, the lamellae were subjected to grazing incidence of the ion beam only, to avoid strong implantation of Ga and beam damage. Control of the thinning process was carried out by SEM, which imaged the lamellae at 52°. However, electron imaging was limited to a minimum and low currents were used to prevent beam damage.

2.3.10   Transmission electron microscopy (TEM)

A FEI Tecnai G2 FEG transmission electron microscope with Schottky emitter (operating at 200 kV) and a Gatan GIF quantum post-column energy filter (Institute of Geosciences, Friedrich Schiller University Jena, Germany) were used for imaging and electron energy loss spectroscopy (EELS), respectively. Selected-area electron diffraction (SAED) patterns were taken at the beginning of the TEM session to ensure minimum electron dose for the sample

and to prevent beam damage. EDXS measurements were performed using a X-MaxN 80T SDD EDXS system (Oxford). Scanning TEM (STEM) images were acquired with a High Angle Annular Dark Field (HAADF) STEM detector (Fischione). EDXS spectra were recorded in scanning TEM mode and semiquantitative evaluation of the spectra was accomplished by the Cliff–Lorimer method using pre-calibrated k-factors and an absorption correction integrated into the Oxford software.

2.3.11 *Electron energy loss spectroscopy (EELS) evaluation and energy dispersion*

Electron energy loss spectra (EELS) were measured in diffraction mode with convergence and collection semi-angles of α = 8 mrad and β = 2.7 mrad, respectively. The energy resolution, measured as width of the zero-loss peak at half maximum, was ca. 0.7 eV. To cover the complete energy range of relevant elements (C, Ca, N, O) from the C *K* to the O *K* edges (ca. 290–530 eV), spectra were acquired with an energy dispersion of 0.25 eV per channel. To calibrate the energy scale, the energy position of the π* peak maximum in the C *K* spectra was assumed to be at 285 eV. EELS spectra were corrected for dark current and channel-to-channel gain variation. To extract the pure single-scattering core-loss signal, an inverse power-law background was subtracted and multiple-scattering contributions were removed by the Fourier-ratio technique using zero-loss spectra.

2.3.12 *NanoSIMS*

High-resolution elemental mapping was performed on the same samples used for SEM. Secondary ion images were acquired using the CAMECA NanoSIMS 50 ion microprobe at the University of Western Australia. Following SEM analysis, the samples were coated with 10 nm of Au to ensure conductivity at high voltage. A Cs^+ primary beam was used to sputter the negative ion species $^{16}O^-$, $^{12}C_2^-$, $^{12}C^{14}N^-$, $^{32}S^-$, and secondary electrons. The primary beam was focused to a beam diameter of 50 nm in high-resolution mode, with a beam current of 0.1 pA. As there were no significant isobaric interferences, it was not necessary to tune the mass spectrometer to high mass resolution. Images were acquired at a resolution of 256 × 256 pixels by rastering the beam over an area of 8 × 8 µm or 15 × 15 µm, with a dwell time of 20 ms per pixel. The relatively short dwell time ensured that the delicate micropearls were not destroyed by the ion beam. The sections would typically "burn through" after two or three images were acquired.

2.4 Results

2.4.1 Occurrence, composition and inner structure of micropearls

Three years of regular observations showed that the micropearls are present all year round in the water column of Lake Geneva, at depths between 2 to 309 m. Micropearls are more numerous in surface water and occur in lower amounts during winter. They always appear in clusters, embedded in a circular or ellipsoidal mucilaginous organic envelope. Clusters can contain ~10 to 200 micropearls (diameter: 0.2–3 µm).
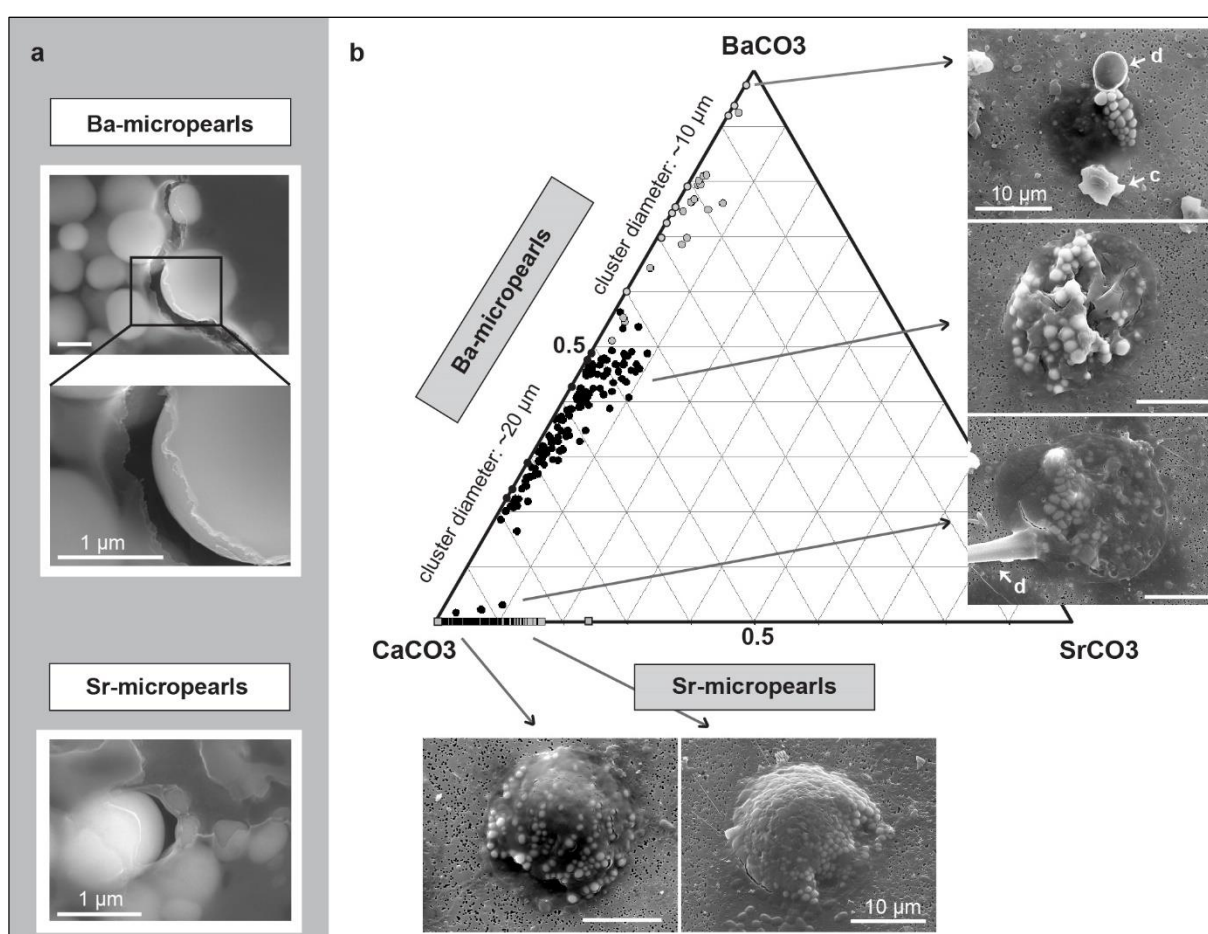
Figure 1 | Sr-and Ba-micropearls, chemical composition, and cluster morphologies.

Figure based on samples collected between July 2012 and December 2014. (a) Micropearl SEM secondary electron images (SEI). (b) Ternary diagram shows 460 EDXS analyses of Ba-micropearls (black and grey circles) and Sr-micropearls (grey squares). Black circles: diameter of Ba-clusters is ~20 µm; grey circles: diameter is ~10 µm. Ca, Ba, and Sr total concentrations are normalized to 100%, not considering other elements (raw EDXS examples: see Table S1 and Fig. S1 and S2). SEI images show dried Ba-and Sr-clusters. Micropearls appear in white/light grey, embedded in a darker organic envelope. Scale bars: (a) 1 µm; (b) 10 µm. d: diatom. c: calcite

Two types of clusters can easily be distinguished on filtered and air-dried samples based on their morphology and the chemical compositions of the micropearls (Figure 1). SEM images and EDXS analysis reveal that micropearls of the first cluster-type contain strontium, while micropearls of the second type are enriched in barium. The main morphological differences are the size of the micropearls (Sr-micropearls: 0.3 to 2 μm diameter; Ba-micropearls: 0.5 to 3 μm diameter), their number (Sr-micropearls: 30 to 200 per cluster; Ba-micropearls: 10 to 60 per cluster), and the shape of the dried organic envelope (Sr-rich: hemispherical mound; Ba-rich: flat ellipsoidal shape).

To identify the Sr-and Ba-containing phases in micropearls, we prepared ultra-thin cross sections for analytical TEM using the focused ion beam (FIB) technology. These TEM foils revealed an internal structure characterized by numerous nanometric concentric layers (Figure 2a).

The alternating brightness of layers in HAADF-STEM images suggests chemical composition oscillations. TEM-EDXS analyses of the two types of micropearls show that the oscillations are zones of alternating Sr/Ca or Ba/Ca ratios. The zonations within the Sr-micropearls are generally wider than those of the Ba-micropearls (minimum thickness: <15 nm) (Figure 2a and Figures 3 and 4). Besides the divalent cations, the micropearls contain no other elements than O and C, suggesting that they are carbonates. To test this assumption and to identify the phase, we used diffraction (SAED) and EELS. SAED patterns showed that the minerals composing the micropearls are in an amorphous state with a broad ring at about 3 Å (Figure 2b), while EELS spectra clearly show that carbon (C K edge with π^* peak) must reside in carbonate groups $(CO_3)^{2-}$ (Figure 2c). The micropearls are highly sensitive under the electron beam. The development of bubbles suggests the liberation of a volatile compound such as water (Fig. S3). Altogether, these observations clearly indicate that the micropearls are made of Sr- and Ba-bearing amorphous calcium carbonate (ACC) with the composition $(Ca,Sr)CO_3 n H_2O$ and $(Ca,Ba)CO_3 \, n H_2O$, respectively. Nevertheless, despite the SAED pattern clearly indicating an amorphous state, the presence of regular internal structures such as the concentric layers hints towards a near-amorphous or poorly crystalline state of the mineral.

To obtain statistically significant data on the overall compositions of the micropearls, we performed a large number of SEM-EDXS analyses. The water content was not considered in the quantification, as the proportion of water cannot be exactly known and does not affect the ratios between the divalent cations. SEM-EDXS has a lower spatial resolution than TEM-EDXS and was performed on micropearls still covered by organic matter. Therefore, elements

(e.g., Na, S…) that have not been detected in the micropearls' cross sections by TEM-EDXS analysis are not taken into account in Figure 1. Using this approach, we find that the Sr- micropearls contain up to 25 mol% of $SrCO_3$ (after normalization to the Ca+Sr+Ba sum) and are devoid of barium. The Ba-micropearls can contain up to 97 mol% of $BaCO_3$, while their $SrCO_3$ content reaches a maximum of 10 mol%. Cluster specimens show little variation in shape and size within one type, except the clusters of Ba-micropearls containing more than 50 mol% of $BaCO_3$. These nearly all have a diameter of ~10 μm instead of ~20 μm for those with lower barium concentrations.
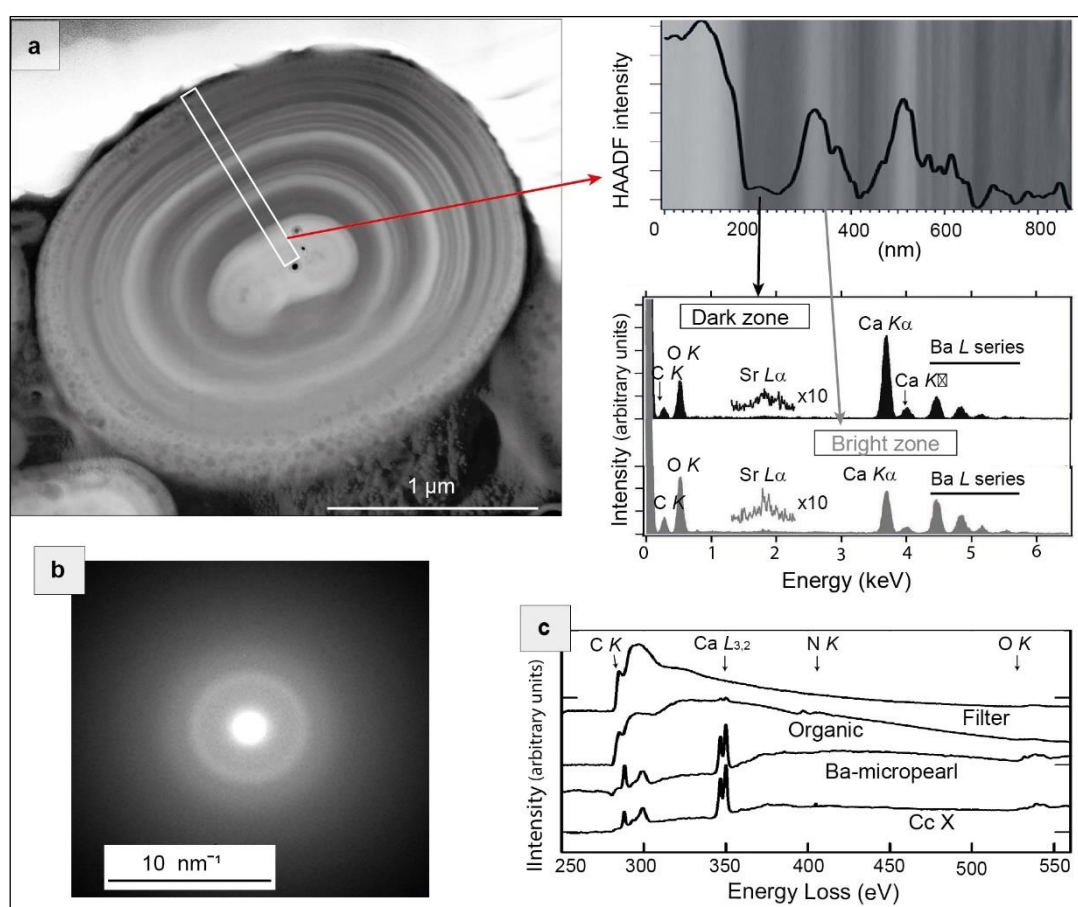
Figure 2 | FIB-cut section of a Ba-micropearl and related TEM analytical data.

(a) STEM-HAADF image showing intense oscillatory zoning in a Ba-micropearl. Black holes in the middle of the micropearl are due to beam damage. An integrated line profile of 50 pixels (upper right) displays more than 20 layers (minimum thickness: <15 nm). The EDXS spectra of the dark and bright zones show that bright zones have a higher Ba content than dark zones. (b) Ba-micropearl SAED pattern. (c) EELS spectra of a Ba-micropearl compared to surrounding organic material [organic], filter material (all from the same FIB section), and a calcite standard [Cc X]
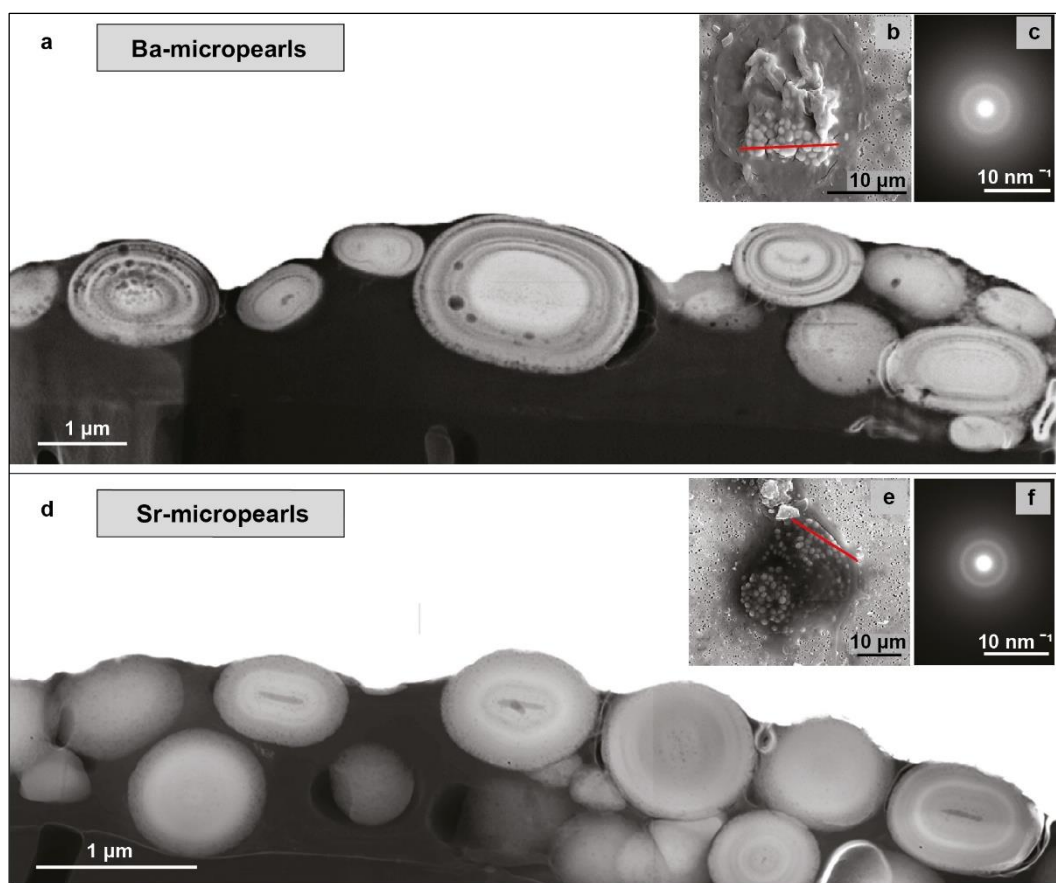
Figure 3 | Comparison of FIB-cut sections through clusters of Sr- and Ba-micropearls.

(a, d) TEM HAADF images of FIB-cut sections through, respectively, clusters of Ba-and Sr-micropearls. Despite noticeable differences (e.g., size, core shape), the common internal structure of micropearls (zonations) and their similar arrangement in the organic envelope clearly show that both types are related. Bubbles inside the micropearls are due to beam damage (resulting from STEM imaging and mapping). The contact between the filter surface and the cluster base can be observed in both cases near the bottom of the image. Filter pores (vertical holes) are also visible inside the filter. (b, e) SEM secondary electron images of the whole clusters; red line: location of the FIB-cut section. (c, f) SAED patterns, from a single micropearl of each FIB-cut section. Both show broad diffraction rings indicative for amorphous material

It is important to note that all the samples used for these measurements did not undergo any fixation prior to drying. The composition of the micropearls is therefore not altered by any chemical interaction, but the morphology of the organisms without mineral skeletal structures is obviously highly impacted (collapse). Nevertheless, even after drying, most organisms still retain enough proper characteristics to allow a comparison based on criteria such as their general shape or size as seen in Figure 1.

Besides the Sr-or Ba-micropearls, some clusters can also contain large inclusions with a very different chemical composition (Fig. S4). These, although still containing important proportions of calcium, are very rich in phosphorous: 30–65% (molar ratio of P over P+Mg+K+Ca+Sr). Proportions for other elements are as follows: 1–8% magnesium, 3–8%

potassium, 26–50% calcium, and 2–4% strontium. Their shape is generally spherical, but can also be angular when they are close to micropearls (Fig. S4).

Sulfur is also present in the SEM-EDXS results (both on carbon-and gold-coated samples) but its concentration never exceeds 5 mol% in the carbon-coated micropearls and ratio of S/Ca always remains below 0.1. Gold-coated samples analyses show similar results, although with a slight underestimation of sulfur (when it was detected), probably due to the overlap of the gold and sulfur emission lines.

2.4.2   Identification of the micropearls as intracellular inclusions in unicellular algae

In April 2015, an important abundance of Sr-micropearls was observed simultaneously with an increased presence of *Tetraselmis* cf. *cordiformis* (Chlorophyta) (Figure 5a). Further observations of fixed samples confirmed the presence of four flagella (or undulipodia) attached to the cells containing Sr-micropearls (Figures 5b and 5c). Moreover, the estimation of the quantity of Sr-clusters during a 9-month survey closely matches the biomass variation
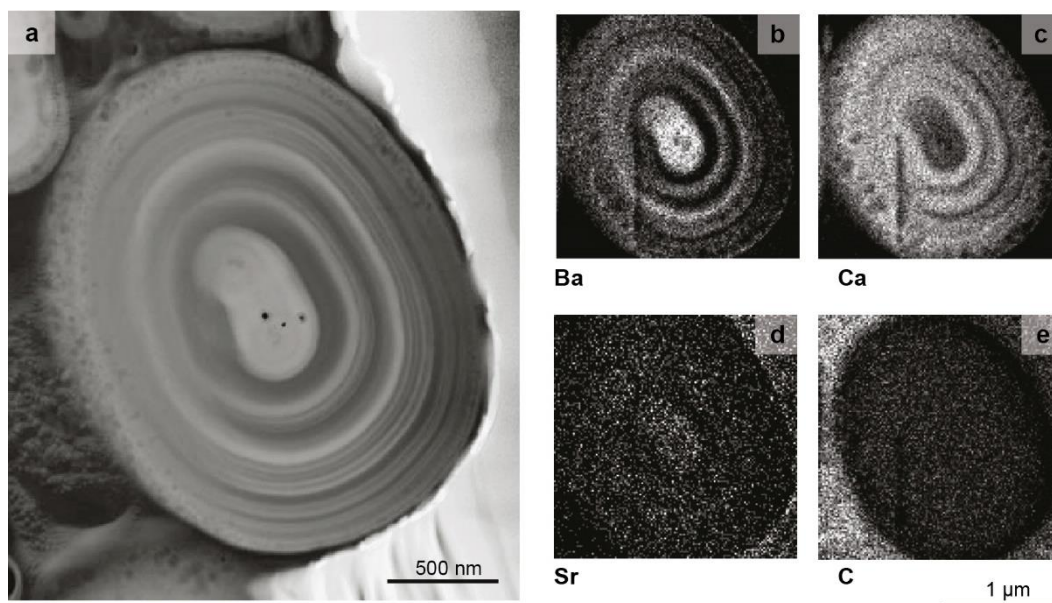
Figure 4 | TEM-EDXS mapping of a Ba-micropearl cross section.

a) TEM HAADF image of FIB-cut section through a Ba-micropearl. The bright material to the right is the protective platinum cover, and the dark material on the left is organic material. (b–e) Elemental EDXS maps show periodic Ba/Ca concentration variations forming the oscillatory zoning. The strontium concentration is overall very low, but the association of strontium with barium is well visible at the centre at the micropearl. The holes in the centre and the vertical black line which appears in the mapping are due at beam damage. The resolution of the mapping is limited by the high beam sensitivity of the sample, rendering long-time acquisitions impossible. Further, a binning of 4 pixels on the original resolution was applied to yield better statistics at the expense of spatial resolution
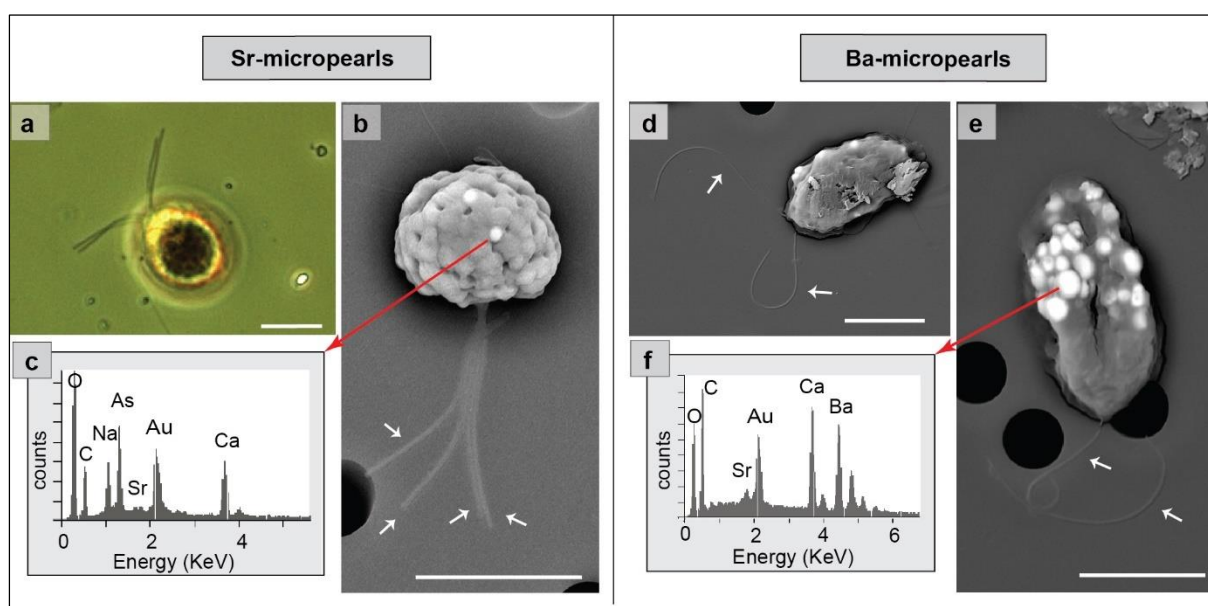
Figure 5 | TEM-EDXS mapping of a Ba-micropearl cross section.

Sr-micropearls in *Tetraselmis* cf. *cordiformis* and Ba-micropearls in a biflagellate alga. (a) *Tetraselmis* cf. *cordiformis*—optical microscope. (b) SEM backscattered image of a fixed Sr-cluster. Intracellular Sr-micropearls appear in lighter grey among organic granules. From a sample taken in GE3 location, at 18 m depth on the 21.04.2015. (c) Sr-micropearl EDXS analysis. Due to the micropearl's small size, the result also includes organic matter (C) and fixative (Na, As) besides the coating (Au). (d, e) SEM backscattered images of a bi-flagellated phytoplankter with intracellular Ba-micropearls (in white). From a sample taken in GE3 location at 20 m depth on the 14.07.2015. (f) Ba-micropearl EDXS analysis. Arrows: flagella. White scale bars: 10 µm

of *Tetraselmis* cf. *cordiformis* (Figure 6). The taxonomic identification of the *Tetraselmis* genus was based on the descriptions presented in *AlgaeBase* (Guiry & Guiry, 2016) and in Ettl (1983). The specimen shown in Figure 5a matches this description (general shape and four equal length flagella are characteristic of *Tetraselmis* sp.). The attribution to the species *cordiformis* is tentative at this stage.

Finally, Sr-micropearls were also observed in three cultured strains of *Tetraselmis cordiformis* (Table S2). Figure 7 shows the composition of micropearls of SAG 26.82 (originally from Münster Castle moat, Germany) and CCAC 0051 (originally from Lake Frühlinger, Germany). In these samples, only a few organisms did not contain micropearls.

Thorough observation of fixed lake samples allowed us to determine that the taxon at the origin of the Ba-micropearls with lower concentrations of barium (black circles in Figure 1) is a biflagellate organism (Figures 5d to 5f).
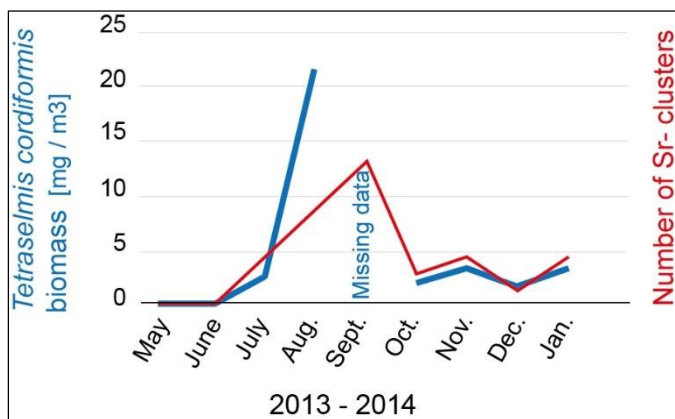
Figure 6 | Concording abundance of Sr-micropearls and *Tetraselmis* cf. *cordiformis*.

Nine-month period correspondence between the Tetraselmis cf. cordiformis biomass (blue line) and the number of Sr-clusters (red line). Note: The September 2013 sample (taken at 27 m depth) value could not be integrated in this figure because the Tetraselmis cf. cordiformis biomass measurement, to which the cluster quantity estimation is compared, was done on an integrated sample taken from 0 to 20 m depth. The comparison was therefore not valid

Element	EDXS results [mol%]
Mg	1.3
K	0.6
Ca	96.8
Sr	1.3

Element	EDXS results [mol%]
Na	0.3
Mg	0.6
K	0.6
Ca	97.9
Sr	0.6
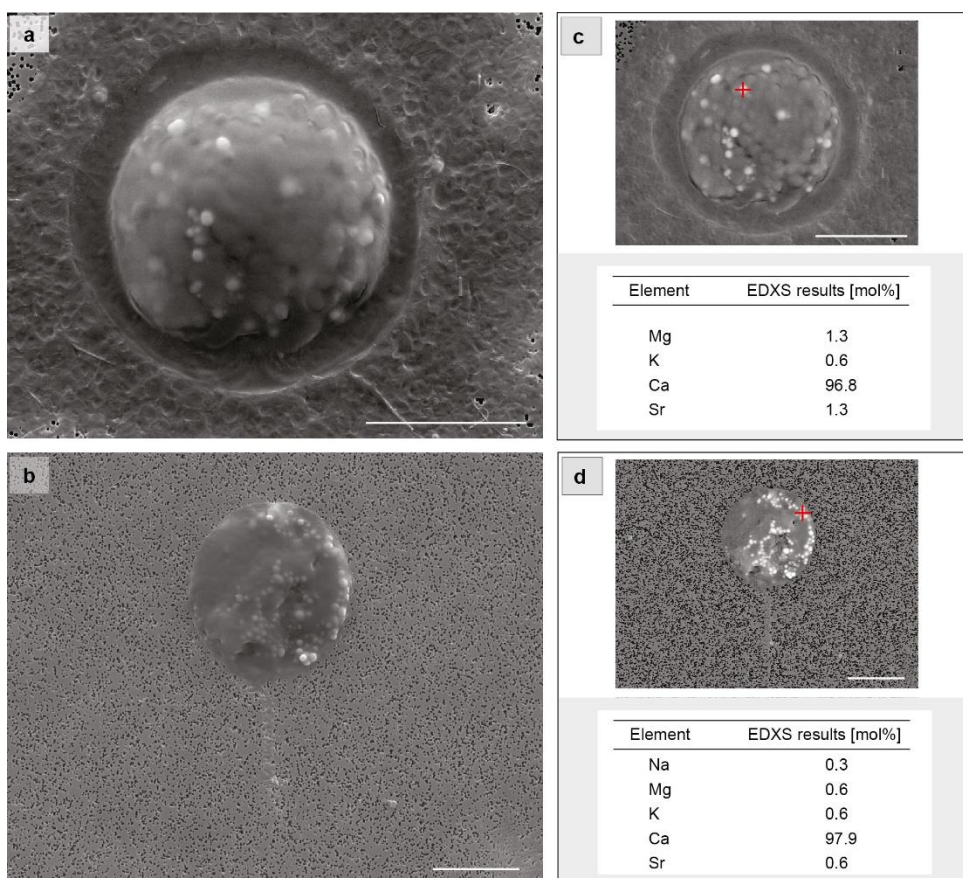
Figure 7 | Sr-micropearls in cultured strains of *Tetraselmis cordiformis*.

Dried samples. Micropearls appear in white or light grey among organic granules. Scale bar: 10 µm. (a) SEM secondary electron image of strain SAG 26.82 (Göttingen; originally from Münster Castle moat). The organism occurs here as a cyst or resting cell (i.e., non-motile). (b) SEM secondary electron image of strain CCAC 0051 (Köln; originally from Lake Frühlinger). (c and d) SEM backscattered electron images and EDXS semiquantitative results in mol%. This observation mode allows to clearly identify the micropearls among the organic granules. The red cross shows the point where the EDXS analysis was performed. These compositions closely resemble the composition of Lake Geneva Sr-micropearls

2.4.3   Inverse correlation with surface water chemistry

Simultaneous water analyses and micropearl-cluster counting showed a good inverse correlation between the abundance of the Ba-micropearl clusters and the concentration of soluble barium in surface waters of Lake Geneva (Figure 8).

2.4.4   Elemental distribution around the micropearls

Micropearls and organic material can be distinguished in NanoSIMS images, using the difference between organic material-derived ions ($^{12}C^{14}N^-$) and mineral-derived ions ($^{16}O^-$). The highest concentrations of CN are found at the borders of the micropearls, where an enrichment in sulfur is also observed (Figure 9). The composite NanoSIMS data confirm the intimate association of sulfur with both Ba-and Sr-micropearls and show significantly higher sulfur levels surrounding the Sr-inclusions than inside them.
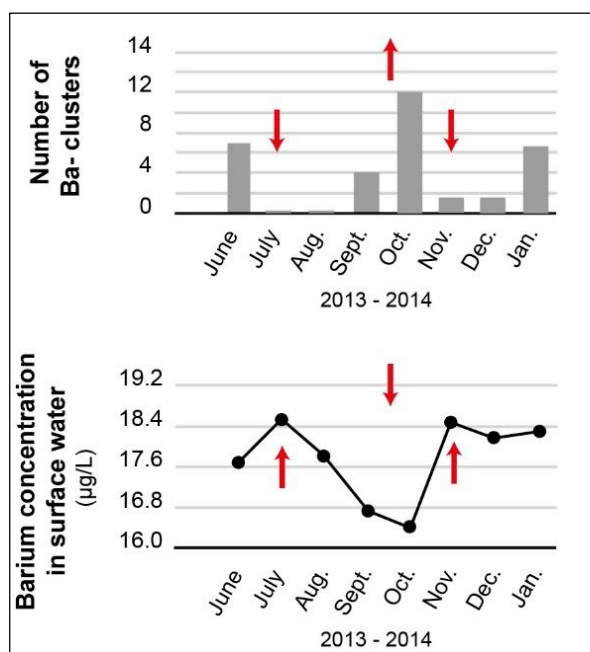
Figure 8 | Surface water barium concentration possibly influenced by the abundance of micro-organisms forming Ba-micropearls.

Eight-month period comparison between barium concentration (black line) and the number of Ba-clusters in surface water of Lake Geneva (grey columns; see methods for calculation details). The inverse correlation (highlighted by arrows) suggests a direct influence of the formation of Ba-micropearls on the barium cycle

2.5   Discussion

2.5.1   *Mineralogy of the micropearls*

While the occurrence of AEM sulfate inclusions are well established (for example, the barium and strontium sulfate crystals in Desmids), non-skeletal intracellular AEM carbonate inclusions have never been observed in unicellular phytoplanktonic eukaryotes until now. However, TEM-EELS and electron diffraction analyses clearly indicate that the micropearls are amorphous (or near-amorphous) carbonate (Figure 2). SEM-EDXS analyses also relate the micropearls to carbonates rather than sulfates, as the observed concentrations of sulfur are very low (molar ratio of S/Ca never exceeds 0.1, compared with the expected value for AEM sulfates: 0.2–0.8). As TEM-EDXS analyses did not identify any other elements than C, O, Ca, Sr, and Ba in the micropearls cross sections, we can unequivocally attribute these low concentrations of sulfur to the organic matter that covers and surrounds the micropearls in the samples analyzed by SEM-EDXS.

The amorphous state of the micropearls is not due to electron or ion beam damage, as calcite milled and observed under the same conditions remains crystalline. Moreover, the micropearls' strong reaction under the electron beam (Fig. S3) indicates that they might be highly hydrated and thus belong to the amorphous calcium carbonate (ACC) family with the general formula $XCO_3 \cdot nH_2O$ with X=Ca, Sr, and/or Ba. A tentative attribution to an amorphous form of benstonite, a mineral also found in cyanobacterial microspheres by Couradeau et al. (2012), was proposed earlier (Jaquet et al., 2013). In its pure form, ACC is unstable and eventually forms either calcite or aragonite crystals (Addadi, Raz, & Weiner, 2003; Weiner & Addadi, 2011; Bots, Benning, Rodriguez-Blanco, Roncal-Herrero, & Shaw, 2012). However, some organisms produce stable ACC (Cartwright, Checa, Gale, Gebauer, & Sainz-Díaz, 2012), which is typically strongly hydrated and may stay in an amorphous state for several days, even if dried (Addadi et al., 2003; Ihli et al., 2014). This is the case for our micropearls.

Interestingly, *in vitro* experiments suggested that the long-term stabilization of an amorphous state for both hydrated barium and calcium carbonates often implies a strong organic control (Addadi et al., 2003; Chen et al., 2009; Cartwright et al., 2012; Cam, Georgelin, Jaber, Lambert, & Benzerara, 2015). In our case, NanoSIMS observations showing high CN concentrations along the surface of some micropearls suggest a link between organic matter-rich regions and the presence of these inclusions.
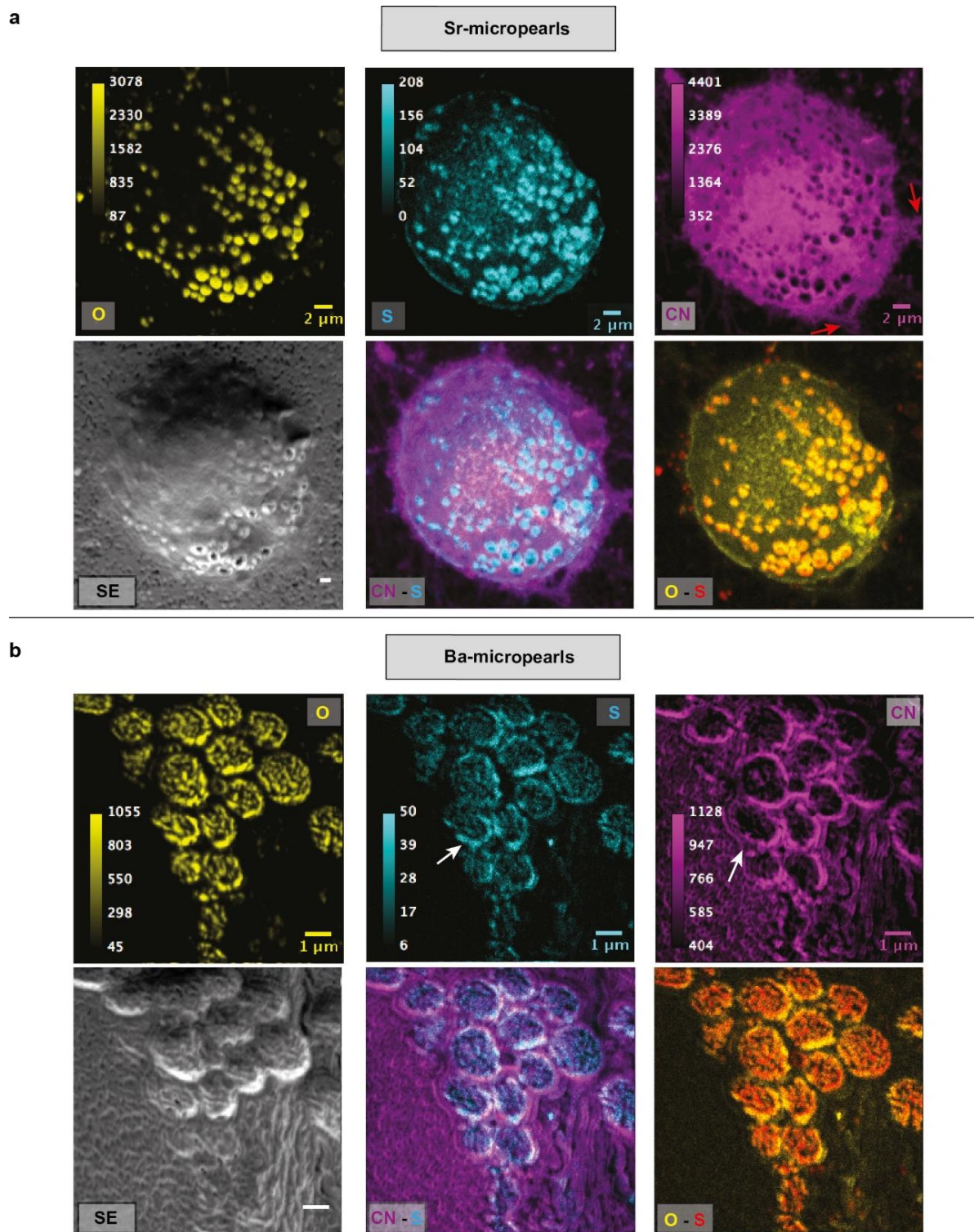
Figure 9 | NanoSIMS images.

(a) Sr-cluster and (b) Ba-cluster. The $^{16}O^-$ clearly shows the micropearl morphology as an indicator of mineral phase; the $^{32}S^-$ reveals the location of S inside and surrounding the micropearls; the $^{26}CN^-$ highlights the organic material and shows an enrichment surrounding the micropearls. The sulfur and CN do not show exactly the same distribution (an example is located by the white arrows). Note the presence of the flagella in two opposite pairs (red arrows) in the Sr-cluster. Overlays of the $^{26}CN^-$ and $^{32}S^-$ along with $^{16}O^-$ and $^{32}S^-$ secondary ion images indicate that S is colocalized with mineral phase in both Sr-and Ba-clusters, and correlate with the enrichment in CN surrounding the micropearls in Sr-clusters. SE: secondary electron images

Organic compounds could be directly associated with ACC formation or be pushed forward as the inclusion grows, thus concentrating at the periphery of the micropearls. Moreover, NanoSIMS results reveal an intimate association of sulfur with the micropearls (Figure 9): Overlapping CN and S suggests that sulfur is part of the organic matter (thus supporting TEM- and SEM-EDXS results), probably as proteinaceous material although the presence of low molecular mass organic sulfur-containing compounds cannot be excluded. The overlapping CN and S distributions (resulting in a mixed color in the composite NanoSIMS image) allows to localize proteinaceous materials in cells (Müller et al., 2010) and may imply the presence of fine-scale mixtures of mineral nanoparticles and organic matter (Moreau et al., 2007). On the other hand, the possibility that the sulfur belongs to isolated sulfates cannot be completely ruled out. Indeed, the presence of different foreign ions in the fluid during $CaCO_3$ crystallization can promote the formation of metastable phases. The very low amount of sulfur detected in the NanoSIMS ion map (Figure 9) could suggest that sulfate is incorporated in the ACC thereby modifying the crystallization pathway of calcium carbonates (Van Santen, 1984; Bots et al., 2012). Such low concentrations are likely beyond the detection limits of the TEM-EDXS. Nevertheless, the observation of high CN concentrations along the surfaces of most micropearls of Ba-clusters seems unfavorable for such a physicochemical control over calcium carbonate formation, rather suggesting an organic control.

Finally, intracellular formation of near-amorphous calcium carbonate requires supersaturation with Ca carbonates in the cytoplasm. Although the present state of our research does not allow to judge, this can be either the result of concentration inside intracellular vesicles or due to high viscosity of the cytoplasm creating local chemical heterogeneities (Li et al., 2016).

2.5.2   *Inner structure and chemistry of the micropearls*

The internal structure of the micropearls is characterized by numerous nanometric concentric layers (Figures 2, 3 and 4), expressing variations in the chemical composition of the carbonates (low or high Sr content for Sr-micropearls; alternating Ba-or Ca-rich composition for Ba-micropearls). To our knowledge, this is the first observation of biomineral oscillatory zoning at the nanoscale. Other similar examples of oscillatory zoning are abiogenic carbonate and sulfate crystals formed during experiments at ambient temperature (Putnis, Fernandez-Diaz, & Prieto, 1992; Prieto, Fernández-González, Putnis, & Fernández-Díaz, 1997; Fernández-González, Prieto, Putnis, & López-Andrés, 1999; Nielsen, Aloni, & De Yoreo, 2014), and

abiogenic natural occurrences formed in hydrothermal or metamorphic conditions (Reeder & Prosky, 1986; Pollok, Jamtveit, & Putnis, 2001). This internal structure indicates that the micropearls' growth was continuous and at sufficient supersaturation, as no Ostwald ripening or interim dissolution appears to have taken place (Putnis & Putnis, 2007).

The exact concentration of barium and strontium needed in a solution for these micropearls to form is difficult to evaluate, as the solubility of metastable hydrated ACC and its variation with barium and strontium content is unknown. Nevertheless, these concentrations must highly exceed those of Lake Geneva's water (Table S5). Indeed, besides the fact that such high barium concentrations have never been described in biogenic ACC, the originality of the micropearls' composition stems from their important enrichment in barium and strontium compared with the surrounding lake water. The Sr/Ca and Ba/Ca molar ratios are, respectively, 13 and 11,000 times higher in the micropearls on average (87 and 800,000 times higher for maximum concentrations) (Table S4 and S5). This implies an important intracellular pre-concentration mechanism of strontium and barium by the organisms producing the micropearls.

2.5.3   A new physiological trait for unicellular eukaryotes

The fact that, apart from early observations in ciliates (Fauré-Fremiet & Gauchery, 1957), intracellular AEM carbonate inclusions have never been described in unicellular eukaryotes before is puzzling, as our results show that micropearls are common in at least two different planktonic organisms (Figures 1, 5 and 7). Perhaps even more so, as the *Tetraselmis* genus, including *Tetraselmis cordiformis*, has been widely studied because several species are potential producers of biofuels (Lim et al., 2012), while others are used as aquaculture feed (Zittelli, Rodolfi, Biondi, & Tredici, 2006). The reason why they have been overlooked so far might be that micropearls appear translucent under the optical microscope and are easily altered, dissolved, or expelled during most sample preparations. For instance, the internal structure of the *Tetraselmis* cell in general (including specimens of *Tetraselmis cordiformis*) has been studied in great detail by Melkonian (1979) and Norris, Hori, and Chihara (1980) in TEM sections without any mention of mineral inclusions. Some electron-transparent features, attributed to starch grains, could perhaps represent the location of dissolved micropearls. Interestingly, a recent study showed that conventional preparation by ultramicrotomy fails in preserving intracellular carbonate inclusions in cyanobacteria (Li et al., 2016).

The presence of micropearls in cultured strains of *Tetraselmis cordiformis* is also interesting. In spite of the fact that the culture media have not been spiked with Sr (Table S3), this element is found in the micropearls (Figure 7), perhaps inherited from the strains' original environment or from the medium where strontium could be present at ultra-trace concentrations. This further reiterates the very strong sequestration capacity of *Tetraselmis* toward strontium in addition to calcium.

The physiological role of these micropearls remains unclear. Some *Tetraselmis* species are known to bioaccumulate metals (Cu, Ag, Pb) in osmiophilic vesicles, in case of exposure to micromole concentrations of these metals (Ballan-Dufrançais, Marcaillou, & Amiard-Triquet, 1991), which is explained as a detoxification strategy. In Lake Geneva, observations indicate that preferential precipitation of strontium or barium is taxon dependent and not opportunistic. Indeed, we often found clusters of Ba-micropearls co-existing with clusters of Sr-micropearls (totally devoid of barium) in the same water sample. The latter observation, in addition to the high concentration of strontium or barium needed inside the cell to form minerals such as the micropearls, may argue for a biologically controlled biomineralization process (Dupraz et al., 2009).

A relationship between the organisms' taxa and the micropearls' chemical composition emerges clearly from our data. Sr-micropearls (grey squares in Figure 1) are systematically assigned to *Tetraselmis* cf. *cordiformis* (Figures 5a to 5c). The Ba-micropearls with lower concentrations of barium always belong to an elongated biflagellate eukaryote of approximately 20 micrometers of diameter (black circles in Figure 1 and Figures 5d to 5f), while the Ba-micropearls with higher concentrations of barium correspond to a round biflagellate eukaryote with a smaller diameter of approximately 7–10 micrometers (grey circles in Figure 1), which might represent a third taxon. These conclusions, based on the analysis and observation of more than 450 clusters, are not unequivocal, but remain striking. A thorough genomic analysis will have to be carried out to precisely identify the organisms responsible for the production of the various micropearl types. What is clear at this stage is that the precipitation of AEM carbonates by *Tetraselmis cordiformis* represents an alternative pathway to the already known sequestration of strontium and barium as sulfates in terminal vacuoles of Desmids (Krejci et al., 2011). Moreover, differences between Sr-and Ba-clusters suggest distinct biomineralization pathways for each cluster-type. Indeed, higher CN and S signals are observed at the periphery of the Sr-micropearls than in the Ba-clusters (Figure 9). The different organisms could use distinct biomineralization processes, both resulting in the formation of micropearls.

2.5.4 Strong concentration capacities may impact the barium geochemical cycle

The widespread intracellular carbonate biomineralization in certain unicellular eukaryotes of Lake Geneva may have large-scale implications. For instance, the inverse correlation observed between the number of the Ba-micropearl clusters and soluble barium concentrations in surface waters (Figure 8) shows that, during strong abundance periods, the production of Ba-micropearls by unicellular organisms impacts the chemical composition of surface water through sequestration of an important part of the available barium. Thus, the occurrence of AEM carbonates as micropearls inside the cells of planktonic unicellular eukaryotes might be considered a key player in the geochemical cycle of strontium and barium in some freshwater environments.

Low concentrations of strontium are also detected in the Ba-micropearls (up to 10 mol%, see Figure 1). Therefore, the strong Ba-and Sr-concentration capacity of both micropearl-forming organisms could lead to new bioremediation solutions for waters polluted by radioactive ^{90}Sr (Krejci et al., 2011).

2.5.5 A similar biomineralization process in bacteria?

It is interesting to note that some bacteria forming intracellular amorphous carbonate inclusions show similar concentration capacities (Gray, 2006; Cam et al., 2015). These otherwise very different organisms also strongly concentrate and sequestrate specific AEM elements. For example, certain *Achromatium* species were reported to have the capacity to scavenge available calcium to form their inclusions from environments with fairly low dissolved calcium concentrations (Head et al., 2000; Gray, 2006). Likewise, some cyanobacteria's AEM inclusions were noted to have very high concentrations of strontium and barium compared with the extracellular solution (up to 1370 times higher for Ba/Ca ratio) (Cam et al., 2015).

Other similarities can be noted with the biomineralization observed in cyanobacteria. Notably, large intracellular phosphorus-rich inclusions are frequently observed to be co-existing with the micropearls, both in Sr-and Ba-clusters (Fig. S4). A very similar feature has been described in cyanobacteria featuring ACC inclusions (Li et al., 2016).

Moreover, the comparison between two cyanobacteria strains producing intracellular ACC inclusions (*Candidatus* Gloeomargarita lithophora C7 and *Candidatus* Synechococcus calcipolaris G9), both cultivated in two different media, showed that the chemical

compositions of the carbonate inclusions varied mostly with the nature of the cyanobacterial strain, independently of the medium in which they were grown (Li et al., 2016). As previously stated, our results similarly indicate that the chemical composition of the micropearls seems characteristic of the eukaryote organism which produces them.

Altogether, these similarities suggest that micropearls observed in unicellular planktonic eukaryotes and intracellular ACC inclusions observed in cyanobacteria might originate from a similar biomineralization process. Recently, this biomineralization process in cyanobacteria was suggested as the possible ancestral evolutionary origin of resembling processes known in multicellular eukaryotes (Benzerara et al., 2014) such as oysters (Addadi et al., 2003; Jacob et al., 2008; Xiang et al., 2014). Unicellular eukaryotes forming micropearls could therefore also be part of this evolutionary lineage.

2.6   Conclusion

We present here the first report of intracellular near-amorphous AEM carbonate inclusions in unicellular eukaryotes. The chemical composition of these micropearls ranges from pure calcium carbonate to other AEM carbonates (Ba and Sr). These mineral inclusions represent a new physiological trait for unicellular eukaryotes, which might have been overlooked until now in numerous species, because traditional sample preparation techniques seem likely to alter or destroy them.

The internal nanometer-scale concentric oscillatory zonations observed on cross sections of the micropearls express chemical variations of the carbonates (low or high contents of Sr, Ba, or Ca). Our results systematically link the unicellular alga *Tetraselmis cordiformis* with micropearls enriched in strontium, while barium-rich micropearls are observed in biflagellate eukaryotes, yet to be identified. Our data suggest that each micropearl-forming organism produces micropearls within a given characteristic chemical composition range, through a novel intracellular biomineralization process. Several similarities suggest that this biomineralization process could be close to the process forming the intracellular carbonate inclusions recently described in cyanobacteria.

The concentrations of strontium and barium needed to form the micropearls greatly exceed those of Lake Geneva's water, implying an important intracellular pre-concentration by the unicellular organism. These strong concentration capabilities suggest micropearl-forming

organisms could be significant players in the geochemical cycle of alkaline-earth metals in some freshwater environments and could potentially lead to new bioremediation solutions.

2.7   References

Addadi, L., Raz, S., & Weiner, S. (2003). Taking advantage of disorder: amorphous calcium carbonate and its role in biomineralization. Advanced Materials, 15, 959–970.

Ballan-Dufrançais, C., Marcaillou, C., & Amiard-Triquet, C. (1991). Response of the phytoplanctonic alga Tetraselmis suecica to copper and silver exposure: vesicular metal bioaccumulation and lack of starch bodies. Biology of the Cell, 72, 103–112.

Benzerara, K., Skouri-Panet, F., Li, J., Férard, C., Gugger, M., Laurent, T., Moreira, D. (2014). Intracellular Ca-carbonate biomineralization is widespread in cyanobacteria. PNAS, 111, 10933–10938.

Bots, P., Benning, L. G., Rodriguez-Blanco, J.-D., Roncal-Herrero, T., & Shaw, S. (2012). Mechanistic insights into the crystallization of amorphous calcium carbonate (ACC). Crystal Growth & Design., 12, 3806–3814.

Cam, N., Georgelin, T., Jaber, M., Lambert, J.-F., & Benzerara, K. (2015). In vitro synthesis of amorphous Mg-, Ca-, Sr-and Ba-carbonates: What do we learn about intracellular calcification by cyanobacteria? Geochimica et Cosmochimica Acta, 161, 36–49.

Cartwright, J. H. E., Checa, A. G., Gale, J. D., Gebauer, D., & Sainz-Díaz, C. I. (2012). Calcium carbonate polyamorphism and its role in biomineralization: how many amorphous calcium carbonates are there? Angewandte Chemie International Edition, 51, 11960–11970.

Chen, L., Shen, Y., Xie, A., Huang, B., Jia, R., Guo, R., & Tang, W. (2009). Bacteria-mediated synthesis of metal carbonate minerals with unusual morphologies and structures. Crystal Growth & Design, 9, 743–754.

CIPEL (2015). Rapports sur les études et recherches entreprises dans le Bassin Lémanique. Programme quinquennal 2011–2015. Campagne 2014. CIPEL, Nyon, Switzerland, pp. 261. Retrieved from http://www.cipel.org/publications/rapports-scientifiques/rapport-2015-campagne-2014/. last accessed on 6 August 2016.

Couradeau, E., Benzerara, K., Gérard, E., Moreira, D., Bernard, S., Brown, G. E. Jr, & López-García, P. (2012). An early-branching microbialite cyanobacterium forms intracellular carbonates. Science, 336, 459–462.

Druart, J. C., Pongratz, E., & Revaclier, R. (1983). Les algues planctoniques du Léman: historique et inventaire. Swiss Journal of Hydrology, 45, 430–457.

Druart, J. C., & Rimet, F. (2008). Protocoles d'analyse du phytoplankton de l'INRA: prélèvement, dénombrement et biovolumes. INRA – SHL Rapport 283. Thonon les Bains, France, pp. 96.

Dupraz, C., Reid, R. P., Braissant, O., Decho, A. W., Norman, R. S., & Visscher, P. T. (2009). Processes of carbonate precipitation in modern microbial mats. Earth-Science Reviews, 96, 141–162.

Ettl, H. (1983). Chlorophyta I Phytomonadina. Süsswasserflora von Mitteleuropa, 9, 141–149.

Fauré-Fremiet, E., & Gauchery, M. (1957). Concrétion minérales intracytoplasmiques chez les ciliés. The Journal of Protozoology, 4, 96–109.

Fernández-González, Á., Prieto, M., Putnis, A., & López-Andrés, S. (1999). Concentric zoning patterns in crystallizing (Cd, Ca)CO3 solid solutions from aqueous solutions. Mineralogical Magazine, 63, 331–343.

Gray, N. D. (2006). The unique role of intracellular calcification in the genus Achromatium. Microbiology Monographs, 1, 299–309.

Guiry, M. D., & Guiry, G. M. (2016). AlgaeBase. World-wide electronic publication, National University of Ireland, Galway. Retrieved from http://www.algaebase.org. searched on 6 August 2016.

Head, I. M., Gray, N. D., Howarth, R., Pickup, R. W., Clarke, K. J., & Jones, J. G. (2000). Achromatium oxaliferum. Understanding the unmistakable. Advances in Microbial Ecology, 16, 1–40.

Ihli, J., Wong, W. C., Noel, E. H., Kim, Y. Y., Kulak, A. N., Christenson, H. K., …, Meldrum, F. C. (2014). Dehydration and crystallization of amorphous calcium carbonate in solution and in air. Nature Communications, 5, 3169. doi: 10.1038/ncomms4169.

Jacob, D. E., Soldati, A. L., Wirth, R., Huth, J., Wehrmeister, U., & Hofmeister, W. (2008). Nanostructure, composition and mechanisms of bivalve shell growth. Geochimica et Cosmochimica Acta, 72, 5401–5415.

Jaquet, J. M., Nirel, P., & Martignier, A. (2013). Preliminary investigations on picoplankton-related precipitation of alkaline-earth metal carbonates in meso-oligotrophic lake Geneva (Switzerland). Journal of Limnology, 72, 592–605.

Konhauser, K. (2007). Introduction to Geomicrobiology (p. 425). Oxford, UK: Blackwell Publishing.

Krejci, M. R., Wasserman, B., Finney, L., McNulty, I., Legnini, D., Vogt, S., & Joester, D. (2011). Selectivity in biomineralization of barium and strontium. Journal of Structural Biology, 176, 192–202.

Li, J., Oliver, I. M., Cam, N., Boudier, T., Blondeau, M., Leroy, E., … Benzerara, K. (2016). Biomineralization patterns of intracellular carbonatogenesis in cyanobacteria: molecular hypothesis. Minerals, 6, 10. doi: 10.3390/min6010010.

Lim, D. K. Y., Garg, S., Timmins, M., Zhang, E. S. B., Thomas-Hall, S. R., Schuhmann, H., … Schenk, P. M. (2012). Isolation and evaluation of oil-producing microalgae from subtropical coastal and brackish waters. PLoS ONE, 7. doi: 10.1371/journal.pone.0040751.

Melkonian, M. (1979). An ultrastructural study of the flagellate Tetraselmis cordiformis Stein (Chlorophyceae) with emphasis on the flagellar apparatus. Protoplasma, 98, 139–151.

Moreau, J. W., Weber, P. K., Martin, M. C., Gilbert, B., Hutcheon, I. D., & Banfield, J. F. (2007). Extracellular proteins limit the dispersal of biogenic nanoparticles. Science, 316, 1600–1603.

Müller, W. E. G., Wang, X., Sinha, B., Wiens, M., Schröder, H.-C., & Jochum, K. P. (2010). NanoSIMS: insights into the organization of the proteinaceous scaffold within Hexactinellid sponge spicules. ChemBioChem, 11, 1077–1082.

Nielsen, M. H., Aloni, S., & De Yoreo, J. J. (2014). In situ TEM imaging of $CaCO_3$ nucleation reveals coexistence of direct and indirect pathways. Science, 345, 1158–1162.

Norris, R. E., Hori, T., & Chihara, M. (1980). Revision of the genus Tetraselmis (Class Prasinophyceae). The Botanical Magazine (Tokyo), 93, 317–339.

Pollok, K., Jamtveit, B., & Putnis, A. (2001). Analytical transmission microscopy of oscillatory zoned grandite garnets. Contributions to Mineralogy and Petrology, 141, 358–366.

Prieto, M., Fernández-González, Á., Putnis, A., & Fernández-Díaz, L. (1997). Nucleation, growth, and zoning phenomena in crystallizing (Ba, Sr) CO_3, Ba(SO_4, CrO_4), (Ba, Sr)SO_4, and (Cd, Ca)CO_3 solid solutions from aqueous solutions. Geochimica et Cosmochimica Acta, 61, 3383–3397.

Putnis, A., Fernandez-Diaz, L., & Prieto, M. (1992). Experimentally produced oscillatory zoning in the (Ba, Sr)SO4 solid solution. Nature, 358, 743–745.

Putnis, A., & Putnis, C. V. (2007). The mechanism of reequilibration of solids in the presence of a fluid phase. Journal of Solid State Chemistry, 180, 1783–1786.

Ragon, M., Benzerara, K., Moreira, D., Tavera, R., & Lopez-Garcia, P. (2014). 16S rDNA-based analysis reveals cosmopolitan occurrence but limited diversity of two cyanobacterial lineages with contrasted patterns of intracellular carbonate mineralization. Frontiers in Microbiology, 5, 331. doi: 10.3389/fmicb.2014.00331.

Raven, J. A., & Giordano, M. (2009). Biomineralization by photosynthetic organisms: Evidence of coevolution of the organisms and their environment? Geobiology, 7, 140–154.

Raven, J. A., & Knoll, A. H. (2010). Non-skeletal biomineralization by eukaryotes: matters of moment and gravity. Geomicrobiology Journal, 27, 572–584.

Reeder, R. J., & Prosky, J. L. (1986). Compositional sector zoning in dolomite. Journal of Sedimentary Research, 56, 237–247.

Rieder, N., Ott, H. A., Pfundstein, P., & Schoch, R. (1982). X-ray microanalysis of the mineral contents of some Protozoa. Journal of Protozoology, 29, 15–18.

Salman, V., Tingting, Y., Berben, T., Klein, F., Angert, E., & Teske, A. (2015). Calcite-accumulating large sulfur bacteria of the genus Achromatium in Sippewissett Salt Marsh. The ISME Journal, 9, 2503–2514.

Saraswati, P. K., & Srinivasan, M. S. (2016). Micropaleontology: Principles and Applications (p. 224). Switzerland: Springer International Publishing.

Sigel, A., Sigel, H., & Sigel, R. K. O. (2008). Metal ions in life sciences, Vol. 4. Biomineralization: from nature to application (pp. 671). Wiley: West Sussex, UK.

Van Santen, R. A. (1984). The Ostwald step rule. The Journal of Physical Chemistry, 88, 5768–5769.

Weiner, S., & Addadi, L. (2011). Crystallization pathways in biomineralization. Annual Review of Materials Research, 41, 21–40.

Weiner, S., & Dove, P. M. (2003). An overview of biomineralization processes and the problem of the vital effect. Reviews in Mineralogy and Geochemistry, 54, 1–29.

Xiang, L., Kong, W., Su, J., Liang, J., Zhang, G., Xie, L., & Zhang, R. (2014). Amorphous calcium carbonate precipitation by cellular biomineralization in mantle cell cultures of Pinctada fucata. PLoS ONE, 9, e:113150. doi: 10.1371/journal.pone.0113150.

Young, J. R., & Henriksen, K. (2003). Biomineralization within vesicles: the calcite of coccoliths. Reviews in Mineralogy and Geochemistry, 54, 189–215.

Zittelli, G. C., Rodolfi, L., Biondi, N., & Tredici, M. R. (2006). Productivity and photosynthetic efficiency of outdoor cultures of Tetraselmis suecica in annular columns. Aquaculture, 261, 932–943.

2.8   Supplementary information
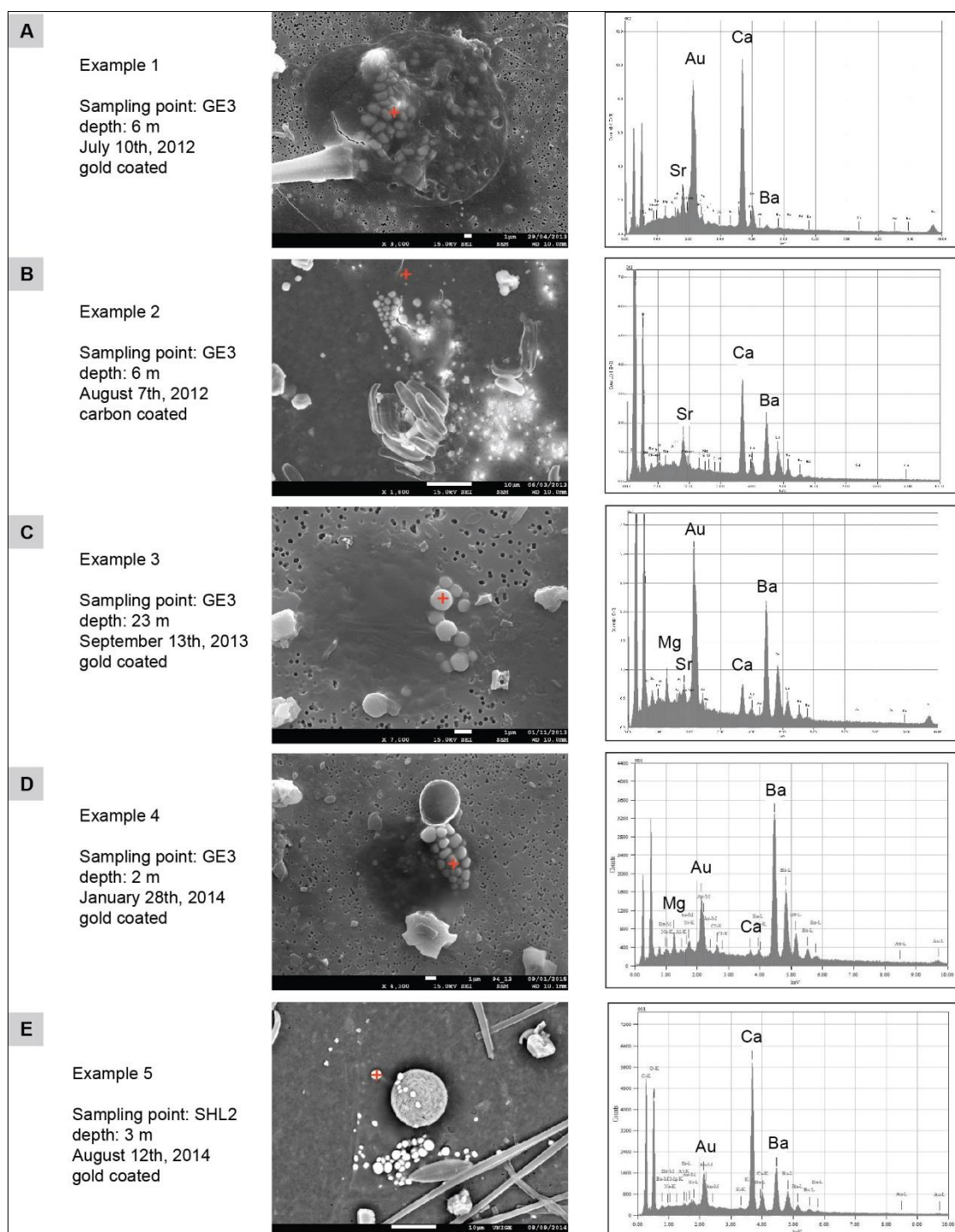
Figure S1 | Examples of EDXS raw data for Ba-micropearl analysis.

The red cross on the SEM images shows the point where the EDXS analysis was performed. The shape of the cluster may not be very visible when other particles were deposited in the same place during filtration (e.g. examples 2 and 4). Resulting EDXS graphs are shown on the right, with the labels of the main peak of major elements enhanced. Carbon and oxygen (the two first peaks on the left of the graphs) are not always labelled; they are not taken into account in the semi-quantitative calculation of the mole percentages per element. Examples 1, 2 and 5 belong to the larger Ba-cluster type, with lower Ba concentrations. Examples 3 and 4 belong to the smaller Ba-cluster type, with higher Ba concentrations.
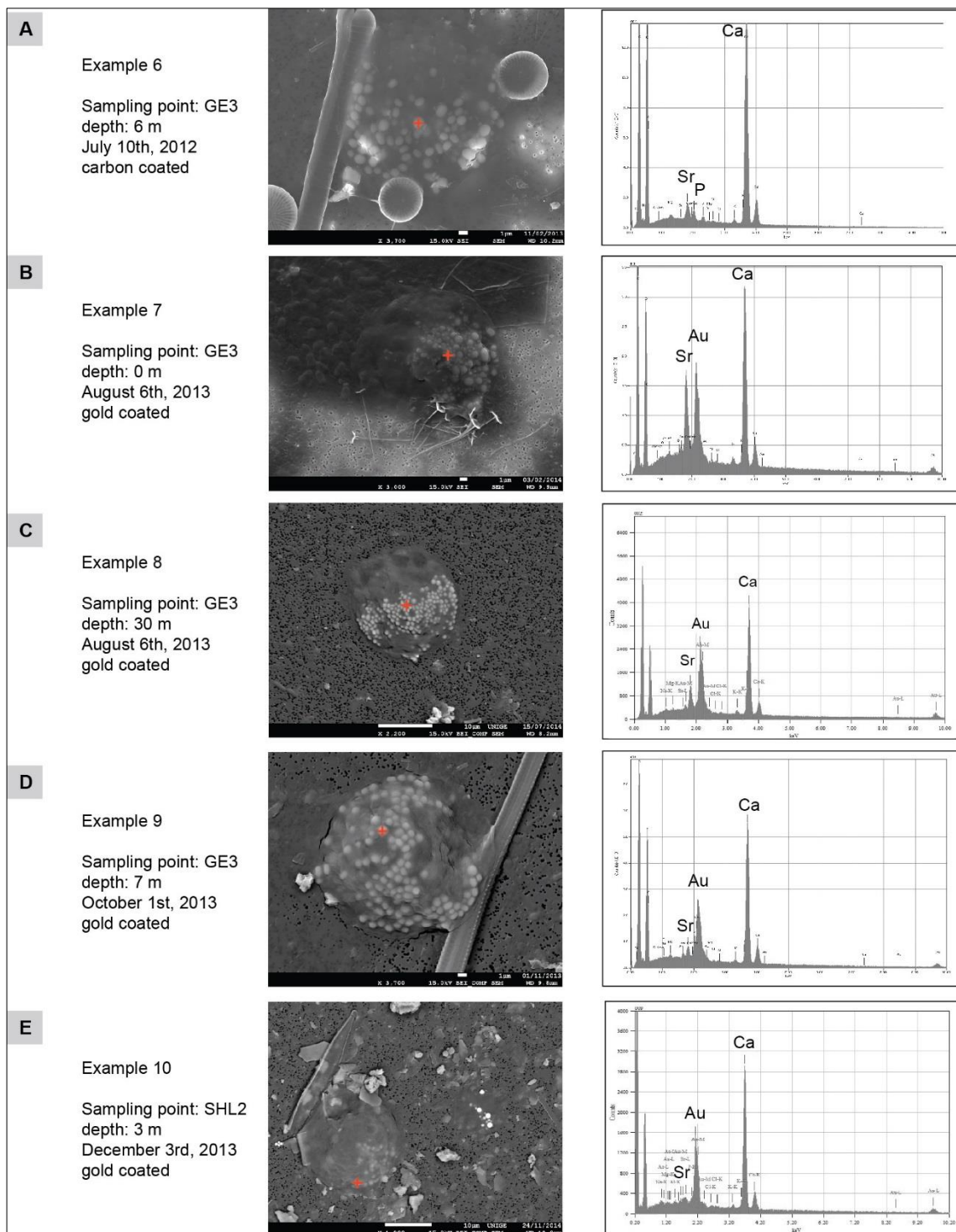
Figure S2 | Examples of EDXS raw data for Sr-micropearl analysis.

The red cross on the SEM images shows the point where the EDXS analysis was performed. Resulting EDXS graphs are shown on the right, with the labels of the main peak of major elements enhanced. Carbon and oxygen peaks (the two first peaks on the left of the graphs) are not always labelled; they are not taken into account in the semi-quantitative calculation of the mole percentages per element.
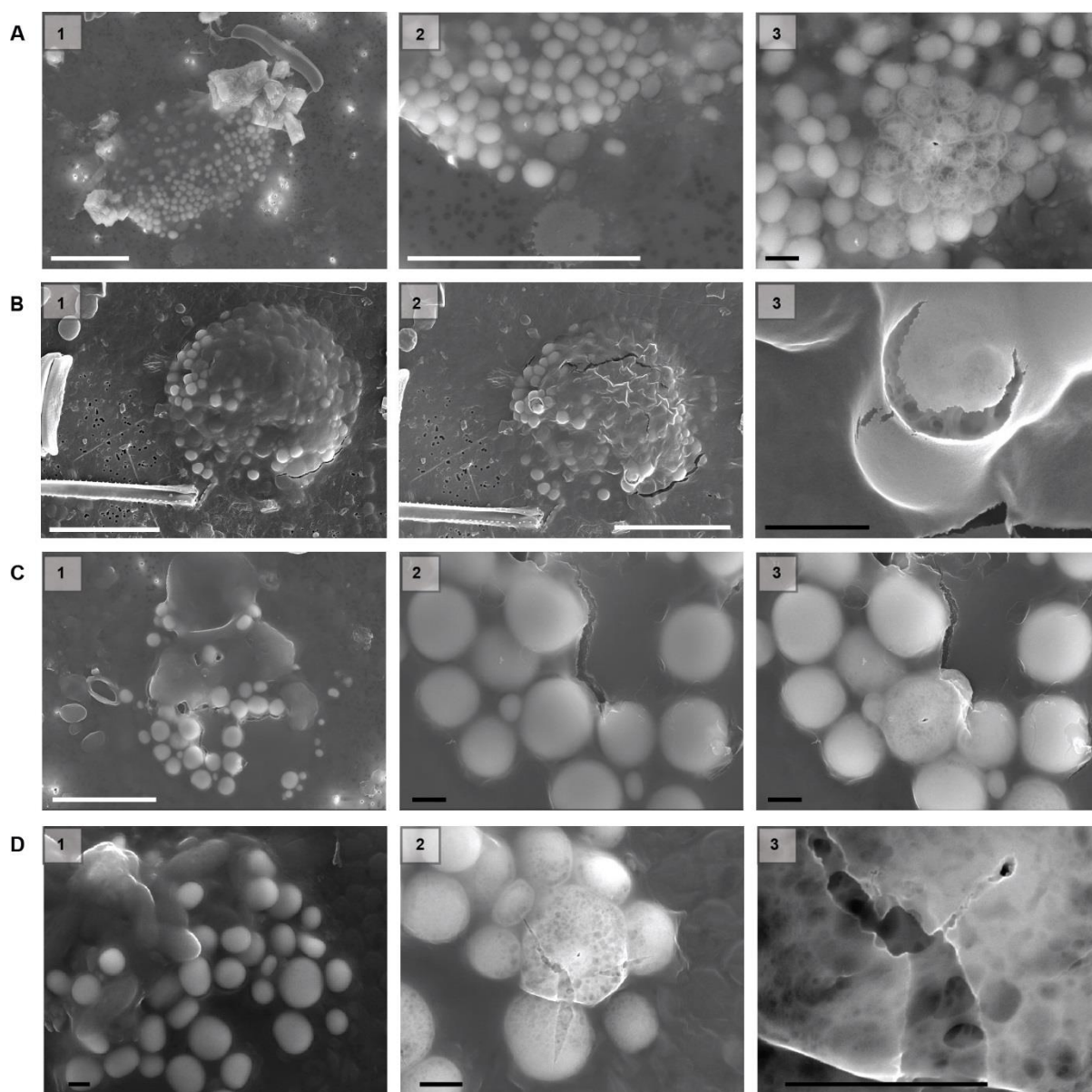
Figure S3 | SEM secondary electron images of SEM-beam damages on Ba- and Sr micropearls.

Prolonged imaging and EDXS analysis produce expanding bubbles inside the micropearls. As a consequence, the gold (A-C) or carbon (D) coating layer cracks. If submitted to a high probe current beam, the organic matter around the micropearls also reacts strongly (see image B1 compared to image B2). Left column (1) shows images of clusters before beam damage. (A) Sr-micropearl cluster. A2 is a medium-zoom of the micropearls before EDXS measurement. Damage after EDXS measurement (central spot) is clearly visible in A3. (B) Sr-micropearls cluster. Long-time exposure to high probe current beam. Micropearls and organic matter both react strongly. Cracks in gold layer reveal the bubbles inside the micropearl in B3. (C) Ba-micropearl cluster. Damage after EDXS measurement (particularly central spot) visible in image C3. Only the analyzed micropearl is affected. (D) Ba-micropearl cluster. Damages after EDXS measurement (central spot visible in D2 and D3) also impact other micropearls, as seen in central image. The bubbles induced in the micropearl are nicely visible through the carbon-coating layer. White scale bar: 10 µm. Black scale bar: 1 µm.
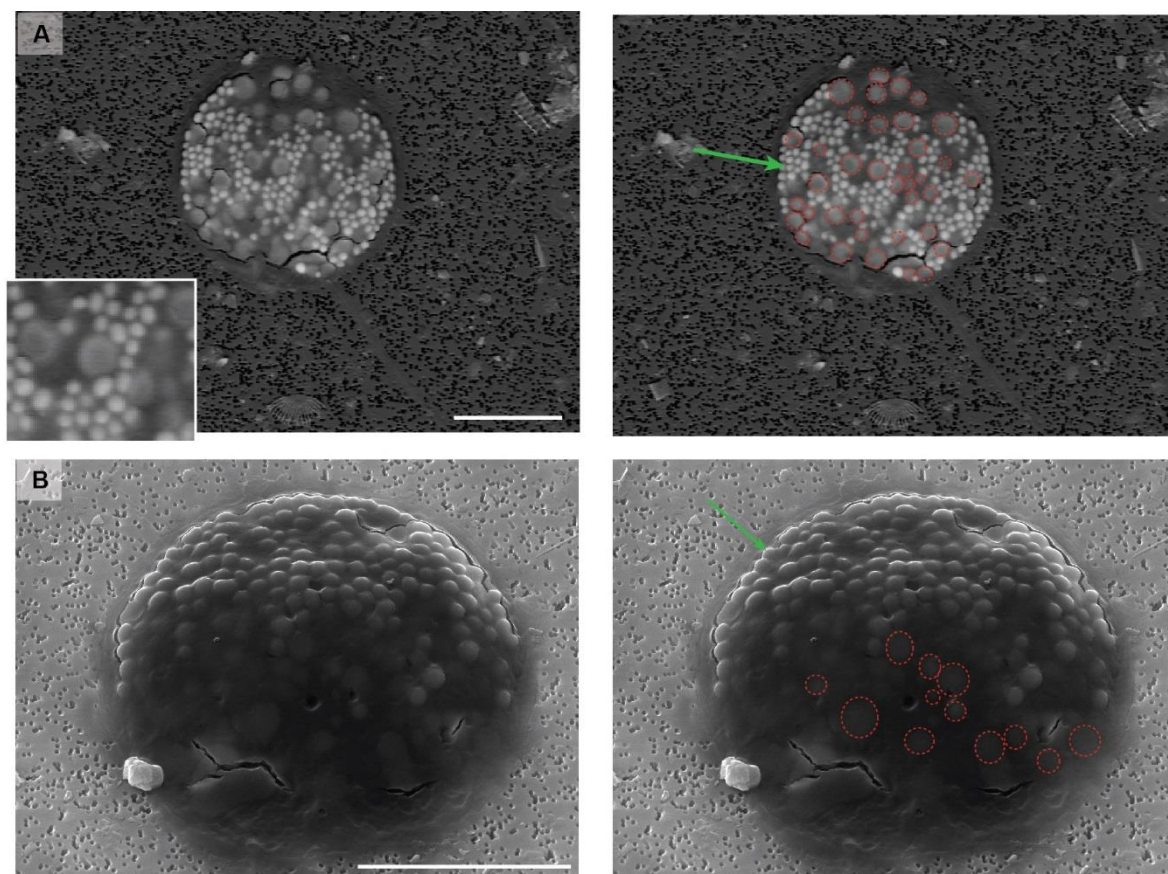
Figure S4 | Two examples of Sr-clusters with large inclusions rich in phosphorus.

Large inclusions rich in phosphorous (surrounded in dotted red lines in the right hand-side pictures) are often observed co-existing with micropearls (light grey spheres, example indicated by a green arrow) in the cell, as in the two above examples of dried Sr-clusters (or *Tetraselmis* sp.). (A) SEM backscattered electron images (BEI). The phosphorus-rich inclusions appear in a darker grey as their atomic mass is lower than the one of the Sr-micropearls. The encarted image in the left image is a zoom of the center of the cluster showing a non-spherical phosphorous-rich micropearl, growing around or between micropearls. EDXS results indicate that these phosphorus-rich inclusions generally contain important amounts of calcium, as well as smaller amounts of Mg and K. (B) Under good conditions, the polyphosphate inclusions can also be seen in SEM secondary electron images (SEI). White scale bar: 10 μm.

Mineral	Additional information	Examples of organisms producing these biominerals	References
Magnetite (Fe_3O_4)	named magnetosomes	some unicellular algae	Bazylinski & Frankel, 2003
Calcium oxalate (Whewellite,CaC_2O_4)	acicular crystals	some unicellular algae	Weiner & Dove, 2003; Baran & Monje, 2008
Barite ($BaSO_4$)	discrete intracellular crystals	some members of the Xenophyophora deep-sea foraminifera	Gooday & Nott, 1982
Barite- Celestite $(Ba,Sr)SO_4$	found in the terminal vacuoles	freshwater Desmids such as *Closterium*	Krejci *et al.*, 2011
Calcium sulfate ($CaSO_4$)		Some Desmids such as *Bambusina* and *Gonatozygon*	Brook, 1981
Sulfur (S)	called sulfur globules	wide variety of eukaryotes	Shively, 2006
Polyphosphates		wide variety of eukaryotes	Shively, 2006; Raven & Knoll, 2010
Sr and Ba "salts"	undetermined mineralogy	prostomatid ciliates *Loxodes* and *Remanella*	Finlay *et al.*, 1983 Lynn, 2010
Ca-containing inclusions	a few were shown to be carbonates; frequently also containing P	several ciliates	Raven *et al.*, 2010; Ruffalo, 1978 ; Jones, 1967 ; Fauré-Fremiet & Gauchery, 1957

Table S1

Mineral nature of non-skeletal biominerals observed as intracellular inclusions in unicellular eukaryotes. Examples of unicellular organisms producing each type of permanently intracellular biominerals are presented, with corresponding literature references.

References for Table S1

Baran EJ, Monje PV (2008) Oxalate biominerals. *Metal Ions in Life Sciences* **4**, 219–254.

Bazylinski DA, Frankel RB (2003) Biologically controlled mineralization in Prokaryotes. *Reviews in Mineralogy and Geochemistry* **54**, 217-247.

Brook AJ (1981) Calcium sulfate inclusions in the desmids *Bambusina* and *Gonatozygon*. *British Phycology Journal* **16**, 267-272.

Fauré-Fremiet E, Gauchery M (1957) Concrétion minérales intracytoplasmiques chez les ciliés. *The Journal of Protozoology* **4**, 96-109.

Finlay BJ, Hetherington NB, Davison W (1983) Active biological participation in lacustrine barium chemistry. *Geochimica et Cosmochimica Acta* **47**, 1325-1329.

Gooday AJ, Nott JA (1982) Intracellular barite crystals in two xenophyophores, *Aschemonella ramuliformis* and *Galatheammina* Sp. (Protozoa: Rhizopoda) with comments on the taxonomy of *A. ramuliformis*. *Journal of the Marine Biological Association UK* **62**, 595-605.

Jones AR (1967) Calcium and phosphorus accumulation in *Spirostomum ambiguum. The Journal of Protozoology* **14**, 220-225.

Krejci MR, Wasserman B, Finney L, McNulty I, Legnini D, Vogt S, Joester D (2011) Selectivity in biomineralization of barium and strontium. *Journal of Structural Biology* **176**, 192-202.

Lynn DH (2010). *The Ciliated Protozoa: Characterization, Classification, and Guide to the Literature.* Springer International Publishing, Amsterdam: pp. 605.

Raven JA, Knoll AH (2010) Non-skeletal biomineralization by eukaryotes: matters of moment and gravity. *Geomicrobiology Journal* **27**, 572-584.

Ruffolo JJ Jr (1978) Intracellular calculi of the ciliate protozoon *Euplotes eurystomus*: morphology, localization, and possible stages in formation. *Transactions of the American Microscopical Society* **97**, 381-386.

Shively JM (2006) Inclusions in prokaryotes. *Microbiology Monographs* **1**, 1-14.

Weiner S, Dove PM (2003) An overview of biomineralization processes and the problem of the vital effect. *Reviews in Mineralogy and Geochemistry* **54**, 1-29.

Strain Number	Original Medium	Origin	Reference
SAG 26.82 (Göttingen)	Diat	Münster Castle moat	http://sagdb.uni-goettingen.de/detailedList.php?str_number=26.82
CCAC 0079B (Köln)	Waris-H	Münster Castle moat	http://webapps.uni-koeln.de/cgi-bin/ccac/recherche
CCAC 0051 (Köln)	SFM	Frühlinger See	http://webapps.uni-koeln.de/cgi-bin/ccac/recherche

Table S2

Information about the cultured strains of *Tetraselmis cordiformis*.

Element	Diat	SFM	Waris-H
Strain	SAG 26.82	CCAC 0051	CCAC 0079B
N	$3.4 \cdot 10^{-4}$	$7.8 \cdot 10^{-4}$	$2.1 \cdot 10^{-3}$
Mg	$1.0 \cdot 10^{-4}$	$2.0 \cdot 10^{-4}$	$8.1 \cdot 10^{-5}$
P	$5.7 \cdot 10^{-5}$	$1.3 \cdot 10^{-5}$	$1.5 \cdot 10^{-4}$
S	$1.1 \cdot 10^{-4}$	$2.0 \cdot 10^{-4}$	$9.9 \cdot 10^{-5}$
Cl			$1.5 \cdot 10^{-6}$
K	$1.1 \cdot 10^{-4}$	$2.6 \cdot 10^{-5}$	$2.0 \cdot 10^{-3}$
Ca	$1.7 \cdot 10^{-4}$	$2.1 \cdot 10^{-4}$	$4.2 \cdot 10^{-4}$
EDTA	$1.4 \cdot 10^{-5}$	$1.2 \cdot 10^{-5}$	$1.3 \cdot 10^{-4}$
HEPES		$1.0 \cdot 10^{-3}$	$3.0 \cdot 10^{-3}$
pH	Adjusted at 7 with NaOH		

Table S3

Information about the culture media. Nominal composition in mol L^{-1} (partial). For further information see the following references:
Diat (Bacillariophycean): http://www.uni-goettingen.de/en/list-of-media-and-recipes/186449.html
Waris-H: http://www.ccac.uni-koeln.de/textfiles/waris-h.htm

Type	BaCaSr (Ba-micropearls)				
Example number	1	2	3	4	5
Sampling point	GE3	GE3	GE3	GE3	SHL2
Sampling date	July 10, 2012	Aug. 7, 2012	Sept. 13, 2013	Jan. 28, 2014	Aug. 12, 2014
Sampling depth	6 m	6 m	23 m	2 m	13 m
Micropearl diameter	1.6 µm	0.8 µm	1.2 µm	1.1 µm	2.4 µm
Na	-	-	-	0.6	-
Mg	1.6	0.4	14.6	11.7	0.3
Al	0.7	1.7	-	1.1	-
Si	-	-	-	2.9	-
P	-	-	-	-	-
S	-	1.6	-	-	-
Cl	1.6	0.8	-	3.5	-
K	0.7	-	-	-	0.5
Ca	87.5	50.8	14.4	2.0	71.3
As	-	-	-	-	-
Sr	5.7	7.7	6.0	-	0.7
Ba	2.2	37.0	65.0	78.2	27.2
Total	100.0	100.0	100.0	100.0	100.0
Ca norm	91.7	53.2	16.9	2.5	71.9
Sr norm	6.0	8.0	7.1	-	0.7
Ba norm	2.3	38.8	76.0	97.5	27.4

Type	CaSr (Sr-micropearls)				
Example number	6	7	8	9	10
Sampling point	GE3	GE3	GE3	GE3	GE3
Sampling date	July 10, 2012	Aug. 6, 2013	Aug. 6, 2013	Oct. 1, 2013	Dec. 3, 2013
Sampling depth	6 m	0 m	30 m	7 m	3 m
Micropearl diameter	1.2 µm	Group of 0.7 µm	0.9 µm	1 µm	1.2 µm
Na	-	-	1.6	0.53	1.2
Mg	0.9	-	1.6	1.8	0.8
Al	-	-	-	-	1.1
Si	-	-	-	-	1.8
P	3.2	-	-	-	0.8
S	1.5	-	-	-	-
Cl	0.5	0.8	0.6	0.8	0.9
K	1.2	2.3	2.3	1.3	1.8
Ca	90.0	80.5	83.7	91.5	89.4
As	-	0.4	-	-	-
Sr	2.7	16.0	10.2	4.1	2.2
Ba	-	-	-	-	-
Total	100.0	100.0	100.0	100.0	100.0
Ca norm	97.1	83.4	89.2	95.7	97.6
Sr norm	2.9	16.6	10.8	4.3	2.4
Ba norm	-	-	-	-	-

Table S4

Ten examples of single micropearl EDXS analysis, raw values (out of the 460 analyses used for ternary diagram of Fig. 1**).** Different sampling dates (summer /winter), depths and barium and strontium concentrations are represented. Concentrations are expressed in mol%. Ca-, Sr- and Ba-"norm" values correspond to normalized values used for the ternary diagram in Fig.1, excluding all the other elements. Note that the size of the smallest micropearls is close to the size of the volume analyzed by EDXS. Minor amounts of different elements could therefore either come from neighboring grains (e.g. clay minerals trapped underneath the dried cluster or polyphosphate intracellular inclusions) or be part of the micropearl's composition. Small quantities of sulfur or phosphorus might be unnoticed here because most samples were coated with gold (P and S present a partial energy peak overlap with Au). Above examples showing sulfur correspond to carbon-coated samples. For examples of EDXS raw data graphs, see Fig. S1 and S2.

Parameter	Units	Value
Temperature	°C	4.6
Conductivity	mS/cm	306.7
pH		7.97
O_2	mg/L	11.5
DOC	mg/L	1.1
Nitrate	mg/L	0.60
Soluble reactive P	mg/L	0.01
SiO_2	mg/L	1.4
Chloride	mg/L	9.7
Sulfate	mg/L	48.5
Alkalinity	meq/L	1.8
Na	mg/L	6.5
Mg	mg/L	5.8
Al	µg/L	1.9
K	mg/L	1.5
Ca	mg/L	43.4
Cr	µg/L	0.32
Mn	µg/L	0.05
Fe	µg/L	2.1
Co	µg/L	0.07
Ni	µg/L	0.95
Cu	µg/L	0.40
Zn	µg/L	0.50
As	µg/L	1.03
Sr	µg/L	467.3
Mo	µg/L	1.4
Ba	µg/L	18.1
Pb	µg/L	0.03

Table S5

Representative water chemistry of Lake Geneva at GE3 station. Average values over 0-70 m depth in February 2012.

Chapter III

Marine and freshwater micropearls : biomineralization producing strontium-rich amorphous calcium carbonate inclusions is widespread in the genus Tetraselmis (Chlorophyta) *

_____

Agathe Martignier, Montserrat Filella, Kilian Pollok, Michael Melkonian, Michael Bensimon, François Barja, Falko Langenhorst, Jean-Michel Jaquet and Daniel Ariztegui

3.1   Abstract

Unicellular algae play important roles in the biogeochemical cycles of numerous elements, particularly through the biomineralization capacity of certain species (e.g., coccolithophores greatly contributing to the "organic carbon pump" of the oceans), and unidentified actors of these cycles are still being discovered. This is the case of the unicellular alga *Tetraselmis cordiformis* (Chlorophyta) that was recently discovered to form intracellular mineral inclusions, called micropearls, which had been previously overlooked. These intracellular inclusions of hydrated amorphous (or near-amorphous) calcium carbonates (ACCs) were first described in Lake Geneva (Switzerland) and are the result of a novel biomineralization process. The genus *Tetraselmis* includes more than 30 species that have been widely studied since the description of the type species in 1878.

The present study shows that many other Tetraselmis species share this biomineralization capacity: 10 species out of the 12 tested contained micropearls, including *T. chui, T. convolutae, T. levis, T. subcordiformis, T. suecica* and *T. tetrathele*. Our results indicate that micropearls are not randomly distributed inside the Tetraselmis cells but are located preferentially under the plasma membrane and seem to form a definite pattern, which differs among species. In *Tetraselmis* cells, the biomineralization process seems to systematically start with a rod-shaped nucleus and results in an enrichment of the micropearls in Sr over Ca (the Sr=Ca ratio is more than 200 times higher in the micropearls than in the surrounding water or growth medium). This concentrating capacity varies among species and may be of interest for possible bioremediation techniques regarding radioactive ^{90}Sr water pollution.

The *Tetraselmis* species forming micropearls live in various habitats, indicating that this novel biomineralization process takes place in different environments (marine, brackish and freshwater) and is therefore a widespread phenomenon.

3.2   Introduction

The biogeochemical cycles of numerous elements are influenced by the biomineralization capacities of certain unicellular organisms. This is the case, for example, of the coccolithophores, which play an important role in the carbon cycle through their production of biogenic calcite (Bolton et al., 2016). Amorphous calcium carbonate (ACC) is also an important actor in the biogenic carbonate cycle because it is a frequent precursor of calcite,

as many organisms use ACC to build biominerals with superior properties (Albéric et al., 2018; Rodriguez-Blanco et al., 2017). For example, the precipitation of calcium carbonate in microbial mats, the Earth's earliest ecosystem, starts with an amorphous calcite gel (Dupraz et al., 2009), and the formation of ACC inside tissue could make coral skeletons less susceptible to ocean acidification (Mass et al., 2017).

In unicellular organisms, intracellular inclusions of ACC had, at first, only been described in cyanobacteria (Couradeau et al., 2012; Benzerara et al., 2014; Blondeau et al., 2018). More recently, similar inclusions have been described in unicellular eukaryotes of Lake Geneva (Switzerland). Consisting of hydrated near-amorphous calcium carbonate, frequently enriched in alkaline-earth elements (e.g., Sr or Ba) and typically displaying internal oscillatory zonation, these inclusions have been named micropearls (Jaquet et al., 2013; Martignier et al., 2017). The internal zonation is due to variations in the Ba/Ca or Sr/Ca ratios.

Until now, micropearls had been observed only in two freshwater species: the unicellular green alga *Tetraselmis cordiformis* (Chlorodendrophyceae, Chlorophyta) producing micropearls enriched in Sr and a second freshwater microorganism producing micropearls enriched in Ba, yet to be identified (Martignier et al., 2017). Since its first description in 1878 (Stein, 1878), the genus *Tetraselmis* has been much studied by biologists because several species are economically important due to their high nutritional value and ease of culture (Hemaiswarya et al., 2011). *Tetraselmis* species are used extensively as aquaculture feed (Azma et al., 2011; Lu et al., 2017; Park and Hur, 2000; Zittelli et al., 2006) and some have been suggested as potential producers of biofuels (Asinari di San Marzano et al., 1981; Grierson et al., 2012; Lim et al., 2012; Montero et al., 2011; Wei et al., 2015). They have also served as models in algal research (Douglas, 1983; Gooday, 1970; Kirst, 1977; Marin et al., 1993; Melkonian, 1979; Norris et al., 1980; Regan, 1988; Salisbury et al., 1984).

The motile cells of *Tetraselmis* have four scale-covered flagella, which emerge from an anterior (or apical) depression of the cell (Manton and Parke, 1965). The *Tetraselmis* genus has a cell wall formation process that is unique among green algae as the cells synthetize small non-mineralized scales in the Golgi apparatus, which undergo exocytosis through Golgi-derived secretory vesicles to form a solid wall (theca) composed of fused scales (Becker et al., 1994; Domozych, 1984; Manton and Parke, 1965). Regarding their habitat, most *Tetraselmis* species are free-living (planktonic or benthic) (Norris et al., 1980), although some species live in specialized habitats, for example as endosymbiont in flatworms (Parke and Manton, 1967; Trench, 1979; Venn et al., 2008). *Tetraselmis cordiformis* is presumably the only freshwater species among the 33 species currently accepted taxonomically in the genus *Tetraselmis*

(Guiry and Guiry, 2018). However, mineral inclusions had never been described in these microorganisms until the recent observation of micropearls in *Tetraselmis cordiformis* (Martignier et al., 2017). The fact that this newly discovered physiological trait had gone unnoticed is puzzling, especially as *Tetraselmis cordiformis* is the type species of the genus. This can probably be explained by the translucence of the micropearls under the optical microscope and their great sensitivity to pH variations, leading to their alteration or dissolution during most sample preparation techniques (Martignier et al., 2017).

Interestingly, several *Tetraselmis* species (e.g., T. subcordiformis) have been mentioned as potential candidates for radioactive Sr bioremediation due to their high Sr absorption capacities (Fukuda et al., 2014; Li et al., 2006), but the precise process by which these microorganisms concentrate this element has never been determined.

The present study investigates 12 species of the genus *Tetraselmis*, including the freshwater *Tetraselmis cordiformis*, with the objective of understanding whether the biomineralization process leading to the formation of micropearls is common to the whole genus or is restricted to *T. cordiformis*. Species living in contrasting environments have been selected to also evaluate if the formation of micropearls is linked to their habitat. Each species is represented by one or several strains, obtained from public algal culture collections. All analyses were carried out on cells sampled from these cultures on the day of their arrival in our laboratory. The micropearls were imaged by scanning electron microscopy (SEM), and their composition was measured by energy-dispersive X-ray spectroscopy (EDXS). The inner structure and chemical composition of micropearls in three different species were studied by transmission electron microscopy (TEM) on focused ion beam (FIB) cross sections.

3.3 Samples and methods

3.3.1 Origin of the samples and pre-treatment methods

Culture samples of 12 different *Tetraselmis* species were obtained from three different algal culture collections and were grown in different media (Table 1). The recipe of each growth medium is available on the website of the respective culture collections (Table S1 in the Supplement). A single strain of each species was studied, except for *T. chui* (two strains) and *T. cordiformis* (three strains). Table 1 lists the strain names. Most cells in these cultures were mature at the time of observation for this study.

Samples for microscopic observation of each strain were prepared directly after the organisms' arrival in our laboratory: small portions of the culture (without any change of the original medium) were filtered under moderate vacuum (-20 to -30 kPa) on polycarbonate filter membranes with 0.2, 1 or 2 µm pore sizes. Volumes filtered (variable depending on culture concentration) were recorded. Species issued from SAG (Sammlung von Algenkulturen – University of Göttingen, Germany) were grown on agar and, therefore, cultures had to be resuspended just before filtration. Filter membranes were dried in the dark at room temperature after filtration. A total of 458 micropearls were analyzed by EDXS.

3.3.2   Water chemistry measurements

Elemental composition of each culture medium was measured at the IsoTraceLab (EPFL, Lausanne, Switzerland), except for the ES medium for which we could not obtain a sample. Blank samples of Milli-Q water were bottled at the same time as growing medium samples and measured in the same way (Table S2). Barium and Sr were measured by inductively coupled plasma sector field mass spectrometry (ICP-SFMS) using a Finnigan™ Element2 high-performance high resolution ICPMS model. The mass resolution was set to 500 to increase analytical sensitivity. Calibration standards were prepared through successive dilutions in cleaned Teflon bottles of 0.1 g L^{-1} ICPMS stock solutions (TechLab, France). Suprapur™-grade nitric acid (65% Merck) was used for the acidification in the preparation of standards. Ultrapure water was produced using Milli-Q™ ultrapure water system (Millipore, Bedford, USA). Rhodium was used as the internal standard for samples and standards to correct signal drift.

At this resolution mode, the sensitivity was better than 1.2 x 10^6 cps ppb^{-1} of ^{115}In. The measurement repeatability expressed in terms of relative standard deviation (RSD) was better than 5 %. The accuracy of the method was tested using a homemade standard solution containing 5.0 ng L^{-1}, used as a reference. The detection limits obtained for Sr and Ba was around 100 ng L^{-1} under these experimental conditions. Note that for the ES medium (not analyzed), the concentrations were set as equivalent to standard seawater, *i.e.*, Sr = 9 x 10^{-5} M and Ca = 10^{-2} M, giving a ratio of Sr/Ca = 9 x 10^{-3}.

	Origin of the sample	Approx. micropearl size	Culture medium	Provider strain no.	Abbreviation
Chlamydomonas					
C. reinhardtii	Freshwater France	no micropearls observed	L-C	TCC 778	–
C. intermedia	Freshwater France, Lake Geneva	no micropearls observed	L-C	TCC 113	–
Tetraselmis					
T. ascus	Marine Spain, Canary Islands, Gran Canaria	no micropearls observed	ASP-12	CCAC 3902	
T. chui	Marine Germany, Heligoland	0.7 μm length	ASP-H	CCAC 0014	chui_cc
	Marine Scotland, Millport, Clyde estuary	0.7 μm length	1/2 SWEg Ag	SAG 8–6	chui_sa
T. contracta	Marine France, Brittany, Île de Batz	1.2 μm length	ASP-H	CCAC 1405	contract_cc
T. convolutae	Marine (symbiotic in flatworm) France, Brittany, Île de Batz	0.8 μm length	ASP-H	CCAC 0100	convol_cc
T. cordiformis	Freshwater Germany, Cologne, Lake Fühlinger	1 μm diameter	SFM	CCAC 0051	cord-F_cc
	Freshwater Germany, Münster, castle ditch	1 μm diameter	Waris – H	CCAC 0579B	cord-M_cc
	Freshwater strain 0579B obtained from CCAC	1 μm diameter	Diat	SAG 26.82	cord-M_sa
T. desikacharyi	Marine France, Île de Batz, Rochigou	0.9 μm length	ASP-H	CCAC 0029	desika_cc
T. levis	Marine France, Saint-Gilles-Croix-de-Vie	0.6 μm length	ES	AC 257	levis_ac
T. marina	Marine strain CA5, from L. Provasoli	no micropearls observed	Porph Ag	SAG 202.8	
T. striata	Marine UK, North Wales, Conwy	0.6 μm length	SWES Ag	SAG 41.85	striata_sa
T. subcordiformis	Marine USA, Connecticut, New Haven	0.4 μm length	Porph Ag	SAG 161-1a	subcord_sa
T. suecica	Marine UK, Plymouth	0.7 μm length	ES	AC 254	suecica_ac
T. tetrathele	Marine –	0.9 μm length	ES	AC 261	tetrath_ac

Table 1 | Specific information for each species and their culture conditions.

Providers include the following. CCAC: Culture Collection of Algae at the University of Cologne (Germany) – http://www.ccac.uni-koeln.de/, last access: 6 July 2018; SAG: Sammlung von Algenkulturen at the University of Göttingen (Germany) – https://www.uni-goettingen.de/de/184982.html, last access: 6 July 2018; AC: Algobank – culture collection of microalgae of the University of Caen (France) – https://www.unicaen.fr/algobank/accueil/, last access: 6 July 2018; TCC: Thonon Culture Collection of the CARRTEL of Thonon-les-Bains (France) – https://www6.inra.fr/carrtel-collection, last access: 6 July 2018. All culture media compositions are given on the corresponding websites (detailed addresses in Table S1).

3.3.3   Scanning electron microscopy (SEM) and EDXS analysis

Small portions of the dried filters were mounted on aluminum stubs with double-sided conductive carbon tape and then coated with gold (ca. 10 nm) using low vacuum sputter coating. A JEOL JSM-7001F scanning electron microscope (Department of Earth Sciences, University of Geneva, Switzerland), equipped with an EDXS detector (model EX- 94300S4L1Q;

JEOL), was used to perform EDXS analyses and to obtain images of the dried samples. Semiquantitative results were obtained using the ZAF correction method. Samples were imaged with backscattered electrons. This method allows us to clearly locate the micropearls inside the organisms thanks to the high difference of mean atomic numbers between the micropearls and the surrounding organic matter. EDXS measurements were acquired with settings of 15 kV accelerating voltage, a beam current of ~7 nA and acquisition times of 30 s. Semiquantitative EDXS analyses of elemental concentrations were made without taking carbon, nitrogen and oxygen into account. EDXS results are all presented as mol %.

3.3.4 Counts and statistics lead on the Tetraselmis culture cells

Counts were performed on the images obtained by SEM. The counts showed that the agar medium seems to hinder the growth of micropearls. These strains were therefore not taken into account for the statistics. Two strains of *Tetraselmis cordiformis* and two strains of *Tetraselmis chui* were analyzed. The samples of the two *Tetraselmis cordiformis* strains taken on their first day of arrival were damaged during sample preparation due to a too high filtration pressure, destroying the arrangement of the micropearls in the cells. A sample obtained from one of these strains 60 days after arrival was therefore taken into account for the statistics, in replacement.

The preservation of the pattern of micropearl arrangement in the cell is difficult during sample preparation, as it is easily disturbed. The following parameters directly influence the preservation of that feature: the fragility of the cells (*T. contracta* cells, for example, seem very solid while *T. chui* cells seem more fragile) and sample preparation methods (*e.g.*, pressure during filtration; see difference between *e* and *f* in Fig. S1 in the Supplement).

3.3.5 Focused ion beam (FIB) preparation

Electron-transparent lamellae for TEM were prepared with a FIB–SEM workstation (FEI Quanta 3D FEG at the Institute of Geosciences, Friedrich Schiller University Jena, Germany). The cells were previously selected based on SEM imaging. To protect the sample, a platinum strap of 15 to 30 μm in length, ~3 μm wide and ~3 μm high was deposited on the cell during lamella preparation, via ion-beam-induced deposition using the gas injection system (GIS). Stepped trenches were prepared on both sides of the Pt straps by GaC ion beam sputtering. This operation was performed at 30 keV energy and a 3 to 5 nA beam current.

The resulting lamellae were then thinned to approximately 1 μm thickness by using sequentially lower beam currents at 30 keV energy (starting at 1 nA and ending at 0.5 or 0.3 nA). The position of the lamellae was chosen to include a maximum of micropearl cross sections. An internal micromanipulator with a tungsten needle was used to lift out the prethinned lamellae and to transfer them to a copper grid.

Final thinning of the sample to electron transparency (~100 to 200 nm) was carried out on both sides of the lamellae by using sequentially lower beam currents (300 to 50 pA at 30 keV energy). The lamellae underwent only grazing incidence of the ion beam at this stage of the preparation. This allows minimization of ion beam damage and surface implantation of Ga. The thinning progress was observed with SEM imaging of the lamellae at 52°. Electron beam damage was further suppressed by using low electron currents and limiting electron imaging to a strict minimum.

3.3.6   Transmission electron microscopy (TEM) and EDXS analysis

TEM investigations were conducted with a FEI Tecnai G^2 FEG transmission electron microscope operating at 200 kV. In order to document the structural state of micropearls in their pristine undamaged form, selected-area electron diffraction (SAED) patterns were taken directly at the beginning of the TEM session with a broad beam. Scanning TEM (STEM) images were then acquired using a high-angle annular dark field (HAADF) STEM detector (Fischione) with a camera length of 80 mm. EDXS measurements were performed with an EDXS system, model XMaxN 80T SDD from Oxford. EDXS spectra and maps were recorded in STEM mode. The semiquantitative calculation of the concentrations (including C) was obtained using the Cliff–Lorimer method using pre-calibrated k factors and an absorption correction integrated into the Oxford software. The absorption correction is based on the principle of electroneutrality, taking into account the valence states and concentrations of cations and oxygen anions. Oxygen is thereby assumed to possess a stoichiometric concentration.

3.4 Results and interpretation

TEM analyses confirmed that the mineral inclusions observed in the Tetraselmis species during this study comply with the definition of micropearls given in Martignier et al. (2017) (intracellular inclusions of near-amorphous hydrated calcium carbonate, frequently enriched in alkaline-earth elements (*e.g.*, Sr or Ba) and typically displaying internal concentric zonation linked to elemental ratio variations). These mineral inclusions will therefore be named micropearls hereafter.

3.4.1 SEM observation of micropearls in Tetraselmis species

SEM observations of 12 different species of *Tetraselmis* (culture strains), on the day of their arrival from the supplier, show that 10 of them contained micropearls (Fig. 1, Table 1). None were observed in *T. ascus* and *T. marina*. The general shape of the micropearls in the marine species is elongated, resembling rice grains (Fig. 1 except 1d), while it is spherical in *T. cordiformis* (the only freshwater species of this study) (Fig. 1d). The micropearls' size (0.4–1.2 µm in length) and shape differ among species. Detailed values for each species are given in Table 1.

Micropearls do not seem to be randomly distributed inside the cells, but rather show a definite location in most species (Figs. 1 and S2). Moreover, for a given species, most cells present a similar micropearl arrangement (Fig. S1). Exceptions are cells that were damaged during sample preparation. Filtration or freshwater rinsing, for example, can disrupt the micropearl distribution pattern (Figs. S1e and f and S3).

In some species, the micropearls are mostly aggregated at one side of the cell, with "pointed" tips appearing at the centre of the cell and on both sides, resulting in a "trident" shape. This is the case for *T. chui, T. suecica* and *T. tetrathele* (Fig. 1a, i, j). *T. striata* shows a similar central micropearl distribution, but the lateral points of the trident are absent (Fig. 1g). In *T. suecica* the central micropearl alignment is generally longer and not necessarily connected to the apical aggregate (Fig. 1i). *T. levis* (Fig. 1f) also shows a similar arrangement, but the aggregate is missing, leaving the micropearls to form three longitudinal alignments (meridians). Altogether, *T. chui, T. levis, T. suecica* and *T. tetrathele* present patterns with an approximately similar trimerous radial organization (although a tetramerous symmetry cannot be totally excluded as dried samples do not allow a definite judgement). Observations seem to indicate
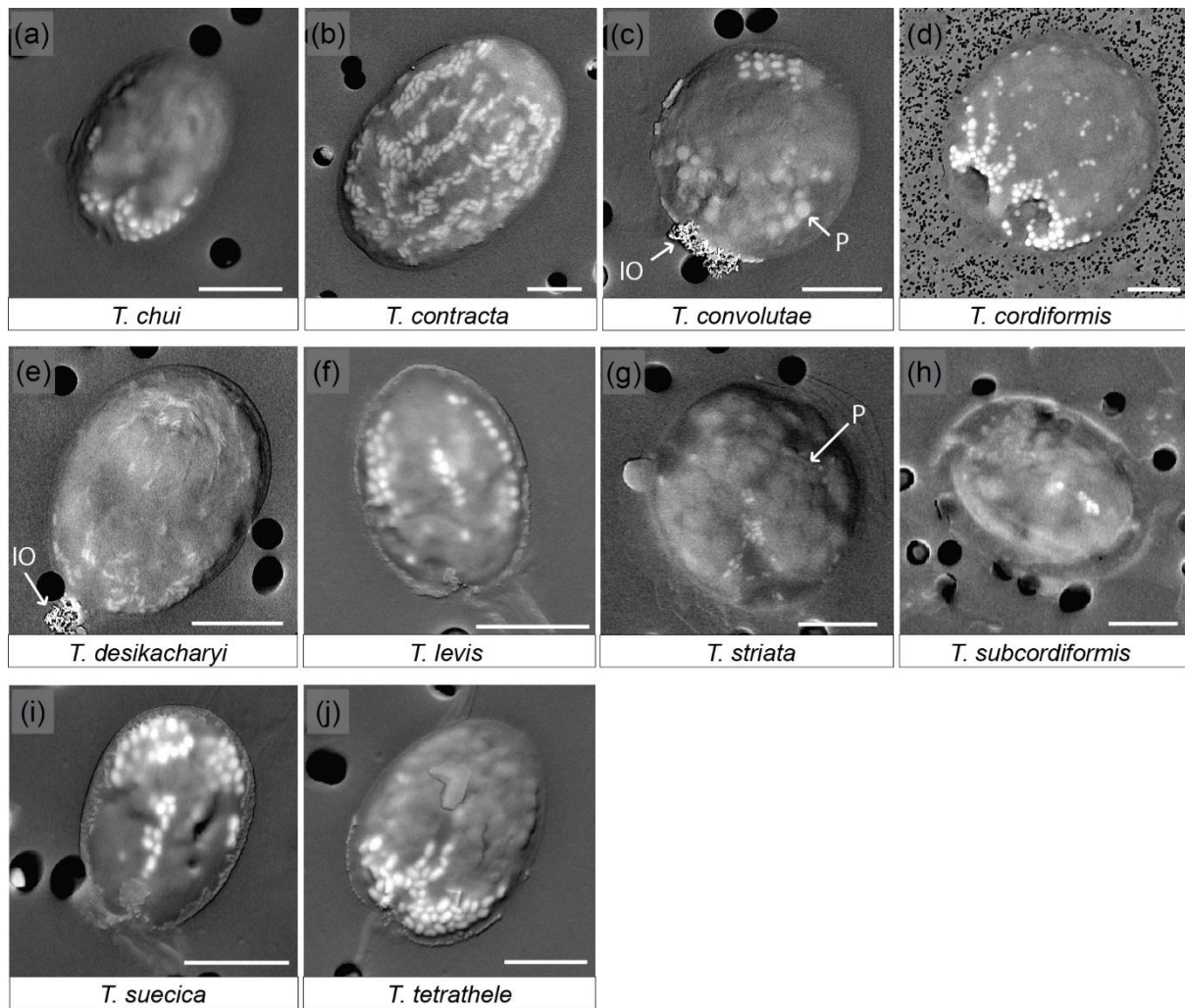
Figure 1 | SEM images of 10 *Tetraselmis* species containing micropearls at the time of observation.

Backscattered electron images of dried samples. The micropearls appear in white or light grey against the darker organic matter, as elongated shapes, except for *T. cordiformis* (d), for which they are spherical. P: the larger and slightly darker inclusions are polyphosphates (c, g). IO: iron oxides. Pores of the filters are visible as black circles in the background (2 μm in diameter except for d: 0.2 μm). Strains are as follows. (a): chui_cc; (d): cord-M_cc; (j):tetrathele_ac. Scale bars are 5 μm.

that, in most species, the micropearl aggregate is located at the apical side of the cell (near the apical depression from which the four flagella emerge) (Fig. S2). In *T. convolutae* (Fig. 1c), the micropearls form a small aggregate at the basal extremity of the cell, while larger polyphosphate inclusions gather at the opposite (apical) side.

A different and interesting organization of the micropearls is displayed by both *T. desikacharyi* (Fig. 1e) and *T. contracta* (Fig. 1b). An apical aggregate of micropearls is generally present, while other micropearls form regularly spaced meridians, which, in *T. contracta*, extend from the apical pole towards the basal part of the cell (Figs. 1b and S2). These meridians are not well expressed in all cells but, when they are clearly visible, there seems to be around eight or

10 of them inside the cell. When well preserved, the micropearl organization in *T. cordiformis* also shows multiple micropearl alignments that depart from a well-developed apical aggregate, although the alignments are generally well arranged only close to the aggregate and the size of micropearls decreases quickly towards the basal end of the cell (Fig. 1d). Finally, samples observed in this study do not allow us to state if there is a definite distribution of the micropearls in *T. subcordiformis* (Figs. 1h and S2).

Polyphosphate inclusions are frequently observed in *Tetraselmis* species. Their distribution seems to be random except in *T. convolutae* (Fig. 1c). Aggregates of small iron oxide minerals were frequently observed in dried samples at one extremity of *T. desikacharyi* and *T. convolutae* (Fig. 1c and e) – probably at the apical extremity. EDXS analyses performed in both polyphosphate inclusions and iron oxide aggregates are shown in Fig. S4.

In order to compare our results with members of another genus, we also analyzed other flagellate species (e.g., *Chlamydomonas reinhardtii* and *Chlamydomonas intermedia*) obtained from algal culture collections (Table 1). No calcium carbonate inclusions were observed in these cells. Thorough observation of samples from Lake Geneva confirms that not all flagellates produce micropearls. This biomineralization process seems to be exclusive to a limited number of species.

Table 2 shows the result of counts carried out on the species producing micropearls. On average, 77% of the cells contained micropearls and amongst these, 51% showed the pattern that is characteristic of their species. This last value is high, considering that all cells do not fall onto the filter with the same orientation and that the only patterns we consider are those obtained when the cell is deposited on its lateral side. Patterns resulting from a deposition of the cells on their apical or basal sides are not considered because the 3-D repartition of the micropearls in the cells is still uncertain.

3.4.2   TEM observation of FIB-cut cross sections of micropearls

FIB-cut cross sections of micropearls produced by *T. chui* and *T. suecica* are shown in Fig. 2, where they are compared to a similar section in a cell of the freshwater species *T. cordiformis* sampled in a natural environment (Lake Geneva). The choice of *T. chui* and *T. suecica* for FIB processing and TEM observation was based on the size of the micropearls and on their strong concentration in Sr. Both features were considered to favor the observation of compositional zonation, as observed in our previous study (Martignier et al., 2017).

Tetraselmis	Strain	Medium	Total cells counted	% cells with mp/ cells	% pattern/ cells with mp	Remarks
T. chui	CCAC 0014	ASP-H	160	93	40	
T. chui	SAG 8-6	1/2 SWEg Ag	121	40	37	Resuspended from agar
T. contracta	CCAC 1405	ASP-H	103	98	79	
T. convolutae	CCAC 0100	ASP-H	100	40	70	
T. cordiformis	CCAC 0051	SFM	115	60	0	Strongly filtered
T. cordiformis*	CCAC 0579B	Waris-H	123	98	46	Gently filtered
T. desikacharyi	CCAC 0029	ASP-H	122	25	13	
T. levis	AC 257	ES	123	94	51	
T. striata	SAG 41.85	SWES (agar)	136	12	25	Resuspended from agar
T. subcordiformis	SAG 161-1a	Porph (agar)	100	1	0	Resuspended from agar
T. suecica	AC 254	ES	105	99	57	
T. tetrathele	AC 261	ES	101	89	56	

Table 2 | Percentage of cells presenting micropearls and specific patterns of micropearl arrangement.

Percentage of cells presenting micropearls for each strain and percentage of these cells showing the typical micropearl arrangement pattern for that species (see Figs. 1 and S1). Two strains have been analyzed for T. chui and T. cordiformis. Please note that strains grown on agar generally show a much lower presence of micropearls and were not considered for the statistics. The asterisk marks a single sample taken 60 days after the strain's arrival in our laboratory, while all the others were observed on the first day after arrival from the provider. This exception allowed us to estimate the number of cells showing the micropearl arrangement pattern of this species, as both samples of T. cordiformis strains taken on the first day were damaged during sample preparation by too strong of a filtration. On the first day after arrival, strain CCAC 0579B gave results similar to those of strain CCAC 0051. mp: micropearls. For details on providers and media, see Table 1.

A FIB cut was also performed in a *Tetraselmis contracta* cell. This result is shown separately in Fig. 3 because the very good conservation of the organic matter in this sample allows the simultaneous observation of other intracellular constituents.

Micropearls in all four species show strong similarities. They are located inside the organic envelope, are amorphous (Figs. 2 and 3) or near-amorphous and, except for the sample with pure Ca (*T. contracta* in Fig. 3), they show a distinct internal concentric zonation (Fig. 2). In all observed species, the cut sections of micropearls suggest the presence of a rod-shaped nucleus in their center (Figs. 2 and S5).

As already pointed out, the micropearls are extremely sensitive to the action of the electron beam (Martignier et al., 2017), indicating a vaporization of some of its components: organic matter associated with water, water contained in the near-amorphous calcium carbonate (Rodriguez-Blanco et al., 2008) or both. This ACC seems to be rather stable, as beam sensitivity persists after more than 5 months of storage of dry samples at room temperature.

TEM–EDXS analyses show that the zonation observed in the marine micropearls of *T. chui* and *T. suecica* (Figs. 2 and S6) is due to changes in the Sr/Ca concentration ratios, similar to the zonation observed in the freshwater micropearls in *Tetraselmis* cf. *cordiformis* (Martignier et

al., 2017). All micropearls within one cell do not necessarily have an identical composition. An example is shown in Fig. 2a, in which one micropearl possesses a composition with a higher atomic mass than the rest (lighter grey level in STEM–HAADF image) due to a higher content of Sr. Furthermore, micropearls within one cell display variable zoning patterns, as thickness and intensity of the zones differ (Fig. 2a and c).

3.4.3   TEM-EDXS mapping: location of the micropearls inside a Tetraselmis contracta cell

The coexistence of micropearls with other cellular constituents and their respective positions in the cell are shown by a TEM image of a FIB-cut section through a *T. contracta* cell (Fig. 3). The micropearls of this species are large and numerous and nearly exclusively consist of calcium carbonate without detectable Sr (Fig. S6). They appear as round to ovoid light grey shapes with smooth surfaces (Fig. 3a). TEM observations also reveal that most micropearls are not randomly scattered throughout the cell but are located preferentially just under the cell wall.

Although Fig. 3a is difficult to interpret because of the atypical preparation of the sample (simply dried instead of more traditional preparations for TEM observation such as chemical fixation or cryosections), the identification of the visible cellular constituents can still be attempted (Figs. 3b and S7). Side views (lower part of the section) and tangential sections of starch grains (upper part of the section) are visible, as well as a glancing view of the chloroplast, which is reticulated in this species. Although micropearls resemble starch grains at first look, it is quite easy to differentiate them. First, they are generally more rounded than starch grains, and secondly they are not located inside the chloroplast; in particular, they are not associated with the prominent pyrenoid.

TEM–EDXS mapping provides compositional information improving the identification of the cellular constituents and organelles visible in the section (Figs. 3c and S8). Micropearls are very visible, based on the high concentration of Ca, with small quantities of K (and sometimes Mg, not shown here). The theca, composed of fused scales, appears as a thin layer between the cell and the filter. Its composition including C, Ca, S and small amounts of K makes it apparent in Fig. 3c (in violet). The theca of these organisms is indeed known to contain 4% of Ca and 6% of S (as sulfate) by weight (Becker et al., 1994, 1998). The two irregular features that are highly enriched in P (in green in Fig. 3c) are identified as being polyphosphate (PolyP)

inclusions, flattened during sample preparation. Finally, the dark grey features, in the center of the section, are probably mitochondrial profiles (mc).
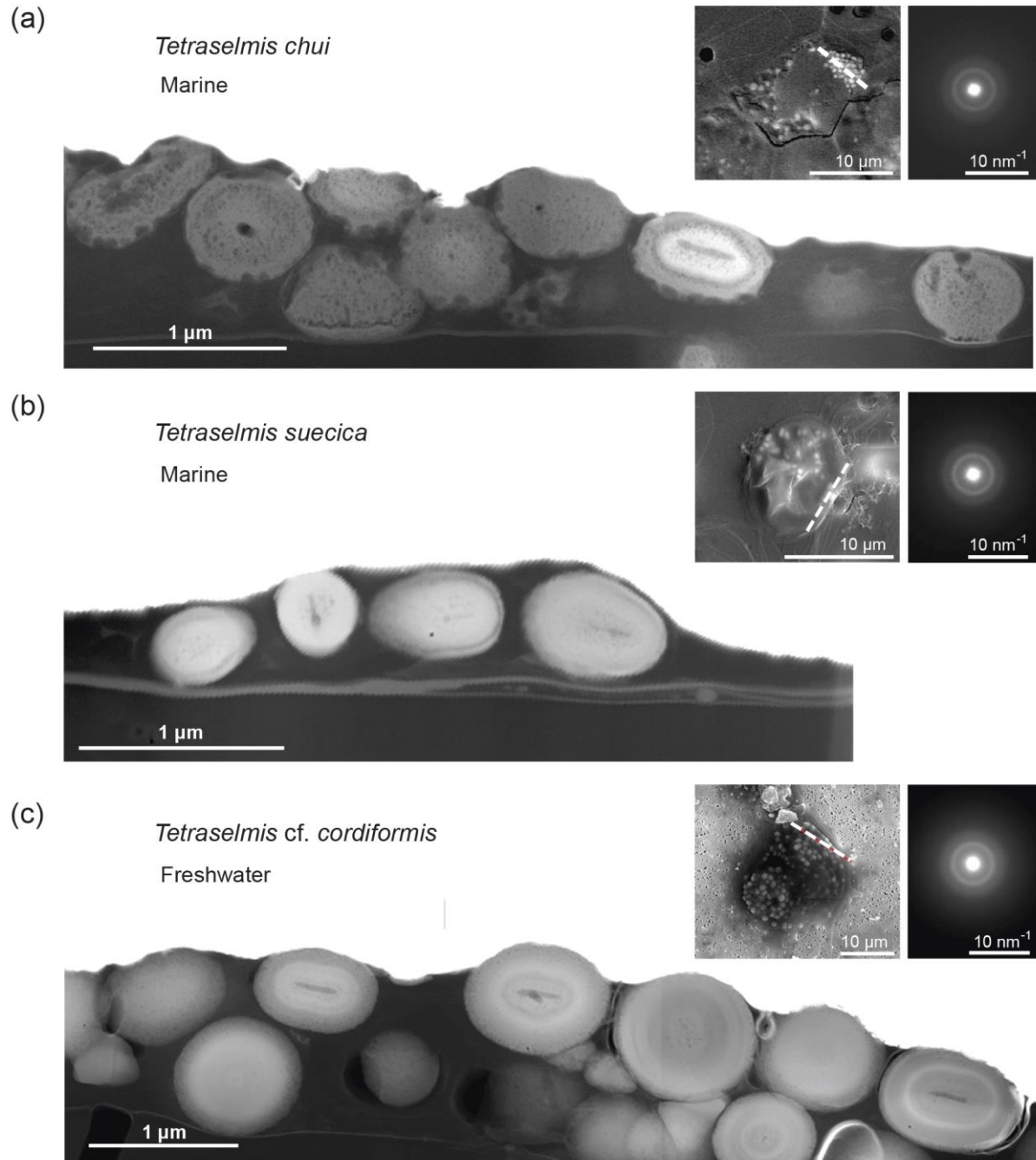
Figure 2 | Comparison of FIB-cut sections of cells of three different Tetraselmis species.

TEM–HAADF images of dried samples: FIB-cut sections through cells of (a) Tetraselmis chui (culture sample), (b) Tetraselmis suecica (culture sample) and (c) Tetraselmis cf. cordiformis (Lake Geneva) (Martignier et al., 2017). Small bubbles inside the micropearls (particularly visible in the marine species) are due to beam damage. The contact between the cell and the filter surface is visible near the bottom in each image. Left top insets: SEM secondary images of the whole cell before FIB preparation indicating the location of the cut with a dashed line. Right top insets: SAED patterns from a single micropearl of each FIB-cut section (broad diffraction rings are indicative of amorphous material).
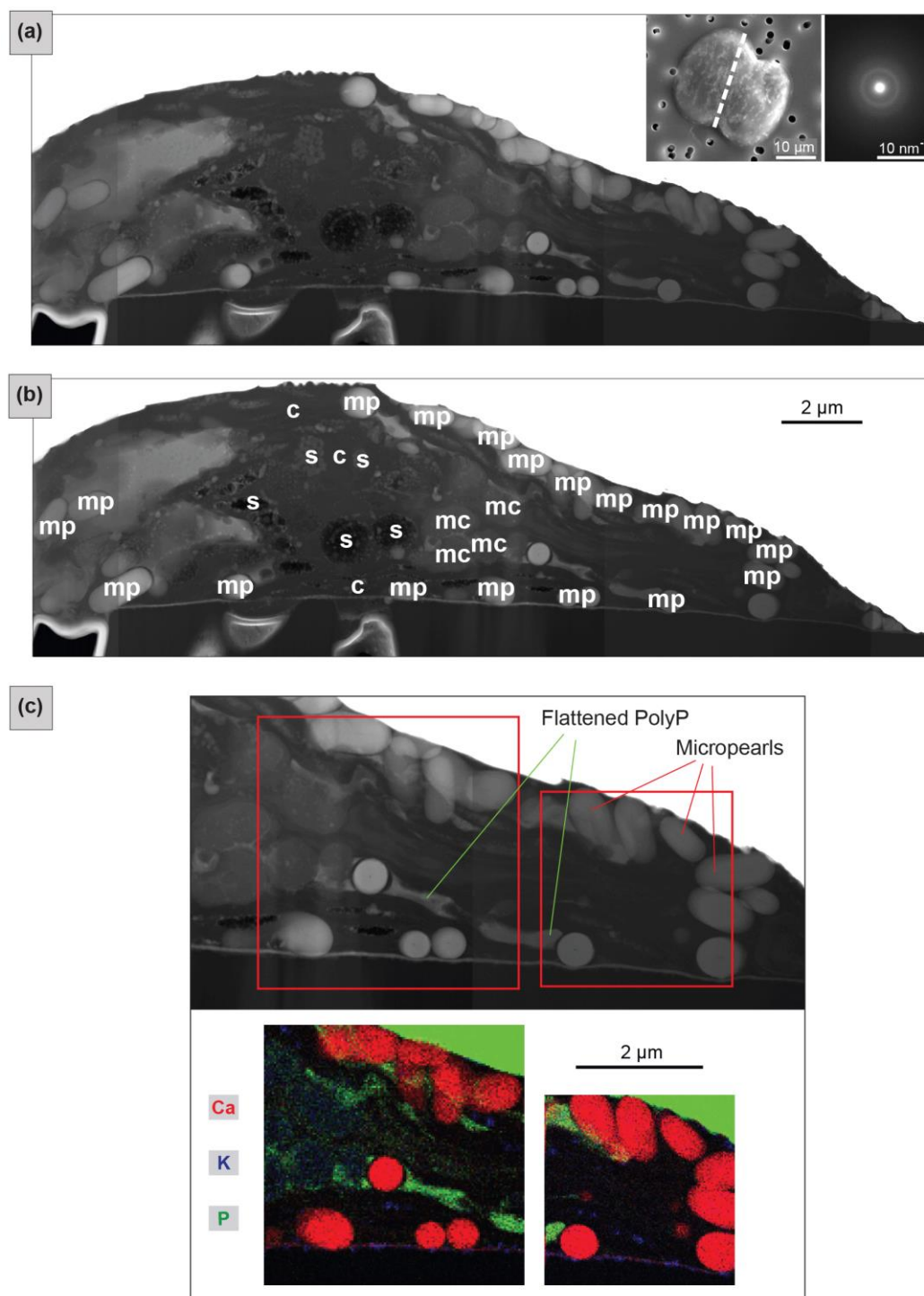
Figure 3 | FIB-cut section through a *Tetraselmis contracta* cell (dried sample).

(a) TEM–HAADF image of the whole FIB-cut section. The micropearls show light or medium grey shades and regular round or oval shapes. Left top inset: SEM secondary image of the whole cell before it was cut, with a dashed line indicating the location of the section. Right top inset: SAED patterns from a single micropearl of this FIB-cut section (diffuse diffraction rings are indicative for amorphous material). (b) Tentative identification of the visible cellular constituents; s: starch grains; c: chloroplast; mp: micropearls; mc: mitochondria. See Fig. S7 for a detailed image. (c) TEM–EDXS mappings – the top image shows the location of the two zones on a TEM–HAADF image of the section. The map shows an RGB image with three superimposed element mappings. Micropearls are mainly composed of Ca, with small quantities of K (and Mg, not shown here). Note that, due to the overlap between the P K peak and secondary Pt L peak, the Pt layer, which was deposited on top of the sample during FIB preparation, is also visible in green.

3.4.4   SEM-EDXS analysis of micropearl composition

The micropearls of most marine species (Fig. 4a) are composed of carbonates, with Ca and Sr as cations. This composition is similar to that measured for micropearls of *T. cordiformis* in Lake Geneva (Martignier et al., 2017). We noted two differences from our previous observations: *T. desikacharyi* forms micropearls containing small amounts of Ba and micropearls of *T. contracta* contain low concentrations of K. However, since growth media had different compositions, these differences need to be taken with care.

Figure 4a compiles the composition of the micropearls for each *Tetraselmis* strain (SEM–EDXS analyses), ranked in increasing order of Sr/Ca median values. Even if low concentrations of K are present in micropearls of *T. contracta*, it was not considered because this element is also present in the surrounding organic matter (Fig. S8), making it impossible to estimate the portion of the measured K that belongs to the micropearls. Magnesium was discarded for the same reason. It should be noted that the size of micropearls is close to or even below the resolution limit of the SEM–EDXS analysis technique. This means that the interaction volume of the electron beam with the sample is often larger than the micropearls themselves. Therefore the technique yields compositions that include the micropearl and the surrounding organic matter or nearby cellular constituents (e.g., polyphosphates).

3.4.5   ICP-SFMS analysis of Sr/Ca ratio in growth media: data and interpretation

The concentrations of Sr and Ba in the culture media are given in Table S2 and represented graphically in Fig. S9. Strontium concentrations range from 3.3×10^{-8} M (freshwater medium SFM) to 7.1×10^{-5} M (seawater SWES medium). All media have lower Sr concentrations than the average seawater (9.1×10^{-5} M). SFM, used to grow *T. cordiformis* – the only freshwater strain under study – has lower Sr concentrations than those measured in Lake Geneva (5.2×10^{-6} M).

The molar ratio Sr/Ca has been calculated for seven growth media (Table S2) and 458 micropearls (Table S3) in order to evaluate a possible influence of the medium on the micropearls' composition. Differences among the species regarding the micropearls' enrichment in Sr compared to their growth medium can be observed. A Sr distribution coeff-
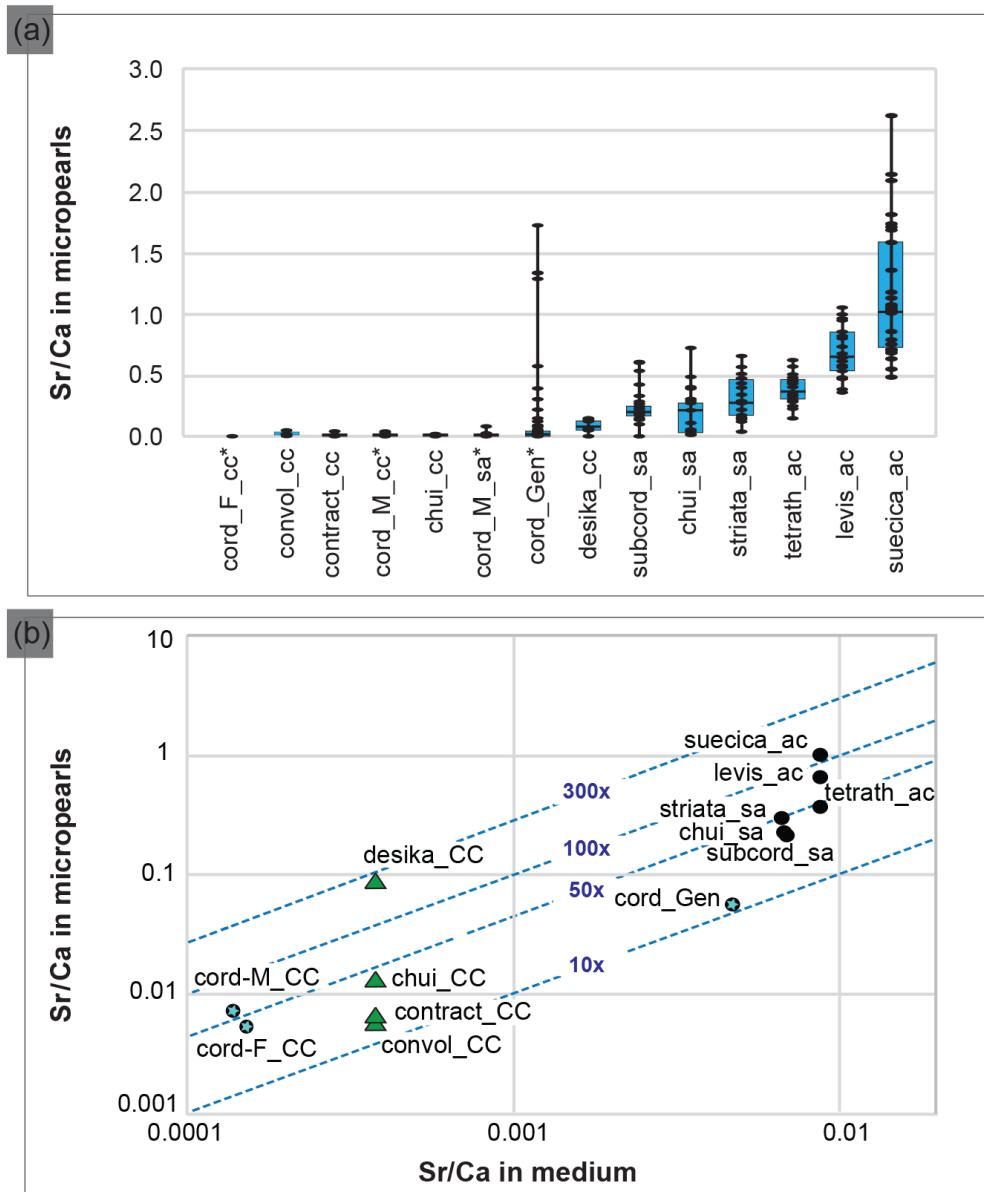
Figure 4 | Composition of the Tetraselmis micropearls and their relation with the growth media composition.

(a) Distribution of the Sr=Ca ratio for each Tetraselmis strain (EDXS analyses), ranked according to the median value of Sr=Ca. At least 20 SEM–EDXS analyses were performed on micropearls of each strain. Asterisks highlight freshwater strains. The range between the minimum and maximum data is shown by black lines. The blue boxes represent the 25–75% inter-quartiles, while the black horizontal line in the boxes shows the median value. (b) Relationship between the composition of the growth media and the composition of the Tetraselmis micropearls, expressed as the Sr=Ca ratio. Each point represents the median Sr=Ca ratio measured in each species' micropearls, related to the Sr=Ca ratio of the growth medium. Points with blue stars highlight freshwater strains. The blue dotted lines define the values of the Sr enrichment factor of the micropearls with respect to the medium (10_, 50_, etc.). Calcium concentrations of the growth media were calculated based on media theoretical composition. Green triangles signal four samples grown in the same medium. The abbreviations and characteristics of each strain are indicated in Table 1 while Sr=Ca values appear in Table S2 (for medium) and S3 (for micropearls). Results from T. cordiformis from Lake Geneva (cord_Gen) (Martignier et al., 2017) are given as a comparison.

-icient (or enrichment factor) was calculated as the molar ratio [(Sr micropearls / Ca micropearls) / (Sr medium / Ca medium)]. Figure 4b shows the relationship between the Sr/Ca ratio measured in the growth media and in the Tetraselmis micropearls. For most of thestrains, the Sr enrichment factor of the micropearls with respect to the medium varies between 10 and 100 times (see Table S3 for exact figures), with the notable exception of *T. desikacharyi* (more than 200 times). It is interesting to observe that both strains of *T. chui* – from different geographic origins (Table 1) – have rather similar Sr distribution coefficients (around 30), while the three strains of *T. cordiformis* show slightly different enrichment factors (25 for Lake Geneva water, 33 for Lake Fühlingen and 51 for Münster castle moat). Broadly speaking, Sr/Ca increases in micropearls together with its increase in the medium. However, the spread in enrichment may be large for a given medium (such as ASP-H for strains of *T. contracta, T. convolutae, T. chui* and *T. desikacharyi*).

3.5   Discussion

Micropearls had been previously interpreted as a feature specifically related to freshwater environments (Martignier et al., 2017). The present results show that the biomineralization process leading to the formation of micropearls can take place in very different environments. The following paragraphs aim to discuss our present knowledge on micropearls in general and on their formation process as well as the newly discovered widespread biomineralization capacity in the *Tetraselmis* genus, involving high concentration capacities of these organisms regarding Sr.

3.5.1   *Marine and freshwater micropearls*

The discovery of micropearls in marine species of *Tetraselmis* shows that this biomineralization process can take place in organisms living in waters of different composition, from freshwater, like Lake Geneva, to seawater (Fig. S9). This highlights the capacity of these organisms to integrate Ca and Sr from different external media.

The production of micropearls is clearly not directly related to a specific habitat since seven *Tetraselmis* species forming micropearls live as phytoplankton in freshwater, marine or brackish waters (Guiry and Guiry, 2018; John et al., 2002); *T. contracta* and *T. desikacharyi* were sampled in the sand, at the bottom of a marine estuary (Marin et al., 1996) or at low

tide; and *T. convolutae* is usually observed as a photosymbiont inside a flatworm (Muscatine et al., 1974). Regarding the only two species that did not show micropearls at the time of observation (*T. ascus* and *T. marina*), it is interesting to note that both live as stalked sessile colonies, with motile life history stages (Norris et al., 1980).

Apart from their elongated shape, marine micropearls have characteristics similar to micropearls formed by the freshwater species *T. cordiformis* (Martignier et al., 2017). Micropearls show a range of possible composition for each species (Fig. 4a and Table S3). The Sr/Ca ratio seems to be influenced by several parameters, amongst which we identified the composition of the culture medium (Fig. 4b) and the Sr concentrating capacity of each *Tetraselmis* species (e.g., green triangles in Fig. 4b). Indeed, the general trend seen in this diagram is an adaptation of the ACC precipitation to the medium composition. However, more relevant information is provided by the enrichment factor (E factor; see Table S4 and dotted isolines in Fig. 4b), which allows us to rank species (Table S4) from low values (12–16) to more than 200. This ranking would need to be confirmed by cultivating the species in different media (*e.g.*, *T. convolutae* group in ES and *T. tetrathele* group in ASP-H) and comparing the new enrichment factor with the current values. The very high E factor for *T. desikacharyi* can tentatively be linked to distinctive morphological features (a six-layered theca, a novel flagellar hair subtype) not found in other strains of Tetraselmis (Marin et al., 1996).

The pattern drawn by the arrangement of the micropearls in the cell is clearly more homogeneous within a strain compared to among strains. Statistics show that these patterns are characteristic for a given species (Table 2 and Fig. S1), which means that the organisms can probably exert a strong control on the number, size and organization of the micropearls in the cells.

3.5.2   Hints about the formation process of micropearls

The biomineralization process leading to the formation of micropearls seems to start in the same way in all *Tetraselmis* species observed in FIB sections (*T. chui, T. contracta, T. cordiformis* and *T. suecica*), with a similar rod-shaped nucleus (Figs. 2, 3 and S5). These nuclei could possibly be of an organic nature given their darker appearance in the STEM–HAADF images that point to a material of lower atomic mass (Fig. S5).

It is important to note that there are many parameters which seem to influence the presence and absence of micropearls in the cells: the state of the culture (fully healthy or suffering from

the transport, for example), the pH of the medium and probably other parameters we are not yet aware of. For example, the use of agar as a culture medium seems to hinder the development of micropearls (Table 2 and Fig. 1g and h). Nevertheless, the composition of the medium does not seem to influence the arrangement of the micropearls in the cell, as demonstrated by *T. chui, T. contracta* and *T. convolutae* (respectively Fig. 1a, c and d), which have different patterns, although all were cultured in the ASP-H medium.

Internal concentric zones are observed in the micropearls formed by cells grown in both the natural environment and cultures (Fig. 2). The presence of this concentric pattern, even when the growth media have a stable composition, may indicate that the zonation is not due to changes in the surrounding water or medium composition during micropearl growth but rather depends on variations in the intracellular fluid composition caused by the biomineralization process itself. In the hypothesis discussed by Thien et al. (2017), it is suggested that the formation of the micropearls results from a combination of a biologically controlled process (preferential intake of specific cations inside the cell) and abiotic physical and chemical mechanisms (mineralization resulting from a nonequilibrium solid-solution growth mechanism, leading to an internal oscillatory zoning). Nevertheless, even that second part of the process does not seem to be purely abiotic, as demonstrated by the long-term amorphous state displayed by micropearls (at least 5 months, according to our observations). Indeed, synthetic ACC with no additives is unstable and rapidly crystallizes into calcite or aragonite (Addadi et al., 2003; Bots et al., 2012; Weiner and Addadi, 2011; Purgstaller, 2016; Alberic et al., 2018), often through the intermediate form of vaterite (Rodriguez-Blanco et al., 2011). In contrast, long-term stabilization of ACC implies the presence of mineral or organic additives (Aizenberg et al., 2002; Sun et al., 2016). Magnesium is known to play a key role in the stabilization of ACC (Politi et al., 2010). This might well be the case for the Tetraselmis-hosted micropearls, in which Mg content is around 2 mol %. Although the phosphate ion has also been reported to inhibit ACC crystallization (Albéric et al., 2018), that does not seem to be the case here since the phosphorus concentration of the micropearls is below the detection level of EDXS. Stabilization of ACC is also enhanced by certain proteins, polyphosphonates, citrates and amino acids (Levi- Kalisman et al., 2002; Addadi et al., 2003; Cam et al., 2015; Cartwright et al., 2012). The presence of these molecules inside the micropearls is suggested by their observed sensitivity to beam damage. As for the possible role of Sr in the ACC long-term stability, we did not find any reference thereof in the literature. However, in an in vitro experiment, Littlewood et al. (2017) found, in the presence of Mg, a correlation between added Sr and the reaction time to transform ACC into calcite (2 h to a maximum of 24 h).

3.5.3   A new intracellular feature in a well-known genus

Our results (Fig. 1) confirm that artifacts can be induced by the usual biological sample preparation techniques (Martignier et al., 2017) and thus introduce bias in observations and even hide some physiological traits in otherwise well-studied organisms. Figure 3c shows that the straightforward sample preparation method used in this study (dried, with no chemical fixation) allows the preservation of the micropearls and yields useful data on the composition of the different elements present inside the cell, without any chemical disturbance.

Micropearls represent a newly discovered intracellular feature. Their systematic presence in most of the analyzed *Tetraselmis* species suggests that they probably play a physiological role. A possible explanation could be that micropearls increase the sedimentation rate of cells that shed their flagella upon N starvation at the end of *Tetraselmis* blooms. An alternative hypothesis is that micropearls represent reserves of Ca for periods when millimolar Ca is not available in the external medium. Indeed, most Chlorodendrophyceae are known to require the presence of Ca^{++} to survive and multiply (Melkonian, 1982). The evolutionary diversification of this class occurs in the marine habitat, where the Ca concentration is constantly around 10 mM (Table 4.1 in Pilson, 1998). The need for Ca is supported by *T. cordiformis*, the only freshwater species of the genus, occurring only in Ca-rich lakes, with a minimum of 1mM of Ca (e.g., Lake Geneva (1 mM) or Lake Fühlinger (2 mM), and tests on cultures showed that *T. cordiformis* cannot develop normally in an environment with 0.42 mM of Ca (Melkonian, 1982). Calcium is needed to support phototaxis (light-oriented movements) and for the construction and maintenance of cell coverage (theca, flagellar scales) (Becker et al., 1994; Halldal, 1957). The Sr found in the composition of the micropearls formed by most *Tetraselmis* spp. (Fig. 4) could be transported by the same transporter as Ca. Indeed, Chlorodendrophyceae have very efficient light-gated Ca channels (channelrhodopsins), which are also essential for phototaxis of these flagellates (Govorunova et al., 2013; Halldal, 1957).

3.5.4   Bioremediation possibilities

The capacity of some organisms to concentrate Sr is of great interest regarding bioremediation. Strontium (^{90}Sr) is one of the radioactive nuclides released in large quantities by accidents such as Chernobyl or Fukushima (Casacuberta et al., 2013) and a major contaminant in wastewater and sludge linked with nuclear activities (Bradley et al., 1996). Its relatively long half-life of ~30 years and high water solubility cause persistent water pollution

(Thorpe et al., 2012; Yablokov et al., 2009). For example, the desmid green alga *Closterium moniliferum*, which can incorporate 45 mol% of Sr in barite crystals, is considered to be a potential candidate as a bioremediation agent (Krejci et al., 2011). The high Sr absorption capacity of several *Tetraselmis* species also led to their mention as potential candidates for radioactive Sr bioremediation (Fukuda et al., 2014; Li et al., 2006). In our experiments, *T. suecica*, for instance, produced a high number of micropearls that contained more than 50 mol% of Sr when cultured in the ES medium (data not shown). Nevertheless, the process allowing these microorganisms to concentrate Sr had not yet been investigated and further studies of micropearl formation processes could therefore lead to new bioremediation techniques. The genus *Tetraselmis* presents the additional advantage of including species living in diverse habitats, which might offer interesting bioremediation applications in different aquatic environments including freshwater, brackish lakes, open sea and hypersaline lagoons (Table 1).

3.6   Conclusions

Until recently, nonskeletal intracellular inclusions of calcium carbonate were considered nonexistent in unicellular eukaryotes (Raven and Knoll, 2010). After the first observation of at least two micropearl-forming organisms in Lake Geneva (Martignier et al., 2017), the present study shows that these amorphous (or near-amorphous) calcium carbonate (ACC) inclusions are widespread in a common phytoplankton genus (*Tetraselmis*), not only in freshwater, but also in seawater and brackish environments. This newly discovered biomineralization process therefore takes place in media of very different composition and our results suggest that it is similar in all studied species: an oscillatory zoning process that starts from an organic rod-shaped nucleus. Although frequent in this well studied genus, these mineral inclusions had been overlooked in the past, possibly destroyed by the usual sample preparation techniques for electron microscopy. Thus, other microorganisms could have similar capacities and intracellular inclusions of ACCs may be more widespread than currently known.

Micropearls represent a new intracellular feature. This study shows that they can be clearly distinguished from other cellular constituents and are not randomly distributed in the cell. On the contrary, micropearls seem to be essentially located just under the cell wall and they draw a pattern that seems to be characteristic for each species. Strong correlations hint that this might have a link with the species habitat.

It appears that, for most of the observed *Tetraselmis* species, the biomineralization process leading to the formation of micropearls enables a selective concentration of Sr. The elements concentrated in the micropearls, as well as their degree of enrichment, seem to be characteristic for each species. Selecting the species with the highest concentration capacities could be of high interest for bioremediation, especially regarding radioactive Sr contaminations linked with nuclear activities.

Edited by: Lennart de Nooijer

Reviewed by: Adrian Immenhauser, Estelle Couradeau and Marie Alberic

3.7   References

Addadi, L., Raz, S., and Weiner, S.: Taking advantage of disorder: Amorphous calcium carbonate and its roles in biomineralization, Adv. Mater., 15, 959-970, https://doi.org/10.1002/adma.200300381, 2003.

Aizenberg, J., Lambert, G., Weiner, S., and Addadi, L.: Factors involved in the formation of amorphous and crystalline calcium carbonate: a study of an ascidian skeleton, J. Am. Chem. Soc., 124, 32–39, https://doi.org/10.1021/ja016990l, 2002.

Albéric, M., Bertinetti, L., Zou, Z., Fratzl, P., Habraken, W., and Politi, Y.: The crystallization of amorphous calcium carbonate is kinetically governed by ion impurities and water, Adv. Sci., 5, 1701000, https://doi.org/10.1002/advs.201701000, 2018.

Asinari di San Marzano, C.-M., Legros, A., Piron, C., Sironval, C., Nyns, E.-J., and Naveau, H. P.: Methane production by anaerobic digestion of algae, in: Energy from biomass: Proceedings

of the EC Contractors' Meeting held in Copenhagen, 23–24 June 1981, edited by: Chartier, P. and Palz, W., Springer Netherlands, Dordrecht, 113–120, 1981.

Azma, M., Mohamed, M. S., Mohamad, R., Rahim, R. A., and Ariff, A. B.: Improvement of medium composition for heterotrophic cultivation of green microalgae, *Tetraselmis suecica*, using response surface methodology, Biochem. Eng. J., 53, 187–195, https://doi.org/10.1016/j.bej.2010.10.010, 2011.

Becker, B., Marin, B., and Melkonian, M.: Structure, composition, and biogenesis of prasinophyte cell coverings, Protoplasma, 181, 233–244, https://doi.org/10.1007/BF01666398, 1994.

Becker, B., Melkonian, M., and Kamerling, J. P.: The cell wall (theca) of *Tetraselmis striata* (chlorophyta): macromolecular composition and structural elements of the complex polysaccharides, J. Phycol., 34, 779–787, https://doi.org/10.1046/j.1529-8817.1998.340779.x, 1998.

Benzerara, K., Skouri-Panet, F., Li, J., Férard, C., Gugger, M., Laurent, T., Couradeau, E., Ragon, M., Cosmidis, J., Menguy, N., Margret-Oliver, I., Tavera, R., López-García, P., and Moreira, D.: Intracellular Ca-carbonate biomineralization is widespread in cyanobacteria, P. Natl. Acad. Sci. USA, 111, 10933–10938, https://doi.org/10.1073/pnas.1403510111, 2014.

Blondeau, M., Sachse, M., Boulogne, C., Gillet, C., Guigner, J.-M., Skouri-Planet, F., Poinsot, M., Ferard, C., Miot, J., and Benzerara, K.: Amorphous calcium carbonate granules form within an intracellular compartment in calcifying cyanobacteria, Front. Microbiol., 9, 1768, https://doi.org/10.3389/fmicb.2018.01768, 2018.

Bolton, C. T., Hernández-Sánchez, M., Fuertes, M.-A., Gonzáles-Lemos, S., Abrevaya, L., Mendez-Vicente, A., Flores, J.-A., Probert, I., Giosan, L., Johnson, J., and Stoll, H. M.: Decrease in coccolithophore calcification and CO_2 since the middle Miocene, Nat. Commun., 7, 10284, https://doi.org/10.1038/ncomms10284, 2016.

Bots, P., Benning, L. G., Rodriguez-Blanco, J.-D., Roncal-Herrero, T., and Shaw, S.: Mechanistic insights into the crystallization of amorphous calcium carbonate (ACC), Cryst. Growth Des., 12, 3806–3814, https://doi.org/10.1021/cg300676b, 2012.

Bradley, D. J., Frank, C. W., and Mikerin, Y.: Nuclear contamination from weapons complexes in the former Soviet Union and the United States, Phys. Today, 49, 40–45, https://doi.org/10.1063/1.881495, 1996.

Cam, N., Georgelin, T., Jaber, M., Lambert, J. F., and Benzerara, K.: In vitro synthesis of amorphous Mg-, Ca-, Sr- and Ba-carbonates: What do we learn about intracellular calcification by cyanobacteria?, Geochim. Cosmochim. Ac., 161, 36–49, https://doi.org/10.1016/j.gca.2015.04.003, 2015.

Cartwright, J. H. E., Checa, A. G., Gale, J. D., and Sainz-díaz, C. I.: Calcium carbonate polyamorphism and its role in biomineralisation?: How many ACCs are there?, Angew. Chemie Int. Edit., 51, 11960–11970, https://doi.org/10.1002/anie.201203125, 2012.

Casacuberta, N., Masqué, P., Garcia-Orellana, J., Garcia-Tenorio, R., and Buesseler, K. O.: [90]Sr and ^{89}Sr in seawater off Japan as a consequence of the Fukushima Dai-ichi nuclear accident, Biogeosciences, 10, 3649–3659, https://doi.org/10.5194/bg-10-3649-2013, 2013.

Couradeau, E., Benzerara, K., Gérard, E., Moreira, D., Bernard, S., Brown Jr., G. E., and López-García, P.: An early-branching microbialite cyanobacterium forms intracellular carbonates, Science, 336, 459–462, https://doi.org/10.1126/science.1216171, 2012.

Domozych, D. S.: The crystalline cell wall of *Tetraselmis convolutae* (Chlorophyta): a freeze fracture analysis, J. Phycol., 20, 415–418, https://doi.org/10.1111/j.0022-3646.1984.00415.x, 1984.

Douglas, A. E.: Uric acid utilization in *Platymonas convolutae* and symbiotic *Convoluta roscoffensis*, J. Mar. Biol. Assoc. UK, 63, 435-447, https://doi.org/10.1017/S0025315400070788, 1983.

Dupraz, C., Reid, R. P., Braissant, O., Decho A. W., Norman, R. S., and Visscher, P. T.: Processes of carbonate precipitation in modern microbial mats, Earth-Sci. Rev., 96, 141–162, https://doi.org/10.1016/j.earscirev.2008.10.005, 2009.

Fukuda, S., Iwamoto, K., Atsumi, M., Yokoyama, A., Nakayama, T., Ishida, K., Inouye, I., and Shiraiwa, Y.: Global searches for microalgae and aquatic plants that can eliminate radioactive cesium, iodine and strontium from the radio-polluted aquatic environment: A bioremediation strategy, J. Plant Res., 127, 79–89, https://doi.org/10.1007/s10265-013-0596-9, 2014.

Gooday, G. W.: A physiological comparison of the symbiotic alga *platymonas convolutae* and its free-living relatives, J. Mar. Biol. Assoc. UK, 50, 199–208, https://doi.org/10.1017/S0025315400000710, 1970.

Govorunova, E. G., Sineshchekov, O. A., Li, H., Janz, R., and Spudich, J. L.: Characterization of a highly efficient blue-shifted channelrhodopsin from the marine alga *platymonas subcordiformis*, J. Biol. Chem., 288, 29911–29922, https://doi.org/10.1074/jbc.M113.505495, 2013.

Grierson, S., Strezov, V., Bray, S., Mummacari, R., Danh, L. T., and Foster, N.: Assessment of bio-oil extraction from *Tetraselmis chui microalgae* comparing supercritical CO2, solvent extraction, and thermal processing, Energ. Fuel., 26, 248–255, https://doi.org/10.1021/ef2011222, 2012.

Guiry, M. D. and Guiry, G. M.: AlgaeBase, World-wide Electron. Publ. Natl. Univ. Ireland, Galw., available at: http://www. algaebase.org, last access: 30 June 2018.

Halldal, P.: Importance of calcium and magnesium ions in phototaxis of motile green algae, Nature, 179, 215–216, https://doi.org/10.1038/179215b0, 1957.

Hemaiswarya, S., Raja, R., Ravi Kumar, R., Ganesan, V., and Anbazhagan, C.: Microalgae: A sustainable feed source for aquaculture, World J. Microb. Biot., 27, 1737–1746, https://doi.org/10.1007/s11274-010-0632-z, 2011.

Jaquet, J. M., Nirel, P., and Martignier, A.: Preliminary investigations on picoplankton-related precipitation of alkaline-earth metal carbonates in meso-oligotrophic lake Geneva (Switzerland), J. Limnol., 72, 592–605, https://doi.org/10.4081/jlimnol.2013.e50, 2013.

John, D. M., Whitton, B. A., and Brook, A. J.: The freshwater algal flora of the British Isles: An identification guide to freshwater and terrestrial algae, Natural History Museum (London) and British Phycological Society, Cambridge University Press, 2002.

Kirst, G. O.: Ion composition of unicellular marine and fresh-water algae, with special reference to *Platymonas subcordiformis* cultivated in media with different osmotic strengths, Oecologia, 28, 177–189, https://doi.org/10.1007/BF00345253, 1977.

Krejci, M. R., Finney, L., Vogt, S., and Joester, D.: Selective sequestration of strontium in Desmid green algae by biogenic co-precipitation with barite, ChemSusChem, 4, 470–473, https://doi.org/10.1002/cssc.201000448, 2011.

Levi-Kalisman, Y., Raz, S., Weiner, S., Addadi, L., and Sagi, I.: Structural differences between biogenic amorphous calcium carbonate phases using X-ray absorption spectroscopy, Adv. Funct. Mater., 12, 43–48, https://doi.org/10.1002/1616- 3028(20020101)12:1<43::AID-ADFM43>3.0.CO;2-C, 2002.

Li, M., Xie, X., Xue, R., and Liu, Z.: Effects of strontiuminduced stress on marine microalgae *Platymonas subcordiformis* (Chlorophyta: Volvocales), Chin. J. Oceanol. Limn., 24, 154–160, https://doi.org/10.1007/BF02842815, 2006.

Lim, D. K. Y., Garg, S., Timmins, M., Zhang, E. S. B., Thomas-Hall, S. R., Schuhmann, H., Li, Y., and Schenk, P. M.: Isolation and evaluation of oil-producing microalgae from subtropical coastal and brackish waters, PLoS One, 7, e40751, https://doi.org/10.1371/journal.pone.0040751, 2012.

Littlewood, J. L., Shaw, S., and Peacock, C. L.: Mechanism of enhanced strontium uptake into calcite via an amorphous calcium carbonate (ACC) crystallisation pathway, Cryst. Growth Des., 17, 1214–1223, https://doi.org/10.1021/acs.cgd.6b01599, 2017.

Lu, L.,Wang, J., Yang, G., Zhu, B., and Pan, K.: Biomass and nutrient productivities of *Tetraselmis chuii* under mixotrophic culture conditions with various C:N ratios, Chin. J. Oceanol. Limn., 35, 303–312, https://doi.org/10.1007/s00343-016-5299-3, 2017.

Manton, I. and Parke, M.: Observations on the structure of two species of *Platymonas* with special reference to flagellar scales and the mode of origin of the theca, J. Mar. Biol. Assoc. UK, 45, 743–754, https://doi.org/10.1017/S0025315400016568, 1965.

Marin, B., Matzke, C., and Melkonian, M.: Flagellar hairs of *Tetraselmis* (Prasinophyceae): Ultrastructural types and intrageneric variation, Phycologia, 32, 213–222, https://doi.org/10.2216/i0031-8884-32-3-213.1, 1993.

Marin, B., Hoef-Emden, K., and Melkonian, M.: Light and electron microscope observations on *Tetraselmis desikacharyi* sp. nov.(Chlorodendrales, Chlorophyta), Nova Hedwigia, 112, 461– 475, 1996.

Martignier, A., Pacton, M., Filella, M., Jaquet, J.-M., Barja, F., Pollok, K., Langenhorst, F., Lavigne, S., Guagliardo, P., Kilburn, M. R., Thomas, C., Martini, R., and Ariztegui, D.: Intracellular amorphous carbonates uncover a new biomineralization process in eukaryotes, Geobiology, 15, 240–253, https://doi.org/10.1111/gbi.12213, 2017.

Mass, T., Giuffre, A. J., Sun, C.-Y., Stifler, C. A., Frazier, M. J., Neder, M., Tamura, N., Stan, C. V., Marcus, M. A., and Gilbert, P. U. P. A.: Amorphous calcium carbonate particles form coral skeletons, P. Natl. Acad. Sci. USA, 114, E7670–E7678, https://doi.org/10.1073/pnas.1707890114, 2017.

Melkonian, M.: An ultrastructural study of the flagellate *Tetraselmis cordiformis* stein (Chlorophyceae) with emphasis on the flagellar apparatus, Protoplasma, 98, 139–151, https://doi.org/10.1007/BF01676667, 1979.

Melkonian, M.: Effect of divalent cations on flagellar scales in the green *flagellate Tetraselmis cordiformis*, Protoplasma, 111, 221– 233, https://doi.org/10.1007/BF01281970, 1982.

Montero, M. F., Aristizábal, M., and García Reina, G.: Isolation of high-lipid content strains of the marine microalga *Tetraselmis suecica* for biodiesel production by flow cytometry and single-cell sorting, J. Appl. Phycol., 23, 1053–1057, https://doi.org/10.1007/s10811-010-9623-6, 2011.

Muscatine, L., Boyle, J. E., and Smith, D. C.: Symbiosis of the acoel flatworm *Convoluta roscoffensis* with the alga *Platymonas convolutae*, P. R. Soc. B, 187, 221–234, https://doi.org/10.1098/rspb.1974.0071, 1974.

Norris, R. E., Hori, T., and Chihara, M.: Revision of the genus *Tetraselmis* (Class Prasinophyceae), Bot. Mag. Tokyo, 93, 317–339, https://doi.org/10.1007/BF02488737, 1980.

Park, J. E. and Hur, S.-B.: Optimum culture condition of four species of microalgae as live food from China, J. Aquac., 13, 107–117, 2000.

Parke, M. and Manton, I.: The specific identity of the algal symbiont in Convoluta roscoffensis, J. Mar. Biol. Assoc. UK, 47, 445–464, https://doi.org/10.1017/S002531540005654X, 1967.

Pilson, M. E. Q.: An introduction to the chemistry of the sea, 2nd Edn., Cambridge University Press, 1998.

Politi, Y., Batchelor, D. R., Zaslansky, P., Chmelka, B. F., Weaver, J. C., Sagi, I., Weiner, S., and Addadi, L.: Role of magnesium ion in the stabilization of biogenic amorphous calcium carbonate: a structure-function investigation, Chem. Mater., 22, 161–166, https://doi.org/10.1021/cm902674h, 2010.

Purgstaller, B., Mavromatis, V., Immenhauser, A., and Dietzel, M.: Transformation of Mg-bearing amorphous calcium carbonate to Mg-calcite – In situ monitoring, Geochim. Cosmochim. Ac., 174, 180–195, https://doi.org/10.1016/j.gca.2015.10.030, 2016.

Raven, J. A. and Knoll, A. H.: Non-skeletal biomineralization by eukaryotes: Matters of moment and gravity, Geomicrobiol. J., 27, 572–584, https://doi.org/10.1080/01490451003702990, 2010.

Regan, D. L.: Other micro-algae, in: Micro-Algal Biotechnology, edited by: Borowitzka, M. A. and Borowitzka, L. J., Cambridge University Press, 135–150, 1988.

Rodriguez-Blanco, J. D., Shaw, S., and Benning, L. G.: How to make "stable" ACC: protocol and preliminary structural characterization, Mineral. Mag., 72, 283–286, https://doi.org/10.1180/minmag.2008.072.1.283, 2008.

Rodriguez-Blanco, J. D., Shaw, S., and Benning, L. G.: The kinetics and mechanisms of amorphous calcium carbonate (ACC) crystallization to clacite, via vaterite, Nanoscale, 3, 265–271, https://doi.org/10.1039/C0NR00589D, 2011.

Rodriguez-Blanco, J. D., Sand, K. K., and Benning, L. G.: ACC and vaterite as intermediates in the solution-based crystallization of CaCO3, in: "New Perspectives on Mineral Nucleation and Growth", edited by: Van Driessche, A. E. S., Kellermeier, M., Benning, L. G., and Gebauer, D., Springer, 93–111, https://doi.org/10.1007/978-3-319-45669-0_5, 2017.

Salisbury, J. L., Baron, A., Surek, B., and Melkonian, M.: Striated flagellar roots: isolation and partial characterization of a calcium-modulated contractile organelle, J. Cell Biol., 99, 962– 970, https://doi.org/10.1083/jcb.99.3.962, 1984.

Stein, F. R.: Der Organismus der Infusionstiere, III, 1. Hälfte Flagellaten, Engelmann, Leipzig, 1878.

Sun, S., Chevrier, D. M., Zhang, P., Gebauer, D., and Cölfen, H.: Distinct short-range order is inherent to small amorhous calcium carbonate clusters (< 2 nm), Angew. Chem. Int. Edit., 55, 12206–12209, https://doi.org/10.1002/anie.201604179, 2016.

Thien, B., Martignier, A., Jaquet, J.-M., and Filella, M.: Linking environmental observations and solid solution thermodynamic modeling: The case of Ba- and Sr-rich micropearls in Lake Geneva, Pure Appl. Chem., 89, 645–652, https://doi.org/10.1515/pac-2017-0205, 2017.

Thorpe, C. L., Lloyd, J. R., Law, G. T. W., Burke, I. T., Shaw, S., Bryan, N. D., and Morris, K.: Strontium sorption and precipitation behaviour during bioreduction in nitrate impacted sediments, Chem. Geol., 306–307, 114–122, https://doi.org/10.1016/j.chemgeo.2012.03.001, 2012.

Trench, R. K.: The cell biology of plant-animal symbiosis, Ann. Rev. Plant Physio., 30, 485–531, https://doi.org/10.1146/annurev.pp.30.060179.002413, 1979.

Venn, A. A., Loram, J. E., and Douglas, A. E.: Photosynthetic symbioses in animals, J. Exp. Bot., 59, 1069–1080, https://doi.org/10.1093/jxb/erm328, 2008.

Wei, L., Huang, X., and Huang, Z.: Temperature effects on lipid properties of *microalgae Tetraselmis subcordiformis* and *Nannochloropsis oculata* as biofuel resources, Chin. J. Oceanol. Limn., 33, 99–106, https://doi.org/10.1007/s00343-015-3346-0, 2015.

Weiner, S. and Addadi, L.: Crystallization pathways in biomineralization, Ann. Rev. Mater. Res., 41, 21–40, https://doi.org/10.1146/annurev-matsci-062910-095803, 2011.

Yablokov, A. V., Nesterenko, V. B., Nesterenko, A. V., and Sherman, J. D.: Chernobyl?: Consequences of the catastrophe for people and the environment, edited by: Sherman-Nevinger, J. D., Annals of the New York Academy of Sciences, 327C39 pp., 2009.

Zittelli, G. C., Rodolfi, L., Biondi, N., and Tredici, M. R.: Productivity and photosynthetic efficiency of outdoor cultures of *Tetraselmis suecica* in annular columns, J. Aquac., 261, 932–943 https://doi.org/10.1016/j.aquaculture.2006.08.011, 2006.

3.8   Supplementary information
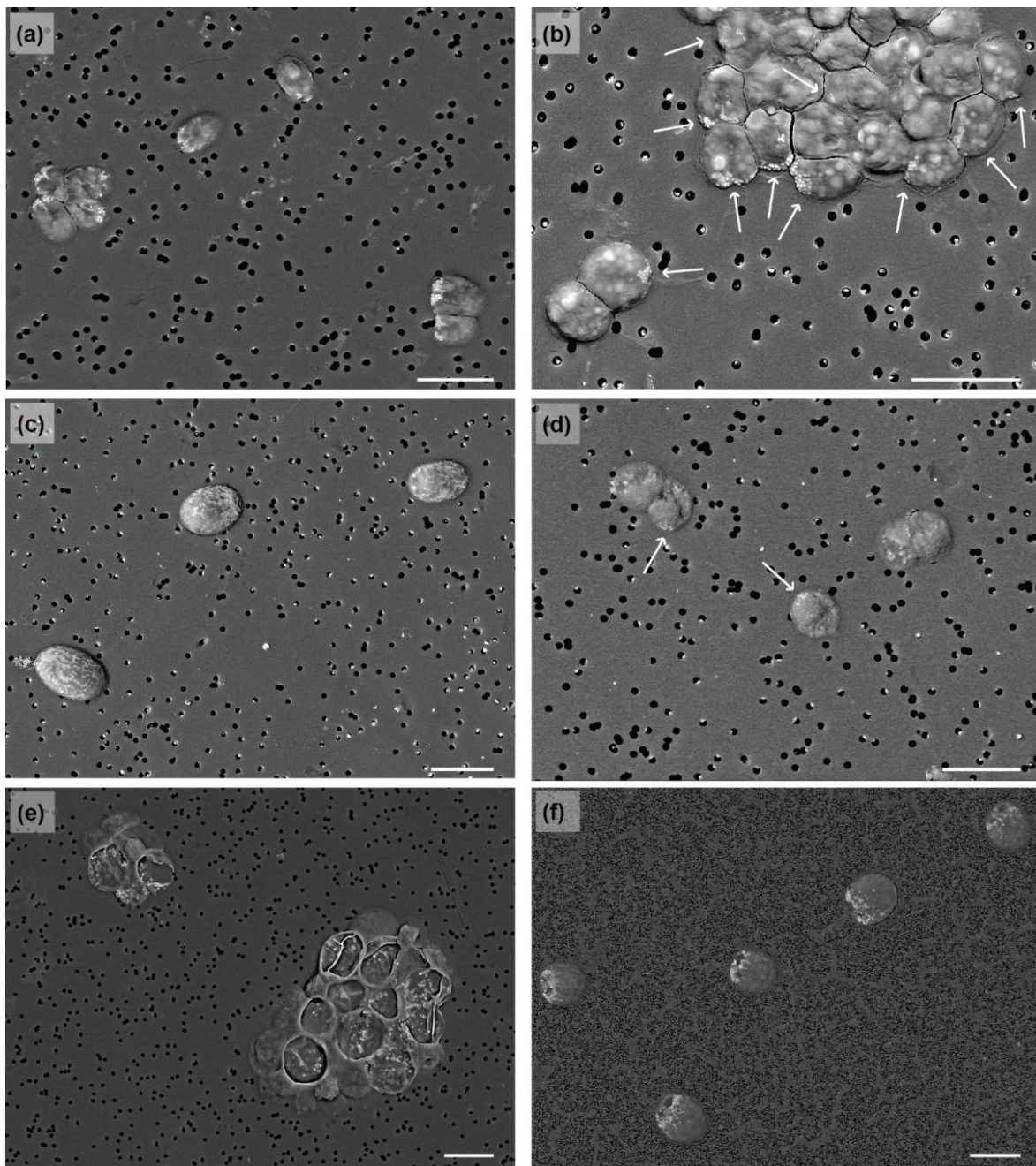
Fig. S1 (part 1): patterns of micropearl arrangement in the different species
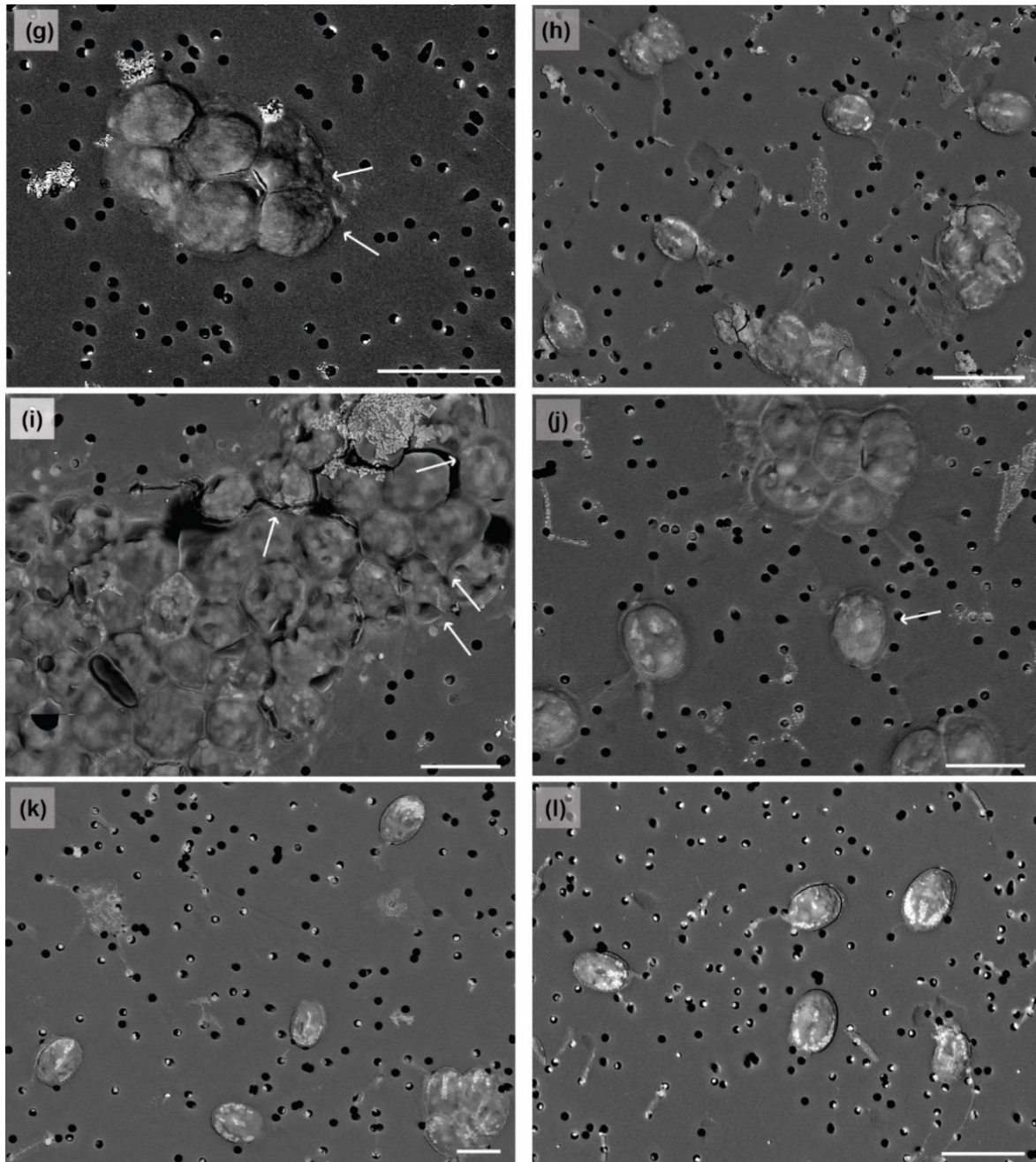
Fig. S1 (part 2): patterns of micropearl arrangement in the different species

SEM backscattered images. (a) *T. chui* (CCAC 0014); (b) *T. chui* (SAG 8-6) ; (c) *T. contracta* (CCAC 1405) ; (d) *T. convolutae* (CCAC 0100) ; (e) *T. cordiformis* (CCAC 0051) ; (f) *T. cordiformis* (CCAC 0579B) ; (g) *T. desikacharyi* (CCAC 0029); (h) *T. levis* (AC 257) ; (i) *T. striata* (SAG 41.85) ; (j) *T. subcordiformis* (SAG 161-1a) ; (k) *T. suecica* (AC 254) ; (l) *T. tetrathele* (AC 261).

These images aim to illustrate the general aspect of the different strains at the time of observation. They correspond to the measurements presented in Table 2. Micropearls appear as white dots inside the cells. In the images where only a few cells contain micropearls, white arrows indicate their position. Note that polyphosphate inclusions (e.g. in (d)) or NaCl crystals (e.g. in (j)) can also appear as white dots. Their distinction was based on their close-up morphology or EDXS analyses. All images were made on the day following the reception of the strains from the provider, except (f), taken 60 days after reception. This exception allows to show the internal pattern of micropearls in *T. cordiformis*,- pattern that was destroyed during our first sample preparation. Note that strains (b), (i) and (j) were maintained on agar, unlike the other strains. Scale bars: 20 μm.
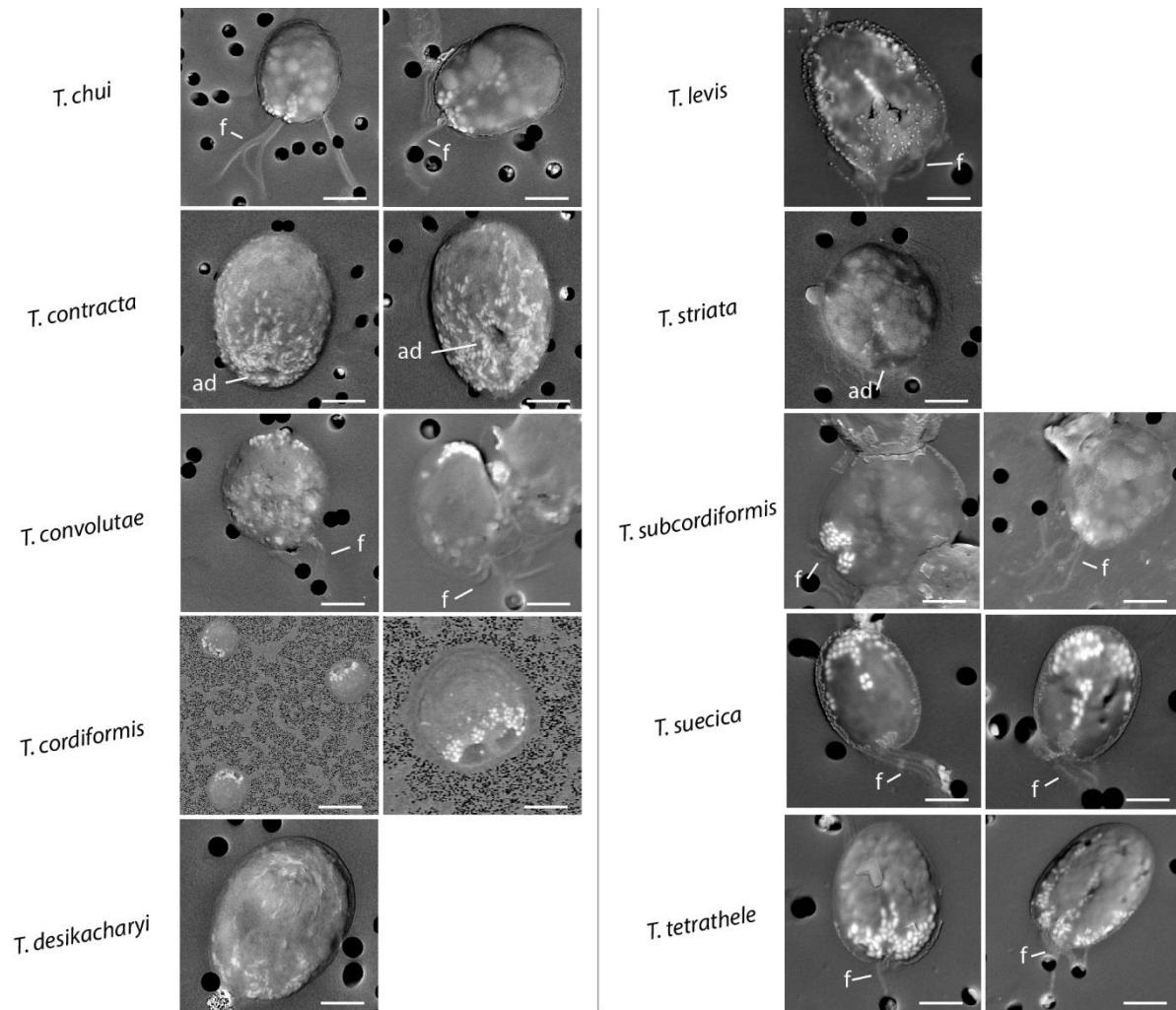
Figure S2: SEM images providing an overview of the micropearl location in *Tetraselmis* species.

Backscattered electron images of dried samples. The micropearls appear in white or light grey against the darker organic matter. The larger and slightly darker inclusions are polyphosphate (observed here in *T. chui*, *T. convolutae*, *T. striata*, *T. subcordiformis*). Pores of the filters are visible as black circles in the background (0.2, 1 or 2 µm of diameter). The location of the micropearls is linked to the observation of flagella (f) or of the apical depression (ad). In *T. cordiformis*, the two contractile vacuoles are clearly visible and are located at the apical side of the cell. Finally, the orientation of *T. desikacharyi* stays completely uncertain, although similar observations in *T. convolutae* seem to indicate that iron oxide minerals (in white) are formed around the (missing) flagella. Scale bars: 5 µm.

Tetraselmis levis	simply dried			
	rinced, then dried			
Tetraselmis suecica	simply dried			
	rinced then dried			
Tetraselmis tetrathele	simply dried			
	rinced then dried			
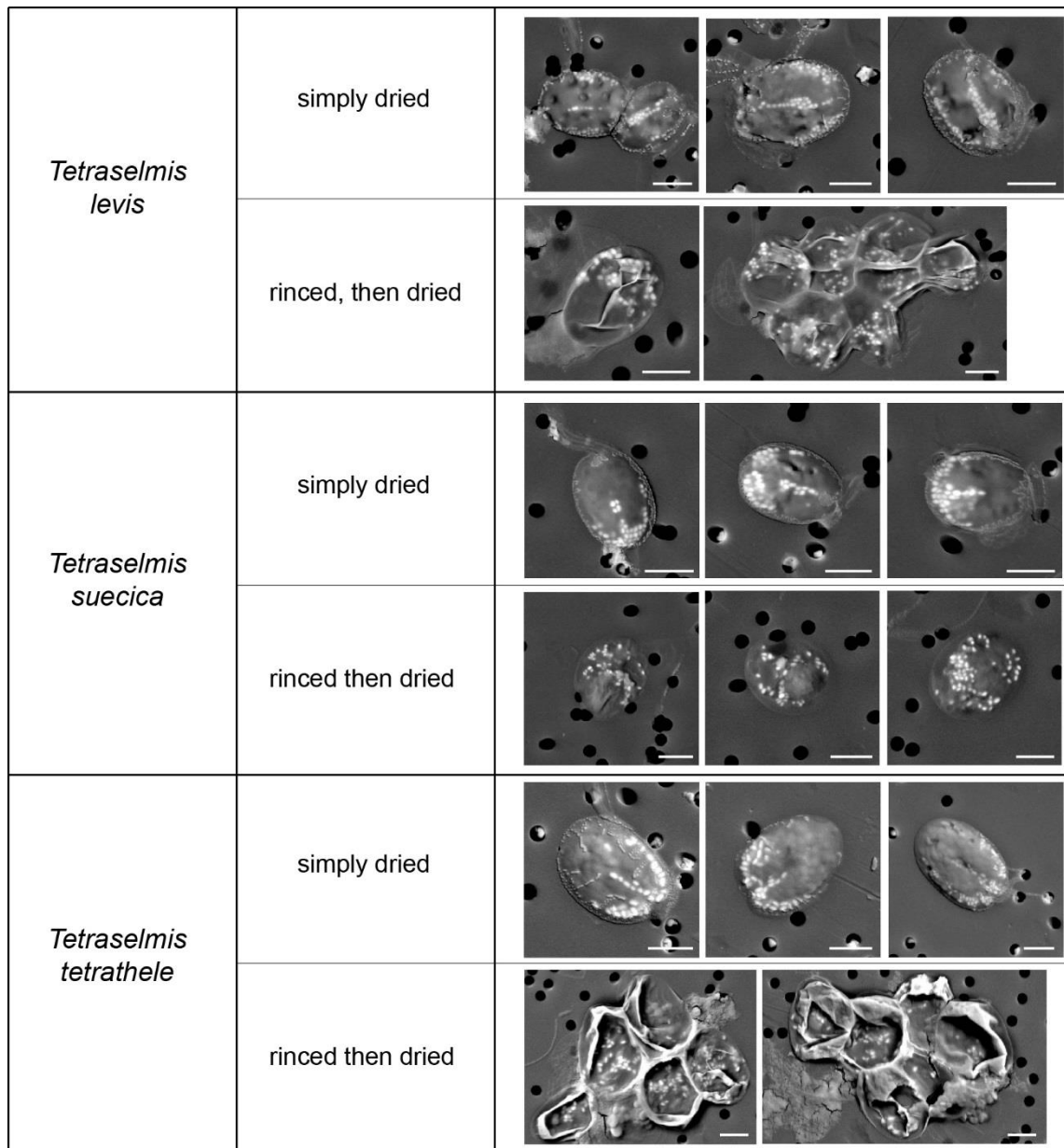
Figure S3: Micropearl distribution inside the cell disrupted by MilliQ water rinsing.

SEM backscattered electron images of dried samples. The micropearls appear in white or light grey against the darker organic matter. Each culture was sampled at the same time, but prepared in two different ways: either simply dried on a filter, or rinsed shortly with MilliQ water and then dried on a filter. The micropearls' distribution inside the cell is not preserved when the sample is rinsed. Scale bars: 5μm.
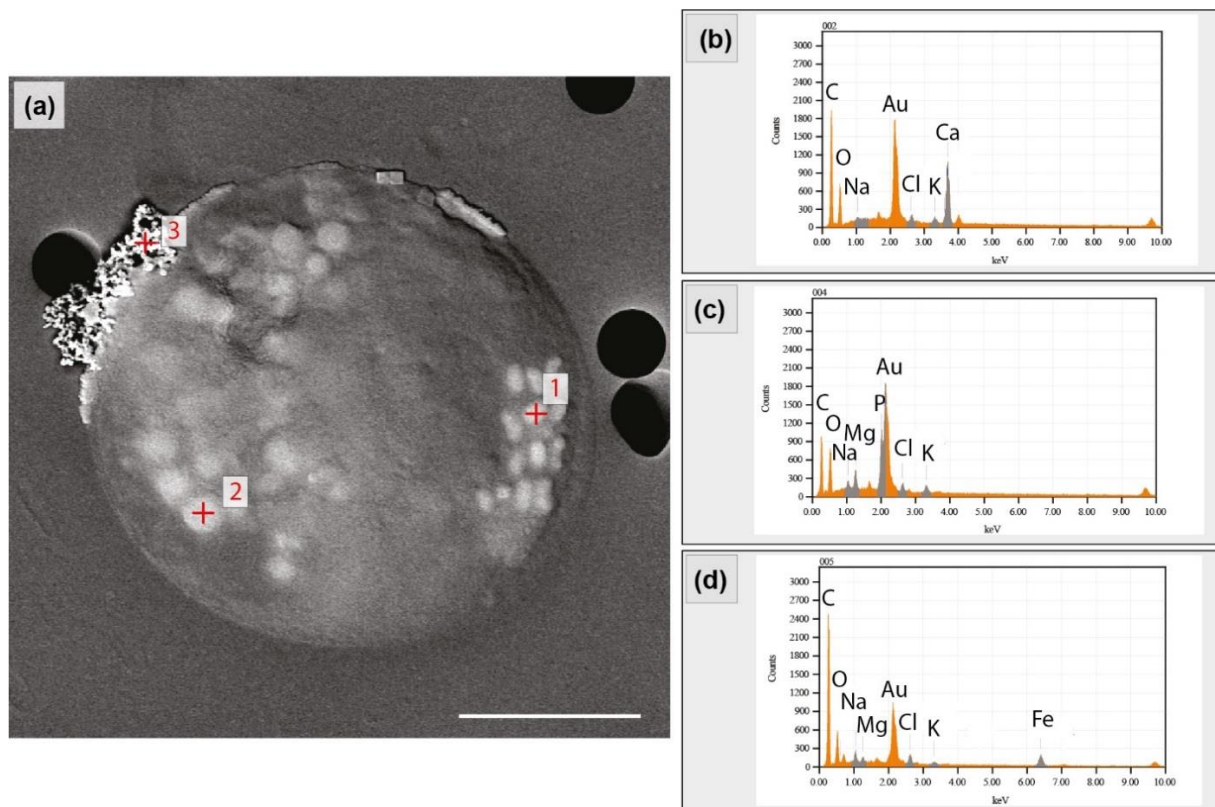
Fig. S4: SEM-EDXS analyses of polyphosphate inclusions and iron oxide aggregate

(a) SEM backscattered image of T.convolutae (Fig. 1c) with localization of the EDXS analyses indicated in red. (b) SEM-EDXS analyses of micropearls. (c) SEM-EDXS analyses of an intracellular polyphosphate inclusion. (c) SEM-EDXS analysis of an extracellular iron oxide aggregate. Due to the small size of the analyzed features, the results may include low percentages of elements coming from the surrounding organic matter (e.g. Na, Cl and possibly K). Presence of gold is due to the coating for SEM observation. Scale bars: 5 µm.

Figure S5: Nucleus shape interpretation for micropearls formed by *Tetraselmis* species.

Cells from algal cultures except *T.*cf *cordiformis,* which was sampled in Lake Geneva (dried samples). (a) Diagram of a possible formation process starting from a rod-shaped nucleus. (b) TEM HAADF images of FIB-cut sections in micropearls formed by *Tetraselmis* species, corresponding to the cross-sections located on the left hand-side drawing. The micropearls measure between 0.7 (*T. chui*) to 1.2 μm (*T. contracta*) in length.

(a) *Tetraselmis chui*

Element	1: bright	2: dark
C	19.2	19.4
Ca	11.2	17.8
Sr	10.0	3.2
O	59.6	59.7

(b) *Tetraselmis suecica*

Element	1: internal	2: external
C	21.9	19.9
Ca	8.3	10.2
Sr	8.8	9.9
O	61.0	60.0

Tetraselmis contracta

Element	1	2
C	24	20
K	1	1
Ca	14	20
O	61	59

Figure S6: TEM-EDXS analyses of *T. contracta, T. chui and T. suecica* micropearls.

Cut-out of single micropearls (left) from STEM – HAADF images of the FIB section shown in Figs 2 and 3. The location of the EDXS analyses (shown in the right hand-side table) is indicated by the corresponding numbers. Results are normalized to 100 at%. O is calculated stoichiometrically based on the cation concentrations (with absorption correction for sample thickness). (a) The micropearl of *T. chui* shows a clear zonation which is well documented in the TEM-EDXS results. (b) The micropearl of *T. suecica* appears almost unzoned, but with a high Sr concentration (Sr/Ca close to 1). Two additional thin zones close to the rim are visible but they are too small to allow meaningful TEM-EDXS analyses.(c) *T. contracta* has a very low concentration of Sr (close to or under the detection limit) in TEM-EDXS. No zoning was detected. In contrast, a low but significant presence of K was detected. However, its analysis n°1 does not fulfil carbonate stoichiometry, which may be due to the excess C from organic matter. Note that the calculation mode for the analyses presented in this figure differ from those presented in the rest of the manuscript, as C and O are included in the composition in order to perform a meaningful absorption correction.
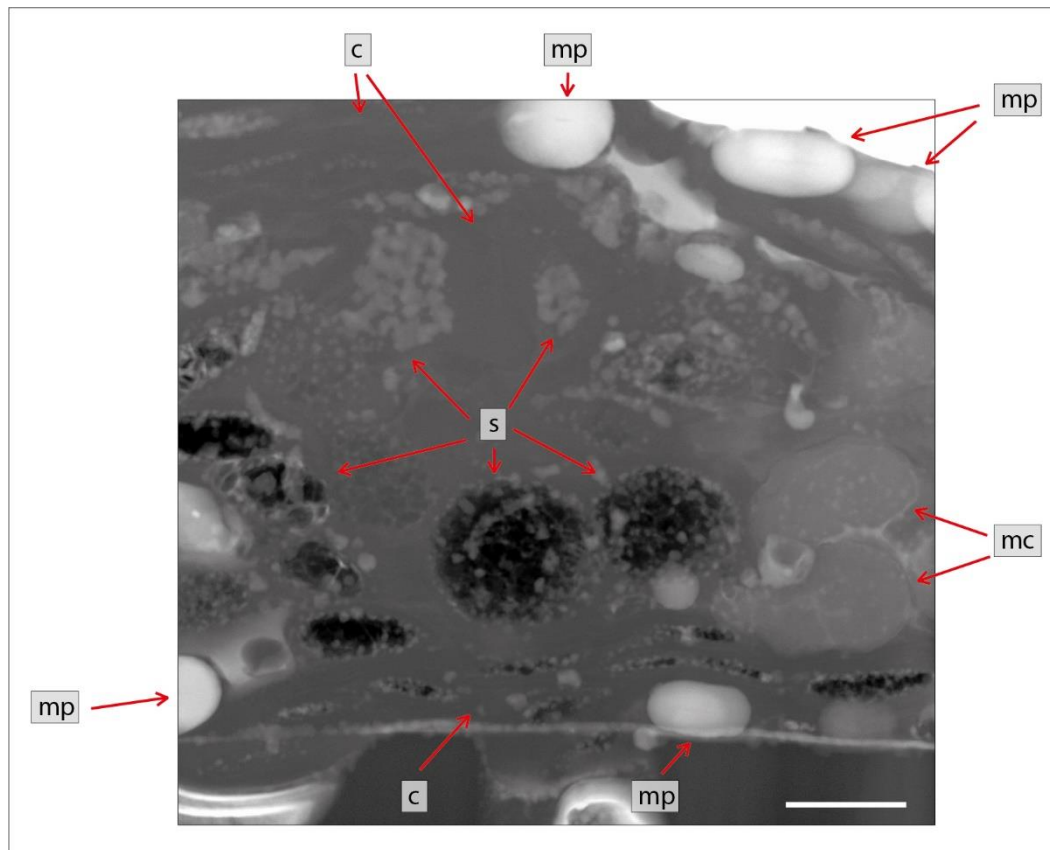
Figure S7: TEM zoom on a FIB-cut section through a *Tetraselmis contracta* cell (dried culture sample).

TEM-HAADF image. Zoomed-in image on a part of Figure 3. The micropearls show light or medium grey shades, regular round or oval shapes. Tentative identification of the visible cellular constituents. s: starch grains; c: chloroplast; mp: micropearls; mc: mitochondria.
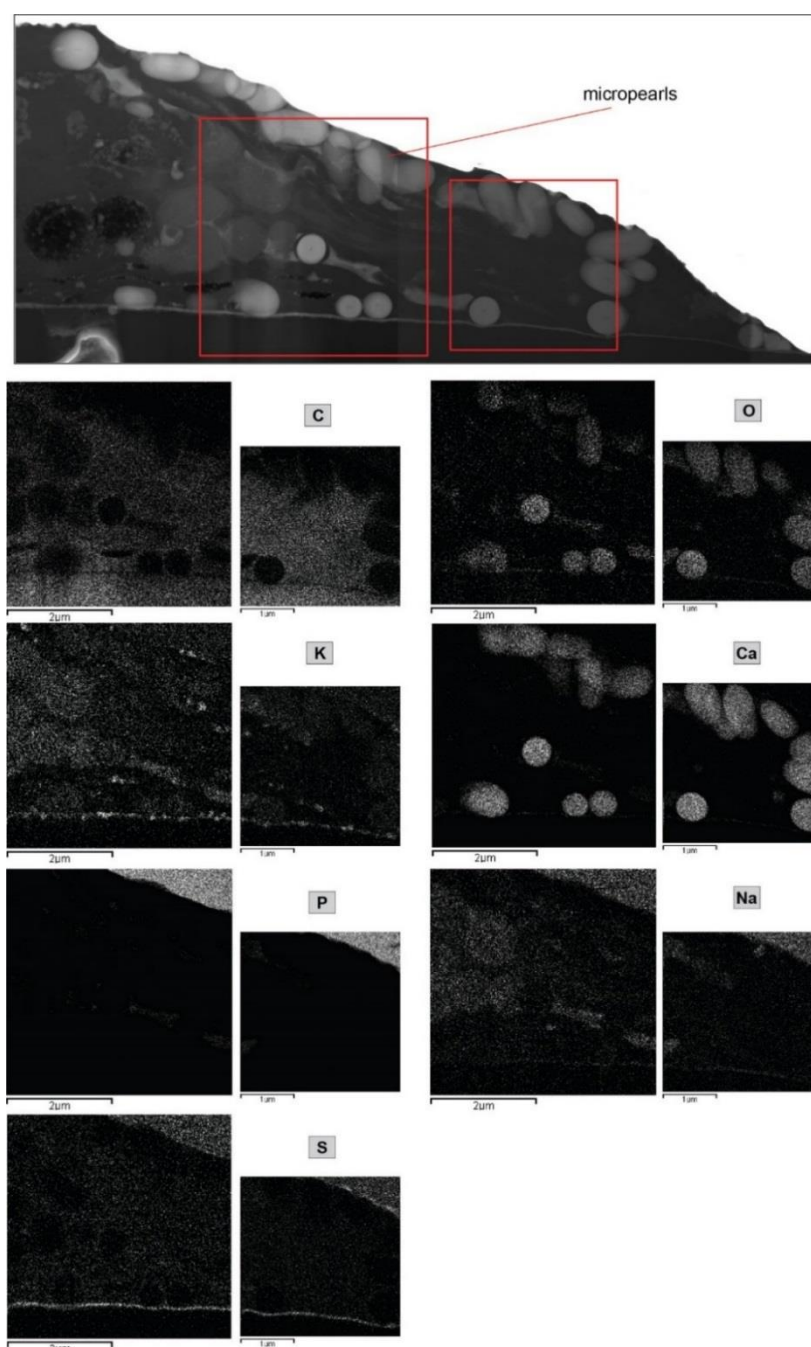
Figure S8: TEM-EDXS mapping results performed on a FIB-cut section through a *Tetraselmis contracta* cell (dried culture sample).

The top image shows the location of the two mappings on a TEM-HAADF image of the section. The maps show the concentration of the different elements: the lighter the color, the more the element is concentrated in that point. Micropearls are mainly composed of Ca, with small quantities of K (and Mg, not shown here). The near-amorphous calcium carbonate appears to contain less C than the surrounding organic matter, because calcite is known to contain 12 wt% of C while the biomass contains 40-50%. Note that, due to the overlap between the P *K* peak and secondary Pt *L* peak, the Pt which was deposited on top of the sample during FIB processing is also visible in green.
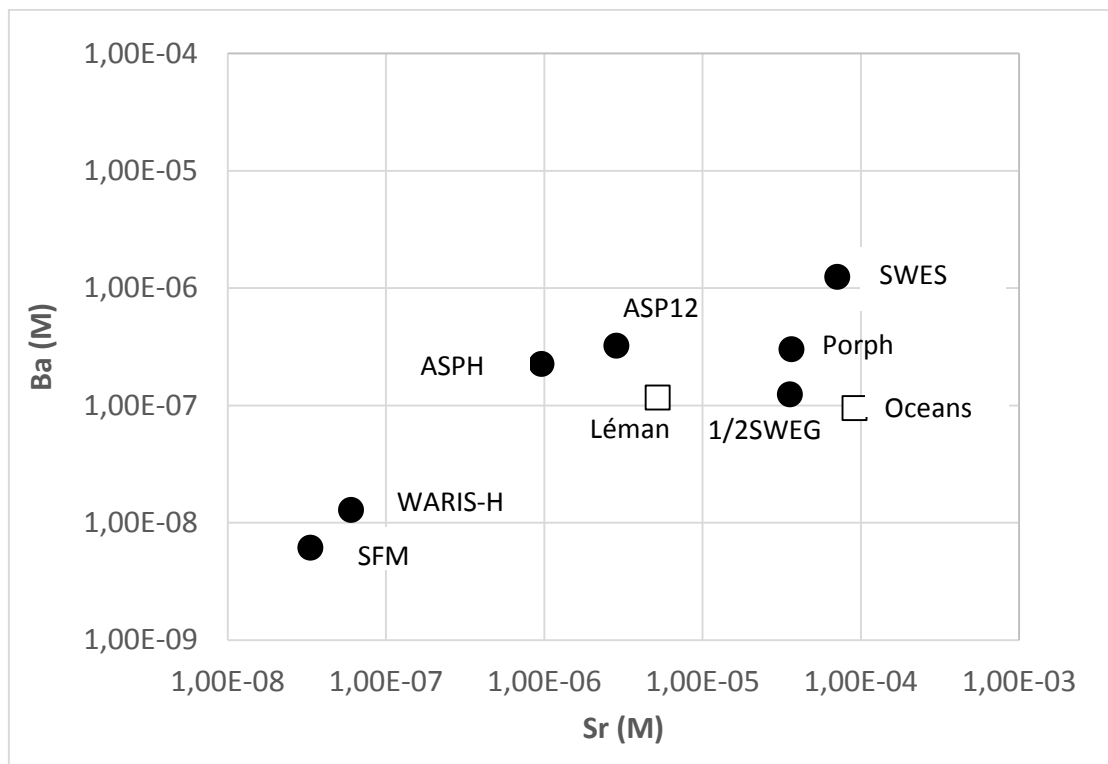
Figure S9: Growth media Sr and Ba concentrations.

Black dots: culture media; white squares: natural waters. Lake Geneva (Jaquet et al. 2013) and oceans (Bruland and Lohan, 2003). Notice the log scale.

References:

Bruland, K.W. and Lohan, M.C.: Controls of Trace Metals in Seawater, In: Treatise on Geochemistry, Volume 6. Elsevier, chapter 6.02, 2003.

Martignier, A., Pacton, M., Filella, M., Jaquet, J. M., Barja, F., Pollok, K., Langenhorst, F., Lavigne, S., Guagliardo, P., Kilburn, M. R., Thomas, C., Martini, R. and Ariztegui, D.: Intracellular amorphous carbonates uncover a new biomineralization process in eukaryotes, Geobiology, 15, 240–253, doi:10.1111/gbi.12213, 2017.

Provider	Internet address
CCAC Culture Collection of Algae at the University of Cologne	http://www.ccac.uni-koeln.de/sidebar/growth-media/
SAG Sammlung von Algenkulturen at the University of Göttingen	http://www.uni-goettingen.de/en/list+of+media+and+recipes/186449.html
AC Algobank Caen University	https://www.unicaen.fr/algobank/infos/recettes.html

Table S1: Sources of the composition of culture media.

	algal collection	dilution	Sr88(LR) [ppb]	Ba138(L) [ppb]	Sr [M]	Ba [M]	Sr /Ca
Blank - MilliQ_Ge	-		2,48	2,71			
Blank - H2O	CCAC		0,68	0,37			
Blank - MilliQ	SAG		23,43	4,14			
Temoin_10ppb	-		9,89	9,83			
Temoin_100ppb	-		99	103,06			
Waris_H	CCAC		5,27	1,77	6.01E-08	1.29E-08	**1.42E-04**
SFM	CCAC		2,91	0,84	3.32E-08	6.12E-09	**1.58E-04**
1_2_SWEG	SAG		3122,6	17,11	3.56E-05	1.25E-07	**6.77E-03**
ASP-12	CCAC	100	249,47	44,42	2.85E-06	3.23E-07	**2.71E-04**
ASP-H	CCAC	100	84,22	31,09	9.61E-07	2.26E-07	**3.84E-04**
Porph	SAG	100	3196,8	41,38	3.65E-05	3.01E-07	**6.93E-03**
SWES	SAG	100	6201,34	170,84	7.08E-05	1.24E-06	**6.72E-03**

Table S2: Concentration of Sr and Ba measured in the growth media.

Sr and Ba: ICP-MS data.Ca concentrations were calculated based on the media theoretical composition. CCAC: Culture Collection of Algae at the University of Cologne (Germany); SAG: Sammlung von Algenkulturen of the University of Göttingen (Germany); Algobank: culture collection of microalgea of the University of Caen (France). Media ES (Algobank) and Diat (SAG) were not available for analysis.

Micropearls	cord-F_cc	convol_cc	contract_cc	cord-M_cc	chui_cc	cord_M_sa	cord_Gen	desika_cc	subcord_sa	chui_sa	striata_sa	tetrath_ac	levis_ac	suecica_ac
Ca norm	0.99	0.99	0.99	0.99	0.99	0.98	0.93	0.90	0.83	0.85	0.77	0.72	0.60	0.49
Sr norm	0.01	0.01	0.01	0.01	0.01	0.02	0.07	0.08	0.17	0.15	0.23	0.28	0.40	0.51
Sr/Ca														
N	48	22	23	68	48	21	70	22	42	31	38	33	29	33
Min	0.000	0.000	0.000	0.000	0.000	0.000	0.000	0.000	0.000	0.013	0.042	0.161	0.374	0.490
Max	0.013	0.050	0.015	0.046	0.025	0.087	1.728	0.154	0.611	0.734	0.667	0.631	1.060	2.620
Mean	0.005	0.015	0.006	0.008	0.013	0.019	**0.118**	0.090	0.218	0.199	0.320	0.391	0.701	1.152
Std. error	0.0005	0.0037	0.0010	0.0008	0.0009	0.0041	0.0369	0.0096	0.0183	0.0306	0.0263	0.0181	0.0394	0.0925
Stand. dev	0.0038	0.0175	0.0046	0.0067	0.0064	0.0190	0.3090	0.0449	0.1187	0.1705	0.1618	0.1042	0.2120	0.5311
Median	**0.005**	**0.006**	**0.006**	**0.007**	**0.013**	**0.015**	**0.025**	**0.085**	**0.208**	**0.225**	**0.290**	**0.376**	**0.661**	**1.030**
25 prcntil	0.001	0.000	0.002	0.004	0.010	0.010	0.004	0.060	0.178	0.040	0.179	0.320	0.545	0.735
75 prcntil	0.008	0.030	0.010	0.011	0.018	0.024	0.057	0.133	0.260	0.290	0.476	0.469	0.902	1.465
Coeff. var	73	116	73	81	49	98	262	50	54	85	51	27	30	46
Medium	**SFM**	**ASP-H**	**ASP-H**	**Waris-H**	**ASP-H**	Diat	**Lake water**	**ASP-H**	**Porph Ag**	1/2 SWEg Ag	SWES Ag	**ES**	**ES**	**ES**
Sr/Ca medium	1.58E-04	3.84E-04	3.84E-04	1.42E-04	3.84E-04		4.73E-03	3.84E-04	6.93E-03	6.77E-03	6.72E-03	9.00E-03	9.00E-03	9.00E-03
Sr/Ca mpearls	5.23E-03	5.50E-03	6.28E-03	7.23E-03	1.25E-02	1.48E-02	5.82E-02	8.43E-02	2.08E-01	2.25E-01	2.90E-01	3.76E-01	6.61E-01	1.03E+00

Table S3: Composition statistics for micropearls formed by *Tetraselmis* species.

Composition statistics for 13 Tetraselmis strains micropearls. Values from Lake Geneva (labelled cord_Gen; *Martignier et al. 2017*) are given for comparison. Ca norm, Sr norm: values normalized to 1.0. In the lower part of the table, Sr/Ca ratios of the micropearls (mp) are compared to the ratios in their growth medium (med). Enrichment = [(Sr/Ca mp) / (Sr/Ca med)]. The concentrations for the ES medium (not analyzed) were set as equivalent to standard seawater, ie. Sr=9 10-5 M. Ca=10-2 M, giving a Ratio Sr/Ca= 9 10-3.

References:

Martignier, A., Pacton, M., Filella, M., Jaquet, J. M., Barja, F., Pollok, K., Langenhorst, F., Lavigne, S., Guagliardo, P., Kilburn, M. R., Thomas, C., Martini, R. and Ariztegui, D.: Intracellular amorphous carbonates uncover a new biomineralization process in eukaryotes, Geobiology, 15, 240–253, doi:10.1111/gbi.12213, 2017.

E factor	Strain	Medium	E factor	Environment
	cord_L	Lake Geneva	12	Freshwater
Low	convol_cc	ASP-H	14	Marine symbiotic
	contract_cc	ASP-H	16	Brackish
	subcord_sa	Porph Ag	30	Marine
Mdium	cord-F_cc	SFM	33	Freshwater
	chui_cc	ASP-H	33	Marine
	chui_sa	1/2 SWEg Ag	33	Marine
	tetrath	ES	42	Brackish
High	striata_sa	SWES Ag	43	Marine
	cord-M_cc	Waris-H	51	Freshwater
Very High	desika_cc	ASP-H	219	Marine sand

Table S4: Ranking of the Enrichment (E) factor amongst species.

Enrichment factor (E) was calculated as the molar ratio [(Sr micropearls / Ca micropearls) / (Sr medium / Ca medium)], on the basis of the data shown in Table S2 and Table S3.

References:

Martignier, A., Pacton, M., Filella, M., Jaquet, J. M., Barja, F., Pollok, K., Langenhorst, F., Lavigne, S., Guagliardo, P., Kilburn, M. R., Thomas, C., Martini, R. and Ariztegui, D.: Intracellular amorphous carbonates uncover a new biomineralization process in eukaryotes, Geobiology, 15, 240–253, doi:10.1111/gbi.12213, 2017.

111

Biomineralization capacities of Chlorodendrophyceae: correlation between chloroplast morphology and the distribution of micropearls in the cell *

_____

Agathe Martignier, Sophie De Respinis, Montserrat Filella, Ines Segovia, Kerstin Hoef-Emden, Birger Marin, Gerd Günther, François Barja, Mauro Tonolla, Jean-Michel Jaquet, Michael Melkonian and Daniel Ariztegui

4.1   Abstract

At least ten species of the genus *Tetraselmis* (Chlorodendrophyceae, Chlorophyta) were recently discovered to possess unsuspected biomineralization capacities: they produce multiple intracellular inclusions of near-amorphous calcium carbonate (ACC), called micropearls. Early microscopists had spotted rows of refractive granules in some species, although without identifying their mineral nature. SEM observation showed that the distribution of the micropearls in the cell can form a pattern, which appears to be characteristic for a given species. The present study shows that this pattern results of the chloroplast shape, which differs between several *Tetraselmis* species, because the micropearls align themselves along the incisions between the chloroplast lobes. This was observed both by SEM and in live cells by light microscopy using Nomarski differential interference contrast. Additionally, phylogenetic analyses, of both the rbcL and ITS gene sequences, associate species in groups presenting similar micropearl arrangement patterns. Thus, the micropearl arrangement pattern might constitute a valid criterion to distinguish phylogenetic groups of the genus *Tetraselmis*.

4.2   Introduction

Biomineralization refers to the process by which organisms form minerals (Weiner and Dove 2003). Some organisms can control the mineralization process (nucleation, growth, morphology and final location of the mineral), which generally takes place in an isolated environment (e.g. vacuole, vesicle) corresponding to a site of controlled chemistry (Mann 2001). The biominerals of intracellular origin mostly become extracellular (e.g. the calcium carbonate scales called coccolithes produced by haptophytes, which undergo rapid exocytosis) (Graham et al. 2016; Paasche 2001; Weiner and Dove 2003). In a less frequently used strategy, some biominerals remain in the cell, either procuring an intracellular structure such as the siliceous frustule of diatoms, or becoming an inorganic intracellular inclusion (Konhauser 2007), like the magnetosomes of magnetotactic bacteria (Faivre and Schüler 2008).

Although calcium carbonate minerals are the most abundant biogenic minerals (Weiner and Dove 2003), intracellular inclusions of calcium carbonate in unicellular organisms were generally thought to be rare. Indeed, intracellular calcium carbonate inclusions had been

described only in a few cyanobacteria species (Couradeau et al. 2012; Benzerara et al. 2014), in the giant sulfur bacteria *Achromatium* (Gray 2006; Head et al. 2000) and in several ciliates (Fauré-Fremiet and Gauchery 1957). Nevertheless, an unsuspected biomineralization capacity was recently discovered in at least ten species of the genus *Tetraselmis* (Chlorodendrophyceae, Chlorophyta), in the form of multiple intracellular inclusions of amorphous (or near-amorphous) calcium carbonate (ACC) called micropearls (Martignier et al. 2017, 2018). These biominerals typically present internal concentric zonation and can be enriched in alkaline earth-elements (e.g. Sr, Ba) (Martignier et al. 2017).

Despite thorough descriptions of these *Tetraselmis* species, the detection of the micropearls by electron microscopy had previously been prevented by the fact that micropearls can be easily dissolved by most of the classic preparations of organic samples. Micropearls produced by *Tetraselmis* species were imaged by Scanning Electron Microscopy (SEM), following an unconventional sample preparation (samples simply dried at room temperature) meant for diatom frustule observation in Lake Geneva waters (Switzerland) (Martignier et al. 2017). This discovery suggests that other well-studied organisms might possess similar, yet unsuspected, biomineralization capacities.

Early microscopists had already observed the micropearls, which they described as refractive granules, without identifying their mineral nature. Carter (1938), Hollande et al. (1954) and Butcher (1959) describe longitudinal rows of these granules, which they observed with light microscopy, using Nomarski differential interference contrast (DIC) at high resolution. The granule rows were observed in the interstice between the lobes of the chloroplast in *Tetraselmis tetrathele* by N. Carter (1938), who also noted that they did not stain with iodine. Later, Norris et al. (1980) disregarded the taxonomic value of the granule rows in *Tetraselmis*. In 1993, K. Hoef-Emden (M.Sc. thesis, Univ. of Cologne, unpublished), studying 60 strains of *Tetraselmis* spp., showed that accumulation of these granules frequently occurs at the apical poles of cells (although more rarely at the posterior pole), but is highly variable and partly related to the age of the culture. Martignier et al. (2018) observed that the micropearls tend to form a pattern in the cell, which is characteristic of a given species. They also stated that two *Tetraselmis* species (*T. marina* and *T. ascus*) do not seem to produce micropearls, suggesting a diverging evolution compared to other species of the genus.

It is generally thought that the class Chlorodendrophyceae is composed of only two genera*: Tetraselmis* F. Stein 1878 and *Scherffelia (Perty)* Pascher 1912, although a third genus (*Prasinocladus* Kuckuck 1894) is sometimes also included (Guiry and Guiry 2019). The class

Chlorodendrophyceae is in need of revision and no comprehensive phylogenetic analyses of the class has yet been published.

Many plastid, mitochondrial or nuclear molecular markers have been tested for phylogenetic studies of algae and the plastid encoded *rbc*L gene was often used for this purpose (see Leliaert et al. 2014 for review): the enzyme Ribulose-1,5-Bisphosphate Carboxylase/Oxygenase (RuBisCO) is involved in carbon fixation during photosynthesis of Archaea, Bacteria and Eukarya (Andersson and Backlund 2008; Kellog and Juliano 1997; Raven 1995;). Form I is composed of eight large (L, about 55,000 Da) and eight small (S, about 13,000 Da) subunits encoded respectively by the plastid encoded genes *rbc*L and *rbc*S (in Viridiplantae rbcS has been transferred from the chloroplast to the nucleus). The gene *rbc*L has been widely used as a molecular marker for phylogenetic analysis of algae and embryophytes at the genus and species level (Palmer et al. 1988; Soltis et al. 2000) but it has been rarely used in the Chlorodendrophyceae (Chantzistrountsiou et al. 2016). Another possible marker for phylogenetic analysis is the nuclear-encoded internal transcribed spacer region (ITS1-5.8S-ITS2 = ITS) of the rRNA operon, which is known to be more variable in sequence than the SSU rRNA gene, and has been often used for species-level discrimination and barcoding of algae (Leliaert et al., 2014). The ITS region was applied to phylogenetic analyses of some *Tetraselmis* species isolated from Chile (Gonzalez et al. 2015). It is nevertheless interesting to note a critical evaluation of this concept (Caisová et al. 2011, 2013). To summarize, currently not much is known about the phylogeny of the Chlorodendrophyceae (Arora et al. 2013; Gonzalez et al. 2015).

The present study investigates thirteen species belonging to the class Chlorodendrophyceae (12 *Tetraselmis* and 1 *Scherffelia* species), with the objective of understanding whether their capacity to form micropearls is related to their phylogeny and whether the arrangement of micropearls in the cell can be correlated with the shape of their chloroplast and be regarded as characteristic for a given species or set of species. Each species is represented by a strain obtained from public algal culture collections. DNA sequences (both ITS and rbcL sequences) were compared to reconstruct the phylogenic relationships among the different strains. Micropearl arrangement in each strain was imaged with SEM. Additionally, micropearls were successfully imaged in live cells using Nomarski DIC at high resolution, while the shape of their chloroplasts were investigated by epifluorescence using chlorophyll autofluorescence.

4.3   Samples and methods

4.3.1 Origin of the samples and pre-treatment methods

Samples were obtained from public algal culture collections hosted in three different universities (Table 1). SAG: the Culture Collection of Algae at the University of Göttingen, Germany (http://sagdb.uni-goettingen.de/); CCAC: the Culture Collection of Algae at the University of Cologne, Germany (www.ccac.uni-koeln.de/); Algobank: the Culture Collection of Algae at the University of Caen, France (www.unicaen.fr/algobank/accueil/). Six different culture media have been used (Table 1). The composition of each growth medium is available on the culture collections websites. A single strain of each species was studied, except for *T. chui* (2 strains) and *T. cordiformis* (2 strains).

Preparation of samples for SEM observation was performed upon arrival at the Geneva University laboratory: a few droplets of each culture were filtered with their original medium under low vacuum (< 10 kPa) on polycarbonate filter membranes (pore sizes of 0.2, 1 or 2 µm diameter). The SAG collection (University of Göttingen) provided species grown on solid media, which were diluted immediately before filtration. Resulting filter membranes were dried at room temperature**.**

4.3.2 Scanning electron microscopy (SEM) and energy-dispersive X-ray spectroscopy (EDXS)

The dried filter membranes were pasted with double-sided conductive carbon tape on aluminum stubs. They were coated with 10 nm of gold by low vacuum sputtering. The images and EDXS analyses were acquired with a JEOL JSM 7001F Scanning Electron Microscope (Department of Earth Sciences, University of Geneva, Switzerland). The EDXS detector was an EX-94300S4L1Q model from JEOL and the EDXS semi-quantitative results were calculated using the ZAF correction method.

Cell images were obtained by using backscattered electrons. In this method, the grey levels represent the mean atomic number of the observed material, which produces a high contrast between the mineral inclusions and the surrounding organic matter. Setting for the EDXS measurements were of 15 kV accelerating voltage with a beam current of ~5 nA during an acquisition of 30 seconds per analyze.

4.3.3 Light microscopy observation and epifluorescence.

Micropearls were successfully observed with light microscopy using Nomarski Differential Interference Contrast (NIC) at high resolution. Light microscopy was performed with a Leica DMLB light microscope using a PL-APO 100/1.40 objective, an immersed condenser with N.A. 1.4 and a Metz Mecablitz 32 Ct3 flash system.

The chloroplasts of some cells were observed by epifluorescence using a Leica DMLB light microscope with epifluorescence attachment, objective 100x oil immersion (N.A. 1.40). The blue excitation light (wavelength 455 nm) was provided by a Cree Royal blue LED. The filter was a Long Pass Barrier Filter 515 nm and the camera was a Canon 5D mark2 DLSR.

Figure 1 | Light microscopy images highlighting the micropearls in live cells

Images made by using Nomarski DIC at high resolution. Micropearls appear as white microspheres against the green color of the chloroplast. They are generally arranged along the interstice between the lobes of the chloroplast, and in some species form agglomerations at the apical extremity of the cell (indicated by white arrows), near the apical depression from which the four flagella emerge. The eyespots (or stigma), involved in light perception, are visible as brown-red spots in the cells.

4.3.4 DNA sequencing

DNA was extracted by phenol-chloroform after a pre-treatment with lysozyme (10mg/mL). The Internal Transcribed Spacer region (ITS, including ITS1, 5.8S rDNA and ITS2) was amplified using universal ITS5 and ITS4 primers for eukaryotes (White et al. 1990). The rbcL partial gene was amplified using primers rbcL-1A1B-Fw and rbcL-1A1B-Rev for phytoplankton (Paul et al. 2000). Sequences were aligned using the MEGA 7.0 (Kumar et al. 2016) to construct a phylogenetic tree by Neighbor-Joining method with the Kimura two-parameter distances bootstrapped with 1000 replicates. If existing, the genetically closest sequences from the National Center for Biotechnology Information (NCBI, http://www.ncbi.nlm.nih.gov) were also included in the phylogenetic tree.

4.4   Results

*4.4.1 Imaging of the micropearls in live cells with light microscopy*

Micropearls were successfully imaged in live cells by light microscopy (Fig. 1 and Fig. S1) using Nomarski Differential Interference Contrast (DIC). These images confirm that the micropearls correspond to the refractive granules described by Carter (1938) and Butcher (1959). Figure 1 also shows that the micropearls are located along incisions of the chloroplast, as stated by Carter (1938) and that they are generally located preferentially near the apical side of the cells (*T. chui* and *T. cordiformis* in Fig. 1), sometimes forming apical aggregates of micropearls (white arrows in Fig. 1).

*4.4.2 SEM images of micropearl arrangement in the cells*

In previous studies, Martignier et al. (2018) showed that the distribution of micropearls in *Tetraselmis* cells is not random and forms a pattern, which is characteristic for a given species. Some of these characteristic patterns are similar and can be combined into groups, which are illustrated in Fig. 2.

Although the micropearls can be observed by light microscopy as shown in Fig. 1, SEM imaging of dried cells provides a complementary technique to visualize these patterns: the dried orga-
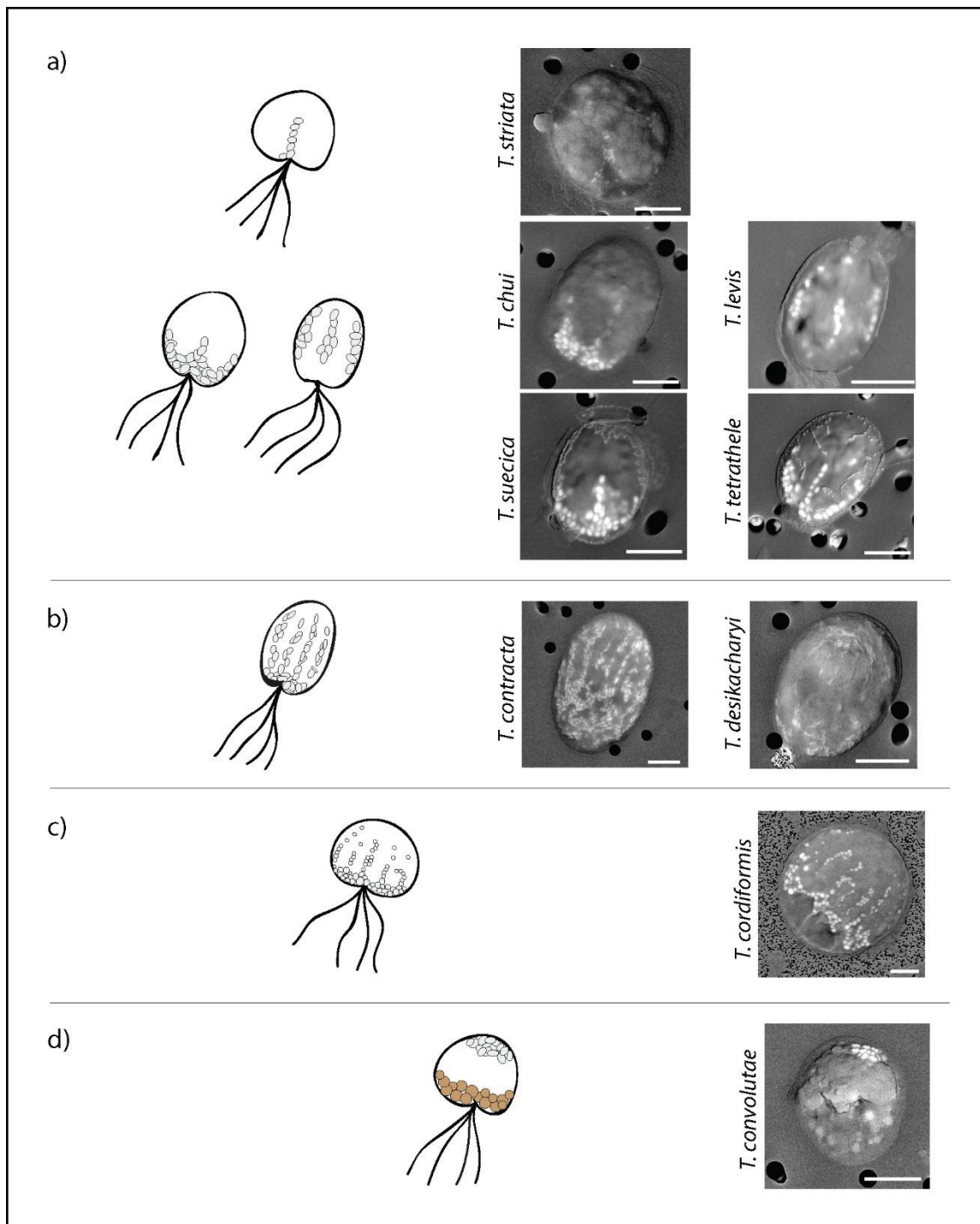
Figure 2 – Main micropearl distribution patterns observed in *Tetraselmis* species

The drawings represent the typical micropearl arrangement pattern for each group: micropearls are in light grey and polyphosphate inclusions in beige. (a) trimerous symmetry (presence apical aggregates and/or trimerous meridians), corresponding to chloroplasts with four apical lobes; (b) apical micropearl aggregation with approx. 8-10 meridians; corresponding to chloroplasts with 8 apical lobes or more; (c) apical micropearl aggregation with short micropearl strings departing towards the basal pole of the cell and a few smaller micropearls scattered elsewhere in the cell, corresponding to net-like chloroplasts; (d) basal micropearl aggregation with apical aggregation of phosphate inclusions (probably polyphosphates), corresponding to cup-shaped chloroplasts. The examples are SEM backscattered images. Micropearls appear in white or light grey embedded in the darker organic matter. Larger polyphosphate inclusions appear in mid-grey tones. The black dots at the back are filter pores. Strain numbers: see Table 1. Scale bars: 5 μm.
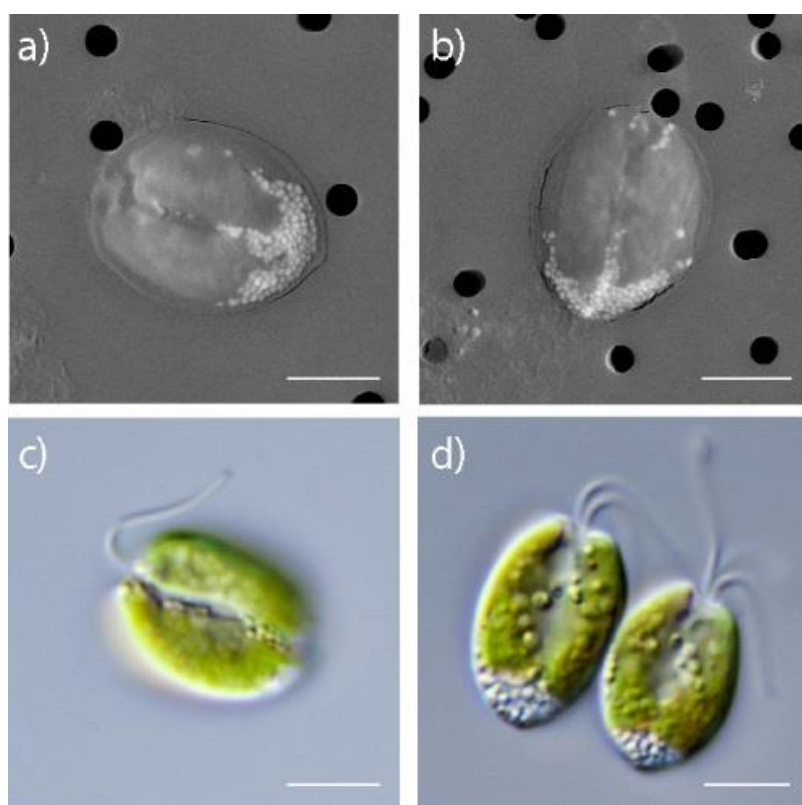
Figure 3 – Micropearls in *Scherffelia dubia*

Top line: SEM backscattered images of *Scherffelia dubia*. The micropearls appear in white against the darker organic matter. The pores of the filter appear in black in the background. Bottom line: light microscope images of *Scherffelia dubia*. The micropearls appear in white against the green chloroplast. Strain number: CCAC 0019. Scale bars: 5 μm.

-nic matter is flattened by desiccation, creating an approximate 2D projection of the location of micropearls within the cell. Figure S1 also illustrates this feature by systematically comparing light microscopy and SEM images for seven different *Tetraselmis* species.

SEM observation of *Scherffelia dubia* revealed that this species, belonging to the second genus of the Chlorodendrophyceae, also produces micropearls (Fig. 3). We have noted that the micropearls of this freshwater species are spherical, similar to the micropearls of *Tetraselmis cordiformis*, the only other (yet) identified freshwater species forming micropearls. In comparison, the micropearls of the marine species of *Tetraselmis* are more elongated ("rice grain" shapes), particularly in *T. contracta* and *T. desikacharyi* (Martignier et al. 2018).

Preliminary results of an ongoing study with new cultures show that in most *Tetraselmis* species, if micropearls are present in the cell, aggregates are frequently observed at the apical pole of the cell, close to the depression from which the flagella emerge. Some micropearls may also form longitudinal alignments, which are not always present (Fig. S2). Thus, the micropearl arrangement in the cell varies to some extent as previously observed by Hoef-Hemden (1993, unpublished). Nevertheless, when micropearl alignments are present, they will appear according to the arrangement pattern, which is characteristic of the species (Fig. 2).

4.4.3 Images of the natural chlorophyll fluorescence of the chloroplasts

Although the incisions of the chloroplast can also be observed in DIC light microscopy (Fig. S3), the observation of the autofluorescence of the chloroplasts by epifluorescence provides a better overview of their different shapes in the different *Tetraselmis* species (Fig. 4). For example, *Tetraselmis chui, striata* and *suecica* show similar four-lobed chloroplast, while *T. convolutae* clearly presents a cup-shaped chloroplast. Four incisions can be observed on the upper side of the *T. desikacharyi* cell illustrated in this figure, highlighting the numerous lobes of its chloroplast.
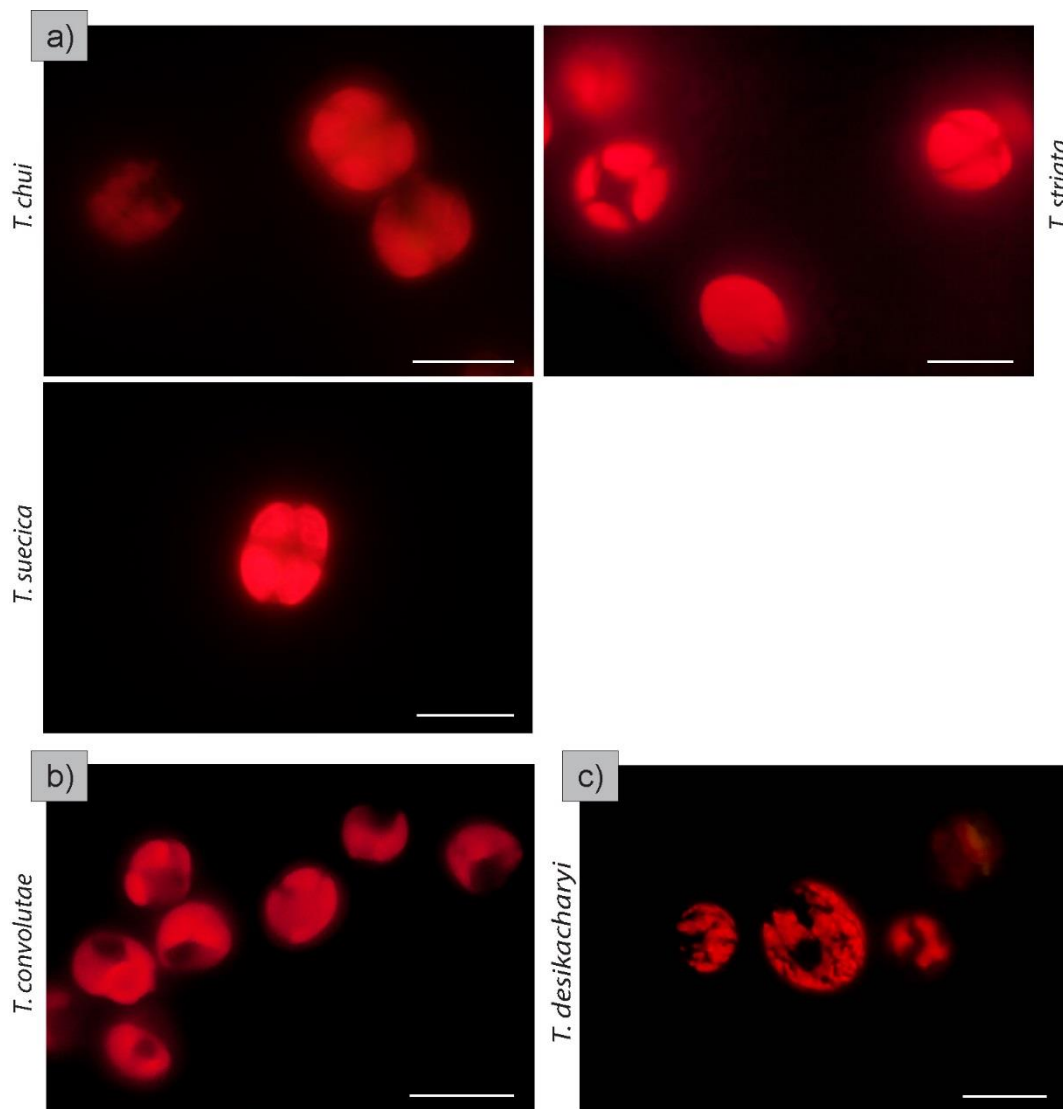
Figure 4 – Different chloroplast shapes observed in *Tetraselmis* species

Epifluorescence images reveal the chloroplast shape of different *Tetraselmis* species, due to the autofluorescence of the chlorophyll. (a) Species with four-lobed chloroplasts. (b) *T. convolutae* presents a cup-shaped chloroplast (c) The chloroplast of *T.desikacharyi* shows multiple lobes, highlighted by four incisions (separating the lobes) which are clearly visible on this side of the cell. Scale bar: 10 μm.

4.4.4 Molecular phylogenetic analysis of the studied species of Chlorodendrophyceae

Phylogenetic analyses of the ITS sequences separated the *Tetraselmis* species in three distinct clades (Fig. 5). The first one contains only *T. cordiformis*, the only freshwater species of the genus. It is clearly divergent from the other species. The second clade includes two *Tetraselmis* species: *T. marina* and *T. ascus*. Finally, the last clade is composed of 10 *Tetraselmis* strains and *Scherffelia dubia*. *S. dubia* is clearly separated from the large group of *Tetraselmis* species, which form two subclades (Fig. 5). Within the two subclades, ITS sequences of the strains are almost identical.

Phylogenetic analyses of the rbcL sequences showed no resolution at the basal branches but identified some monophyletic lineages (Fig. 6): one clade consisted of the *T. marina/T. ascus* sequences, the second clade consisted of 5 *Tetraselmis* strains including *T. chui*, and the third clade again of 5 strains including *T. suecica/T. striata*. The two strains of *T. cordiformis* also formed a clade (Fig. 6).

All other strains of *Tetraselmis* formed single branches with unresolved relationships. With respect to these three clades, the ITS2 and rbcL phylogenies were congruent.

4.5 Discussion

*4.5.1 A biomineralization capacity present in all the Chlorodendrophyceae*

According to Melkonian and Preisig (1986), there are only two genera in the Chlorodendrophyceae: *Scherffelia* and *Tetraselmis*. The present results show that micropearls occur in both of them, demonstrating that all Chlorodendrophyceae potentially have this biomineralization capacity and suggesting that the last common ancestor of the two genera also possessed the capacity to produce micropearls.

The functional role of the micropearls might be linked to motility, flagellar shedding and regeneration as well as scale formation and stability (Melkonian 1982; Salisbury et al. 1984; Reize and Melkonian 1987). Salisbury et al. (1984), in their study on *T. striata*, stated that "the striated flagellar roots are simple ion-sensitive contractile organelles composed predominantly of 20,000 Mr calcium-binding phosphoprotein and (…) this protein is largely responsible for the motile behavior of these organelles". Their article described for the first
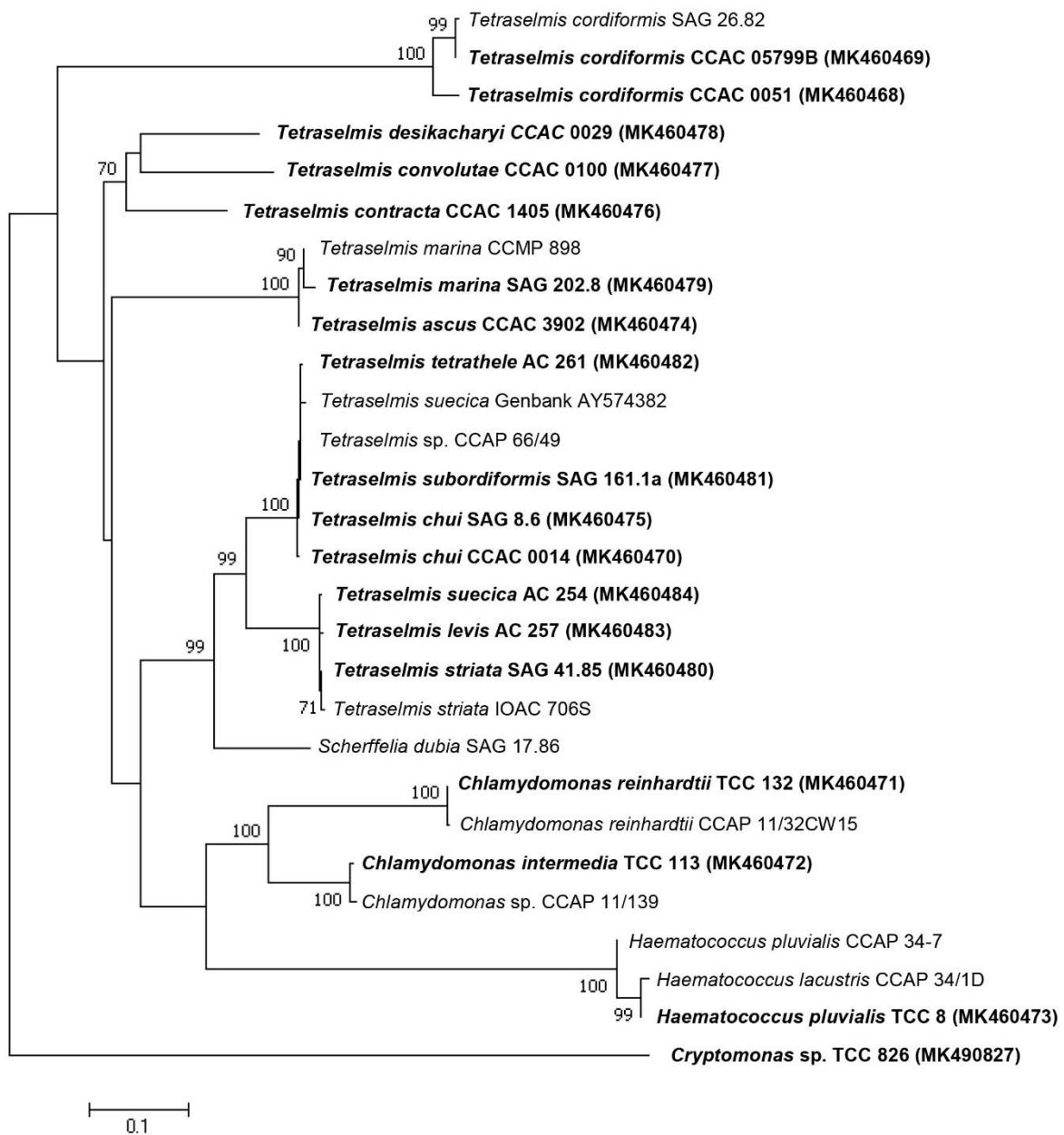
Fig. 5 – Phylogenetic tree of Chlorodendrophyceae inferred from ITS sequences.

Constructed by using the "Neighbor joining" method. The ITS sequences produced during the present study appear in bold characters. The others come from databases.
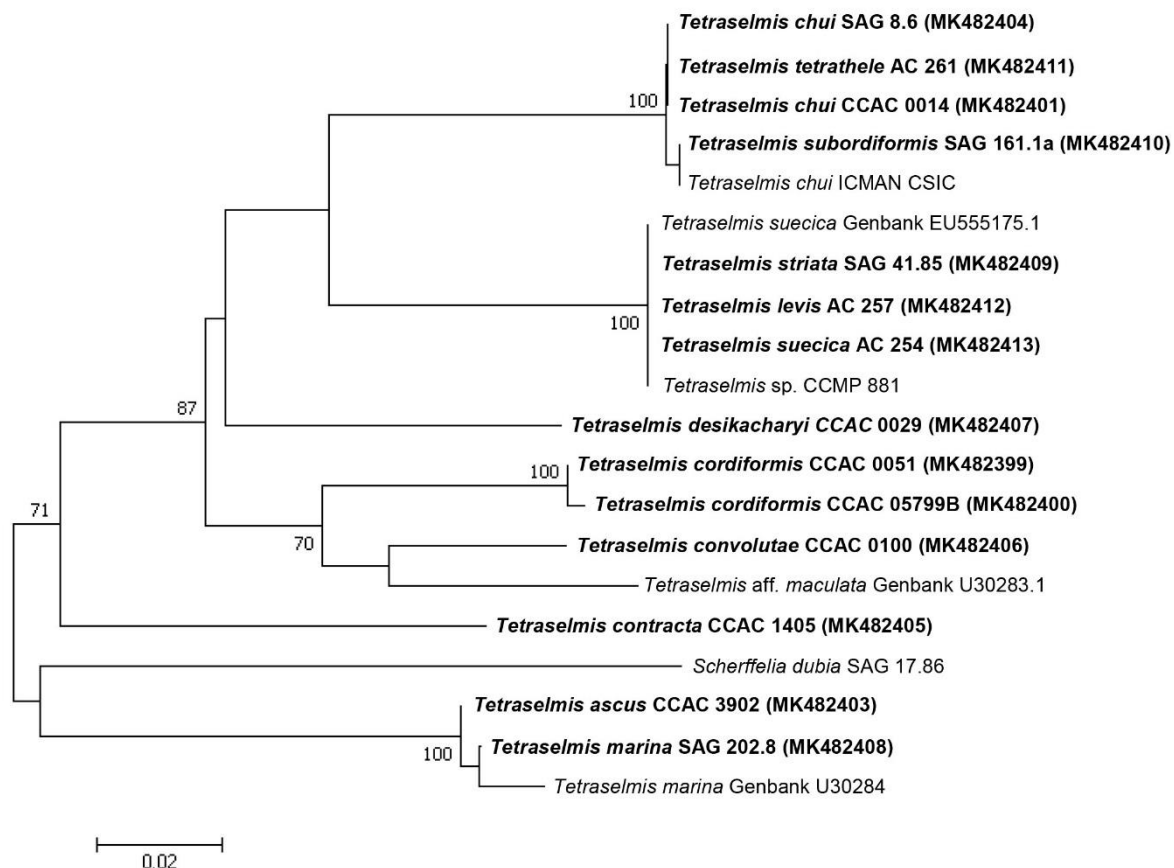
Fig. 6 – Phylogenetic tree of Chlorodendrophyceae inferred from rbcL sequences.

Constructed by using the "Neighbor joining" method. The rbcL sequences produced during the present study appear in bold characters. The others come from databases.

---

time in the striated flagellar roots/rhizoplasts of *T. striata* an EF-hand Calcium-binding protein involved in motility of eukaryotic flagellate organisms and associated with basal bodies/centrioles, later named centrins. Centrins are now known to be a family of calcium-binding phosphoproteins, which are present in many organisms including humans. They are required for the duplication of centrioles (Salisbury et al. 2002) and may play a role in severing microtubules (Sanders and Salisbury 1994). Interestingly, centrin has also been found in the basal body complexes of *Scherffelia dubia* (Bhattacharya et al. 1993), another species producing micropearls (Fig. 3). Given the location of the micropearl aggregate in most of the observed species, which is close to the flagellar apparatus, we suggest that the micropearls could play a role as calcium storage in the Chlorodendrophyceae, in relation with the different roles calcium plays in their metabolism along their life cycle history.

4.5.2 The distribution of the micropearls in the cell is linked to the chloroplast morphology

Most *Tetraselmis* species present an apical aggregate of micropearls, but some of the micropearls can also form additional longitudinal alignments in the cell (Fig. S2). These "meridians" draw the main lines of the species-characteristic pattern described by Martignier et al. (2018). The light microscopy images of micropearls in live cells, shown in this study by Nomarski DIC at high resolution (Fig. 1 and Fig. S1), confirm that these meridians are the result of micropearls aligned along the incisions between the chloroplast lobes. Carter (1938) was apparently the first to observe the micropearls in the light microscope. She had already suggested that the arrangement of these "refractive granules", as she called them, depended on the shape of the chloroplast. Indeed, the shape of the chloroplast is known to differ in some *Tetraselmis* species (Table S1). The epifluorescence images depicted in Fig. 4 provide a clear documentation of the chloroplast morphology in some of the studied species.

The comparison between Fig. 2 and Fig. 4 supports, for these 5 species, the hypothesis that micropearl arrangement correlates with the shape of the chloroplast. More specifically, we can state that the species presenting four-lobed chloroplasts (*T. striata*, *T. chui*, *T. levis*, *T. suecica and T. tetrathele*) all have a micropearl arrangement presenting a trimerous symmetry (*i.e.* trident shape or three equidistant lines, see Fig. 2), representing micropearls aligned along incisions between the chloroplast lobes. The fourth line of micropearls is "hidden", underneath the flattened cell. The only exception is *T. striata*: we suggest that this is due to the cell morphology, which allows only one (or two) of the very thin micropearl alignments to be visible at the same time in SEM images (Fig. 2). The chloroplast of both *T. desikacharyi* (Fig. 4) and *T.contracta* presents more than eight lobes, which corresponds to the numerous meridians of micropearls forming the characteristic patterns of these species (Fig. 2). The net-like chloroplast of *Tetraselmis cordiformis* (Table S1) causes the apical aggregate of this species to be accompanied by scattered micropearls, sometimes added of small micropearl alignments (Fig. 2), which may even form volutes. Finally, the well-delimited micropearl aggregate of *T. convolutae* (Fig. 2) generally seems to be located at the posterior end of the cell, at the "top" of the cup-shaped chloroplast (Fig. 4), while the anterior end is occupied by large polyphosphate vacuoles.

Accordingly, the trident pattern formed by the micropearls inside the cell of *Scherffelia dubia* (Fig. 3) suggests a four-lobed chloroplast (confirmed by transmission electron microscopy (Melkonian and Preisig 1986)), which might be the ancestral situation in the Chlorodendrophyceae. It must be noted that the cell shape of *S. dubia* (Fig. 3) suggests that

the micropearls, in this species, are aggregated in the basal part of the cell rather than in the apical part, unlike most *Tetraselmis* species.

4.5.3 Clade-specific micropearl patterns

The phylogenetic trees produced by the analysis of the ITS (Fig. 5) and the rbcL sequences (Fig. 6) differ somewhat. Nevertheless, it must be highlighted that three clusters of sequences are identically grouped in both trees, suggesting a particularly strong genetic similarity inside each group. The first is composed only of *T. ascus* and *T. marina*, which is interesting as these two species are the only ones described by Martignier et al. (2018) not to produce any micropearls. The second group is the sub-clade containing *T. suecica/T. striata* and the third is the sub-clade containing *T. chui* and *T. tetrathele* (see part 4.4.4), both showing an arrangement pattern of micropearls that follows a trimerous symmetry (Fig. 2). In the ITS phylogeny the two latter subclades were recovered as sister lineage with strong support (Fig.5).

In general, our results suggest that the non-random patterns of micropearl distribution in the Chlorodendrophyceae (Figs 2 and 3) reflect the chloroplast morphology (Fig. 4). In turn, figure 7 illustrates the strong correlation between the groups formed by species with similar micropearl arrangement patterns and the clades resulting of their phylogenetic position (Fig. 5). This consequently means that the chloroplast shape differs between each phylogenetic clades of the genus *Tetraselmis*. Thus, we suggest that the micropearl arrangement pattern, when present, may be characteristic enough to constitute a valid criterion allowing to distinguish some of the different phylogenetic groups of the genus *Tetraselmis* (*e.g.* the "*suecica-tetrathele*" clade). Even considering the variations of the micropearl distribution pattern during a cell's life cycle (Fig. S2), when the micropearl alignments are present, the micropearl distribution pattern of a given clade is clearly distinct from the pattern of other clades.

The position of *Scherffelia dubia* in the phylogenetic tree inferred from ITS sequence analyses is worth noting (Figs 5 and 7). Indeed, although it does not belong to the *Tetraselmis* genus, *S. dubia* appears as the closest species to the "*suecica-tetrathele*" clade (which includes all the
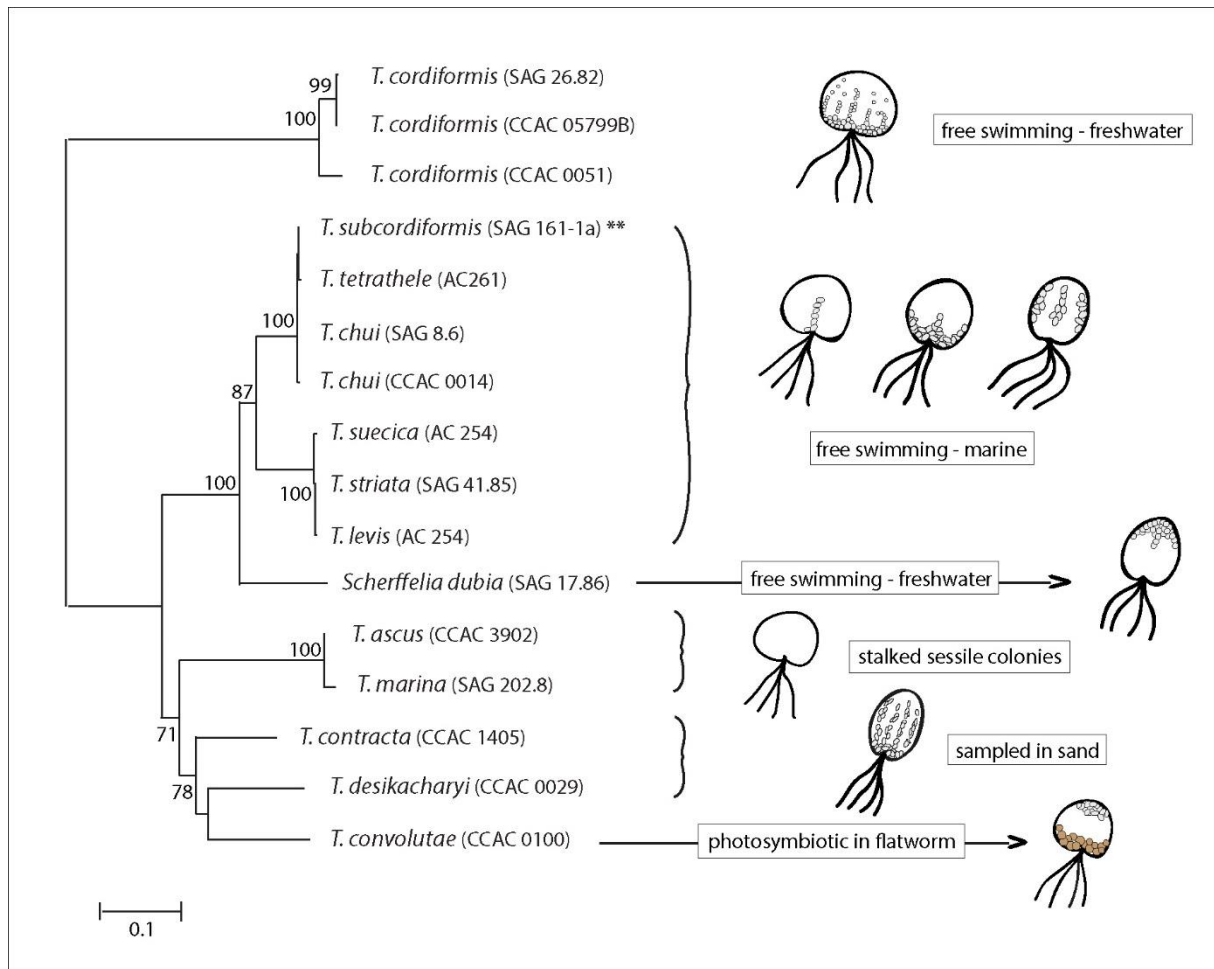
Fig. 7 – Correspondence between the phylogenetic tree based on ITS sequence analyses and the micropearls distribution in the cells.

The asterisks following *T. subcordiformis* signal that this specie is the only one in which the micropearl distribution could not be clearly identified. The text boxes add information on the habitat of the different species. Compared to the original ITS phylogenetic tree (Fig. 5), this figure only contains the Chlorodendrophyceae sequences produced during this study, apart from the *Scherffelia dubia* sequence, taken from Genbank.

species displaying a trimerous symmetry in their micropearl arrangement pattern). The fact that the micropearl arrangement pattern of *S. dubia* is precisely of the same symmetry (Fig. 3) suggests that this arrangement could be ancestral in the Chlorodendrophyceae. This is corroborated by the observation that species of the early-diverging prasinophyte genus *Pyramimonas* (e.g. *P. orientalis*, Carter 1938) also exhibits a trimerous symmetry of refractive granules, which may correspond to micropearls.

4.5.4 Evolution linked with habitat constraints?

Interestingly, the *Tetraselmis* species sharing the same micropearls arrangement patterns (most of which correspond to distinct clades Fig. 7) share the same habitat (Table 1). All members of the *suecica-tetrathele* clade (*T. tetrathele, T. suecica, T. subcordiformis, T. chui*, *T. striata* and *T. levis)* live as free-swimming phytoplankton in the marine environment (Guiry and Guiry 2019; John et al. 2002). The two members of the *ascus-marina* clade are the only species mentioned by Martignier et al. (2018) not to produce micropearls and both live as stalked sessile colonies (Norris et al. 1980). *T. cordiformis*, which forms a clearly divergent clade is the only freshwater species of the genus (Ettl 1983; Melkonian 1979). Finally, *T. desikacharyi* and *T. contracta* were both sampled as benthic organisms in sand (Marin et al. 1996, http://www.ccac.uni-koeln.de/), while *T. convolutae* lives as a photosymbiont in a flatworm (Muscatine et al. 1974). We must therefore consider the possibility that the habitat of these organisms has a link with the morphology of their chloroplasts and the distribution of the micropearls inside the cells. The correlations between these characteristics and the phylogenetic position of the species studied poses the question of a possible genetic basis for the distributions of micropearls and functional implications in relation to habitat constraints met by the different *Tetraselmis* species.

4.6 Conclusions

The recently discovered biomineralization capacities of 10 *Tetraselmis* species is shown here to be shared by at least one species of the genus *Scherffelia* (*S. dubia*), and thus potentially extends to the whole class Chlorodendrophyceae. The numerous intracellular inclusions of near-amorphous calcium carbonate (ACC), called micropearls, can be observed by light microscopy in live cells using Nomarski differential interference contrast (DIC) at high resolution, corroborating previous SEM observations. The present results show that this pattern correlates with the different shapes of the chloroplasts in diverse strains/species, because the micropearl alignments follow the incisions between the chloroplast lobes. Thus, although the arrangement of micropearls has been shown to vary to some extent, when the alignments are expressed, they will form the pattern characteristic for a given species. Moreover, we highlight a correlation between the distribution of micropearls and the phylogenetic position of the studied species of Chlorodendrophyceae, as exemplified by ITS and rbcL phylogenies. When present, the pattern of micropearl arrangements therefore may

be used as one criterion to distinguish some of the phylogenetic groups in the genus *Tetraselmis*. It is also interesting to note that species presenting similar micropearls arrangement share the same habitat, which hints towards a possible influence of the habitat constraints on a genetic-based distribution of the micropearls in the cells.

4.7   References

Andersson I, Backlund A (2008) Structure and function of Rubisco. Plant Physiol Biochem 46:275-291

Arora M, Anil AC, Leliaert F, Delany J, Mesbahi E (2013) Tetraselmis indica (Chlorodendrophyceae, Chlorophyta), a new species isolated from salt pans in Goa, India, Eur J Phycol, 48:61-78, doi:10.1080/09670262.2013.768357

Benzerara K, Skouri-Panet F, Li J, Ferard C, Gugger M, Laurent T, Couradeau E, Ragon M, Cosmidis J, Menguy N, Margaret-Oliver I, Tavera R, Lopez-Garcia P, Moreira D (2014) Intracellular Ca-carbonate biomineralization is widespread in cyanobacteria. Proc Nat Acad. Sci 111:10933–10938

Bhattacharya D, Steinkötter J, Melkonian M (1993) Molecular cloning and evolutionary analysis of the calcium-modulated contractile protein, centrin, in green algae and land plants. Plant Mol Biol 23:1243-1254

Butcher RW (1959) An introductory account of the smaller algae of British coastal waters Part I: introduction and Chlorophyceae. Fish Investig 4:1-74

Caisova L, Marin B, Melkonian M (2011): A close-up view on ITS2 evolution and speciation - a case study in the Ulvophyceae (Chlorophyta, Viridiplantae). BMC Evol Biol 11:262, doi:10.1186/1471-2148-11-262

Caisová L, Marin B, Melkonian M (2013): A consensus secondary structure of ITS2 in the Chlorophyta identified by phylogenetic reconstruction. Protist 164:482-496, doi:10.1016/j.protis.2013.04.005

Carter N (1938) New or interesting algae from brackish water. Arch Protistenk 90:1-68

Chantzistrountsiou X, Tzovenis I, Parmakelis A, Economou-Amilli A (2016) Characterization of *Tetraselmis verrucosa* f. *rubens* (Chlorodendrophyceae) strains from coastal lagoons of Western Greece using a multivariate approach. Phytotaxa 278:225-240

Couradeau E, Benzerara K, Gérard E, Moreira D, Bernard S, Brown GE Jr, López-García P (2012). An early-branching microbialite cyanobacterium forms intracellular carbonates. Science 336:459–462.

Ettl H (1983) Chlorophyta I Phytomonadina. Süsswasserflora von Mitteleuropa. Springer, vol 9, pp 141–149

Faivre D, Schüler D (2008) Magnetotactic bacteria and magnetosomes. Chem Rev 108:4875-4898

Fauré-Fremiet E, Gauchery M (1957) Concrétions minerals intracytoplasmiques chez les ciliés. Journ Protozool 4:96-109

Gray ND (2006) The unique role of intracellular calcification in the genus *Achromatium*. Microbiol Monographs 1: 299-309

Gonzalez MA, Aguayo PA, Inostroza IL, Castro PA, Fuentes GA, Gomez PI (2015) Ultrastructural and molecular characterization of *Tetraselmis* strains (Chlorodendrophyceae, Chlorophyta) isolated from Chile. Gayana Bot 72:47-57

Graham LE, Graham JM, Wilcox LW, Cook ME (2016) Algae (Third Edition). LJLM Press, Madison, Wisconsin, ISBN 978-0-9863935-3-2

Guiry MD, Guiry GM (2019) AlgaeBase, World-wide Electron. Publ Natl Univ Ireland, Galway. http://www.algaebase.org, searched on: 03 February 2019

Head IM, Gray ND, Howarth R, Pickup RW, Clarke KJ, Jones JG (2000) *Achromatium oxaliferum*: understanding the unmistakable. Adv In Microbiol Ecology 16:1-40

Hollande A, Enjumet M, LaFaurie F (1954) Contribution a l'étude des Volvocales: études des genres Platymonas West et Stephanoptera Dangeard. Ann Scie nat Zool 16 :283-292

John DM, Whitton BA, Brook AJ (2002) The freshwater algal flora of the British Isles: an identification guide to freshwater and terrestrial algae. Natural History Museum (London) and British Phycological Society, Cambridge University Press, London

Kellogg EA, Juliano ND (1997) The structure and function of RuBisCO and their implications for systematic studies. Am J Bot 84:413-428

Konhauser K (2007) Introduction to Geomicrobiology. Blackwell Publishing, Oxford, 425 p

Kumar S, Stecher G, Tamura K (2016) MEGA7: Molecular Evolutionary Genetics Analysis Version 7.0 for Bigger Datasets. Mol Biol and Evol 33:1870–1874, doi:10.1093/molbev/msw054

Leliaert F, Verbruggen H, Vanormelingen P, Steen F, Lopez-Bautista JM, Zuccarello GC, De Clerck O (2014) DNA-based species delimitation in algae. Eur J Phycol 49:179-196

Mann S (2001) Biomineralization: Principles and concepts in bioinorganic materials chemistry. Oxford University Press, New York, 198 p

Marin B, Hoef-Emden K, Melkonian M (1996) Light and electron microscope observations on *Tetraselmis desikacharyi* sp. nov. (Chlorodendrales, Chlorophyta). Nova Hedwigia Beih. 112: 461–475

Martignier A, Pacton M, Filella M, Jaquet JM, Barja F, Pollok K, Langenhorst F, Lavigne S, Guagliardo P, Kilburn MR, Thomas C, Martini R, Ariztegui D (2017) Intracellular amorphous carbonates uncover a new biomineralization process in eukaryotes. Geobiology 15:240–253

Martignier A, Filella M, Pollok K, Melkonian M, Bensimon M, Barja F, Langenhorst F, Jaquet JM, Ariztegui D (2018) Marine and freshwater micropearls: biomineralization producing strontium-rich amorphous calcium carbonate inclusions is widespread in the genus *Tetraselmis* (Chlorophyta). Biogeosciences 15: 6591-6605

Melkonian M (1979) An ultrastructural study of the flagellate *Tetraselmis cordiformis* Stein (Chlorophyceae) with emphasis on the flagellar apparatus. Protoplasma 98:139–151

Melkonian M (1982) Effect of divalent cations on flagellar scales in the green flagellate *Tetraselmis cordiformis*. Protoplasma 111:221-233

Melkonian M, Preisig HR (1986) A light and electron microscopic study of *Scherffelia dubia*, a new member of the scaly green flagellates (Prasinophyceae). Nord J Bot 6:235-256

Muscatine L, Boyle JE, Smith DC (1974) Symbiosis of the acoel flatworm *Convoluta roscoffensis* with the alga *Platymonas convolutae*, P R Soc B, 187, pp 221–234

Norris RE, Hori T, Chihara M (1980) Revision of the genus *Tetraselmis* (Class Prasinophyceae). Bot Mag Tokyo 93:317–339

Paasche E (2001) A review of the coccolithophorid *Emiliania huxleyi* (Prymnesiophyceae), with particular reference to growth, coccolith formation, and calcification-photosynthesis interactions. Phycologia 40:503-529

Palmer JD, Jansen RK, Michaels HJ, Chase MW, Manhart JR (1988) Chloroplast DNA variation and plant phylogeny. Ann Missour Bot Garden 75:1180-1206

Paul JH, Alfreider A, Wawrik B (2000) Micro- and macrodiversity in rbcL sequences in ambient phytoplankton populations from the southeastern gulf of Mexico. Mar Ecol Prog Series 198:9-18

Raven JA (1995) Inorganic carbon assimilation by marine biota. J Exp Mar Biol Ecol 203:39-47

Reize IB, Melkonian M (1987): Flagellar regeneration in the scaly green flagellate *Tetraselmis striata* (Prasinophyceae): regeneration kinetics and effect of inhibitors. Helgol Meerersunters 41:149-164

Salisbury JL, Baron A, Surek B, Melkonian M (1984) Striated flagellar roots: isolation and partial characterization of a calcium-modulated contractile organelle. doi:10.1083/jcb.99.3.962

Salisbury JL, Suino KM, Busby R, Springett M (2002) Centrin-2 is required for centriole duplication in mammalian cells. Curr. Biol. 12:1287–92

Sanders MA, Salisbury JL (1994) Centrin plays an essential role in microtubule severing during flagellar excision in *Chlamydomonas reinhardtii*. J Cell Biol 124: 795-805

Soltis ED, Soltis PS, Chase MW, Mort ME, Albach DC, Zanis M, Savolainen V, Hahn WH, Hoot SB, Fay MF, Axtell M, Swensen SM, Prince LM, Kress WJ, Nixon KC, Farris JS (2000) Angiosperm phylogeny inferred from 18S rDNA, rbcL, and atpB sequences. Bot J Linn Soc 133:381-461

Weiner S, Dove PM (2003) An overview of biomineralization processes and the problem of the vital effect. Rev Min Geochem 54:1-29

	natural environment	provider (culture collection of algae)	GenBank n° ITS	GenBank n° rbcL
Tetraselmis chui	marine (tide pools and estuaries)	SAG[a] 8.6	MK460475	MK482404
		CCAC[b] 0014	MK460470	MK482401
Tetraselmis contracta	brackish	CCAC[b] 1405	MK460476	MK482405
Tetraselmis convolutae	marine (photosymbiotic in flatworm)	CCAC[b] 0100	MK460477	MK482406
Tetraselmis cordiformis	freshwater	CCAC[b] 0051	MK460468	MK482399
		CCAC[b] 05799B	MK460469	MK482400
Tetraselmis desikacharyi	marine (in sand, bottom of estuary)	CCAC[b] 0029	MK460478	MK482407
Tetraselmis levis	marine (salt marshes / coastal)	Algobank[c] 257	MK460483	MK482412
Tetraselmis striata	marine (brackish water and tide pool above high tide level)	SAG[a] 41.85	MK460480	MK482409
Tetraselmis. subcordiformis	marine	SAG[a] 161.1a	MK460481	MK482410
Tetraselmis suecica	marine (tidal pools and open sea)	Algobank[c] 254	MK460484	MK482413
Tetraselmis tetrathele	brackish	Algobank[c]261	MK460482	MK482411
Scherffelia dubia	freshwater	CCAC[b] 0019	-	-
Tetraselmis ascus	marine (benthic as sessile stalked colonies, with motile stage)	CCAC[b] 3902	MK460474	MK482403
Tetraselmis marina	marine (benthic as sessile stalked colonies, with motile stage)	SAG[a] 202.8	MK460479	MK482408

Table 1 - Studied Chlorodendrophyceae species.

Species without micropearls are listed separately at the bottom of the table. [a] University of Göttingen, Germany: http://sagdb.uni-goettingen.de/. [b] University of Cologne, Germany: www.ccac.uni-koeln.de/. [c] University of Caen, France: www.unicaen.fr/algobank/accueil/. No DNA analyses were performed on *Scherffelia dubia* because its biomineralization capacities were discovered late in the study.

4.8   Supplementary information

Light microscopy   SEM

T. chui

T. contracta

T. convolutae

T. cordiformis
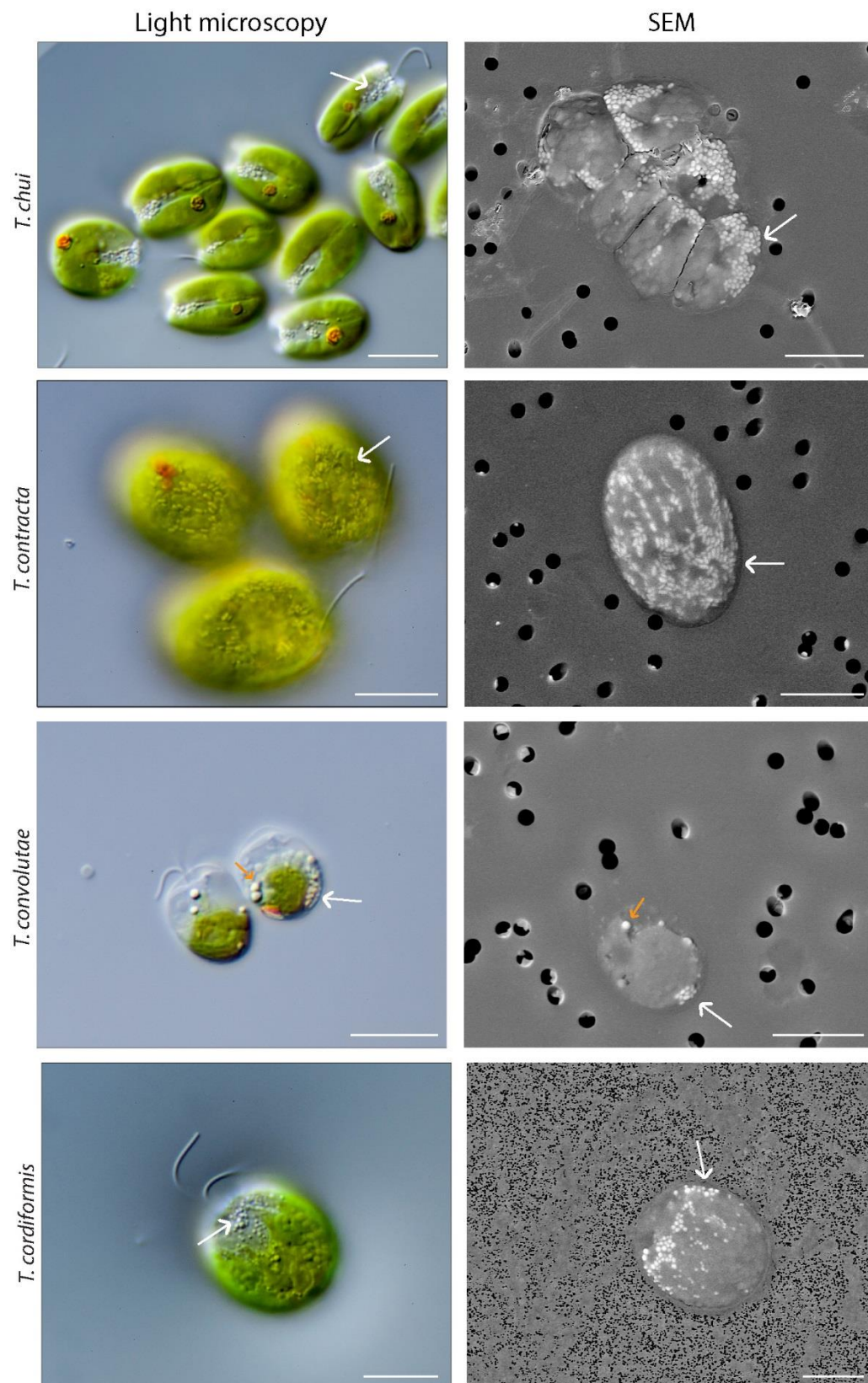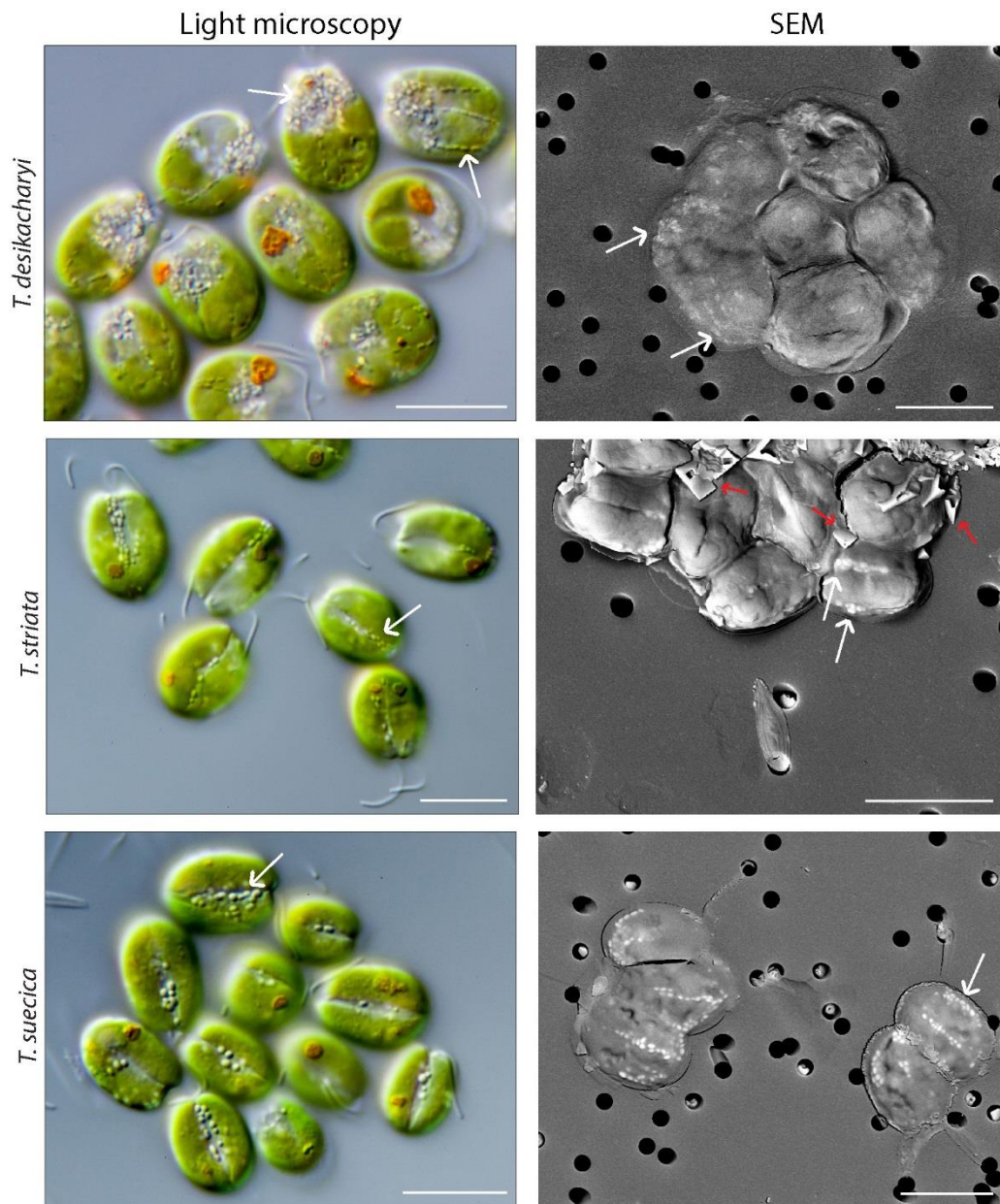
**Figure S1 – Comparison between Light microscopy (DIC) and SEM images.**

In light microscopy images taken with Nomarski differential interference contrast at high resolution, the micropearls appear white (or transparent in the case of *T. contracta* and *T. desikacharyi*) against the green chloroplast. In each image, one or two white arrows points at an example of micropearls. In SEM images, the micropearls appear in white, against the dark grey color of the organic matter. The micropearl arrangement pattern characteristic of each species can be observed in both type of images. Nevertheless, it is easier to observe in SEM images (better contrast) and the collapse due to desiccation allows to see more micropearl alignments at once than in live cells (approximate 2D projection, particularly visible in *T. suecica* and *T. chui*). Small red arrows (in *T. striata*) point at halite crystals (salt). Small orange arrows (in *T. convolutae*) point at large polyphosphate inclusions, often seen in this species alongside the micropearls. Scale bars: 10 µm.
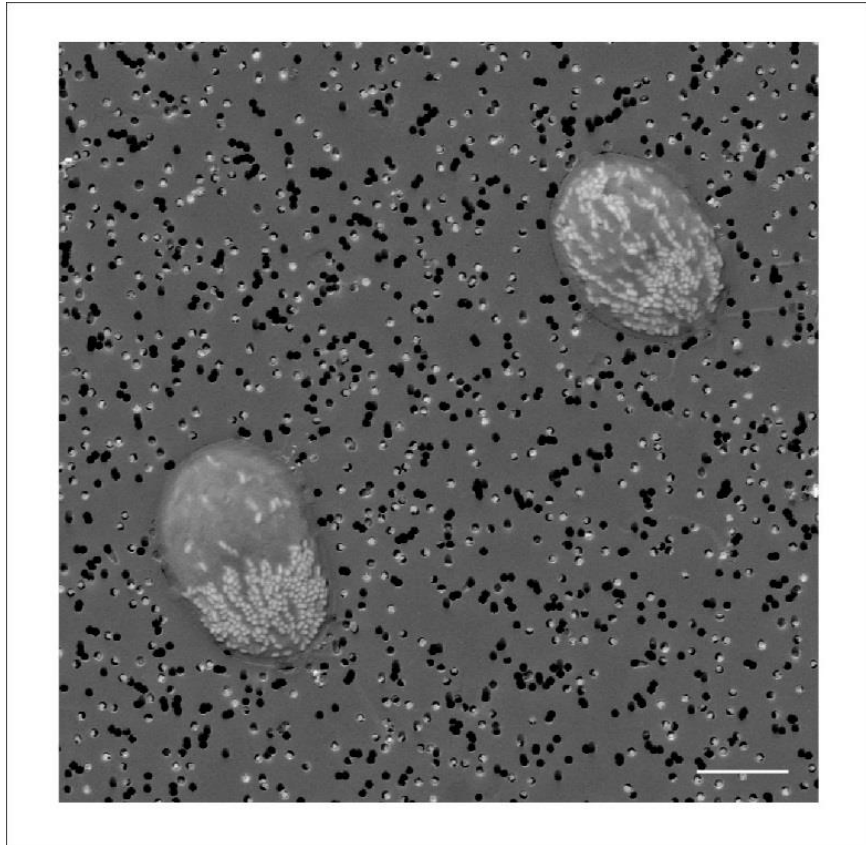
Figure S2 – Different micropearl distribution pattern in a same species.

SEM backscattered images of *Tetraselmis contracta* cells. In this same species, the micropearls either can form an apical aggregate (bottom-left cell) or be aligned along multiple "meridians" (top-right cell). These different micropearl distribution patterns could be linked to different stages in the cell's life cycle. The micropearl distribution pattern observed when the alignments are visible (top-right cell) is characteristic of this species. Scale bar: 10 µm.
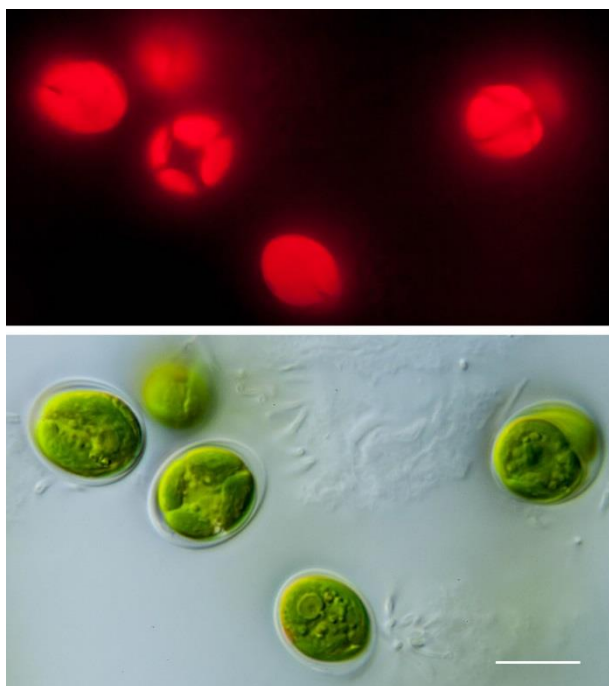
Figure S3 – Comparison of epifluorescence and DIC images of the four-lobed chloroplast of *Tetraselmis striata*

Top image: chlorophyll auto-fluorescence imaging of the chloroplast of *T. striata*. Bottom image: corresponding image in DIC. Scale bar: 5 µm.

Species	chloroplast shape described in literature	references
T. ascus	chloroplast large, forming four lobes extending forward in the anterior half of the cell, becoming reticulate at the level of the pyrenoid in the cell posterior, having four (or more) lobes in the posterior part of the cell	Hori et al. 1982
T. chui	chloroplast finely lobed at the posterior part	Hori et al. 1986
T. contracta	two large and two small apical lobes	Arora et al. 2013 ; Carter 1937 ; Butcher 1959
T. convolutae	unlike other members of the subgenus Tetraselmis, *T. convolutae* has little or no posterior lobing of the chloroplast and little tendency to be reticulate.	Hori et al. 1982
T. cordiformis	chloroplast large, highly reticulate in the posterior regions, having cytoplasmic channels occurring throughout;	Hori et al. 1982 ; Melkonian, 1979 ; Melkonian and Robenek, 1979
T. desikacharyi	cup shaped and divided into more than 6 lobes anteriorly	Arora et al. 2013 ; Marin et al. 1996
T. levis	chloroplast lobed finely in the posterior end	Hori et al. 1986
T. marina	chloroplast massive, almost cup-shaped, located peripherally, with four anterior lobes extending forward into the cell lobes, irregularly lobed posteriorly	Hori et al. 1983
T. striata	chloroplast dorsiventraly lobed into two posterior sections	Hori et al. 1986
T. subcordiformis	a shorter posterior lobe and two lateral lobes	Arora et al. 2013 ; Butcher 1959
T. suecica	chloroplast cup-shaped, usually simple, rarely bilobed in the posterior part	Hori et al. 1986
T. tetrathele	shorter posterior lobe and two lateral lobes	Arora et al. 2013; West 1916; Carter 1937; Butcher 1959

Table S1: Chloroplast morphology of the studied *Tetraselmis* species, as described in the literature.

Species highlighted in grey did not have any micropearls at the time of observation.

References for Table S1

Arora M, Anil AC, Leliaert F, Delany J, Mesbahi E (2013) *Tetraselmis indica* (Chlorodendrophyceae, Chlorophyta), a new species isolated from salt pans in Goa, India. Eur J Phycol 48:61-78

Butcher RW (1959) An introductory account of the smaller algae of British coastal waters Part I: introduction and Chlorophyceae. Fish Investig 4:1-74

Carter N (1937) New or interesting algae from brackish water. Arch Protistenk 90:1-68

Hori T, Norris RE, Chihara M. (1982) Studies on the ultrastructure and taxonomy of the genusTetraselmis (Prasinophyceae): I. Subgenus *Tetraselmis*. Bot Mag Tokyo 95:49

Hori T, Norris RE, Chihara M. (1983) Studies on the ultrastructure and taxonomy of the genusTetraselmis (Prasinophyceae): II. Subgenus *Prasinocladia*. Bot Mag Tokyo 95:49

Hori T, Norris RE, Chihara M (1986) Studies on the ultrastructure and taxonomy of the genusTetraselmis (Prasinophyceae): III. Subgenus *Parviselmis*. Bot Mag Tokyo 99: 123

Marin B, Hoef-Emden K, Melkonian M (1996) Light and electron microscope observations on Tetraselmis desikacharyi sp. nov. (Chlorodendrales, Chlorophyta). Nova Hedwigia Beih. 112: 461–475

Melkonian M (1979) An ultrastructural study of the flagellate *Tetraselmis cordiformis* Stein (Chlorophyceae) with emphasis on the flagellar apparatus. Protoplasma 98:139–151

Melkonian M, Robenek H (1979) The eyespot of the flagellate *Tetraselmis cordiformis* stein (Chlorophyceae): Structural spezialization of the outer chloroplast membrane and its possible significance in phototaxis of green algae. Protoplasma 100: 183

West GS (1916) Algological notes XVIII-XXII. J Bot London 54:1-10

Characterization of the organism(s) producing Ba-rich micropearls in Lake Geneva

_____

5.1 Abstract

Recent studies revealed unsuspected biomineralization capacities of at least 11 species in the class Chlorodendrophyceae (genus *Tetraselmis* and *Scherffelia*). These species produce intracellular inclusions of amorphous (or near-amorphous) calcium carbonate (ACC), called micropearls, which can be enriched in Sr. In Lake Geneva (Switzerland), a different organism, yet unidentified, was described to produce similar mineral inclusions, distinguished clearly by the micropearls' composition which is highly enriched in barium or even reaching the barium carbonate composition (up to > 90 Ba/Ca mol%). The present research introduces the first light microscopy images of this species and describes novel characteristics allowing to precise its phenotype. SEM observations provide new details of its morphology, while epifluorescence showed that its organic matter produces a strong characteristic autofluorescence signal (approx. 580 nm emission). These results allow to restrict the list of potential species corresponding to the organism producing the Ba-carbonate micropearls of Lake Geneva.

5.2 Introduction

Calcium carbonates are the minerals, which most frequently involved in natural biomineralization processes (Weiner and Dove, 2003). Apart from dolomite (for example Krause et al., 2012; Petrash et al., 2017), other carbonate compounds are rarely mentioned in this context. A few examples include: siderite (Sanchez-Roman et al., 2014; Roh et al., 2003), manganese carbonate (Li et al., 2016) or strontianite (Li et al., 2015). As far as we know, only one organism has been described as having the capacity to produce barium carbonate by biomineralization (Martignier et al., 2017). The existence of this organism was discovered in Lake Geneva (Switzerland), but its precise identification has not yet been successfully achieved. It produces large quantities of intracellular inclusions, called micropearls, with compositions ranging from near-amorphous calcium carbonates (ACC) highly enriched in barium to near-amorphous barium carbonates (Ba/Ca ratio may be up to more than 90 mol%). These micropearls' composition also often include small concentrations of strontium (up to 10 mol%) (Martignier et al., 2017).

Other organisms known to produce intracellular inclusions of ACC enriched in barium include only *Tetraselmis desikacharyi*, one of the marine species of the genus *Tetraselmis* (Martignier et al., 2018), and a few cyanobacteria species (Couradeau et al., 2012; Benzerara et al., 2014).

Nevertheless, the low concentration of barium observed in these ACC inclusions (Cam et al., 2015; Martignier et al., 2018) cannot be compared to those observed in Lake Geneva. Interestingly, another species of Lake Geneva also forms micropearls, but only enriched in strontium, without any barium: it is the unicellular green alga *Tetraselmis cordiformis*. Both organisms can be found simultaneously in the same water sample, each forming micropearls of their own characteristic compositions (Martignier et al., 2017).

The organism producing Ba-rich micropearls (OPBaM) which was described in Lake Geneva had, to this day, only been observed with Scanning Electron Microscopy. Indeed, the identification of the OPBaM under light microscopy has been prevented by the translucent appearance of micropearls (similar to starch inclusions). The morphological characteristics already observed with SEM by Martignier et al. (2017) are not sufficient for identification. Nevertheless, two different types of OPBaM were distinguished by their size and the composition of the micropearls. One type has a smaller size of approximately 5-8 μm, and typically produces micropearls with very high barium concentrations corresponding to barium carbonate compositions (50-95 mol%). The second type is larger, with a length of 20-25 μm, and produces micropearls with 5 – 55 mol% of barium. It has not yet been determined whether both types are distinct species or if they are different stages of the life cycle of a single species. Both types appeared to possess two flagella.

The identification of the OPBaM clearly requires the use of additional investigation methods. Epifluorescence microscopy is a commonly used tool to make a first distinction between big groups of phytoplanktonic organisms based on pigment autofluorescence. For example, under blue-wavelength excitation, phytoplankton generally appears red, due to chlorophyll-a fluorescence while cyanobacteria appear yellow, due to phycocyanin molecules present in the cell (Callieri, 2007). The spectral signature is considered as one aspect of the organism's phenotype and may therefore constitute an important characteristic to help identification.

The goal of the present research is to determine additional characteristics of these organism(s), aiming to facilitate their identification. Thorough SEM observations have been carried out on different sample preparations (dried or fixed with different agents) and were completed by numerous SEM-EDXS analyses. Additional images have been acquired by epifluorescence, as well as light microscopy. Finally, metagenomic analyses were performed on a water sample of Lake Geneva taken during a period of high productivity of the OPBaM.

5.3   Samples and methods

5.3.1 Origin of the samples and pre-treatment methods

Lake water was sampled by lowering a plastic bottle at the depth of maximum *Chl a* concentration, which was determined by using a FLNTUB probe (WetLabs, Philomath, OR 97370, USA). Sampling was performed during monthly campaigns (with rare exceptions) between June 2012 and November 2018, systematically at the same location of Lake Geneva (Switzerland) named *GE3* (6.2197 ° E/ 46.2994 ° N). At this location, the water depth reaches 72 m.

Debris and large organisms were discarded from the samples for microscopic observation by pre-filtration through a 64 µm mesh sieve. The water sample was then filtered on polycarbonate filter membranes under a vacuum lower than 20 kPa. Pore size varied between 0.2 to 5 µm.

These filter membranes were either directly dried at room temperature in the dark before SEM observation, or were first observed immediately after filtration with an epifluorescence microscope, prior to desiccation.

5.3.2 Sample fixation

Different fixation techniques were applied on certain samples, in order to preserve as much as possible the original shape of the organisms organic matter while avoiding to dissolve the micropearls. The fixation protocols were tested on fresh water samples from Lake Geneva, considering: different fixation time (from a few minutes to several hours), with or without buffers (cacodylate or phosphate buffer (Na_2HPO_4)) and different concentration of different fixatives (glutaraldehyde, formaldehyde, methanol, lugol, alkaline lugol and mixtures of the previous). The best results were obtained either with 2% glutaraldehyde fixation during 5-10 minutes and rinsing with cacodylate buffer (pH 8.2), or with alkaline lugol (in which the acetic acid is replaced by sodium acetate (CH_3COONa)) during 1-2 minutes.

5.3.3 Scanning electron microscopy (SEM) and energy-dispersive X-ray spectroscopy (EDXS)

Small areas of the membrane filters were cut and stuck on an aluminum stub with a double-sided conductive carbon tape. The samples were vacuum sputtered, producing gold coating of approximately 10 nm thickness. Backscattered and secondary electron imaging, as well as EDXS analyses, were performed by a JSM 7001F Scanning Electron Microscope from JEOL (Department of Earth Sciences, University of Geneva, Switzerland). The model of the EDXS detector is EX-94300S4L1Q, from JEOL. ZAF correction method was applied to obtain the semi-quantitative results. EDXS measurements were performed with a beam current of ~4 nA, acquisition times of 30 s and 15 kV acceleration. Carbon, nitrogen, oxygen and gold were not taken into account for the calculation of the elemental concentrations (expressed as mol%).

5.3.4 Light microscopy observation and epifluorescence.

The images of *Tetraselmis* cf. *cordiformis* (Figure S1) were made with an inverted optical microscope (Axiovert 35 Zeiss), under phase-contrast illumination by the Service de l'Ecologie de l'Eau (SECOE) of Canton Geneva.

The light microscopy and epifluorescence imaging of OPBaMs on filter membranes were performed with a Nikon Eclipse 80i widefield microscope (Department of Botany and Plant Biology, University of Geneva). The fluorescence filters used were the following: DAPI filter (Semrock F36-500), GFP filter (Semrock F36-528), YFP filter (Semrock F36-525), CFP filter (Semrock F36-544) and GFP longpass filter (Chroma 49012).

5.3.5 DNA analysis of water samples

Two water samples from Lake Geneva (300 ml) were filtered on polycarbonate filter membranes (Whatman Nuclepore Track-Etch Membrane, 47 mm diameter, 1 µm pore size). The filters were extracted using the Blood and Tissue Kit (Qiagen) with an incubation in the lysis buffer of 24h at 56°C. For the DNA amplification, we used two different universal genetic markers: the V4 region of the 18S rRNA (Stoeck et al., 2010) and COI gene (Leray et al., 2013). For the V4 marker, PCR cycles included an initial denaturation at 95 °C for 5min, followed by 9 cycles of denaturation at 94 °C for 30s, annealing at 52 °C for 45s and elongation at 72 °C for 1min. Then a second set of 25 cycles was performed with denaturation at 94 °C for 30s, annealing at 47 °C for 45s and elongation at 72 °C for 1min. A final elongation step at 72 °C

was performed for 5 minutes. For the COI marker, the PCR cycles included an initial denaturation at 95 °C for 5min, followed by 16 cycles of denaturation at 95 °C for 10s, a touchdown annealing from 62 to 47 °C for 30s and elongation at 72 °C for 1min. Then a second set of 25 cycles was performed with denaturation at 95 °C for 10s, annealing at 46 °C for 30s and elongation at 72 °C for 1min. A final elongation step at 72 °C was performed for 2 minutes. For each sample, 3 PCR reactions and a negative control were performed. All PCR replicates were pooled and quantified with capillary electrophoresis using QIAxcel instrument (Qiagen) and then purified using High Pure PCR Product Purification kit (Roche Applied Science). One library per genetic marker was performed using Illumina TruSeq® DNA PCR-Free Library Preparation Kit. The libraries were finally quantified with qPCR using KAPA Library Quantification Kit and sequenced on a MiSeq instrument using paired-end sequencing for 500 cycles with nano kit v2. Raw FASTQ reads were quality-filtered by removing any sequence with a mean quality score of 30, and also removing all sequences with ambiguous bases or mismatch in the primers. These extremely stringent parameters ensure that we keep only high-quality reads. Then, paired-end reads were assembled by aligning them into a contiguous sequence with highest similarity. Chimera removing, strict dereplication and the OTUs clustering at 97% were performed using *vsearch* (Rognes, 2016). A BLAST analysis was then performed on all OTUs against the NCBI database with at least 97% of coverage for taxonomic assignment.

5.4   Results

5.4.1 SEM imaging of the organisms forming Ba-rich micropearls

In general, the morphology of organisms without mineral shells is difficult to image with SEM, if samples are simply dried, due to the loss of organic matter structure during desiccation. Nevertheless, it remains possible to identify a general shape and thereby to distinguish between different organisms as already performed in Martignier et al. (2017). Figure 1 shows the two different types of OPBaM observed in Lake Geneva: the large (Fig. 1a) and the small types (Fig. 1d). Each of them is compared to *Tetraselmis* cf. *cordiformis* (Chlorodendrophyceae), another organism present in Lake Geneva, which produces micropearls enriched in strontium.
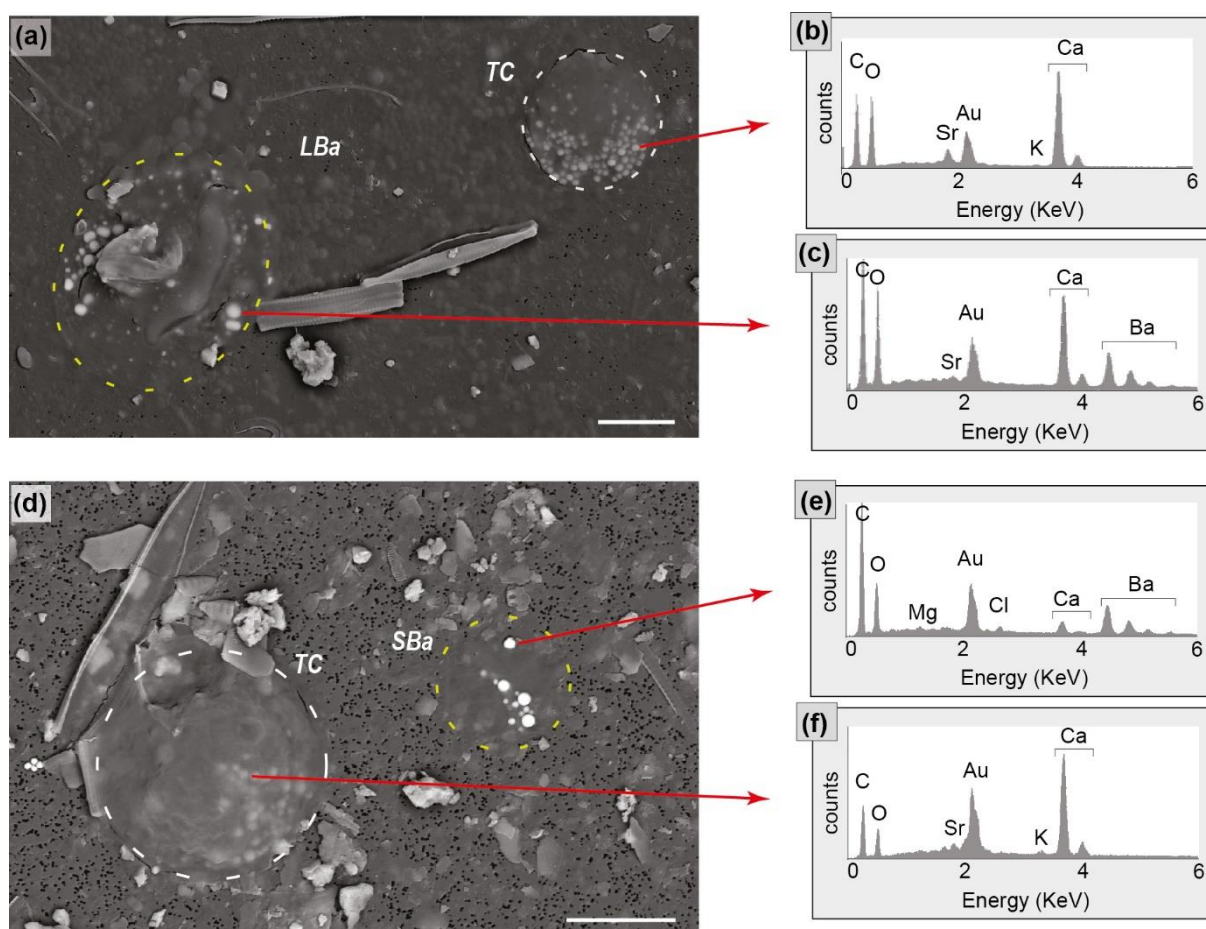
Figure 1 – Comparison between organisms forming Ba-rich micropearls and *Tetraselmis cordiformis*

Dried samples. (a) and (d) backscattered SEM images of a sample taken at location GE3 in Lake Geneva respectively on the 10th of July 2012 at 6 m depth and on the 3rd of December 2013 at 3.5 m depth. The micropearls appear in white or light grey against the darker organic matter. The external limit of the cells is highlighted by dotted lines. *TC*: *Tetraselmis cordiformis*; LBa: Large type of organism forming Ba-rich micropearls; SBa: small type of organism forming Ba-rich micropearls. (b), (c), (e) and (f): EDXS spectra of one micropearl formed by each organism. The black dots at the back are filter pores. Scale bars: 10 μm.

In order to obtain a better representation of the OPBaMs' original shapes, samples from Lake Geneva have been fixed with chemicals. The micropearls being easily dissolved, multiple tests showed that if micropearls are to be preserved, any decrease in *pH* must be avoided. The best results were obtained by fixations with glutaraldehyde or alkaline lugol.

A too long exposure to glutaraldehyde dissolves the micropearls, implying that it is impossible to obtain an optimal fixation of the organic matter if the mineral inclusions are to be preserved. A selection of the best images produced by this method are shown in Figure 2. Fig. S1 allows to compare the effect of this same sample preparation on another organism, (*Tetraselmis cordiformis*). Note that images of Fig. S1 and those of Fig. 2a to 2c were made on the same filter.

Figure 2 confirms that the large type of OPBaM always possesses two flagella or "appendages". The latter term will be preferentially used in this manuscript, as the nature of these organisms seems unsure. The size of the fixed cells ranges approximately from 15 to 20 μm. The general shape appears ovoid (Fig. 2a to 2d) to spherical (Fig. 2e), depending on how the cell was deposited on the filter. The micropearls are generally agglomerated at one extremity of the cell, where the two appendages are also located. Few micropearls can also be located elsewhere in the cell, and can sometimes form longitudinal alignments (e.g. Fig. 2b and 2d).
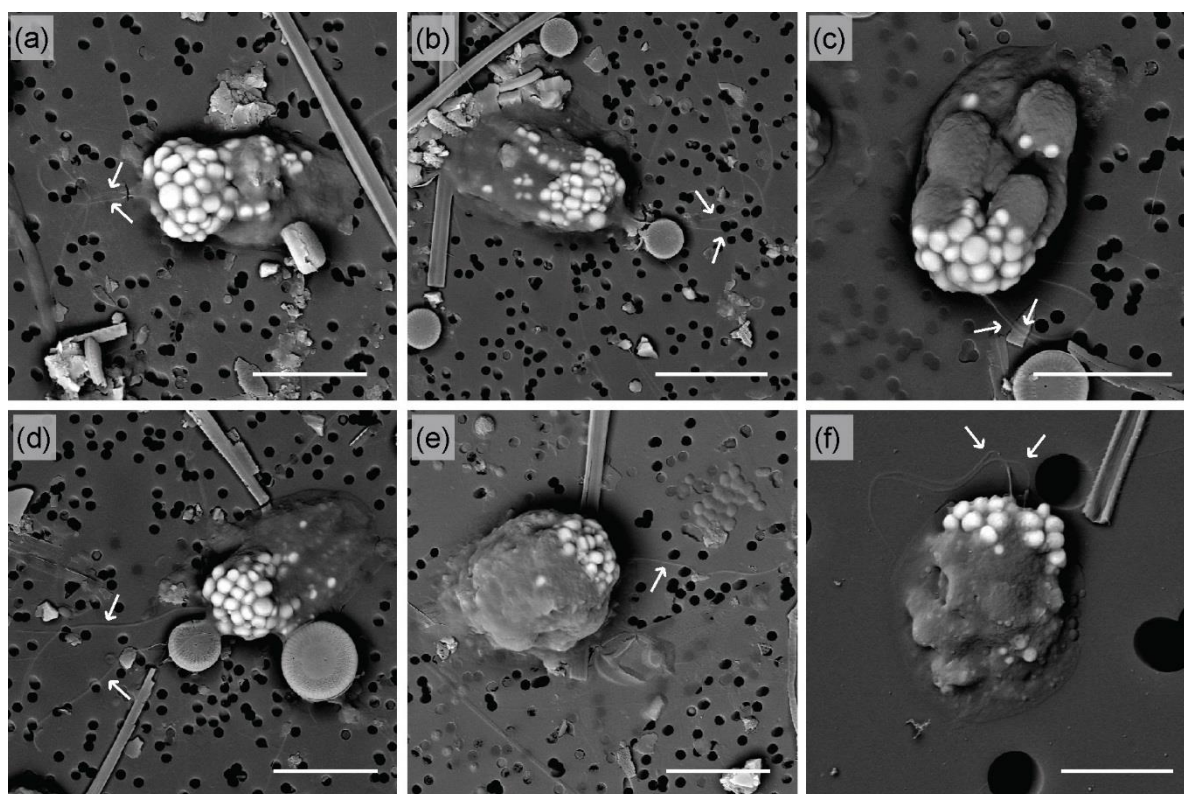
Figure 2 – SEM images of the large type of organisms forming Ba-rich micropearls – glutaraldehyde
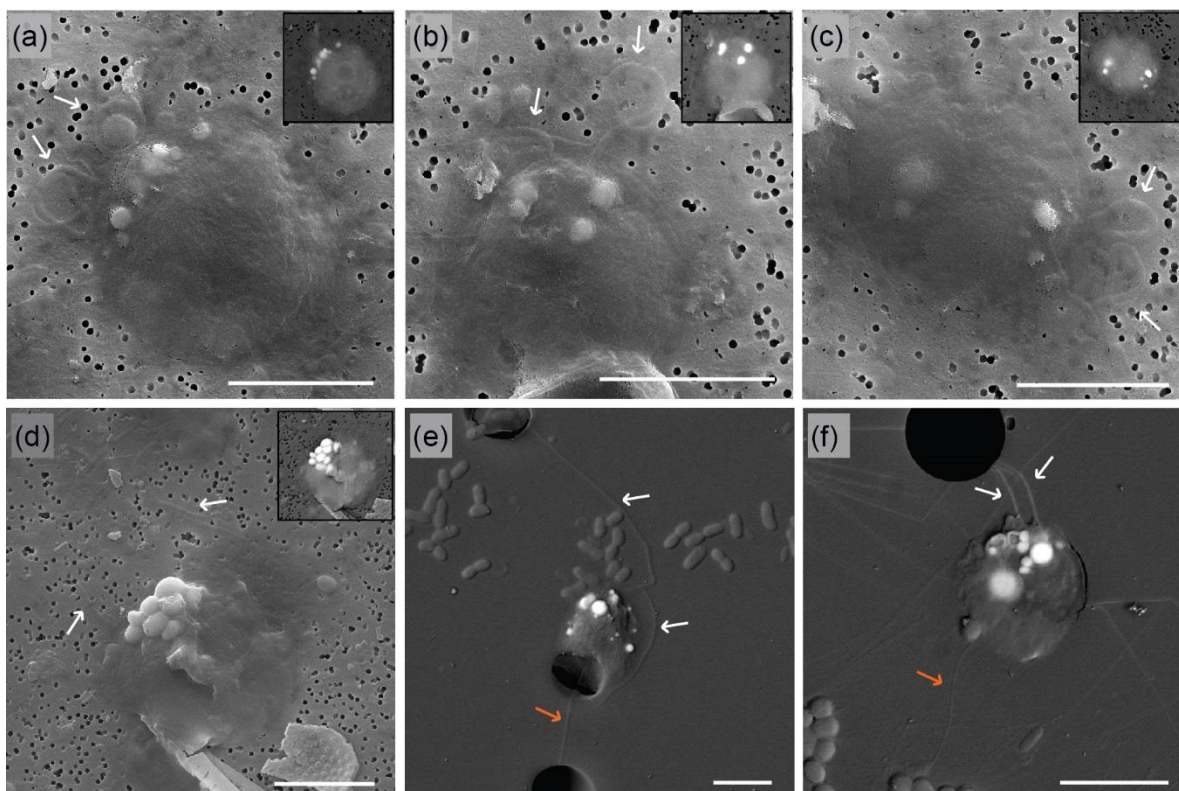
Water samples coming from Lake Geneva, fixed with 2% glutaraldehyde during approx. 5 minutes in order to maintain as much as possible the original shape of the organic matter. Micropearls appear in white or light grey against the darker organic matrix. White arrows indicate the visible motile appendages. (a) to (c): organisms sampled on the 12th of June 2018 at 11 m depth; (d) and (e): organisms sampled on the 10th of July 2018 at 13 m depth; (f) sampled on the 14th of June 2016 at 10 m depth. The black dots at the back are filter pores (filter porosity: 1 μm in a) to e) and 5 μm in f)). Scale bars: 10 μm.
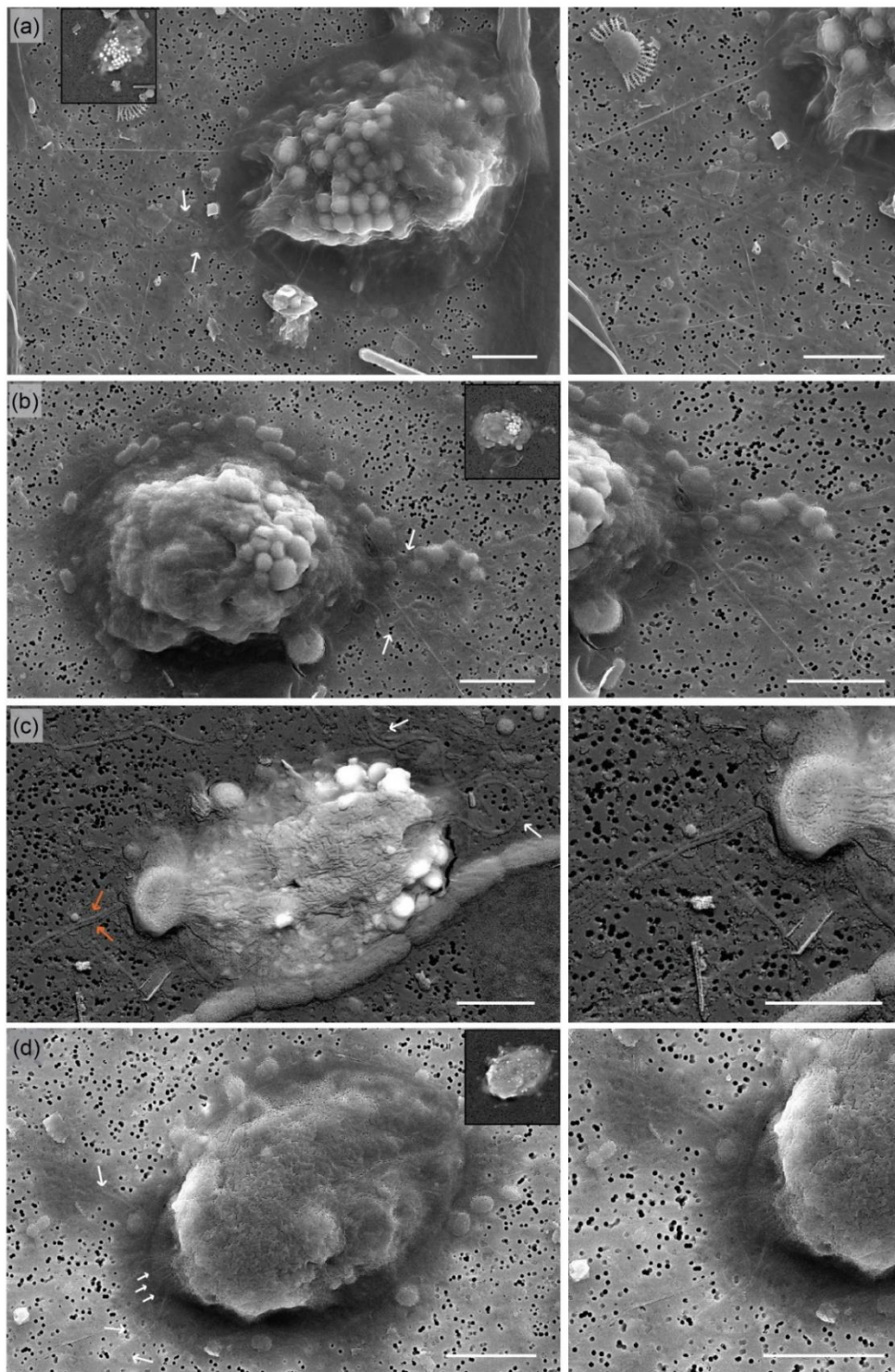
Figure 3 | SEM images of the large type of organisms forming Ba-rich micropearls – alkaline lugol

Water sampled in Lake Geneva (a): on the 19th of May 2015 at 18 m depth; (b) to (d): on the 3rd of November 2015 at 10 m depth and then fixed with alkaline lugol during approx. 90 seconds in order to preserve as much as possible the original shape of the organic matter. White arrows point at the visible motile appendages. Orange arrows point at two appendages, which seem attached to the other end of the cell. Zooms are shown in the right hand-side column. Images (a), (b) and (d) were taken with secondary electrons (for a better topographic detection, to enhance the shape of the motile appendages). Backscattered image (figuring the micropearls in white or light grey against the darker organic matter, as the grey levels relate to the atomic mass of the material) are shown in small boxes. The black dots at the back are filter pores. Scale bars: 5 µm.

Figure 4 – SEM images of the small type of organisms forming Ba-rich micropearls

Water samples coming from Lake Geneva. Micropearls appear in white or light grey against the darker organic matter. White arrows indicate the two motile appendages (see Fig. S2 for zooms). Orange arrows show a third appendage, attached to the opposite side of the cell. Organisms (a) to (d) were fixed with alkaline lugol; organisms (e) and (f) with glutaraldehyde. Note the difference of preservation of the motile appendages. Images (a) to (d) were taken with the secondary electron mode (highlighting the morphology of the sample), and backscattered images (where grey levels represent the atomic mass) are integrated as boxes in the top-right corner of the image. (a) to (c): organisms sampled on the 17th of May 2016 at 10 m depth; (d) sampled on the 21st of April 2016 at 10 m depth; (e) and (f): organisms sampled on the 12th of July 2016 at 18 m depth. The black dots at the back are filter pores (filter porosity: 0.2 μm in a) to d) and 5 μm in e) and f)). Scale bars: 5 μm.

Figure 3 shows a selection of the best SEM images of the large type of OPBaM obtained from samples fixed with alkaline lugol. The appendages seem to be better preserved with this sample preparation, and these images suggest that the large type of OPBaM might in fact possess more motile appendages than just two. Indeed, at least two long appendages can be seen on the other end of the cell in Fig. 3c and Fig. 3d. Figures 3e and f even suggest that additional shorter appendages might be present between the two main "flagella".

The smaller type of OPBaM is more difficult to observe because of its size and lesser abundance. Figure 4 shows the best SEM images of this organism, taken from samples fixed with both glutaraldehyde and alkaline lugol. The small type seems more spherical than the large type and its size varies between 6 to 10 μm. Similarly to the large type, the small type possesses at least two appendages, which are located on the cell extremity where the

micropearls agglomerate (Fig. S2). Interestingly, an additional appendage also seems to be present on the opposite side of the cell (figure 4e and 4f).

5.4.2 Intrinsic fluorescence signal combined with SEM imaging

Each month, between July and October 2018, small areas of freshly filtered samples of Lake Geneva waters were imaged with epifluorescence microscopy, in order to obtain the intrinsic (or auto-) fluorescence signal of the different organisms present on the filter. Subsequent SEM observation of exactly this same area allowed to locate precisely the OPBaM. Only the large type was observed in July, August and October. Ba-rich micropearls were totally absent in September 2018.

Fig. S3 shows fluorescence microscope images of a single OPBaM specimen, acquired with different emission filters. The GFP longpass emission filter was chosen to proceed to further analyses, because it is the most useful type as it allows to visualize a large range of wavelengths corresponding to different intrinsic fluorescent responses from the sample.

The intrinsic fluorescence signal of the large type of OPBaM was identical in all samples. As illustrated on Fig. 5a, these organisms produce a bright yellow signal with a greenish hue (approx. 580 nm) under blue excitation (460-500 nm). This seems to be quite characteristic, as no other organism of our samples produced the same signal. Fig. 5b shows a SEM image of all the organisms producing this yellow-greenish signal in the illustrated zone, confirming that each belongs to the large type of OPBaM.

Note that the organisms seem larger in Fig. 5 than in Fig. 2 or Fig. 3, due to the fact that the organic matter was chemically fixed in the latter samples and therefore collapsed less during sample preparation.

The second and third columns of Fig. 6 show close-up images of the large type of OPBaM. The yellow-green intrinsic fluorescence clearly comes from the organic matter, whereas the micropearls can be distinguished as non-luminescent spots inside the cell (Fig. 6a, 6b and 6d). The intensity of the yellow-green luminescence signal can directly be linked with the thickness of the organic matter preserved after filtration: when intracellular components are preserved, the thicker organic matter produces a signal with greater intensity (Fig. 6b and 6c). This is particularly visible in Fig. 6b and 6c.
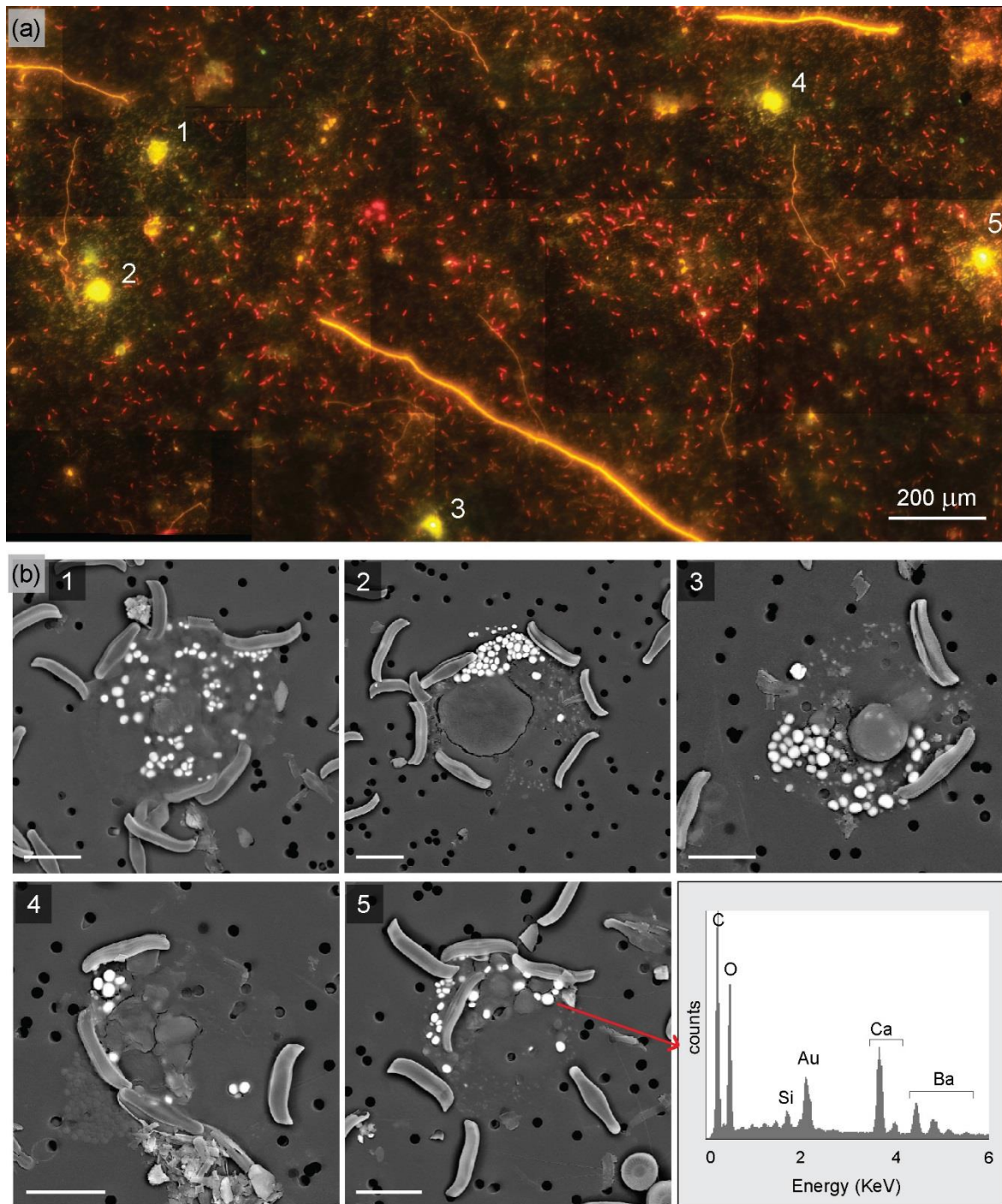
Figure 5 – Correlation between autofluorescence and SEM imaging of freshly filtered filters

Water sample coming from Lake Geneva, taken on the 2nd of October 2018 at 17 m depth. Dried sample. (a) panorama showing the autofluorescence of all the living organisms present on this part of the filter. The red autofluorescence is typically produced by the chloroplasts of all phytoplankters. The bright yellow-orange signal is produced by cyanobacteria (shapes vary from long string for filamentous cyanobacteria to aggregates of tiny dots). White numbers from 1 to 5 label each of the occurrences of the bright yellow-greenish color identified as the autofluorescence signal of the large type of organisms producing Ba-rich micropearls. (b) SEM backscattered images of the organisms found at the corresponding locations. The micropearls appear in white. The composition of the micropearls of the fifth organism is given as an example. Notice the bloom of small diatoms (*Achnantidium catenatum*). Scale bars in part (b): 10 µm.
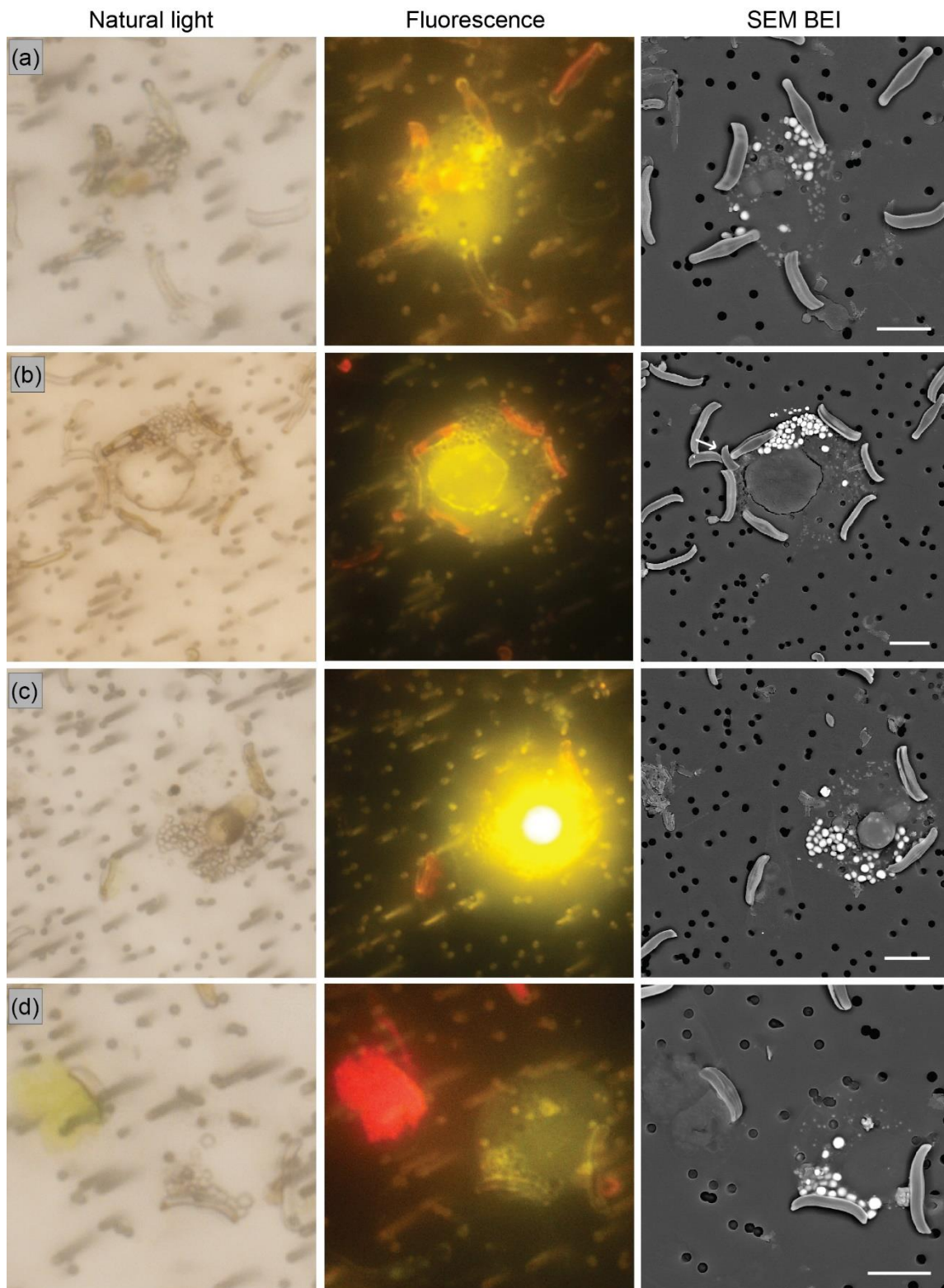
Figure 6 – Correlation between natural light, fluorescence and SEM imaging

Water sample coming from Lake Geneva, sampled on the 2nd of October 2018 at 17 m depth. Dried sample. (a) to (d): each line compares the images obtained for the same specimen of organism forming Ba-rich micropearls (large type), by natural light with optical microscope, by fluorescence microscope and by SEM imaging (Backscattered Electron Images). The red autofluorescence is typically produced by the chloroplasts of all phytoplankton cells. Note that the pores of the filter are colored in brown in natural light, yellow in fluorescence and black in SEM images. The micropearls appear in white in SEM images. Scale bars: 10 μm.

It is interesting to note that apart from a few specimens (e.g. Fig. 6a), the OPBaMs do not show red fluorescence signal inside their cells (which generally correspond to the autofluorescence signal of phytoplankton chloroplasts).

5.4.3 Natural light images of OPBaM

The characteristic autofluorescence signal produced by the large type of OPBaM allowed us to locate these organisms without SEM and to observe them with light microscopy. The first column of Figure 6 presents the first images of these organisms in natural light. The comparison with SEM and autofluorescence images provides a complete set of information for each specimen.

The natural light images of Fig. 6 indicate that the large type of OPBaM is completely transparent. No color can be distinguished inside the cells, apart in Fig. 6a (where two green areas suggest the presence of chloroplasts). The micropearls, although clearly distinguishable, appear translucent, similarly to the micropearls produced by *Tetraselmis cordiformis* (Martignier et al., 2017).

5.4.4 Metagenomic analyses

Epifluorescence and SEM observations showed that many OPBaM of the large type were present in the water sample taken from Lake Geneva on the 2nd of October 2018. Tables S1 and S2 present the list of genomes detected by metagenomic analyses performed on this sample, by analyzing respectively the COI gene and the V4 region of the 18S rRNA. Amongst the identified organisms, the presence of a member of the haptophytes (*Chrysochromulina sp.*) has been noted. Nevertheless, other species show several characteristics similar to those of the OPBaM organisms, such as a member of the Katablepharids, two *Cryptomonas* species, a member of the Bicosoecida or of the Cercomonadida as well as several ciliates (e.g. Cercozoa).

We also note the presence of two different *Tetraselmis* species: *Tetraselmis aff. maculata* (normally known as a marine species) and *Carteria sp. (*possibly *Tetraselmis cordiformis*, as *Carteria cordiformis* is a homotypic synonym of *Tetraselmis cordiformis*)

It is important to state that as nearly 86% of the detected genomes have not been successfully identified, there is no guaranty that the genome of the OPBaM is amongst the identified ones.

5.5 Discussion

5.5.1 Observed characteristics of the organisms producing Ba-rich micropearls

SEM images made on samples fixed with glutaraldehyde and alkaline lugol (Figs 2 to 4) show that the morphological characteristics of both the large and small types of OPBaM can be observed repeatedly in all cells if they did not suffer too much damage during filtration. The large type is generally ovoid (15 to 20 µm) (Figs 2 and 3), while the small type seems more spherical (6 to 10 µm) (Fig. 4). In both cases, the Ba-rich micropearls aggregate on one side of the cell, from which two appendages emerge (Figs 2 to 4). Although the interpretation of SEM images made on fixed samples needs to be taken with caution due to possible artefacts (Read et al., 1983; Fratesi et al., 2004), the concordant results of two different sample preparation methods support the reality of the observed elements.

It may be discussed whether the two appendages are flagella or not. It is important to note that SEM observations suggest that both these organisms possess in fact more than just two appendages. These additional appendages, in both types, emerge from the opposite side of the cell and seem thinner than the two "main" ones (orange arrows in Figs 3c, 4e and 4f). Finally, shorter appendages have also been observed in the large type, between the two "main" motile appendages (Fig 3c). This could point towards cilia rather than flagella. In the present state of knowledge, the nature and function of these appendages remains unclear.

The particular intrinsic fluorescence signal of the large type of OPBaM under blue excitation (Fig. 5 and 6), producing a yellow-green spectral signature, is definitely an interesting characteristic of this organism phenotype. This specific autofluorescence signal does not relate to the descriptions of the classic "large groups" of plankton defined by their autofluorescence (e.g. phytoplankton: red; cyanobacteria: yellow-orange, etc.) (Callieri, 2007; Simis et al., 2012; Huisman et al., 2005). Fig. S1 shows, as a comparison, an image of the standard red fluorescence of *Tetraselmis cordiformis*, emitted by the chlorophyll-*a* present in the chloroplast. The occasional presence of red fluorescence areas inside a few OPBaM (Fig. 6a) suggests that these organisms do not possess any chloroplast of their own. The red fluorescence can be explained either by small phytoplanktonic organisms deposited beneath the OPBaM during filtration, or by small algae having been "ingested" by the OPBaM.

The small type of OPBaM was, unfortunately, not present during the four-month observations in epifluorescence. Its intrinsic fluorescence signal has therefore not been determined. We possess less information on the small type in general. Nevertheless, the few characteristics

which have been observed confirm that they are very similar to the large type (part 5.1.1), supporting the hypothesis of a close parentage, either as a species of the same genus or as a different life-stage of the same organism.

5.5.2 Tentative identification of the large type of organism producing Ba-rich micropearls

To date, the only species producing micropearls, which have been identified, are green algae, part of the class Chlorodendrophyceae (Martignier et al., 2018). The composition of the micropearls differs from the composition of the micropearls produced by OPBaM as they are enriched in strontium, instead of barium. Nevertheless, the mineral nature of the micropearls, as well as their internal structure, is extremely similar (Martignier et al., 2017). Moreover, the location of the micropearls in the cell is also similar: in most *Tetraselmis* species, as in the OPBaM, the micropearls are aggregated at the side of the cell wherefrom the appendages emerge (Figs 2 to 4 and Martignier et al., 2018). Finally, the alignment of micropearls observed in Figs 2a, 2b and 2d resemble the longitudinal alignments of micropearls described in several *Tetraselmis* species (Martignier et al., 2018).

Our first hypothesis is therefore that the OPBaM are also part of the phytoplankton of Lake Geneva. The metagenomic analysis carried out on a water sample where numerous OPBaM (large type) were present (Table S1), showed that the genome belonging to a haptophyte (*Chrysochromulina* sp.) was identified more than 2000 times in the sample. It had already been shown that freshwater haptophytes could constitute an important part of the phytoplankton of Lake Bourget, which is geographically close to Lake Geneva (Lepère et al., 2010). These authors also suggest that the haptophyte group may play an important role in other freshwater ecosystems and point out its possible mixotrophy. Interestingly, the small type of OPBaM could also belong to this group, as it was demonstrated that small haptophytes constitute an important part of the picoplankton of certain freshwater lakes, particularly oligotrophic lakes, even if most of these minuscule species have not yet been described (Lepère et al., 2010; Liu et al., 2009). Currently, only a dozen species of haptophytes are known in freshwater or terrestrial habitats (Nicholls, 2015). The absence of chloroplast in some specimens could be explained by the fact that Chrysochromulina is extremely fragile (Southard 2005).

If we consider other hypothesis regarding the identity of this organism, the specific autofluorescence signal produced by the large-type of OPBaM can provide interesting leads. Phycobiliproteins, for example, are intrinsic fluorophores, which cause the autofluorescence of certain algae with a yellow emission color and include phycoerythrin and phycocyanin (Dennis et al., 2011; Warwick, 1983). These fluorophores, widely used as fluorescent probes (Roman et al., 2002), have been observed mainly in cyanobacteria, cryptomonads, red algae (Dasgupta, 2015) and glaucophytes (Jackson et al., 2015). Interestingly, literature indicates that phycoerythrin emits in the green-yellow wavelengths - approx. 580 nm (Sonani et al., 2016), which corresponds to the signal of the OPBaM. Therefore, the abundant presence of two Cryptomonas species (*C. pyrenoidifera* and *C. curvata*), revealed by the metagenomics analyses, is of interest, as well as the presence of an uncultured katablepharid (colorless flagellates closely related to the cryptophytes (Okamoto et al., 2009)). Nevertheless, apart from the last one, these hypotheses do not explain the colorless appearance of the OPBaM in natural light.

If we do take into account the absence of chloroplasts in the observed cells and the colorless appearance (Fig. 6), then we have to consider the possibility that the OPBaM could in fact be part of the heterotrophic or mixotrophic organisms present in Lake Geneva. A member of the Cercromonads, for example, was identified by the metagenomics analysis. These zooflagellates are widespread in freshwater and present two ventral posterior microtubular roots as well as an anterior dorsal root (Karpov et al., 2006), which could correspond to our morphological observations. Nevertheless, the multiple appendages observed on one of the OPBaM specimens (Fig. 3c and 3d) could rather hint towards ciliates. The latter hypothesis is supported by the fact that intracellular inclusions of calcium carbonate as well as salts containing barium and strontium have already been described in some ciliate species (Fauré-Fremiet and Gauchery, 1957; Rieder et al., 1982). Numerous ciliate genomes were found in the second run of metagenomics analyses, such as members of the subclass Choreotrichia or *Cyclidium glaucoma*. Also, the occurrence, in this analysis of the DNA sequence of an uncultured Cercozoa seems of high interest. Indeed, this group includes amoeboids, some of which bear permanent flagella in addition to cilia (Bass et al., 2009), which would correspond to the SEM observations made on fixed samples (Figs 3 and 4).

It appears, at this stage of the research, that multiple organisms still need to be considered as valid candidates for the OPBaM. In further studies, the use of flow cytometry would be highly indicated to clearly identify the large type of OPBaM, as this technique allows the cells to be isolated in function of their intrinsic fluorescence wavelength (Dennis et al., 2011).

5.6   Conclusions

The freshwater unicellular organisms, which form intracellular barium-rich micropearls, were first observed in Lake Geneva (Switzerland) by Martignier et al., 2018. These mineral inclusions are near-amorphous and have compositions ranging from barium carbonates to carbonates enriched in Ba, and frequently also present low concentrations of Sr. This research produces evidence for previously undescribed characteristics of these yet undetermined organisms. Our SEM observation of samples fixed with glutaraldehyde or alkaline lugol confirm the existence of two different types of OPBaM (small and large types) and provide more details regarding their morphology. The micropearls aggregate at one extremity of the cell, from which two "main" appendages emerge. Our observations also strongly suggest that additional appendages protrude from the other end of the cell. Moreover, the large type of OPBaM showed a characteristic yellow-green autofluorescence signal under blue excitation, approximately corresponding to the spectral signature of phycoerythrin.

Tentative identification of the large type of OPBaM results in different hypotheses:

1) the metagenomic analyses of a water sample containing many OPBaMs showed the presence of the haptophyte *Chrysochromulina* sp. Several characteristics listed during this research could correspond to a haptophyte species. This is supported by the fact that a significant part of the picoplankton of several freshwater lakes has been shown to belong to the haptophyte group, which could correspond to the small type of OPBaM. Nevertheless, the observation of the cells by light microscopy did not confirm the presence of any chloroplast, although this absence could be explained by possible damages due to filtration. *Chrysochromulina* species are indeed known to be particularly fragile.

2) The characteristic autofluorescence signal emitted by the large type of OPBaM resembles the signal emitted by phycoerythrin. This fluorophore is known to be present in cryptophytes. Therefore, the two species of Cryptomonas and the

uncultured Katablepharid organism detected by metagenomics in Lake Geneva elect them as potential OPBaM candidates.

3) The lack of chloroplasts observed in light microscopy could also suggest that the OPBaM are heterotoph eukaryotes. Moreover, the multiple short appendages imaged on one specimen, between the two main appendages might even hint towards an affiliation to the ciliates. Interestingly, mineral intracellular inclusions with chemical characteristics corresponding to the Ba-rich micropearls have already been mentioned in literature to be produced by ciliates. Also, metagenomic analyses confirmed the presence of zooflagellates and of different ciliates, including an uncultured Cercozoa (flagella-bearing amoeba).

Altogether, the present results confirm that a second organism living in Lake Geneva, different from the already identified Chlorodendraceae *Tetraselmis cordiformis*, has the capacity to produce near-amorphous calcium carbonate intracellular inclusions. We propose that the final identification of the organism(s) producing Ba-rich micropearls could be completed by using single-cell flow cytometry that would allow to clearly separate them from the rest of the picoplankton.

### *Collaborations and acknowledgements*

5.7   References

Bass, D., Chao, E.E.Y., Nikolaev, S., YabukicKen-ichiroIshida, A., Berney, C., Pakzad, U., Wylezich, C. and Cavalier-Smith, T.: Phylogeny of novel naked filose and reticulose Cercozoa: Granofilosea cl. n. and Proteomyxidea revised. *Protist,* 160(1), 75-109, doi:10.1016/j.protis.2008.07.002, 2009.

Benzerara, K., Skouri-Panet, F., Li, J., Férard, C., Gugger, M., Laurent, T., Couradeau, E., Ragon, M., Cosmidis, J., Menguy, N., Margret-Oliver, I., Tavera, R., López-García, P., and Moreira, D.: Intracellular Ca-carbonate biomineralization is widespread in cyanobacteria. *P. Natl. Acad. Sci. USA*, 111, 10933–10938, doi:10.1073/pnas.1403510111, 2014.

Callieri, C.: Picophytoplankton in Freshwater Ecosystems: The Importance of Small-Sized Phototrophs. *Freshwater Rev.*, 1, 1-28, doi: 10.1608/FRJ-1.1.1, 2007.

Cam, N., Georgelin, T., Jaber, M., Lambert, J.-F. and Benzerara, K.: In vitro synthesis of amorphous Mg-, Ca-, Sr-and Ba-carbonates: What do we learn about intracellular calcification by cyanobacteria? *Geochim. Cosmochim. Acta*, 161, 36–49, 2015.

Choudhury, H. and Cary, R.: Barium and barium compounds, Concise International Chemical Assessment document 33. Geneva, WHO, 2001.

Couradeau, E., Benzerara, K., Gérard, E., Moreira, D., Bernard, S., Brown Jr., G. E., and López-García, P.: An early-branching microbialite cyanobacterium forms intracellular carbonates. *Science*, 336, 459–462, doi:10.1126/science.1216171, 2012.

Dasgupta, C.N.: Algae as a source of phycocyanin and other industrially important pigments. In: Algal biorefinery: An Integrated Approach. Ed: Das, D., Springer, doi:10.1007/978-3-319-22813-6_12, 2015.

Dennis, M.A., Landman, M., Wood, S.A. and Hamilton, D.: Application of flow cytometry for examining phytoplankton succession in two eutrophic lakes. *Water Sci. Technol.*, 64(4), 999-1008, 2011.

Fauré-Fremiet, E. and Gauchery, M.: Concrétion minérales intracytoplasmiques chez les ciliés. *J. Protoz.*, 4, 96–109, 1957.

Fratesi, S.E., Lynch, F.L., Kirkland¸B.L. and Brown, L.R.: Effects of SEM preparation techniques on the appearance of bacteria and biofilms in the Carter sandstone. *J. Sed. Res.*, 74(6), 858-867, doi:10.1306/042604740858, 2004.

Huisman, J., Matthijs, H.C.P. and Visser, P.M.: Harmful cyanobacteria. Aquatic ecology series 3, Springer, 2005.

Jackson, C., Clayden, S. and Reyes-Prieto, A.: The Glaucophyta: the blue-green plants in a nutshell. *Acta Soc. Bot. Pol.*, 84(2),149–165, doi:10.5586/asbp.2015.020, 2015.

Karpov, S.A., Bass, D., Mylnikov, A.P., and Cavalier-Smith, T.: Molecular Phylogeny of Cercomonadidae and Kinetid Patterns of Cercomonas and Eocercomona gen. nov. (Cercomonadida, Cercozoa). Protist, 157, 125—158, 2006.

Krause, S., Liebetrau, V., Gorb, S., Sánchez-Román, M., McKenzie, J.A. and Treude, T.: Microbial nucleation of Mg-rich dolomite in exopolymeric substances under anoxic modern seawater salinity: New insight into an old enigma. *Geology*, 40(7), 587-590, doi:10.1130/G32923.1, 2012.

Lepère, C., Masquelier, S., Mangot, J.-F., Debroas, D. and Domaizon, I.: Vertical structure of small eukaryotes in three lakes that differ by their trophic status: a quantitative approach. ISME J., 4, 1509–1519, 2010.

Leray, M., Yang, J.Y., Meyer, C.P., Mills, S.C., Agudelo, N., Ranwez, V., Boehm, J.T., Machida, R.J.: A new versatile primer set targeting a short fragment of the mitochondrial COI region for metabarcoding metazoan diversity: application for characterizing coral reef fish gut contents. *Frontiers in Zoology*, 10(1), 34, doi:10.1186/1742-9994-10-34, 2013.

Li, Q., Csetenyi, L., Paton, G.I. and Gadd, G.M.: $CaCO_3$ and $SrCO_3$ bioprecipitation by fungi isolated from calcareous soil. *Envir. Microbiol*., 17(8), 3082–3097, doi:10.1111/1462-2920.12954, 2015.

Li, Q., Liu, D., Jia, Z., Csetenyi, L. and Gadd, G.M.: Fungal biomineralization of manganese as a novel source of electrochemical materials. *Current Biol*., 26, 950–955, doi:10.1016/j.cub.2016.01.068, 2016.

Liu, H., Probert, I., Uitz, J., Claustre, H., Aris-Brosou, H., Frada, M., Not, F. and de Vargas, C.: Extreme diversity in noncalcifying haptophytes explains a major pigment paradox in open oceans. PNAS, 106(31), 12803-12808, doi:10.1073/pnas.0905841106, 2009.

Martignier, A., Pacton, M., Filella, M., Jaquet, J. M., Barja, F., Pollok, K., Langenhorst, F., Lavigne, S., Guagliardo, P., Kilburn, M. R., Thomas, C., Martini, R. and Ariztegui, D.: Intracellular amorphous carbonates uncover a new biomineralization process in eukaryotes, *Geobiology*, 15(2), 240–253, doi:10.1111/gbi.12213, 2017.

Martignier, A., Filella, M., Pollok, K., Melkonian, M., Bensimon, M., Barja, F., Langenhorst, F., Jaquet, J.M., Ariztegui, D.: Marine and freshwater micropearls: biomineralization producing strontium-rich amorphous calcium carbonate inclusions is widespread in the genus *Tetraselmis* (Chlorophyta). *Biogeosciences*, 15, 6591-6605, doi: 10.5194/bg-15-6591-2018, 2018.

Nicholls, K.H.: Haptophyte Algae. In: Freshwater Algae of North America (Second Edition), Eds: Wehr, J., Sheath, R. and Kociolek, J.P., Academic Press, pp. 587-605, doi: 10.1016/B978-0-12-385876-4.00013-X, 2015.

Okamoto, N., Chantangsi, C., Horak, A., Leander, B.S.and Keeling, P.J.: Molecular Phylogeny and Description of the Novel Katablepharid *Roombia truncate* gen. et sp. nov., and establishment of the Hacrobia Taxon nov. PLoS ONE 4(9), e7080, doi:10.1371/journal.pone.0007080, 2009.

Oskarsson, A.: Barium. In: Handbook on the Toxicology of Metals (Fourth Edition), vol. 2. Eds: Nordberg, G., Fowler, B., Nordberg, M., pp. 625-634, doi:10.1016/B978-0-444-59453-2.00029-9, 2015.

Petrash, D.A., Bialik, O.M., Bontognali, T.R.R., Vasconcelos, C., Roberts, J.A., McKenzie and J.A., Konhauser, K.O.: Microbially catalyzed dolomite formation: From near-surface to burial. *Earth-Sci. Rev*., 171, 558-582, doi:10.1016/j.earscirev.2017.06.015, 2017.

Read, N.D., Porter, R. and Beckett, A.: A comparison of preparative techniques for the examination of the external morphology of fungal material with the scanning electron microscope. *Can. J. Bot.*, 61(8), 2059-2078, doi:10.1139/b83-223, 1983.

Rieder, N., Ott, H.A., Pfundstein, P. and Schoch, R.: X-ray microanalysis of the mineral contents of some Protozoa. *J. Protoz*., 29, 15–18, 1982.

Rognes, T., Flouri, T., Nichols, B., Quince, C., Mahé, F.: VSEARCH: a versatile open source tool for metagenomics. *PeerJ.;*4:e2584, doi:10.7717/peerj.2584, 2016.

Roh, Y., Zhang, C., Vali, H., Lauf, R., Zhou, J. and Phelps, T.: Biogeochemical and environmental factors in Fe biomineralization: Magnetite and siderite formation, *Clay Miner.*, 51, 83–95, doi:10.1346/CCMN.2003.510110, 2003.

Román, R.B., Alvárez-Pez, J.M., Fernández, F.G.A., Grima, E.M.: Recovery of pure B-phycoerythrin from the microalga *Porphyridium cruentum*. *J. Biotechnol.*, 93(1), 73-85, doi:10.1016/S0168-1656(01)00385-6, 2002.

Sánchez-Román, M., Fernández-Remolar, D., Amils, R., Sánchez-Navas, A., Schmid, T., San Martin-Uriz, P., Rodríguez, N., McKenzie, J.A. and Vasconcelos, C.: Microbial mediated formation of Fe-carbonate minerals under extreme acidic conditions. *Sci. Rep.*, 4, 4767, 2014.

Simis, S.G.H., Huot, Y., Babin, M., Seppälä, J. and Metsamaa, L.: Optimization of variable fluorescence measurements of phytoplankton communities with cyanobacteria. *Photosynth. Res.*, 112, 13-30, doi:10.1007/s11120-012-9729-6, 2012.

Sonani, R.R., Rastogi, R.P., Patel, R. and Madamwar, D.: Recent advances in production, purification and applications of phycobiliproteins. *World J Biol Chem.*, 7(1), 100-109, doi:10.4331/wjbc.v7.i1.100, 2016.

Southard, G.M.: Microscopy and *Prymnesium parvum*: observations and challenges. In: Management of *Prymnesium parvum* at Texas State Fish Hatcheries. Report n°PWD RP T3200-1138 (9/05), 2005.

Stoeck, T., Bass, D., Nebel, M., Christen, R., Jones, M.D.M., Breiner, H.-W., Richards, T.A.: Multiple marker parallel tag environmental DNA sequencing reveals a highly complex eukaryotic community in marine anoxic water. *Mol. Ecol.,* 19(Suppl 1):S21–S31, doi:10.1111/j .1365-294X.2009.04480.x, 2010.

Warwick, F.V.: Fluorescence properties of the freshwater phytoplankton: Three algal classes compared. *Brit. Phycol. J.*, 18(1), 5-21, doi:10.1080/00071618300650021, 1983.

Weiner, S. and Dove, P.M.: An overview of biomineralization processes and the problem of the vital effect. *Rev. Min. Geochem.,* 54, 1-29, 2003.

5.8   Supplementary information
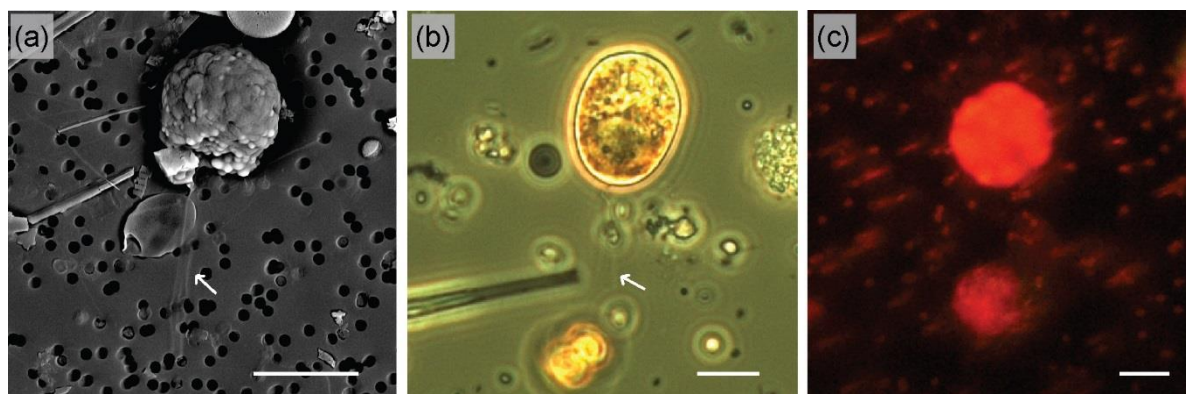
Figure S1: images of *Tetraselmis* cf *cordiformis*

(a) SEM image of a sample form Lake Geneva, fixed with glutaraldehyde in order to maintain the original shape of the organic matter. Images of Fig.2 were taken from this same sample. Micropearls of near-amorphous calcium carbonate enriched in Sr appear in white or light grey against the darker organic matter. The black dots at the back are filter pores. (b) Optical microscope image. The water sample is the same as the one used to prepare the sample for image (a). White arrow indicate the position of the four flagella of *Tetraselmis* cf. *cordiformis* on each picture. (c) Epifluorescence image of a *Tetraselmis cordiformis* cell (culture sample), illustrating the red autofluorescence of the chloroplast (blue excitation). Scale bars: 10 µm.
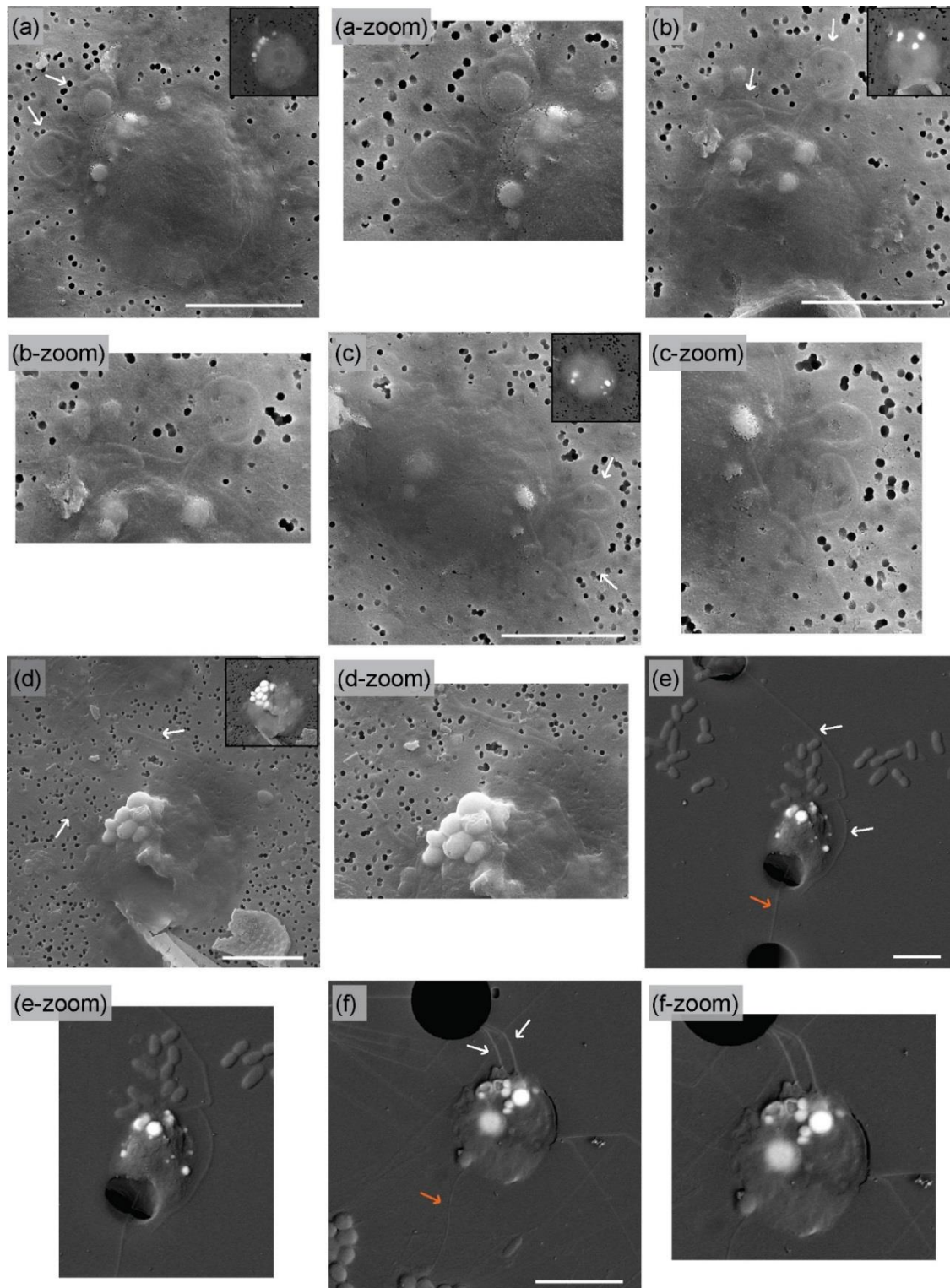
Figure S2: Zoom-in images of Figure 4.

SEM images of the small type of organisms forming Ba-rich micropearls. Water samples coming from the water column of Lake Geneva. Micropearls appear in white or light grey against the darker organic matter. White arrows indicate the two motile appendages. Orange arrows show a third appendage, attached to the opposite side of the cell. Organisms (a) to (d) were fixed with alkaline lugol; organisms (e) and (f) with glutaraldehyde. (a) to (c): organisms sampled on the 17th of May 2016 at 10 m depth; (d) sampled on the 21st of April 2016 at 10 m depth; (e) and (f): organisms sampled on the 12th of July 2016 at 18 m depth. The black dots at the back are filter pores (filter porosity: 0.2 µm in (a) to (d) and 5 µm in (e) and (f)). Scale bars: 5 µm.
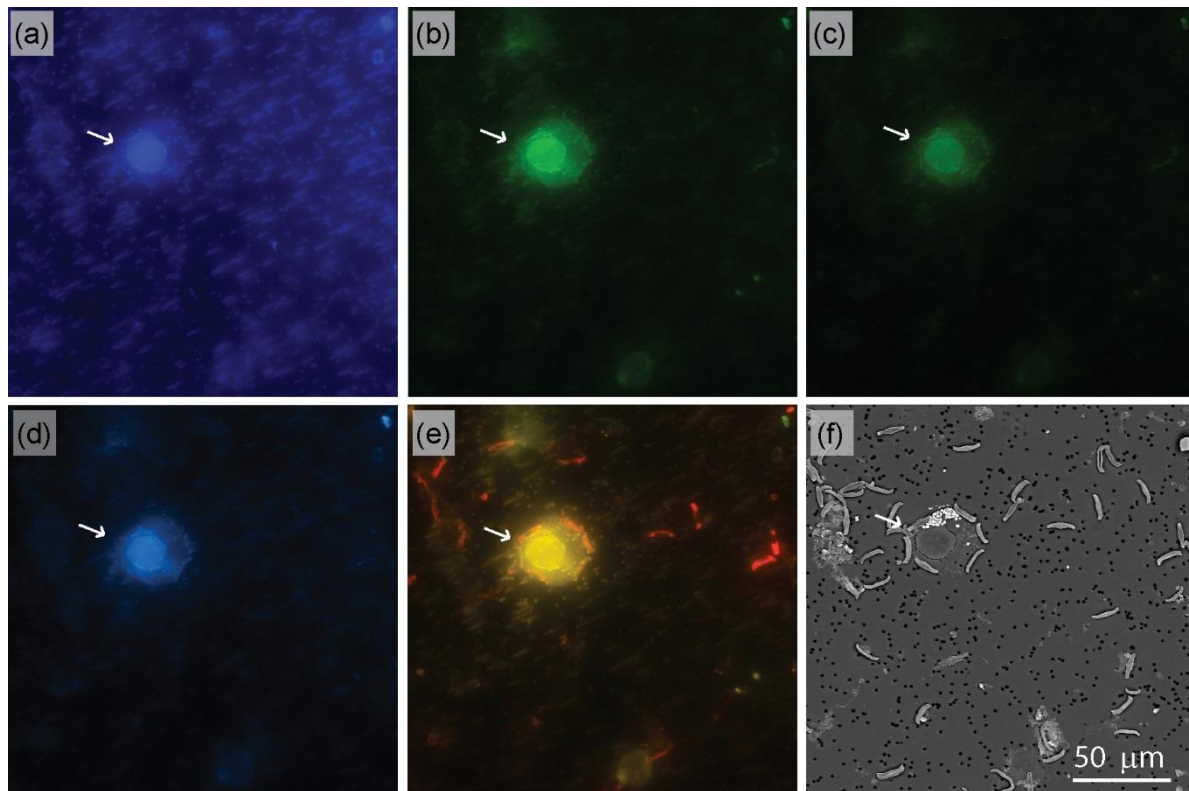
Figure S3: Comparative imaging of a freshly filtered water sample from Lake Geneva with different filter of fluorescence microscope and SEM.

(a) to (e): images, taken with a fluorescence microscope, of a freshly filtered water sample from Lake Geneva, sampled on the 2nd of October 2018 at 17 m depth. The filters are, respectively: (a) DAPI filter, excitation: UV/violet (352-402 nm), emission: blue (417-477 nm); (b) GFP filter, excitation: blue (457-487 nm), emission: green (502-537 nm); (c) YFP filter, excitation: blue/green (488-512 nm), emission: green (528-555 nm); (d) CFP filter, excitation: violet (426-450 nm), emission: blue (467-499 nm); (e) GFP longpass filter, excitation: blue (460-500 nm), emission: green, yellow, orange, red (>510 nm). (f) SEM image of the same zone. The white arrow points to a large type of the organism producing Ba-rich micropearls. The phytoplankton's chloroplast intrinsic fluorescence can be seen in red in (e). Only the diatoms that are still alive are visible, as can be seen by comparing with image (f).

Table S1: Metagenomics, DNA analysis of the COI gene.

Water sample taken in Lake Geneva on the 2nd of October 2018, at 17 m depth. This sample was chosen because of the high number of large-type of OPBaM present at that time.

Grand Total	418220
#N/A	359604
Rotifera;Monogononta;Ploima;Keratella cochlearis	37027
Rotifera;Monogononta;Ploima;Synchaeta kitina	9753
Rotifera;Monogononta;Ploima;Polyarthra dolichoptera complex sp. UO-2013	5756
NA;NA;Prymnesiales;Chrysochromulina sp. CCMP291	2811
Arthropoda;Branchiopoda;Diplostraca;Macrothrix sp. HE-364	936
Chordata;Mammalia;Primates;Homo sapiens	907
Ascomycota;Eurotiomycetes;Eurotiales;Penicillium sclerotiorum	158
NA;Dinophyceae;Gonyaulacales;Alexandrium tamarense	69
Ascomycota;Dothideomycetes;Capnodiales;Cladosporium sp. BM-2009-5	64
Streptophyta;NA;Solanales;Solanum lycopersicum	64
NA;NA;NA;Vermamoeba vermiformis	55
Rotifera;Monogononta;Ploima;Ascomorpha ovalis	51
Mollusca;Gastropoda;NA;Ancilla sp. MNHN IM 2013-55401	47
Arthropoda;Arachnida;Mesostigmata;Cheiroseius sp. BOLD:ACE1640	45
NA;Dinophyceae;NA;uncultured dinoflagellate	44
Basidiomycota;Agaricomycetes;Agaricales;Clitocybe robusta	40
NA;Oomycetes;Pythiales;uncultured Pythium	40
Mollusca;Gastropoda;NA;Physella gyrina	37
Rotifera;Monogononta;Ploima;Polyarthra sp. UO-2013	33
Mollusca;Gastropoda;NA;Physella johnsoni	28
Arthropoda;Arachnida;Mesostigmata;Typhloseiulus rodopiensis	25
Bacteroidetes;Sphingobacteriia;Sphingobacteriales;Sphingobacterium sp. 21	25
Firmicutes;Clostridia;Clostridiales;Clostridium autoethanogenum	18
Chordata;Actinopteri;Carangiformes;Carangoides armatus	17
Platyhelminthes;Cestoda;Cyclophyllidea;Mesocestoides corti	17
Mollusca;Bivalvia;Mytiloida;Modiolus barbatus	16
NA;Chrysophyceae;NA;Apoikiospumella mondseeiensis	15
Platyhelminthes;Trematoda;Plagiorchiida;Homalometron manteri	15
NA;NA;NA;invertebrate environmental sample	14
Arthropoda;Arachnida;Araneae;Nippononeta sp. 12 SL-2010	13
Chlorophyta;Chlorodendrophyceae;Chlorodendrales;Tetraselmis aff. maculata	12
Arthropoda;Arachnida;Araneae;Heptathela sp. 4 XX-2016	11
Chordata;Aves;Apterygiformes;Apteryx australis	11
Arthropoda;Insecta;Hymenoptera;Ectatomma ruidum	10
Chordata;Actinopteri;Beloniformes;Oryzias uwai	10
Mollusca;Cephalopoda;Sepiida;Sepia pharaonis	10
Firmicutes;Bacilli;Bacillales;Staphylococcus agnetis	9

Arthropoda;Malacostraca;Decapoda;Anomura sp. LPdivOTU90	8
Echinodermata;NA;NA;Eleutherozoa sp. COT003_L204	8
Mollusca;Gastropoda;NA;Physella ancillaria	8
Mollusca;Gastropoda;Thecosomata;Creseis clava	8
NA;Dinophyceae;Gonyaulacales;Azadinium dalianense	8
NA;Dinophyceae;Lophodiniales;Woloszynskia sp. CS-341	8
NA;Dinophyceae;Suessiales;Polarella glacialis	8
Nematoda;Chromadorea;Rhabditida;Angiostrongylus cantonensis	8
NA;Oligohymenophorea;Peniculida;Frontonia didieri	7
Rotifera;Monogononta;Ploima;Lecane papuana	7
Arthropoda;Arachnida;Mesostigmata;Blattisociidae sp. BOLD:ACJ0472	6
Arthropoda;Insecta;Trichoptera;Leptonema simulans	6
Basidiomycota;Microbotryomycetes;Sporidiobolales;Rhodotorula taiwanensis	6
NA;Dinophyceae;Peridiniales;Thoracosphaera heimii	6
NA;Oomycetes;Saprolegniales;Saprolegnia eccentrica	6
Nematoda;Chromadorea;Spirurida;Gongylonema pulchrum	6
Arthropoda;Insecta;Diptera;Cecidomyiidae sp. BOLD-2016	5
Arthropoda;Insecta;Diptera;Chironomidae sp. BOLD:AAV6026	5
Arthropoda;Malacostraca;Amphipoda;Niphargus subtypicus	5
Ascomycota;Sordariomycetes;Hypocreales;Fusarium solani	5
Chordata;Mammalia;NA;Ovis canadensis	5
Mollusca;Gastropoda;NA;Opisthostoma laidlawi	5
Arthropoda;Chilopoda;Craterostigmomorpha;Craterostigmus tasmanianus	4
Arthropoda;Insecta;Diptera;Cecidomyiidae sp. BOLD:ACA7477	4
Arthropoda;Insecta;Thysanoptera;Thrips sp. BOLD:AAG0728	4
Bacillariophyta;Mediophyceae;Hemiaulales;Eucampia zodiacus	4
Chordata;Actinopteri;NA;Pseudochromis sp. MBS1109301	4
Mollusca;Bivalvia;Mytiloida;Gigantidas tangaroa	4
NA;Oomycetes;Pythiales;Pythium ultimum	4
Nematoda;Chromadorea;Rhabditida;Nippostrongylus brasiliensis	4
Rotifera;Monogononta;Ploima;Polyarthra dolichoptera	4
Acanthocephala;Palaeacanthocephala;Echinorhynchida;Rhadinorhynchus sp. MGV-2005	3
Annelida;Clitellata;Haplotaxida;Lumbricus castaneus	3
Arthropoda;Arachnida;Mesostigmata;Cheiroseius sp. BOLD:ABY2050	3
Arthropoda;Arachnida;NA;Raoiella indica	3
Arthropoda;Insecta;Diptera;Metopomyza flavonotata	3
Arthropoda;Insecta;Hymenoptera;Prasmodon sp. Janzen11	3
Basidiomycota;Agaricomycetes;Agaricales;Lepiota sp. MUSH114-07	3
Chordata;Mammalia;Primates;Macaca fascicularis	3
Cnidaria;Scyphozoa;Rhizostomeae;Crambionella helmbiru	3
Mollusca;Gastropoda;NA;Nerita longii	3
NA;Dinophyceae;Lophodiniales;Woloszynskia sp. ES1-2	3
NA;Dinophyceae;Peridiniales;Scrippsiella precaria	3

Nematoda;Chromadorea;Rhabditida;Heligmosomoides polygyrus	3
Tenericutes;Mollicutes;Entomoplasmatales;Spiroplasma kunkelii	3
Apicomplexa;Coccidia;Eucoccidiorida;Eimeria brasiliensis	2
Arthropoda;Arachnida;Mesostigmata;Varroa destructor	2
Arthropoda;Insecta;Coleoptera;Microrhopala excavata	2
Arthropoda;Insecta;Coleoptera;Pristonema sp. AG02	2
Arthropoda;Insecta;Diptera;Megaselia sp. BOLD-2016	2
Arthropoda;Insecta;Hymenoptera;Diolcogaster sp. Choi57	2
Arthropoda;Insecta;Hymenoptera;Phanerotoma bonbonensis	2
Bacteroidetes;Sphingobacteriia;Sphingobacteriales;Pedobacter steynii	2
Chordata;Actinopteri;Beloniformes;Oryzias latipes	2
Chordata;Actinopteri;Gobiiformes;Rhyacichthys aspro	2
Chordata;Mammalia;Scandentia;Tupaia chinensis	2
Mollusca;Bivalvia;Mytiloida;Bathymodiolus platifrons	2
Mollusca;Gastropoda;NA;Mastigeulota kiangsinensis	2
Mollusca;Gastropoda;NA;Radix natalensis	2
Mollusca;Gastropoda;Nudibranchia;Tenellia sp. 1 AF-2006	2
NA;Dinophyceae;Gonyaulacales;Ceratium hirundinella	2
NA;Dinophyceae;Peridiniales;Pfiesteriaceae sp. CCMP2836	2
NA;Oligohymenophorea;Hymenostomatida;Tetrahymena sp. BOLD:AAO5057	2
NA;Oomycetes;Pythiales;Pythium megalacanthum	2
Rotifera;Monogononta;Ploima;Synchaeta cf. tremula/oblonga UO-2012	2
Streptophyta;NA;Brassicales;Camelina sativa	2
Streptophyta;NA;Malvales;Theobroma cacao	2
Actinobacteria;Actinobacteria;Micrococcales;Brevibacterium linens	1
Annelida;Clitellata;Rhynchobdellida;Placobdella multilineata	1
Annelida;Polychaeta;Phyllodocida;Odontosyllis globulocirrata	1
Annelida;Polychaeta;Terebellida;Grassleia cf. hydrothermalis MHE-2016	1
Apicomplexa;Aconoidasida;Haemosporida;Plasmodium malariae	1
Arthropoda;Arachnida;Araneae;Calisoga sp. K1 DHL-215	1
Arthropoda;Arachnida;Araneae;Floronia bucculenta	1
Arthropoda;Arachnida;Araneae;Hasarius adansoni	1
Arthropoda;Arachnida;Araneae;Heptathela sp. 2 XX-2016	1
Arthropoda;Arachnida;Araneae;Heptathela sp. XUX-2012-309	1
Arthropoda;Arachnida;Araneae;Maeota simoni	1
Arthropoda;Arachnida;Araneae;Neriene sp. 5 LT-2015	1
Arthropoda;Arachnida;Araneae;Tomopisthes varius	1
Arthropoda;Arachnida;Astigmata;Trouessartia inexpectata	1
Arthropoda;Arachnida;Mesostigmata;Amblyseius largoensis	1
Arthropoda;Arachnida;Mesostigmata;Digamasellidae sp. BOLD:ACE4876	1
Arthropoda;Arachnida;Mesostigmata;Mesostigmata sp. BOLD:ACI6949	1
Arthropoda;Arachnida;Mesostigmata;Ologamasidae sp. BOLD:ABA8135	1
Arthropoda;Arachnida;Mesostigmata;Parasitidae sp. BOLD:AAN6694	1

Arthropoda;Arachnida;NA;Calyptostoma sp. BOLD:ABV4196	1
Arthropoda;Arachnida;NA;Microtrombidiidae sp. BOLD:ACG6273	1
Arthropoda;Arachnida;NA;Sperchon sp. BOLD:ACO5111	1
Arthropoda;Arachnida;Oribatida;Oribatulidae sp. BOLD:ACM1667	1
Arthropoda;Insecta;Coleoptera;Atomaria fuscata	1
Arthropoda;Insecta;Coleoptera;Lycidae sp. BOLD:ACC9914	1
Arthropoda;Insecta;Coleoptera;Malvapion malvae	1
Arthropoda;Insecta;Coleoptera;Mycetina perpulchra	1
Arthropoda;Insecta;Coleoptera;Phengodes plumosa	1
Arthropoda;Insecta;Coleoptera;Poecilonota variolosa	1
Arthropoda;Insecta;Coleoptera;Pterostichus jurinei	1
Arthropoda;Insecta;Coleoptera;Staphylinidae sp. BMNH 1274637	1
Arthropoda;Insecta;Coleoptera;Staphylinidae sp. BOLD:ACG6295	1
Arthropoda;Insecta;Coleoptera;Sternidius alpha	1
Arthropoda;Insecta;Diptera;Anthomyiidae sp. BOLD:AAL7523	1
Arthropoda;Insecta;Diptera;Drosophila busckii	1
Arthropoda;Insecta;Diptera;Ophiomyia sp. Opcam-1	1
Arthropoda;Insecta;Ephemeroptera;Rhithrogena sp. 10 LV-2015	1
Arthropoda;Insecta;Hemiptera;Anoecia sp. BOLD-2016	1
Arthropoda;Insecta;Hemiptera;Chinannus bierigi	1
Arthropoda;Insecta;Hemiptera;Eratoneura aculeata	1
Arthropoda;Insecta;Hemiptera;Halyomorpha halys	1
Arthropoda;Insecta;Hymenoptera;Apanteles sp. Rodriguez213	1
Arthropoda;Insecta;Hymenoptera;Campopleginae sp. BOLD-2016	1
Arthropoda;Insecta;Hymenoptera;Cheloninae sp. BOLD:AAH0556	1
Arthropoda;Insecta;Hymenoptera;Chelonus sp. Yu01	1
Arthropoda;Insecta;Hymenoptera;Microgastrinae sp. ASPNI546-09	1
Arthropoda;Insecta;Hymenoptera;Phanerotoma sp. RK113	1
Arthropoda;Insecta;Hymenoptera;Pteromalidae sp. BOLD-2016	1
Arthropoda;Insecta;Hymenoptera;Rhabdepyris sp. ON-2002	1
Arthropoda;Insecta;Hymenoptera;Stenomacrus sp. BOLD:AAJ5372	1
Arthropoda;Insecta;Lepidoptera;Argyresthia goedartella	1
Arthropoda;Insecta;Lepidoptera;Catoptria conchella	1
Arthropoda;Insecta;Lepidoptera;Cyclophora punctaria	1
Arthropoda;Insecta;Lepidoptera;Nisoniades sp. UK31	1
Arthropoda;Insecta;Lepidoptera;Phigalia titea	1
Arthropoda;Insecta;Neuroptera;Myrmeleontidae sp. MAMAN250-12	1
Arthropoda;Insecta;Strepsiptera;Elenchus sp. 2 DPM-2011	1
Arthropoda;Insecta;Thysanoptera;Frankliniella schultzei	1
Arthropoda;Insecta;Thysanoptera;Thrips palmi	1
Arthropoda;Insecta;Thysanoptera;Thrips urticae	1
Arthropoda;Insecta;Trichoptera;Ptilostomis semifasciata	1
Arthropoda;Malacostraca;Cumacea;Diastylopsis thilenuisi	1

Bacteroidetes;Cytophagia;Cytophagales;Bernardetia litoralis	1
Bacteroidetes;Cytophagia;Cytophagales;Cyclobacterium marinum	1
Bacteroidetes;Cytophagia;Cytophagales;Hymenobacter sp. PAMC 26554	1
Bacteroidetes;Flavobacteriia;Flavobacteriales;Salegentibacter sp. T436	1
Basidiomycota;Agaricomycetes;Agaricales;Pleurotus populinus	1
Basidiomycota;Agaricomycetes;Polyporales;Cerrena unicolor	1
Basidiomycota;Agaricomycetes;Polyporales;Ganoderma applanatum	1
Chordata;Actinopteri;Cypriniformes;Cyprinus carpio	1
Chordata;Actinopteri;Cypriniformes;Danio rerio	1
Chordata;Actinopteri;Perciformes;Erisphex pottii	1
Chordata;Actinopteri;Siluriformes;Neoplecostomus selenae	1
Chordata;Amphibia;Anura;Arthroleptis variabilis	1
Chordata;Amphibia;Anura;Gephyromantis leucocephalus	1
Chordata;Mammalia;Chiroptera;Myotis riparius PS2	1
Chordata;Mammalia;Didelphimorphia;Monodelphis domestica	1
Chordata;Mammalia;Primates;Pan troglodytes	1
Chordata;Mammalia;Rodentia;Mus musculus	1
Chordata;Mammalia;Rodentia;Myodes rufocanus	1
Chordata;Mammalia;Tubulidentata;Orycteropus afer	1
Chordata;NA;Squamata;Chamaeleo zeylanicus	1
Chordata;NA;Squamata;Madatyphlops arenarius	1
Chytridiomycota;Chytridiomycetes;Spizellomycetales;Spizellomyces punctatus	1
Cnidaria;Anthozoa;Actiniaria;Actiniaria sp. BOLD:ACQ4394	1
Cnidaria;Anthozoa;Scleractinia;Acanthastrea ishigakiensis	1
Cnidaria;Hydrozoa;Anthoathecata;Coryne eximia	1
Cnidaria;Hydrozoa;Leptothecata;Clytia folleata	1
Cnidaria;Hydrozoa;Leptothecata;Clytia hemisphaerica	1
Cnidaria;Hydrozoa;Leptothecata;Clytia sp. 1 SL-2013	1
Cnidaria;Hydrozoa;Leptothecata;Obelia sp. MZUSP 3356	1
Cnidaria;Hydrozoa;Siphonophorae;Chuniphyes multidentata	1
Cnidaria;Hydrozoa;Siphonophorae;Halistemma sp. 1 BO-2009	1
Euryarchaeota;Thermoplasmata;Methanomassiliicoccales;Candidatus Methanomassiliicoccus intestinalis	1
Eustigmatophyceae;NA;Eustigmatales;Nannochloropsis limnetica	1
Gastrotricha;NA;Chaetonotida;Diuronotus aspetos	1
Mollusca;Bivalvia;Ostreoida;Crassostrea virginica	1
Mollusca;Cephalopoda;Teuthida;Magnapinna sp. ARL-2008	1
Mollusca;Gastropoda;NA;Achatinella fuscobasis	1
Mollusca;Gastropoda;NA;Biomphalaria sp. CJS-2010	1
Mollusca;Gastropoda;NA;Dendropoma rhyssoconchum	1
Mollusca;Gastropoda;NA;Elysia pusilla	1
Mollusca;Gastropoda;NA;Erato environmental sample	1
Mollusca;Gastropoda;NA;Erosaria erosa	1

Mollusca;Gastropoda;NA;Gulella natalensis	1
Mollusca;Gastropoda;NA;Meghimatium fruhstorferi	1
Mollusca;Gastropoda;NA;Scabrotrophon maltzani	1
Mollusca;Gastropoda;NA;Sinumelon expositum	1
Mollusca;Gastropoda;Nudibranchia;Dirona albolineata	1
NA;Bangiophyceae;Bangiales;Pyropia vietnamensis	1
NA;Dinophyceae;Gonyaulacales;Alexandrium fundyense	1
NA;Dinophyceae;Peridiniales;uncultured Thecadinium	1
NA;Florideophyceae;Corallinales;Amphiroa ephedraea	1
NA;Florideophyceae;Gigartinales;Ramicrusta aranea	1
NA;Florideophyceae;Nemaliales;Dichotomaria sp. SMB-2013g	1
NA;NA;Bicosoecida;Caecitellus parvulus	1
NA;NA;Kinetoplastida;Leishmania peruviana	1
NA;NA;NA;NA	1
NA;Oomycetes;Peronosporales;Phytophthora hydrogena	1
NA;Oomycetes;Peronosporales;Phytophthora thermophila x moyootj	1
Nematoda;Chromadorea;Ascaridida;Parascaris equorum	1
Nematoda;Chromadorea;Oxyurida;Enterobius vermicularis	1
Nematoda;Chromadorea;Rhabditida;Haemonchus placei	1
Nematoda;Chromadorea;Rhabditida;Strongylus vulgaris	1
Nematoda;Chromadorea;Spirurida;Onchocerca flexuosa	1
Nematoda;Enoplea;Trichocephalida;Trichuris ovis	1
Phaeophyceae;NA;Ectocarpales;Ectocarpus sp. 12 AP-2014	1
Phaeophyceae;NA;Fucales;Sargassum polycystum	1
Phaeophyceae;NA;Laminariales;Laminaria setchellii	1
Platyhelminthes;Cestoda;Diphyllobothriidea;Schistocephalus solidus	1
Platyhelminthes;Trematoda;Plagiorchiida;Dicrocoelium dendriticum	1
Proteobacteria;Alphaproteobacteria;Rickettsiales;Ehrlichia ruminantium	1
Proteobacteria;Betaproteobacteria;Burkholderiales;Pandoraea sputorum	1
Rotifera;Monogononta;Ploima;Brachionus quadridentatus	1
Streptophyta;Liliopsida;Alismatales;Spirodela polyrhiza	1
Streptophyta;Liliopsida;Poales;Hordeum vulgare	1
Streptophyta;NA;Proteales;Nelumbo nucifera	1

Table S2: Metagenomics, DNA analysis of the V4 region of the 18S rRNA.

Water sample taken in Lake Geneva on the 2nd of October 2018, at 17 m depth. This sample was chosen because of the high number of large-type of OPBaM present at that time.

Grand Total	418220
#N/A	359604
Rotifera;Monogononta;Ploima;Keratella cochlearis	37027
Rotifera;Monogononta;Ploima;Synchaeta kitina	9753
Rotifera;Monogononta;Ploima;Polyarthra dolichoptera complex sp. UO-2013	5756
NA;NA;Prymnesiales;Chrysochromulina sp. CCMP291	2811
Arthropoda;Branchiopoda;Diplostraca;Macrothrix sp. HE-364	936
Chordata;Mammalia;Primates;Homo sapiens	907
Ascomycota;Eurotiomycetes;Eurotiales;Penicillium sclerotiorum	158
NA;Dinophyceae;Gonyaulacales;Alexandrium tamarense	69
Ascomycota;Dothideomycetes;Capnodiales;Cladosporium sp. BM-2009-5	64
Streptophyta;NA;Solanales;Solanum lycopersicum	64
NA;NA;NA;Vermamoeba vermiformis	55
Rotifera;Monogononta;Ploima;Ascomorpha ovalis	51
Mollusca;Gastropoda;NA;Ancilla sp. MNHN IM 2013-55401	47
Arthropoda;Arachnida;Mesostigmata;Cheiroseius sp. BOLD:ACE1640	45
NA;Dinophyceae;NA;uncultured dinoflagellate	44
Basidiomycota;Agaricomycetes;Agaricales;Clitocybe robusta	40
NA;Oomycetes;Pythiales;uncultured Pythium	40
Mollusca;Gastropoda;NA;Physella gyrina	37
Rotifera;Monogononta;Ploima;Polyarthra sp. UO-2013	33
Mollusca;Gastropoda;NA;Physella johnsoni	28
Arthropoda;Arachnida;Mesostigmata;Typhloseiulus rodopiensis	25
Bacteroidetes;Sphingobacteriia;Sphingobacteriales;Sphingobacterium sp. 21	25
Firmicutes;Clostridia;Clostridiales;Clostridium autoethanogenum	18
Chordata;Actinopteri;Carangiformes;Carangoides armatus	17
Platyhelminthes;Cestoda;Cyclophyllidea;Mesocestoides corti	17
Mollusca;Bivalvia;Mytiloida;Modiolus barbatus	16
NA;Chrysophyceae;NA;Apoikiospumella mondseeiensis	15
Platyhelminthes;Trematoda;Plagiorchiida;Homalometron manteri	15
NA;NA;NA;invertebrate environmental sample	14
Arthropoda;Arachnida;Araneae;Nippononeta sp. 12 SL-2010	13
Chlorophyta;Chlorodendrophyceae;Chlorodendrales;Tetraselmis aff. maculata	12
Arthropoda;Arachnida;Araneae;Heptathela sp. 4 XX-2016	11
Chordata;Aves;Apterygiformes;Apteryx australis	11
Arthropoda;Insecta;Hymenoptera;Ectatomma ruidum	10
Chordata;Actinopteri;Beloniformes;Oryzias uwai	10
Mollusca;Cephalopoda;Sepiida;Sepia pharaonis	10
Firmicutes;Bacilli;Bacillales;Staphylococcus agnetis	9

Arthropoda;Malacostraca;Decapoda;Anomura sp. LPdivOTU90	8
Echinodermata;NA;NA;Eleutherozoa sp. COT003_L204	8
Mollusca;Gastropoda;NA;Physella ancillaria	8
Mollusca;Gastropoda;Thecosomata;Creseis clava	8
NA;Dinophyceae;Gonyaulacales;Azadinium dalianense	8
NA;Dinophyceae;Lophodiniales;Woloszynskia sp. CS-341	8
NA;Dinophyceae;Suessiales;Polarella glacialis	8
Nematoda;Chromadorea;Rhabditida;Angiostrongylus cantonensis	8
NA;Oligohymenophorea;Peniculida;Frontonia didieri	7
Rotifera;Monogononta;Ploima;Lecane papuana	7
Arthropoda;Arachnida;Mesostigmata;Blattisociidae sp. BOLD:ACJ0472	6
Arthropoda;Insecta;Trichoptera;Leptonema simulans	6
Basidiomycota;Microbotryomycetes;Sporidiobolales;Rhodotorula taiwanensis	6
NA;Dinophyceae;Peridiniales;Thoracosphaera heimii	6
NA;Oomycetes;Saprolegniales;Saprolegnia eccentrica	6
Nematoda;Chromadorea;Spirurida;Gongylonema pulchrum	6
Arthropoda;Insecta;Diptera;Cecidomyiidae sp. BOLD-2016	5
Arthropoda;Insecta;Diptera;Chironomidae sp. BOLD:AAV6026	5
Arthropoda;Malacostraca;Amphipoda;Niphargus subtypicus	5
Ascomycota;Sordariomycetes;Hypocreales;Fusarium solani	5
Chordata;Mammalia;NA;Ovis canadensis	5
Mollusca;Gastropoda;NA;Opisthostoma laidlawi	5
Arthropoda;Chilopoda;Craterostigmomorpha;Craterostigmus tasmanianus	4
Arthropoda;Insecta;Diptera;Cecidomyiidae sp. BOLD:ACA7477	4
Arthropoda;Insecta;Thysanoptera;Thrips sp. BOLD:AAG0728	4
Bacillariophyta;Mediophyceae;Hemiaulales;Eucampia zodiacus	4
Chordata;Actinopteri;NA;Pseudochromis sp. MBS1109301	4
Mollusca;Bivalvia;Mytiloida;Gigantidas tangaroa	4
NA;Oomycetes;Pythiales;Pythium ultimum	4
Nematoda;Chromadorea;Rhabditida;Nippostrongylus brasiliensis	4
Rotifera;Monogononta;Ploima;Polyarthra dolichoptera	4
Acanthocephala;Palaeacanthocephala;Echinorhynchida;Rhadinorhynchus sp. MGV-2005	3
Annelida;Clitellata;Haplotaxida;Lumbricus castaneus	3
Arthropoda;Arachnida;Mesostigmata;Cheiroseius sp. BOLD:ABY2050	3
Arthropoda;Arachnida;NA;Raoiella indica	3
Arthropoda;Insecta;Diptera;Metopomyza flavonotata	3
Arthropoda;Insecta;Hymenoptera;Prasmodon sp. Janzen11	3
Basidiomycota;Agaricomycetes;Agaricales;Lepiota sp. MUSH114-07	3
Chordata;Mammalia;Primates;Macaca fascicularis	3
Cnidaria;Scyphozoa;Rhizostomeae;Crambionella helmbiru	3
Mollusca;Gastropoda;NA;Nerita longii	3
NA;Dinophyceae;Lophodiniales;Woloszynskia sp. ES1-2	3
NA;Dinophyceae;Peridiniales;Scrippsiella precaria	3

Nematoda;Chromadorea;Rhabditida;Heligmosomoides polygyrus	3
Tenericutes;Mollicutes;Entomoplasmatales;Spiroplasma kunkelii	3
Apicomplexa;Coccidia;Eucoccidiorida;Eimeria brasiliensis	2
Arthropoda;Arachnida;Mesostigmata;Varroa destructor	2
Arthropoda;Insecta;Coleoptera;Microrhopala excavata	2
Arthropoda;Insecta;Coleoptera;Pristonema sp. AG02	2
Arthropoda;Insecta;Diptera;Megaselia sp. BOLD-2016	2
Arthropoda;Insecta;Hymenoptera;Diolcogaster sp. Choi57	2
Arthropoda;Insecta;Hymenoptera;Phanerotoma bonbonensis	2
Bacteroidetes;Sphingobacteriia;Sphingobacteriales;Pedobacter steynii	2
Chordata;Actinopteri;Beloniformes;Oryzias latipes	2
Chordata;Actinopteri;Gobiiformes;Rhyacichthys aspro	2
Chordata;Mammalia;Scandentia;Tupaia chinensis	2
Mollusca;Bivalvia;Mytiloida;Bathymodiolus platifrons	2
Mollusca;Gastropoda;NA;Mastigeulota kiangsinensis	2
Mollusca;Gastropoda;NA;Radix natalensis	2
Mollusca;Gastropoda;Nudibranchia;Tenellia sp. 1 AF-2006	2
NA;Dinophyceae;Gonyaulacales;Ceratium hirundinella	2
NA;Dinophyceae;Peridiniales;Pfiesteriaceae sp. CCMP2836	2
NA;Oligohymenophorea;Hymenostomatida;Tetrahymena sp. BOLD:AAO5057	2
NA;Oomycetes;Pythiales;Pythium megalacanthum	2
Rotifera;Monogononta;Ploima;Synchaeta cf. tremula/oblonga UO-2012	2
Streptophyta;NA;Brassicales;Camelina sativa	2
Streptophyta;NA;Malvales;Theobroma cacao	2
Actinobacteria;Actinobacteria;Micrococcales;Brevibacterium linens	1
Annelida;Clitellata;Rhynchobdellida;Placobdella multilineata	1
Annelida;Polychaeta;Phyllodocida;Odontosyllis globulocirrata	1
Annelida;Polychaeta;Terebellida;Grassleia cf. hydrothermalis MHE-2016	1
Apicomplexa;Aconoidasida;Haemosporida;Plasmodium malariae	1
Arthropoda;Arachnida;Araneae;Calisoga sp. K1 DHL-215	1
Arthropoda;Arachnida;Araneae;Floronia bucculenta	1
Arthropoda;Arachnida;Araneae;Hasarius adansoni	1
Arthropoda;Arachnida;Araneae;Heptathela sp. 2 XX-2016	1
Arthropoda;Arachnida;Araneae;Heptathela sp. XUX-2012-309	1
Arthropoda;Arachnida;Araneae;Maeota simoni	1
Arthropoda;Arachnida;Araneae;Neriene sp. 5 LT-2015	1
Arthropoda;Arachnida;Araneae;Tomopisthes varius	1
Arthropoda;Arachnida;Astigmata;Trouessartia inexpectata	1
Arthropoda;Arachnida;Mesostigmata;Amblyseius largoensis	1
Arthropoda;Arachnida;Mesostigmata;Digamasellidae sp. BOLD:ACE4876	1
Arthropoda;Arachnida;Mesostigmata;Mesostigmata sp. BOLD:ACI6949	1
Arthropoda;Arachnida;Mesostigmata;Ologamasidae sp. BOLD:ABA8135	1
Arthropoda;Arachnida;Mesostigmata;Parasitidae sp. BOLD:AAN6694	1

Arthropoda;Arachnida;NA;Calyptostoma sp. BOLD:ABV4196	1
Arthropoda;Arachnida;NA;Microtrombidiidae sp. BOLD:ACG6273	1
Arthropoda;Arachnida;NA;Sperchon sp. BOLD:ACO5111	1
Arthropoda;Arachnida;Oribatida;Oribatulidae sp. BOLD:ACM1667	1
Arthropoda;Insecta;Coleoptera;Atomaria fuscata	1
Arthropoda;Insecta;Coleoptera;Lycidae sp. BOLD:ACC9914	1
Arthropoda;Insecta;Coleoptera;Malvapion malvae	1
Arthropoda;Insecta;Coleoptera;Mycetina perpulchra	1
Arthropoda;Insecta;Coleoptera;Phengodes plumosa	1
Arthropoda;Insecta;Coleoptera;Poecilonota variolosa	1
Arthropoda;Insecta;Coleoptera;Pterostichus jurinei	1
Arthropoda;Insecta;Coleoptera;Staphylinidae sp. BMNH 1274637	1
Arthropoda;Insecta;Coleoptera;Staphylinidae sp. BOLD:ACG6295	1
Arthropoda;Insecta;Coleoptera;Sternidius alpha	1
Arthropoda;Insecta;Diptera;Anthomyiidae sp. BOLD:AAL7523	1
Arthropoda;Insecta;Diptera;Drosophila busckii	1
Arthropoda;Insecta;Diptera;Ophiomyia sp. Opcam-1	1
Arthropoda;Insecta;Ephemeroptera;Rhithrogena sp. 10 LV-2015	1
Arthropoda;Insecta;Hemiptera;Anoecia sp. BOLD-2016	1
Arthropoda;Insecta;Hemiptera;Chinannus bierigi	1
Arthropoda;Insecta;Hemiptera;Eratoneura aculeata	1
Arthropoda;Insecta;Hemiptera;Halyomorpha halys	1
Arthropoda;Insecta;Hymenoptera;Apanteles sp. Rodriguez213	1
Arthropoda;Insecta;Hymenoptera;Campopleginae sp. BOLD-2016	1
Arthropoda;Insecta;Hymenoptera;Cheloninae sp. BOLD:AAH0556	1
Arthropoda;Insecta;Hymenoptera;Chelonus sp. Yu01	1
Arthropoda;Insecta;Hymenoptera;Microgastrinae sp. ASPNI546-09	1
Arthropoda;Insecta;Hymenoptera;Phanerotoma sp. RK113	1
Arthropoda;Insecta;Hymenoptera;Pteromalidae sp. BOLD-2016	1
Arthropoda;Insecta;Hymenoptera;Rhabdepyris sp. ON-2002	1
Arthropoda;Insecta;Hymenoptera;Stenomacrus sp. BOLD:AAJ5372	1
Arthropoda;Insecta;Lepidoptera;Argyresthia goedartella	1
Arthropoda;Insecta;Lepidoptera;Catoptria conchella	1
Arthropoda;Insecta;Lepidoptera;Cyclophora punctaria	1
Arthropoda;Insecta;Lepidoptera;Nisoniades sp. UK31	1
Arthropoda;Insecta;Lepidoptera;Phigalia titea	1
Arthropoda;Insecta;Neuroptera;Myrmeleontidae sp. MAMAN250-12	1
Arthropoda;Insecta;Strepsiptera;Elenchus sp. 2 DPM-2011	1
Arthropoda;Insecta;Thysanoptera;Frankliniella schultzei	1
Arthropoda;Insecta;Thysanoptera;Thrips palmi	1
Arthropoda;Insecta;Thysanoptera;Thrips urticae	1
Arthropoda;Insecta;Trichoptera;Ptilostomis semifasciata	1
Arthropoda;Malacostraca;Cumacea;Diastylopsis thilenuisi	1

Bacteroidetes;Cytophagia;Cytophagales;Bernardetia litoralis	1
Bacteroidetes;Cytophagia;Cytophagales;Cyclobacterium marinum	1
Bacteroidetes;Cytophagia;Cytophagales;Hymenobacter sp. PAMC 26554	1
Bacteroidetes;Flavobacteriia;Flavobacteriales;Salegentibacter sp. T436	1
Basidiomycota;Agaricomycetes;Agaricales;Pleurotus populinus	1
Basidiomycota;Agaricomycetes;Polyporales;Cerrena unicolor	1
Basidiomycota;Agaricomycetes;Polyporales;Ganoderma applanatum	1
Chordata;Actinopteri;Cypriniformes;Cyprinus carpio	1
Chordata;Actinopteri;Cypriniformes;Danio rerio	1
Chordata;Actinopteri;Perciformes;Erisphex pottii	1
Chordata;Actinopteri;Siluriformes;Neoplecostomus selenae	1
Chordata;Amphibia;Anura;Arthroleptis variabilis	1
Chordata;Amphibia;Anura;Gephyromantis leucocephalus	1
Chordata;Mammalia;Chiroptera;Myotis riparius PS2	1
Chordata;Mammalia;Didelphimorphia;Monodelphis domestica	1
Chordata;Mammalia;Primates;Pan troglodytes	1
Chordata;Mammalia;Rodentia;Mus musculus	1
Chordata;Mammalia;Rodentia;Myodes rufocanus	1
Chordata;Mammalia;Tubulidentata;Orycteropus afer	1
Chordata;NA;Squamata;Chamaeleo zeylanicus	1
Chordata;NA;Squamata;Madatyphlops arenarius	1
Chytridiomycota;Chytridiomycetes;Spizellomycetales;Spizellomyces punctatus	1
Cnidaria;Anthozoa;Actiniaria;Actiniaria sp. BOLD:ACQ4394	1
Cnidaria;Anthozoa;Scleractinia;Acanthastrea ishigakiensis	1
Cnidaria;Hydrozoa;Anthoathecata;Coryne eximia	1
Cnidaria;Hydrozoa;Leptothecata;Clytia folleata	1
Cnidaria;Hydrozoa;Leptothecata;Clytia hemisphaerica	1
Cnidaria;Hydrozoa;Leptothecata;Clytia sp. 1 SL-2013	1
Cnidaria;Hydrozoa;Leptothecata;Obelia sp. MZUSP 3356	1
Cnidaria;Hydrozoa;Siphonophorae;Chuniphyes multidentata	1
Cnidaria;Hydrozoa;Siphonophorae;Halistemma sp. 1 BO-2009	1
Euryarchaeota;Thermoplasmata;Methanomassiliicoccales;Candidatus Methanomassiliicoccus intestinalis	1
Eustigmatophyceae;NA;Eustigmatales;Nannochloropsis limnetica	1
Gastrotricha;NA;Chaetonotida;Diuronotus aspetos	1
Mollusca;Bivalvia;Ostreoida;Crassostrea virginica	1
Mollusca;Cephalopoda;Teuthida;Magnapinna sp. ARL-2008	1
Mollusca;Gastropoda;NA;Achatinella fuscobasis	1
Mollusca;Gastropoda;NA;Biomphalaria sp. CJS-2010	1
Mollusca;Gastropoda;NA;Dendropoma rhyssoconchum	1
Mollusca;Gastropoda;NA;Elysia pusilla	1
Mollusca;Gastropoda;NA;Erato environmental sample	1
Mollusca;Gastropoda;NA;Erosaria erosa	1

Mollusca;Gastropoda;NA;Gulella natalensis	1
Mollusca;Gastropoda;NA;Meghimatium fruhstorferi	1
Mollusca;Gastropoda;NA;Scabrotrophon maltzani	1
Mollusca;Gastropoda;NA;Sinumelon expositum	1
Mollusca;Gastropoda;Nudibranchia;Dirona albolineata	1
NA;Bangiophyceae;Bangiales;Pyropia vietnamensis	1
NA;Dinophyceae;Gonyaulacales;Alexandrium fundyense	1
NA;Dinophyceae;Peridiniales;uncultured Thecadinium	1
NA;Florideophyceae;Corallinales;Amphiroa ephedraea	1
NA;Florideophyceae;Gigartinales;Ramicrusta aranea	1
NA;Florideophyceae;Nemaliales;Dichotomaria sp. SMB-2013g	1
NA;NA;Bicosoecida;Caecitellus parvulus	1
NA;NA;Kinetoplastida;Leishmania peruviana	1
NA;NA;NA;NA	1
NA;Oomycetes;Peronosporales;Phytophthora hydrogena	1
NA;Oomycetes;Peronosporales;Phytophthora thermophila x moyootj	1
Nematoda;Chromadorea;Ascaridida;Parascaris equorum	1
Nematoda;Chromadorea;Oxyurida;Enterobius vermicularis	1
Nematoda;Chromadorea;Rhabditida;Haemonchus placei	1
Nematoda;Chromadorea;Rhabditida;Strongylus vulgaris	1
Nematoda;Chromadorea;Spirurida;Onchocerca flexuosa	1
Nematoda;Enoplea;Trichocephalida;Trichuris ovis	1
Phaeophyceae;NA;Ectocarpales;Ectocarpus sp. 12 AP-2014	1
Phaeophyceae;NA;Fucales;Sargassum polycystum	1
Phaeophyceae;NA;Laminariales;Laminaria setchellii	1
Platyhelminthes;Cestoda;Diphyllobothriidea;Schistocephalus solidus	1
Platyhelminthes;Trematoda;Plagiorchiida;Dicrocoelium dendriticum	1
Proteobacteria;Alphaproteobacteria;Rickettsiales;Ehrlichia ruminantium	1
Proteobacteria;Betaproteobacteria;Burkholderiales;Pandoraea sputorum	1
Rotifera;Monogononta;Ploima;Brachionus quadridentatus	1
Streptophyta;Liliopsida;Alismatales;Spirodela polyrhiza	1
Streptophyta;Liliopsida;Poales;Hordeum vulgare	1
Streptophyta;NA;Proteales;Nelumbo nucifera	1

177

Conclusions and outlook

_____

6.1   Micropearls: discovery of a widespread phenomenon

The present work allowed to uncover a yet undescribed biomineralization process, which results in the formation of micropearls. These intracellular mineral inclusions, composed of metastable near-amorphous calcium carbonate (ACC), are produced by unicellular planktonic organisms. Alkaline-earth metal carbonate inclusions had never been described before in unicellular eukaryotes. This enhances the significance of our results, which show that this biomineralization capacity seems widespread amongst the whole class Chlorodendrophyceae. We identified eleven micropearl-producing species, living in very different habitats and environments: estuarine, marine (both in open water and on the sea floor), brackish and freshwater environments. Thus, the production of micropearls is not directly related to a specific habitat and may take place in water of various types, from freshwater to seawater. The composition of the micropearls imply that their formation is a biologically-controlled process: the micropearl-forming organisms have the capacity to integrate and concentrate specific elements (such as Ca, Ba and/or Sr), which they extract from their environment, to form the micropearls.

During this study, the presence of micropearls has been identified in water samples coming from seven different lakes around the world, both freshwater and brackish: Lake Geneva (Switzerland / France), Lake Lucerne (Switzerland), Lake Lugano (Switzerland), Lake Bourget (France), Lake Annecy (France), Lake Kournas (Greece) and Lake Titicaca (Peru / Bolivia). This is coherent with the fact that *Tetraselmis cordiformis*, the micropearl-forming organism identified in Lake Geneva, is described as having a "worldwide distribution, in freshwater lakes or ponds" (Guiry and Guiry, 2019). Moreover, the occurrence of marine micropearl-producing species, cited in the literature, show that their geographical extent is also widespread in marine waters (Fig. 1).

Furthermore, our results indicate that Chlorodendrophyceae are not the only taxa to produce micropearls. At least one additional organism produces micropearls, although of different composition: in natural conditions, Chlorodendrophyceae produce micropearls of pure calcium carbonate or slightly enriched in strontium, while the "unidentified organism of Lake Geneva" produces micropearls highly enriched in barium (up to >90mol% Ba/Ca). The presently known characteristics of this organism (listed in Chapter V) are sufficient to state that it is not a close relative of the Chlorodendrophyceae and even suggest that it could be part of the heterotroph eukaryotes (zooflagellates) or mixotroph eukaryotes.
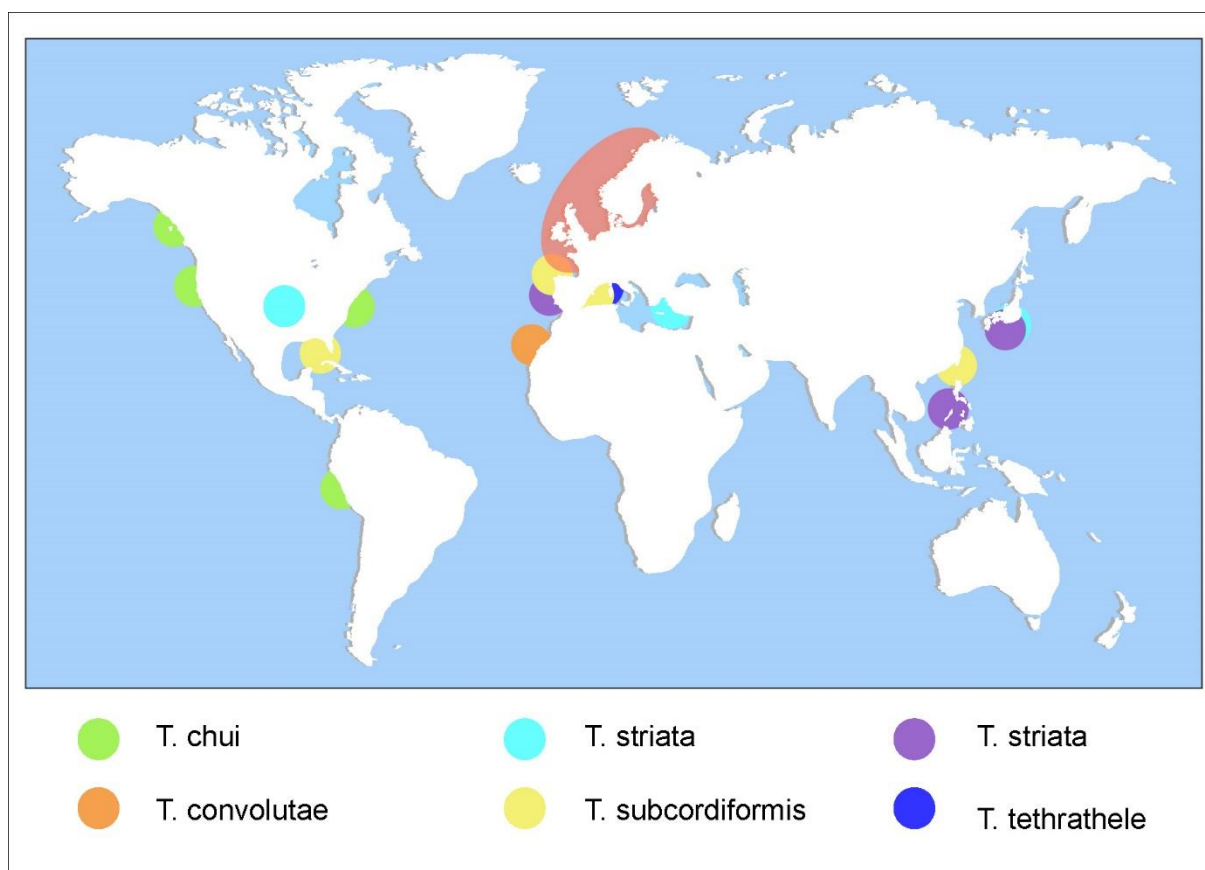
Figure 1 – Occurrences described in the literature of six marine micropearl-producing *Tetraselmis* species.

Red zone: most of the above-mentioned species were observed in that area, probably because it was subject to several extensive works. Note that *T. striata* was also observed in a hypersaline lake of Oklahoma (USA). Data from Guiry and Guiry (2019).

6.2   An innovating method

Most of the species, which were discovered to produce micropearls during this research, had already been thoroughly studied by biologists. Early microscopists did spot the alignments of micropearls in some *Tetraselmis* species, although without identifying their mineral nature (Carter 1938; Hollande et al. 1954; Butcher 1959). These inclusions, which they named "refractive granules", are scarcely mentioned in literature, probably because they were considered as having no taxonomic value (Norris et al. 1980). The advent of electronic imagery techniques did not allow the immediate discovery of micropearls' real nature, because most sample preparation procedures, used to fix the organic matter, dissolve the micropearls.

Micropearls were finally identified as mineral inclusions through a basic sample preparation for SEM microscopy, which we used in the present study: originally meant for diatom frustule imaging, it consists of simply drying the sample, thus deteriorating the organic matter but preserving the mineral material. Successful improvements of this procedure, coupled with mineralogical technics, demonstrated that SEM allows to image the arrangement of the mineral inclusions in the cell and to obtain semi-quantitative elemental analyses of their composition. TEM analyses of FIB-cut cross-sections can then lead to further investigations (mineralogical state of the material, nano-scale imaging of the inner structure of the biominerals, EELS analysis, etc.).

The sample preparation mishap inducing the dissolution of micropearls, resulted in hiding one of the physiological features of otherwise well-studied organisms. This is possibly not an isolated phenomenon. Therefore, other thoroughly studied organisms, besides those mentioned in this manuscript, could share a yet unnoticed capacity to produce micropearls or similar ACC inclusions.

6.3   Micropearls in the cell

In *Tetraselmis* species, it appears that micropearls are not randomly scattered throughout the cell but are located preferentially just under the cell wall (plasma membrane). Moreover, at certain stages of their life cycle, the micropearl arrangement in the cell forms a pattern, which is characteristic for a given species (e.g. longitudinal alignments). Our results show that this pattern is linked to the shape of the chloroplast, which differs amongst *Tetraselmis* species.

ITS and rbcL phylogenetic analyses carried out on the ten studied *Tetraselmis* species showed that species of a given clade all seem to present similar micropearl arrangement patterns. This assumption should be confirmed by further phylogenetic analyses on other *Tetraselmis* species, but these results suggest that, when it is present, the micropearl arrangement pattern may constitute a valid criterion to distinguish different phylogenetic groups in the genus *Tetraselmis*.

Finally, it appears that species sharing the same pattern of micropearl arrangement generally also share the same habitat, thus suggesting a possible genetic basis for the distribution of the micropearls in the cell, in relation with functional needs linked to the species' specific habitat.

6.4 High alkaline-earth element concentration capacities

The mineralogical analyses of micropearls shows that their formation is associated, in some species, with the selective concentration of specific alkaline-earth elements. Indeed, microalgae of the genus *Tetraselmis* form micropearls exclusively enriched in strontium, while the "unidentified micropearl-producing organism of Lake Geneva", which lives simultaneously in the same water, concentrates high quantities of barium, with occasional minor amounts of strontium. In the same way, the marine species *Tetraselmis desikacharyi* was observed to produce micropearls slightly enriched in barium and strontium, while other species of *Tetraselmis*, cultured in the same medium, form micropearls enriched in strontium only (*T. chui*), or composed of pure calcium carbonate (*T. contracta* and *T. convolutae*).

Moreover, these concentration capacities seem to be very strong in certain species. For instance, the "unidentified organism producing Ba-rich micropearls" in Lake Geneva succeeds to form micropearls with a Ba/Ca ratio up to 800 000 times higher than in the surrounding lake water. Our measurements showed that in periods of high productivity, the metabolic activity of these organisms can influence the barium concentration of the Lake Geneva surface waters.

6.5 Mineralogy of the micropearls and formation process

The process leading to the formation of micropearls seems to be the same in all the species observed by TEM. The micropearls form around a nucleus, possibly of organic nature, which is rod-shaped in the *Tetraselmis* species, but appears u-shaped in the "unidentified micropearl-producing organism of Lake Geneva".

The internal structure of the micropearls is characterized by a concentric oscillatory zoning on a nanometric scale, expressing variations in the chemical composition of the micropearls (Sr/Ca or Ba/Ca ratios). These structures indicate that the growth of the micropearl takes place at sufficient supersaturation and is continuous. By applying a solid solution thermodynamic model to this case, Thien et al. (2017) showed that micropearl formation could potentially be explained by the combination of the organisms' high pre-concentration capacities and an abiotic non-equilibrium solid solution growing mechanism (Annex II). Their results lead to estimate the formation time of a micropearl to an order of a few days. Nevertheless, the long-term amorphous state displayed by the micropearls, even after the organism's death (up to 2

years, according to our observations), implies a strong biological control of the mineralization, through the presence of mineral or organic additives needed to prevent the crystallization of ACC.

6.6 Outlook

The discovery of unsuspected biomineralization capacities in numerous species, some with high selective concentration potentials, opens new possibilities of research in various directions. For example:

Bioremediation

A PhD research project started recently, aiming to investigate the potential development of bioremediation methodologies based on micropearl-forming organisms. The capacity to concentrate selectively specific alkaline-earth elements beside calcium is of great interest for bioremediation (Krejci et al., 2011, Fukuda et al., 2014), particularly in areas polluted by radioactive strontium, in link with nuclear activities or accidents or in areas with barium pollutions issued from sludge deposits due to oil production. Preliminary laboratory tests on a *Tetraselmis* species forming Sr-rich micropearls showed that the absorption of the element is rapid: already a few days after addition of Sr in the culture medium, micropearls' Sr content was greatly increased (Segovia-Campos, oral communication). Further experiments are ongoing.

Understanding the biological process leading to the formation of micropearls

It is of great interest to understand the biological processes underlying biomineralization. Unicellular organisms are easier to culture and to study than large pluricellular organisms. The study of different species of the same genus, some producing micropearls and others not, could allow to compare their genome and potentially to understand what genes and proteins are implicated in the biomineralization process. The affinity of a given species for one alkaline-earth metal rather than another could also be addressed in this way. Moreover, markers could be used to follow the path taken respectively by calcium, strontium and barium to understand how these organisms extract these elements from the environment and metabolize them.

Identifying the organism producing barium-rich micropearls in Lake Geneva

The successful identification of this organism could lead to interesting potential applications. It would, for example, allow to compare the genomes of Chlorodendrophyceae producing micropearls with the genome of this other unicellular organism, using the same biomineralization process, but with a distant phylogeny. Potential similar genes between these different organisms could help to identify those playing a role in the biomineralization of ACC.

Stable ACC

The micropearl-forming organisms are perfect candidates to study the formation of stable (or metastable) ACC. Indeed, they are relatively easy to culture and the calcium carbonate endures for years in a near-amorphous state after the organisms have been dried. Investigating the additives implied in the stabilization of ACC is currently the focus of numerous material studies and investigating this particular case could potentially produce interesting results.

Micropearls in lakes with different water chemistry

The phytoplanktonic assemblages vary greatly with different chemistry of the lake water. Thus, investigating samples from lakes with drastically different water chemistry would give the opportunity to discover other micropearl-forming organisms, potentially with the capacity to concentrate different elements than those already studied during this research.

The fate of micropearls

Micropearl-forming organisms play a role in the biogeochemical cycles of Lake Geneva, as was mentioned earlier. Given their widespread geographical distribution, they probably also play a role in the biogeochemical cycles of numerous other water bodies. Thus, understanding their fate would allow to deepen our understanding of this phenomenon: are micropearls dissolved after the organisms' death, or do they sink to the bottom and are buried in sediments, thus taking these chemical elements into a sedimentary sink? Moreover, the presence of mineral elements with such exotic compositions in the sediments could help to interpret chemical anomalies, which are not yet understood (e.g. sediment layers enriched in barium and/or strontium).
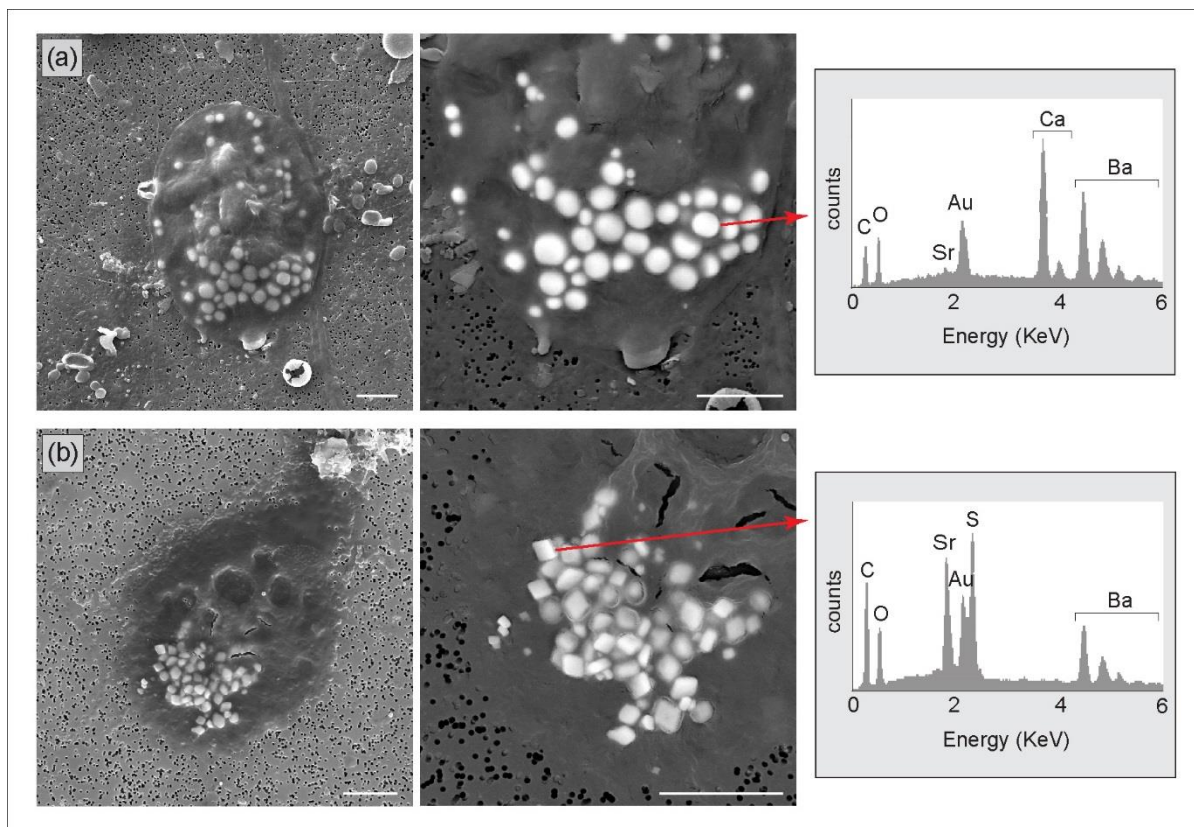
Figure 2 – Possible crystallization of Ba-rich micropearls: from Ba-rich ACC to BaSO₄?

(a) Organism forming Ba-rich micropearls. Sample taken from Lake Geneva, at the *GE3* location, on the 19th of May 2015 at 18 m depth. The micropearls are composed of near-amrophous Ba-rich hydrated calcium carbonate. (b) Organism with intracellular Ba-rich crystals; possibly dying because it appears badly delimited and invaded by numerous bacteria. The mineral observed is probably barite ($BaSO_4$). Sample taken in Lake Geneva, at the *SHL2* location, on the 19th of February 2015 at 308 m depth. - Left hand-side images show the whole organisms (SEM secondary electron images). Right hand-side images are zooms on the intracellular minerals (SEM backscattered images) and are linked to EDXS analyses of one of the minerals. Scale bars: 5 μm.

This last point being of particular interest for sedimentologists, a research on the subject is already ongoing, raising new interesting questions. Preliminary results show no clear micropearl-equivalent in lacustrine sediments, maybe because of dilution by other components. Nevertheless, water samples taken at the bottom of Lake Geneva, at 308 m depth, have provided interesting results. At these depths, we found no trace of the micropearls enriched in strontium, produced by Chlorodendrophyceae. On the other hand, several organisms producing Ba-rich micropearls have been observed, seemingly in good shape.

Others, very similar although less well delimited (which we interpreted as dying), present minerals with crystalline shapes instead of micropearls (Fig. 2). Surprisingly, the composition of these minerals hints towards Ba and Sr sulfates rather than Ba carbonates. A preliminary

working hypothesis, based on the fact that high sulfur concentrations were detected in the organic matter of ageing *Tetraselmis* cells, is that dying cells might provide enough sulfur to permit the crystallization of sulfates. We can also consider the alternative possibility that these are different organisms, living in the deep waters of Lake Geneva, and producing intracellular barite inclusions. Further investigations will, hopefully, allow a better understanding of the fate of micropearls once they reach the sediment and of their implication within the Ba and Sr biogeochemical cycles of Lake Geneva.

6.7   References

Butcher RW (1959) An introductory account of the smaller algae of British coastal waters Part I: introduction and Chlorophyceae. Fish Investig 4:1-74

Carter N (1938) New or interesting algae from brackish water. Arch Protistenk 90:1-68

Fukuda S, Iwamoto K, Atsumi M, Yokoyama A, Nakayama T, Ishida K, Inouye I, Shiraiwa Y (2014) Global searches for microalgae and aquatic plants that can eliminate radioactive cesium, iodine and strontium from the radio-polluted aquatic environment: A bioremediation strategy. J Plant Res, 127:79–89

Guiry MD, Guiry GM (2019) AlgaeBase, World-wide Electron. Publ Natl Univ Ireland, Galway. http://www.algaebase.org, searched on: 03 February 2019

Hollande A, Enjumet M, LaFaurie F (1954) Contribution a l'étude des Volvocales: études des genres Platymonas West et Stephanoptera Dangeard. Ann Scie nat Zool 16 :283-292

Krejci, MR, Wasserman B, Finney L, McNulty I, Legnini D, Vogt S, Joester D (2011). Selectivity in biomineralization of barium and strontium. J Struct Biol, 176:192–202

Norris RE, Hori T, Chihara M (1980) Revision of the genus *Tetraselmis* (Class Prasinophyceae). Bot Mag Tokyo 93:317–339

Thien B, Martignier A, Jaquet JM, Filella M (2017) Linking environmental observations and solid solution thermodynamic modeling : the case of Ba- and Sr-rich micropearls in Lake Geneva. Pure Appl Chem 89:645-652

Acknowledgements / Remerciements

_____

I want to thank all the people who contributed to this project, in one way or another! Originally, the research presented in this manuscript is the result of a conjunction of circumstances, which allowed the discovery of the micropearls during a SEM session with a totally different focus. After that, although I have been leading this research in the last four years, I feel it is, in a way, a collective endeavour: indeed, this work would not have been possible without the continuous support and the collaboration of people issued from very diverse backgrounds, all motivated to share their respective knowledge for the pleasure of trying to unravel the mystery of these intriguing little micropearls.

I want to thank especially Jean-Michel Jaquet, who was present all along this long adventure, from the discovery of the first micropearls to the thesis defense. He made me discover the marvel of the lacustrine microscopic biomineralization world, and his perpetual enthusiasm and curiosity were as strong a support as his wide scientific knowledge of traditional "naturalist", combining geology, biology, environment and technical applications. Thank you Jean-Michel!

I want to thank also Daniel Ariztegui, for his kind and efficient direction of my work. He was always available and receptive and I greatly appreciated his supportive attitude and excellent advice all along these years, as well as the deep scientific knowledge he shared. He was particularly a great support during all the difficult moments and a driving force to widen the scope of this project. Thank you Daniel!

I want to thank also Montserrat Filella, who has been a cornerstone of this project all along, providing extremely useful contacts, bringing me all her expertise in environmental chemistry, her meticulousness, positive energy and continuous support. Thank you Montserrat! I also thank Muriel Pacton, who was an important driver at the beginning of this project: amongst other things, I am particularly grateful to her for helping me to take my first steps into the "biological side" of biomineralization. I thank François Barja, for welcoming me warmly in his lab, although my sample preparation methods probably seemed barbaric for a biologist, for his continued help and support and for his positive energy all along the years! I am also

Appendices

_____

Preliminary investigations on picoplankton-related precipitation of alkaline-earth metal carbonates in meso-oligotrophic lake Geneva (Switzerland)

Jean-Michel JAQUET,[1*] Pascale NIREL,[2] Agathe MARTIGNIER[1]

[1]Section des Sciences de la Terre et de l'Environnement, Université de Genève, 13 rue des Maraîchers, CH-1205 Geneva; [2]Service d'Ecologie de l'Eau, Département de l'Intérieur, Mobilité et Environnement (DIME), 23 rue Ste. Clotilde, CH-1211 Geneva, Switzerland
*Corresponding author: jean-michel.jaquet@unige.ch

ABSTRACT

In the course of a routine water-quality survey in meso-oligotrophic lake Geneva (Switzerland), suspended matter was collected by filtration on 0.2 μm membranes in July and August 2012 at the depth of maximal chlorophyll a (Chl a) concentration (2 mg m^{-3}). Examination by scanning electron microscopy revealed the presence of numerous dark and gelatinous patches occluding the pores of the membranes, containing high numbers of picoplanktonic cells and, in places, clusters of medium-to-high-reflectance smooth microspheres (0.6 μm in diameter). Their chemical composition, determined by semi-quantitative, energy-dispersive X ray spectrometry (EDS) showed magnesium (Mg), calcium (Ca), strontium (Sr) and barium (Ba) (alkaline earth metals) to be the dominant cations. Among the anions, phosphorus (P) and carbon (C) were present, but only the latter is considered here (as carbonate). The microspheres were subdivided into four types represented in a Ca-Sr-Ba ternary space. All types are confined within a domain bound by Ca>45, Sr<10 and Ba<50 (in mole %). Type I, the most frequent, displays a broad variability in Ba/Ca, even within a given cluster. Types II and III are devoid of Ba, but may incorporate P. Type IV contains only Ca. The Type I composition resembles that of benstonite, a Group IIA carbonate that was recently found as intracellular granules in a cyanobacterium from alkaline lake Alchichica (Mexico). Lake Geneva microspheres are solid, featureless and embedded in a mucilage-looking substance in the vicinity of, but seemingly not inside, picoplanktonic cells morphologically similar to Chlorella *and* Synechococcus. *In summer 2012, the macroscopic physico-chemical conditions in lake Geneva epilimnion were such as to allow precipitation of Ca but not of Sr and Ba carbonates. Favourable conditions did exist, though, in the micro-environment provided by the combination of active picoplankton and a mucilaginous envelope. Further studies are ongoing to investigate the vertical distribution of the microspheres, their internal structure and their exact mineralogical composition, as well as the taxonomy of the picoplankton and the nature of the mucilage, in order to gain a proper understanding of this intriguing process of alkaline-earth metals sequestration.*

Key words: Bio-mediated carbonate precipitation, alkaline-earth metals, freshwater, picoplankton.

Received: March 2013. Accepted: June 2013.

INTRODUCTION

Calcium carbonate ($CaCO_3$) precipitation in lacustrine environment is now a well-documented phenomenon. It occurs in hard- to moderately hard-water lakes such as, for example, Constance (Stabel, 1986), Zurich (Kelts and Hsu, 1978) and Bourget (Groleau *et al.,* 2000). An earlier work on lake Geneva showed calcite to be oversaturated in the epilimnion between April and August (Jaquet *et al.,* 1983).

Autochtonous calcite precipitation is dependent on water temperature and pH, the latter increasing with phytoplanktonic primary production. Particulate matter, whether living (plankton and bacteria) or inert (organic or mineral detritus), plays an important role in heterogeneous calcite nucleation, a process at work in natural waters in which saturation index (*SI*) is too low to trigger homogeneous nucleation (Stabel, 1986).

Picoplankton, as prokaryotic cyanobacteria (*e.g. Synechococcus*), or small eukaryotic phototrophs (*e.g. Chlorella*), is now recognised as a significant part of autotrophic plankton in lakes as diverse as Baikal (Belykh and Sorokovikova, 2003), Huron (Fahnenstiel *et al.,* 1991), Tahoe (Winder, 2009) and Maggiore (Callieri and Piscia, 2002). In this last case, it is said to successfully compete with nanoplankton in periods of phosphorus (P) limitation. Picoplankton can be an important actor in $CaCO_3$ precipitation process, as confirmed by laboratory experiments and field study in lake Lucerne (Dittrich *et al.,* 2004; Dittrich and Obst, 2004). Various strains of *Synechococcus* have been tested for their potential to sequestrate atmospheric CO_2 (Lee *et al.,* 2006; Jansson and Northen, 2010). This genus has also been found to be active in calcite ooid formation in western lake Geneva (Plée *et al.*, 2008), closely associated to biofilms.

The presence of extracellular polymeric substances (EPS) in biofilms is a key factor in the model of Dupraz *et al*. (2009), which states that organomineralisation can be divided into two coupled elements: i) an alkalinity engine, driven internally by microbial metabolism or externally by the environment (temperature); and ii) an organic

matrix in which mineralisation will take place. Cyanobacteria (Pereira *et al.,* 2009; Dittrich and Sibler, 2010) and some strains of *Chlorella* (Watanabe *et al.,* 2006) are known to secrete extracellular polysaccharides, which may act as binding sites for Ca^{2+} and CO_3^{2-}. The importance of biofilms in freshwater carbonate precipitation has been demonstrated by Rogerson *et al.* (2008) in their experiments on tufa systems.

In contrast to $CaCO_3$, data on precipitation of other alkaline-earth metals (AEM) such as strontium (Sr) and barium (Ba) are scarcer. This is understandable, as the concentration of these elements in lake water is much lower (molar ratio Ba:Sr:Mg:Ca is of the order of 1:40:1900:8200 in lake Geneva), with saturation indices for Sr and Ba carbonates well below zero under normal physico-chemical conditions.

In the marine environment, biogenic Ba preferably precipitates as sulfate (barite) within dead phytoplankton aggregates (abiotic precipitation) (Jeandel *et al.,* 2000), or under the direct influence of biological processes (Gonzalez-Muñoz *et al.,* 2012).

In lake Constance, Sr has been found to co-precipitate with calcium (Ca) in calcite, while a Ca-independent Sr uptake by biota is negligible (Stabel *et al.,* 1986; Stabel, 1989). According to Stabel *et al.* (1991), the water of this lake is always undersaturated with respect to $SrCO_3$ (strontianite), not to mention $BaCO_3$ (witherite).

Barium and Sr sulfates (barite and celestite) are known to be present as biominerals in the terminal vacuoles of freshwater Desmids such as *Closterium* and *Micrasterias* (Brook, 1980; Wilcock *et al.,* 1989; Krejci *et al.,* 2011). Barium carbonate (as witherite) has been reported to be precipitated as fibrous crystals by bacteria (Sanchez-Moral *et al.,* 2004). Another avenue for precipitation of AEM is given by the prostomatid ciliates *Loxodes* and *Remanella*, whose müllerian vesicles contain, respectively, Ba and Sr salts (Finlay *et al.,* 1983; McGrath *et al.,* 1989; Lynn, 2010).

It is only recently that a well-identified amorphous carbonate containing magnesium (Mg), Ca, Sr and Ba (attributed to a benstonite-like phase) was found in highly alkaline lake Alchichica microbialites by Couradeau *et al.* (2012). In this case, the carbonate is precipitated as *intracellular* inclusions in a novel cyanobacterium (candidatus *Gloeomargarita lithophora*).

Within the framework of ongoing water-quality surveys undertaken by the *Service de l'écologie de l'eau* (SECOE) in Petit-Lac (the southwestern part of lake Geneva), suspended matter was collected in 2012 by filtration at the depth of maximum chlorophyll *a* (Chl *a*) concentration. Examination by scanning electron microscopy (SEM) coupled to energy-dispersive X-ray spectrometry (EDS) revealed, in July and August samples, the presence of Mg-Ca-Sr-Ba-containing microspheres, seemingly related to mucilage packaging picoplanktonic cells.

We present here preliminary investigations conducted by SEM/EDS on the microsphere samples currently available. This study is part of a series of geomicrobiological analyses conducted in lake Geneva (Jaquet *et al.,* 1982; Plée *et al.,* 2008; Glas-Haller, 2010).

METHODS

Petit-Lac represents the southwest portion of Léman or lake Geneva. After undergoing eutrophication in the 1980s and 1990s (Anneville and Pelletier, 2000), this hard-water lake is now in the process of re-oligotrophication. Data on physico-chemistry, phytoplankton, zooplankton and fish production is available in the French-Swiss Commission yearly reports (CIPEL, 2011; Lazarotto and Klein, 2012). Recent studies on phytoplankton can be found in Anneville *et al.* (2002) and Gallina *et al.* (2011).

Monthly measurements of physico-chemistry and water samples were taken at GE3 station (6.22°E/46.30°N) at 10 different depths ranging 0 to 70 m with a plastic Niskin® bottle. Also, continuous recording of Chl *a* and turbidity was done by means of a Wet Labs® probe (Wet Labs, Philomath, OR, USA). Phytoplankton was collected by means of an integrating sampler over the top 20 m, and taxa were identified and counted following Utermöhl method. A larger water volume (10-15 L) was sampled at the depth of maximum Chl *a* concentration, followed by gentle vacuum filtration in the lab within a few hours on return from the field. For gravimetry, Whatman® GF/F membranes (Whatman Ltd., Maidstone, UK) were used, and Schleicher & Schuell® nitrocellulose (NC 60; 0.6 μm) (Schleicher & Schuell BioScience GmbH, Dassel, Germany) as well as Millipore® polycarbonate (PC GTTP; 0.2 μm) (Millipore, Billerica, MA, USA) for SEM/EDS. Filters were air-dried, and no fixation was applied on this first set of samples. Sub-samples of filters were mounted on aluminum stubs covered with double-sided conductive carbon tape. A coating of gold (*ca* 15 nm) or carbon (*ca* 15 nm) was then deposited on the samples prior to imaging with a Jeol® JSM 7001F SEM (Jeol Ltd., Tokyo, Japan) (Department of Earth Sciences, Section of Earth and Environmental Sciences, University of Geneva, Switzerland) with an acceleration voltage of 15 kV. Semi-quantitative elemental analyses were performed with a JED2300 EDS detector (Jeol Ltd.; working distance: 10 mm).

Carbonate species concentrations and calcite saturation index [SI=log (IAP/K_S)] were calculated using the software Aqion 2.5.1 (www.aqion.de), based on USGS PHREEQC (Parkhurst and Appelo, 1999) and the thermodynamical database *wateq4f* (Ball and Nordstrom, 1991).

This preliminary study concerns two suspended matter samples in which microspheres were present. They were collected in 2012: i) on 10th July at 6 m depth [polycarbonate (PC) filter numbers 16 and 17, carbon coated] and ii) on 7th August at 6 m depth [(PC filters 20, 21 (carbon coated) and 30 (gold coated)]. Clusters of microspheres

were identified visually on the stubs at a magnification of 1000x and numbered as specimens (*Spx_y-z,* where *x*=1 for 10.07.12, *x*=2 for 07.08.12; *y*=cluster number and *z*=microsphere number).

In order to verify the analytical results obtained by EDS on the microspheres, the mineral benstonite [Mg Ca$_6$ (Ba$_x$Sr$_y$) (CO$_3$)$_{13}$] (with x+y=6) was synthesised following a modification of Hood and colleagues' procedure (Hood and Steidl, 1973; Hood *et al.*, 1974). The precipitate was aged for three days prior to SEM/EDS analysis. It consists of spherical aggregates of nanoparticles (Supplementary Fig. 1), similar in shape to CaCO$_3$ or SrCO$_3$ polymorphs reported by Wu *et al.* (2004), Sun *et al.* (2006) and Sondi and Matijevic (2003). The precipitate attribution to benstonite was confirmed by X-ray diffraction (XRD) (Supplementary Fig. 2) and Raman spectroscopy (Supplementary Fig. 3).

RESULTS

Limnological context

The microsphere-containing suspended matter samples were collected both times in fairly similar conditions

(Fig. 1a): at 6 m in the metalimnion, corresponding to the peak concentration of Chl *a* (2 mg m^{-3} on both dates) and with a turbidity around 1 NTU.

The water was saturated, with respect to calcite, down to 7 m in July and 10 m in August (Tab. 1, Fig. 1b). Other interesting features are the molar ratios (in solution) Sr/Ca, around 0.0050, similar to lake Constance values as mentioned by Stabel *et al.* (1986), and Sr/Ba, which is higher in the epilimnion (43-45.5; Fig. 1c), practically mimicking the Chl *a* profile (Fig. 1a). Analytical results (Tab. 1) indicate, at 5 m depth, higher temperature, pH, Sr/Ba and calcite saturation values (0.34 *vs* 0.13) in August. These Sr/Ba maximums were not observed during our other campaigns in 2012 (data not shown).

Fig. 2 shows the phytoplankton groups found in July and August integrated over the top 20 m of the water column. Because of the integration, this may not represent exactly the taxa living at 6 m depth. Moreover, apart from *Chlorella* sp., it does not include picoplankton, which is omnipresent in the SEM images. In terms of biomass, diatoms (Bacillariophyceae) largely dominate in July, with
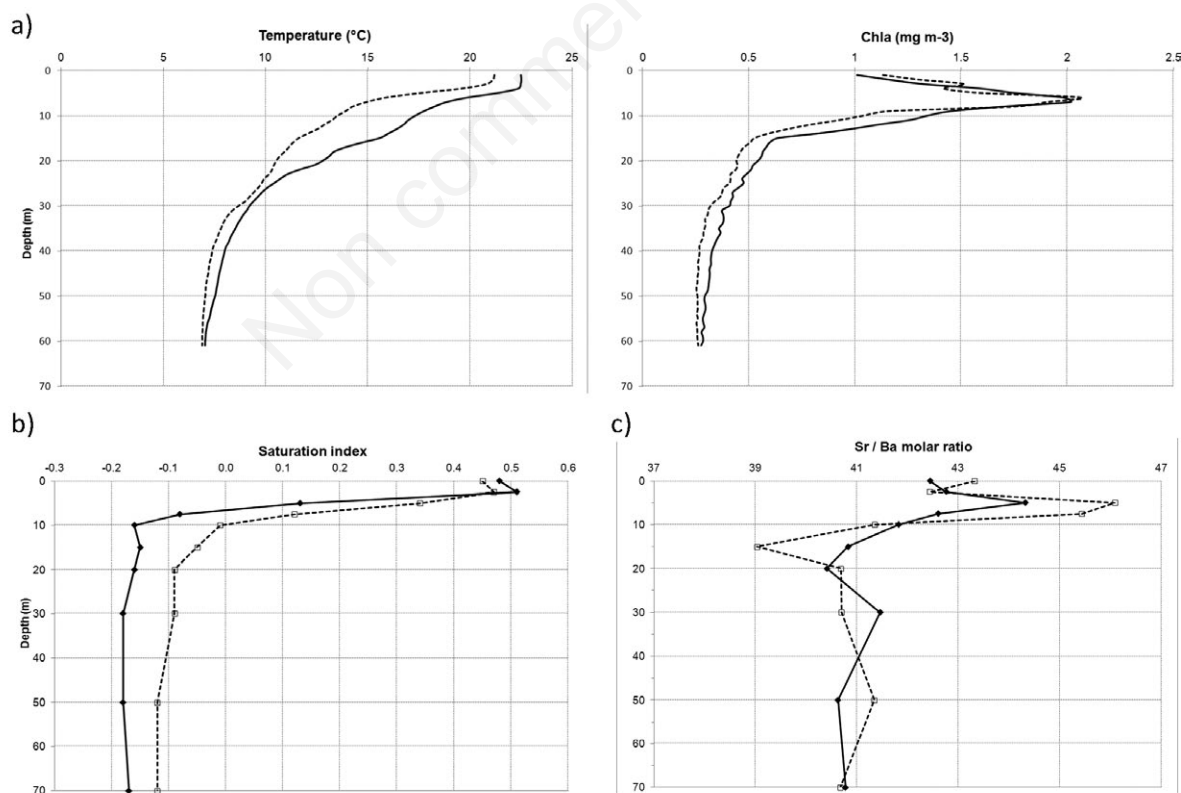
Fig. 1. a) Temperature and chlorophyll *a* concentration profiles at GE3 station on 10th July (dashed line) and 7th August (solid line) 2012; b) corresponding calcite saturation index (samples with saturation index>0 are saturated with respect to calcite); c) Sr/Ba molar ratio.

lesser amounts of Chlorophyceae, Cryptophyceae and Dinophyceae. In August, the diatoms biomass decreases at the expense of the Chlorophyceae (mostly *Chlorella* sp., with abundance around 2×10^3 cell mL^{-1}). No measurements were carried out for water samples at the Chl *a* maximum. However, for lake Geneva in August (upper 15 m), Personnic *et al.* (2009) report picocyanobacterial abundance values up to 3×10^5 cell mL^{-1}.

Overall morphology of suspended matter

The general aspect of the suspended matter collected on 10th July (concentration: 2.6 mg L^{-1}) and 7th August (concentration: 1.8 mg L^{-1}) is shown in Figs. 3 and 4, respectively. An obvious feature of both samples is the presence of dark patches, very likely of mucilaginous nature, which obliterate the membrane pores.

Low reflectance picoplanktonic cells, either spherical (Fig. 5a, right) or ellipsoidal (Fig. 6a), are densely packed within the mucilage patches. Their dimension is of the order of the μm. In places, the patches contain clusters of high-reflectance, spherical or subspherical bodies (Fig. 5a), with diameters varying between 0.6 and 3 μm. These

microspheres are described in detail below. The mucilage embedding the clusters and picoplanktonic is electronically quasi-transparent, and its limits can be quite sharp and sub-circular (white arrows in Fig. 6a and 6b), suggesting an originally spherical shape prior to the deposition on the filter and subsequent collapse through drying. The presence of this organic matrix is further confirmed by a fortunate feature stemming from electron damage, visible on Fig. 6c: whereas most of the microspheres' contours are blurred by the organic coating (Hernández Mariné *et al.,* 2004), the cracks reveal the presence of underlying, *bare*, sharply delimited microspheres (within white frames in Fig. 6c).

Calcium carbonate is present as isolated crystals (>5 μm) or aggregates (Fig. 6a), showing signs of corrosion (Fig. 5a). These do not have any visible relationship with mucilage.

In July (Fig. 3), suspended matter contained, in addition to picoplankton, nano- and microplankton (Fig. 2): centric and pennate diatoms and chrysophyte siliceous scales. *Ceratium hirundinella* and diatoms (*Achnanthes* sp.) (Fig. 4) were present in August.

Tab. 1. Chemical composition of water at GE3 station (selected elements) and in lake Alchichica aquarium (from Couradeau *et al.,* 2012).

Depth (m)	T (°C)	pH	Alkalinity (μM L-1)	Mg (μM L-1)	Ca (μM L-1)	Sr (μM L-1)	Ba (μM L-1)	*SI* calcite
				10.07.2012				
0	20.6	8.52	1570	235	910	5.2	0.12	0.48
2.5	20.0	8.55	1590	235	930	5.2	0.12	0.51
5*	16.0*	8.14*	1730*	235*	1004*	5.3*	0.12*	0.13*
7.5	13.3	7.92	1810	235	1059	5.4	0.13	-0.08
10	12.2	7.86	1820	235	1059	5.3	0.13	-0.16
15	10.6	7.84	1870	240	1094	5.5	0.13	-0.15
20	9.6	7.83	1880	240	1104	5.4	0.13	-0.16
30	7.4	7.84	1880	240	1109	5.5	0.13	-0.18
50	6.4	7.86	1890	240	1104	5.5	0.13	-0.18
70	6.4	7.86	1890	240	1124	5.5	0.14	-0.17
Alchichica aquarium	24	8.9	13617	6955	47	0.013	0.001	0.158
				05.08.2012				
0	22.4	8.5	1480	232	868	5.0	0.12	0.45
2.5	21.8	8.52	1480	233	882	5.0	0.12	0.47
5*	19.4*	8.38*	1560*	232*	924*	5.0*	0.11*	0.34*
7.5	17.4	8.11	1620	241	994	5.1	0.11	0.12
10	16.4	8	1650	235	986	5.2	0.12	-0.01
15	13.6	7.91	1720	238	1052	5.1	0.13	-0.05
20	11.3	7.89	1790	236	1072	5.2	0.13	-0.09
30	8.2	7.88	1880	249	1145	5.5	0.13	-0.09
50	6.7	7.9	1880	244	1123	5.4	0.13	-0.12
70	6.3	7.9	1880	245	1131	5.5	0.13	-0.12

Mg, magnesium; Ca, calcium; Sr, strontium; Ba, barium; SI, *saturation index of calcite (aragonite in Alchichica).* *Approximate depth of occurrence of studied microspheres.*

Alkaline-earth metals precipitates

Structure

Fifty-five individual microspheres were characterised by SEM and analysed by EDS (Tab. 2). Their morphology can be inferred from SEM photographs in Figs. 5 and 6. They are spherical or sub-spherical and, prior to EDS analysis at least, display a very smooth and featureless surface. Their diameter varies between 0.6 and 3 μm. When struck by the electron beam, a small hole generally appears in the microsphere, which then exhibits damage consisting of cracks and surface alteration (darker punctuations; Figs. 5b and 5c). These features seem to be the expression of bubbles developing inside the microspheres. Notice that adjacent microspheres are also affected, being within the electron beam interaction volume of a few cubic μm (white circle in Fig. 5b). In some other instances (Fig. 5c), the electron action induces desquamation of the microspheres, which then appear to be composed of several successive layers a few nm thick. In all cases, these bodies seem to consist of a solid, seemingly amorphous substance (at least at the magnification of the SEM, and pending verification by electron diffraction).

Chemical composition

The microspheres investigated so far have been grouped in five types on the basis of their chemical composition, determined by EDS semi-quantitative analyses

checked by reference to a synthetic benstonite standard. The type numbers and names with averages and minima/maxima are listed in Tab. 2, and the individual microspheres' positions in the Ca-Sr-Ba molar ternary space are shown in Fig. 7. So far, we found 35 microspheres belonging to type I, seven from type II and V, three from type III and only one from type IV. Because of the relatively small sample size (55 clusters), these numbers do not necessarily reflect the true proportion of the various types.

In Tab. 2, the major potential cations are Ca (always present), Ba and Sr, with minor amounts of Mg and potassium (K). Only in type V could P act as a potential anion. However, in this type, there is a severe charge imbalance (Tab. 2, last columns) if P is under the orthophosphate form. This anomaly is hitherto unexplained. In the other groups, we had to postulate the presence of CO_3^{2-}, because carbon cannot be validly analysed with the EDS configuration at our disposal. This can be justified by the carbonate hardness of lake Geneva water and by the findings by Couradeau *et al*. (2012), who report the presence of intracellular granules of an unusual benstonite-like phase, a carbonate (Tab. 3, last column) very similar to our microspheres. In the present paper, we shall deal only with types I, II, III and IV (alkaline-earth metal carbonates), setting aside type V to a further study.

Energy-dispersive X-ray spectrometry mapping was carried out to check the distribution of, chiefly, Mg, Ca, Sr and Ba among the various components of suspended matter. An example is given in Fig. 8a (cluster *Sp2_4*,
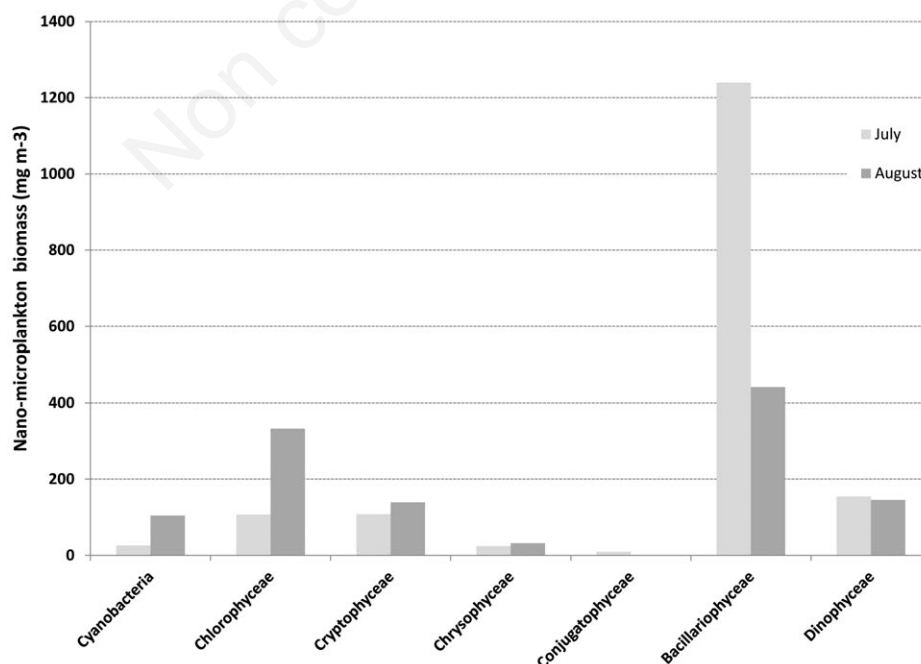

Fig. 2. Biomass of nano-microphytoplankton groups at GE3 station (0-20 m integration) in July and August 2012.

**Tab. 2.** Microspheres average composition (atom %).

Type	I				II				III				IV		V			
Name	CaSrBa				CaSr				CaPSr				Ca		CaP			
Element	Mean	N	Min	Max	Mean	N	Min	Max	Mean	N	Min	Max	Mean	N	Mean	N	Min	Max
Mg	0.5	35	0.0	2.2	0.4	7	0.3	0.8	1.2	3	0.8	1.7	1.0	1	3.5	7	1.4	10.6
P	1.2	3	0.0	2.0					5.0	3	3.4				53.5	7	45.0	60.2
S									2.5	1	2.5	2.5			12.4	2	1.3	23.4
K															8.4	2	7.2	9.5
Ca	32.0	35	19.5	64.1	90.1	7	87.0	92.4	82.7	3	76.3	87.5	99.0	1	37.1	7	23.0	43.1
Sr	4.7	35	0.4	10.1	9.5	7	7.3	12.2	10.3	3	6.6	16.0						
Ba	62.8	35	30.7	75.5	0.0	7												
As 100%*																		
Ca	32.2		19.6	64.4	90.5		87.3	92.8	88.9		82.1	94.2	100.0		100.0			
Sr	4.7		0.4	10.1	9.5		7.3	12.3	11.1		7.1	17.2	0.0		0.0			
Ba	63.1		30.9	76.0	0.0				0.0				0.0		0.0			

*N, number of analyses for a given element; Min, minimum; Max, maximum; Mg, magnesium; P, phosphorus; S, sulphur; K, potassium; Ca, calcium; Sr, strontium; Ba, barium. *Three last rows: Ca, Sr and Ba normalised to 100%.*

Tab. 3. Composition (atom %, alkaline-earth elements) of benstonite varieties.

Ratio	$(Ba_{5.5}Sr_{0.5})$ theoretical* 1	$(Ba_{4.5}Sr_{1.5})$ theoretical* 2	$(Ba_{4.5}Sr_{1.5})$ synthetic° EDS	$(BaSr)_6$ Anthony *et al.* (2012)	$(Ba_{2.7}Sr_{1.0}Mg_{1.4}Ca_{0.9})$ Couradeau *et al.* (2012)
Mg	2.3	2.4	1.3	2.3	18.0
Ca	22.6	23.7	20.8	22.9	53.2
Sr	4.1	13.0	11.2	4.1	8.1
Ba	71.0	60.9	66.7	70.7	20.7

*EDS, energy dispersive X-ray spectrometry; Mg, magnesium; Ca, calcium; Sr, strontium; Ba, barium. *Computed from formula; °analysed semi-quantitatively by EDS on a polished surface. First row: variable cations, in addition to fixed $Mg_1 Ca_6$; last column: recomputed from Table S2 in Couradeau* et al. *(2012).*
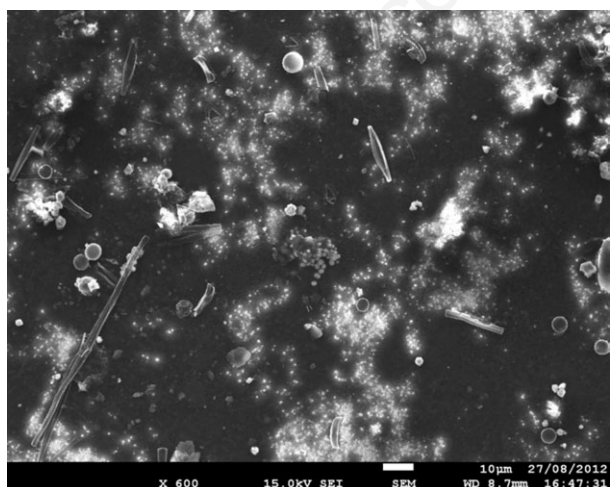
Fig. 3. General view of suspended matter from 10th July 2012 (6 m depth), deposited on 0.2 µm polycarbonate membrane, carbon coated. Scale bar: 10 µm. Centric and pennate diatoms, CaCO₃ as white aggregates. Darker parts are interpreted as mucilage packaging picoplanktonic cells (see Figs. 5-7 for further details). *Sp1_1* cluster of microspheres is visible at the centre of the figure.
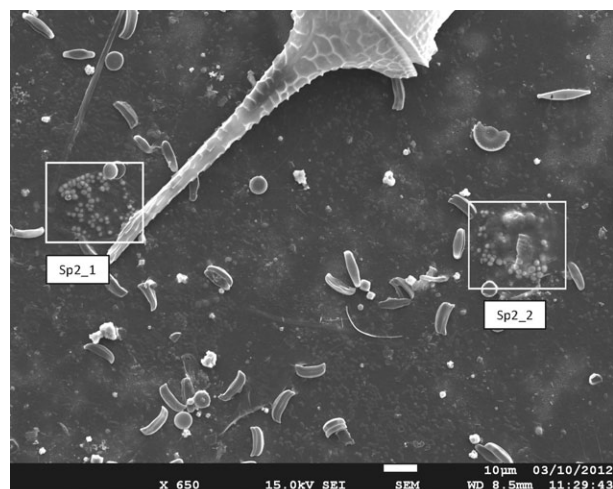
Fig. 4. General view of suspended matter from 7th August 2012 (6 m depth), deposited on 0.2 µm polycarbonate membrane, gold coated. Scale bar: 10 µm. Apical horn of *Ceratium hirundinella*. Numerous *Achnanthes* sp. diatoms, CaCO₃ are also visible. Darker parts are believed to be mucilage packaging picoplanktonic cells (see Fig. 6a and 6b for further details). Two clusters of microspheres are labelled *Sp2_1* and *Sp2_2* (in white frames).

07.08.2012). In this specimen, Ca and Ba are exclusively concentrated in the microspheres, some of which may be rather small. The Sr and silicon (Si) maps are similar due to peak overlaps (Fig. 8b).

DISCUSSION

Chemical composition in terms of dissolved alkaline-earth metals

The concentrations of Ca, Sr, Ba and their seasonal variations are quite similar in lake Geneva and lake Constance (Stabel *et al.,* 1991), where these elements are depleted in epilimnion during summer. In lake Geneva, the ratios $[Me]_{5m}/[Me]_{70m}$ computed from Tab. 1 were, in August 2012, Mg: 0.95, Ca: 0.82, Sr: 0.90 and Ba: 0.85. Hence, it seems that Ca and Ba are slightly more depleted

than Mg and Sr, as an echo to the composition of the microspheres, Ca and Ba representing more than 90% of the cations (Tab. 2) in type I microspheres. In lake Constance, Sr and Ba are said to co-precipitate with calcite at an almost constant stoichiometry in particulate material (molar Sr/Ca=0.0084; atom Sr/Ca=0.018). This could also be the case in lake Geneva, with additional scavenging by the biologically mediated precipitation of specific amorphous AEM carbonates. In contrast, there is no sign of a decrease in Ba concentration towards the bottom (Tab. 1), as in lake Biwa, through adsorption on hydrous manganese oxides (Sugiyama *et al.,* 1992).

Physico-chemical framework for microspheres precipitation

It is not known whether amorphous AEM carbonate
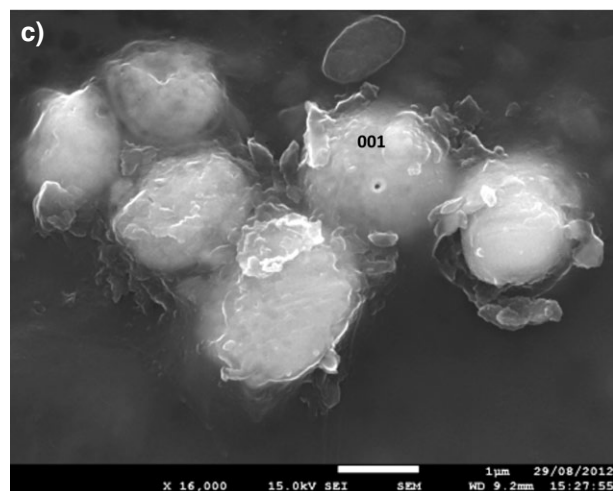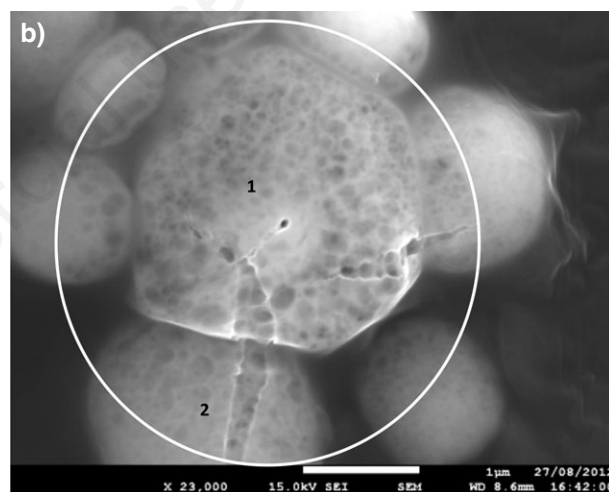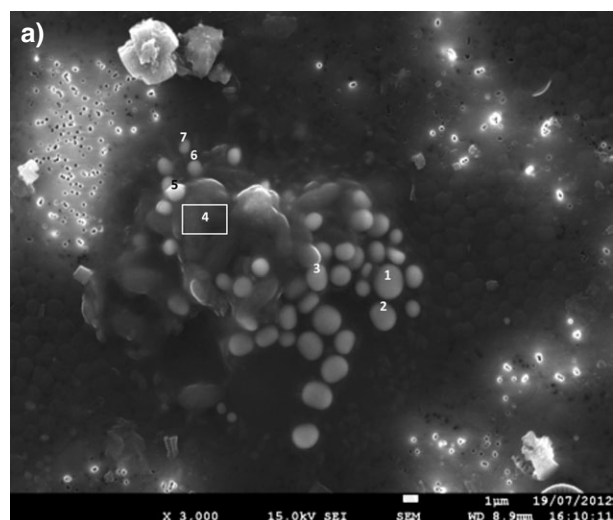
Fig. 5. a) Close-up view of microsphere cluster *Sp1_1* (10.07.2012; from centre of Fig. 3). Scale bar=1 μm, carbon coated. Parts of membrane uncovered by extracellular polymeric substances are lighter, with 0.2 μm pores well visible. Extracellular polymeric substances-covered parts are darker, and show densely-packed, spherical cells 1 μm or less in diameter, with associated microspheres. Numbers refer to individual microspheres that have been analysed by energy-dispersive X-ray spectrometry (EDS) (as points or rectangle). A large CaCO₃ grain is visible on top. Scanning electron microscopy photograph taken prior to EDS analysis of microspheres (compare with Fig. 5b); b) close-up view of microspheres 1 and 2 in cluster *Sp1_1* (10.07.2012). Scale bar: 1 μm. Scanning electron microscopy photograph taken after EDS analysis. Notice bubbly structure and cracks due to electron ray action within the volume of primary excitation of energy-dispersive X ray spectrometry (EDS) analysis (white circle); c) close-up view of microspheres in cluster *Sp1_2* (10.07.2012). Scale bar: 1 μm. Microspheres seem to consist of several successive pellicles. Notice the hole due to EDS point analysis in *Sp1_2-001*. Image taken after EDS analysis.

(AAEMC) microspheres existed at other depths and dates than those found by chance in summer 2012. We only know they occurred in the thermocline, near the Chl *a* concentration or biomass maximum, in waters saturated with respect to calcite and at a depth where the dissolved Sr/Ba molar ratio was maximal (Fig. 1). It is, therefore, not unreasonable to postulate that there is a link between microsphere precipitation and phytoplanktonic primary production (PP) (primary production and phytoplankton biomass maxima generally coincide in lake Geneva) (Tadonleke, 2012). This is substantiated by the close spatial association of microspheres and picoplankton visible in SEM images (Figs. 5a and 6a).

If the macroscopic physico-chemical conditions (saturation index>0; Tab. 1) enable the precipitation of calcite crystals, the situation is different for the AAEMC. Although we were not able to find a value for the solubility constant K_s of crystalline benstonite (let alone for its amorphous, various species), we can approach the question by considering Stabel *et al*.'s (1991) data: these authors have computed, for lake Constance in summer, the $[Sr^{2+}]=3.16\ 10^{-5}$ M L^{-1} and $[Ba^{2+}]=7.08\ 10^{-5}$ M L^{-1} concentrations necessary to allow precipitation of strontianite ($SrCO_3$; $Ks=10^{-9.03}$) and witherite ($BaCO_3$; $Ks=10^{-8.3}$). Extending these figures to our case, it is obvious that Sr and Ba concentrations given in our Tab. 1 are much lower, meaning that these AEM carbonates cannot precipitate under the *macroscopic* pH and temperature conditions in lake Geneva. This is likely to apply also to benstonite-like minerals, the precipitation of which will necessitate micro-environments with extreme conditions (elevated pH, increased ionic concentration and alkalinity).
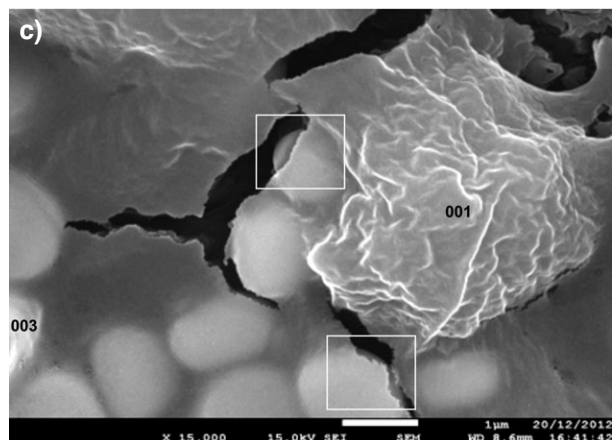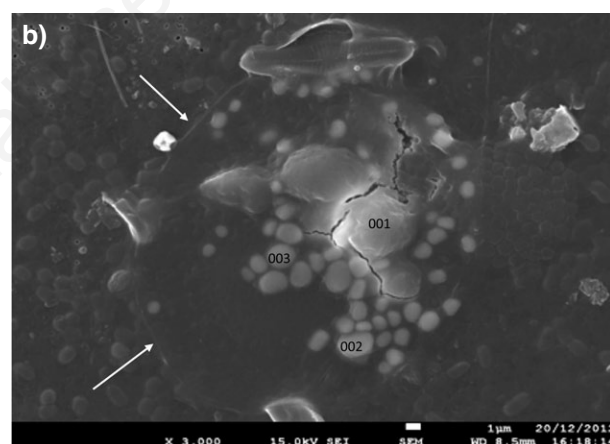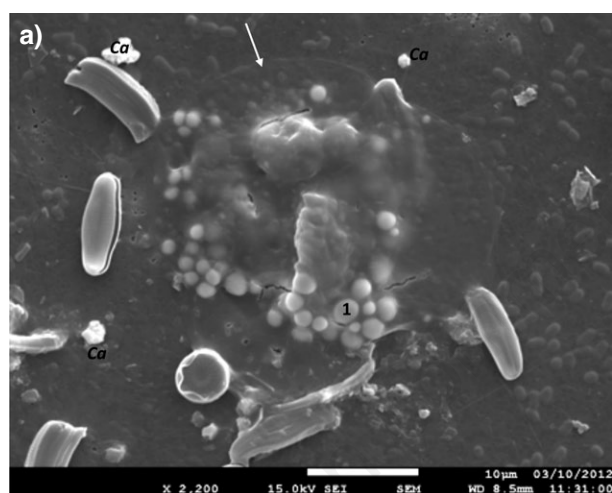
Fig. 6. a) View of microsphere cluster *Sp2_2* (07.08.2012; from right part of Figure 4). Scale bar=10 μm. Most parts of membrane are covered by mucilage (0.2 μm pores not visible), with a well-defined circular mass at centre (upper limit: white arrow). Numerous picoplankton spherical and subspherical cells 1 μm or less in diameter. For analysis of microsphere *Sp2_2-001* (1 at centre), see Tab. 2. A few CaCO$_3$ (*Ca*) grains are visible. Diatoms are *Achnanthes* sp. Photograph taken prior to energy-dispersive X ray spectrometry (EDS) analysis of microspheres; b) view of microsphere cluster *Sp2_3* (07.08.2012). Scale bar: 1 μm. The microspheres are embedded in a subcircular mucilagineous mass, the left limit of which is quite sharp (arrows). Part 001 is heavily coated with mucilage, whereas 002 and 003 are much less so. Numerous picoplankton spherical and subspherical cells 1 μm or less in diameter. Image taken prior to EDS analysis; c) close-up view of microspheres in cluster *Sp2_3* (07.08.2012) after EDS analysis. Scale bar: 1 μm. Mucilagenous part 001 has shrunk (compare with Fig. 6b), and the cracks in mucilagenous matrix have widened. In white frames: *bare* microspheres partially visible under torn mucilage.

Micro-environment

This micro-environment is provided by the combination of picoplanktonic cells and a mucilage-like matrix in which microspheres have been observed to be embedded. Mucilage or EPS (exopolymeric substances) excreted by micro-organisms consists mainly of polysaccharides, which may contain functional groups for metal binding (Tien, 2002; Dittrich and Sibler, 2006, 2010). For instance, Alvarado Quiroz *et al.* (2006) have reported the strong binding capacity of *sticky* EPS-derived acid polysaccharide compounds for thorium (IV). Likewise, Acharya *et al.* (2009) showed that the ability of *Synechococcus elongatus* to bind uranium was due to its complexation with ligands within the EPS coating cell surface. Extracellular polymeric substances are known to stabilise microbial cells against high-energy environments and to provide a chemically protective microenvironment. They also serve to bind and concentrate Ca^{2+} and Mg^{2+} ions and raise the alkalinity of the surrounding water (Decho *et al.,* 2005; Couradeau *et al.,* 2012).

Mucilage has not yet been chemically characterised in the samples under study, but we interpret the low reflectance portions of the polycarbonate membranes (Fig. 3) as extra-cellular mucilage because of the following characteristics: obliteration of the 0.2 μm pores (Figs. 5a and 6a); coating of microspheres and presence of numerous picoplanktonic cells (Fig. 6b) in their midst; patch size reaching several tens of micrometers, thereby ruling out their attribution to flattened cells; and, of course, existence of AAEMC precipitates, which were never found *outside* the dark parts of the membranes.

The taxonomic attribution of the picoplankton associated with the mucilage will be clarified in a follow-up study. At the present stage, the densely packed, coccoid cells visible in July sample (Fig. 5a) could be tentatively attributed to two taxa: a member of i) the Chlorellaceae (*Chlorella, Dictyosphaerium*) or ii) the Chroococcaceae (*Aphanocapsa, Aphanothece*). *Chlorella* has been identified in the integrated phytoplankton counts, and these colonial taxa may have mucilaginous envelopes (Bock *et al.,* 2011; Watanabe *et al.,* 2006). Grouped under a *small eukaryotes* category, they have been found in summer in lakes Annecy, Bourget and Geneva (Personnic *et al.,* 2009). The cyanophyta *Aphanocapsa* and *Aphanothece* have also been counted in the integrated phytoplankton sample. In August, most of the micro-organisms found close to the AAEMC microspheres (Fig. 6a) seem morphologically similar to a species of *Synechococcus* (Callieri and Stockner 2002), a cyanobacterium known for its association with EPS (Alvarado Quiroz *et al.,* 2006). Besides, it is possible that *Synechococcus* and *Chlorella* co-exist in the so-called *association Z* reported by Callieri *et al.* (2006) in lake Maggiore. Epifluorescent microscopy, necessary to discriminate between pro- and eukaryotes (Callieri, 2010), could not be done at the time of sampling

in summer 2012. However, water samples collected at the same GE3 station in June 2013 were examined by a combination of SEM and confocal laser scanning microscopy. Under blue excitation we found coccoid and rod-shaped cells appearing yellow [*PE-cells* of Callieri (2010)], and larger (1-2 μm) cocci emitting in light red (pico-eukaryotes). This finding somewhat supports the taxonomic attribution presented for the summer samples.

On the basis of only SEM images, we cannot know whether the microspheres have precipitated next to, or at the expense of, picoplanktonic cells. The microspheres' aggregation in clusters and their almost perfectly spherical shape would stand in favour of the former alternative, whereas the presence of a pellicle surrounding an internal part might indicate precipitation at the cell surface, as observed by Schultze-Lam and Beveridge (1994) for a *Synechococcus* strain.

The mineral phase

Medium-magnification SEM images do not reveal any clear features on the microspheres' surface (Fig. 6c). They seem to be solid and compact inside, and the bubbly texture seen in Fig. 5b is an artifact clearly due to EDS analysis. This points towards an amorphous nature for the microspheres, characterising also the AAEMC intracellular granules of lake Alchichica (Couradeau *et al.,* 2012). Interestingly, Addadi *et al.* (2003) stress the role of amorphous $CaCO_3$ (ACC or vaterite) in biomineralisation, as temporary storage deposits in various vesicles and transient precursor of calcite or aragonite (Konhauser and Riding, 2012; Mori *et al.,* 2009; Gower, 2008). Finally, similar spherical shapes have been reported in amorphous barite precursors (Gonzalez-Muñoz *et al.*, 2012).

Strictly speaking, types I to IV microspheres should take place in a tetraedric space with Mg, Ca, Sr and Ba apices to account for the composition given in Tab. 2. However, we have chosen to reduce this representation to a ternary Ca-Sr-Ba system: never exceeding a few atom percents, the Mg analytical results are somewhat doubtful and thus can be temporarily disregarded. The ternary plot of Fig. 7a shows the microspheres to be confined within the domain Ca>45; Sr<10; Ba<50 (expressed here as %). The Ba/Ca molar ratio varies between 0 and 1.1, indicating a very broad mixture of these cations compared to a relatively narrow Sr variability. In terms of a possible influence of the sampling date on the composition, the domains of occurrence of July and August microspheres on Fig. 7b being separated in places, while overlapping in others, the question cannot be solved for the moment. The plot of Fig. 7c has been used to establish a provisional typology of the microspheres (Tab. 4). The reality of five *discrete* types will have to be checked through the analysis of further microspheres, with consideration of the limited accuracy of EDS analyses. This will establish whether the chemical compo-

sition forms a continuous series. What is clear from Fig. 7c, though, is the impossibility of subdividing type I, as a great variability in the Ba/Ca ratio exists between microspheres *within* a given cluster (represented in the figure as a line joining the squares). Type III differs from type II by

the presence of P and S (Tab. 2). Type IV is, so far, represented by only one individual.

We have attributed type I microspheres to a benstonite-like amorphous phase. The benstonite mineral species is part of the Nickel-Struntz 05.AB Alkali-earth carbonates

Tab. 4. Indices of approximate stoichiometric formulae for microspheres.

Microspheres	Mg	Ca	Sr	Ba
		$Mg_w Ca_x (Sr_y Ba_z) (CO_3)_{13}$		
Type I: average	0.18	7.57	0.55	4.71
Type I: max Ba	0.09	5.76	0.64	6.51
Type I: max Sr	0.24	6.28	1.27	5.21
Type I: min Ba	0.35	10.83	0.31	1.52
Type II: average	0.09	12.31	0.59	0.00
Lake Alchichica	2.4	6.9	1.0	2.7
Benstonite (from Tab. 3)	1.0	6.0	1.5	4.5

Mg, magnesium; Ca, calcium; Sr, strontium; Ba, barium. Lake Alchichica benstonite-like phase stoichiometry is recomputed from Couradeau et al. *(2012).*
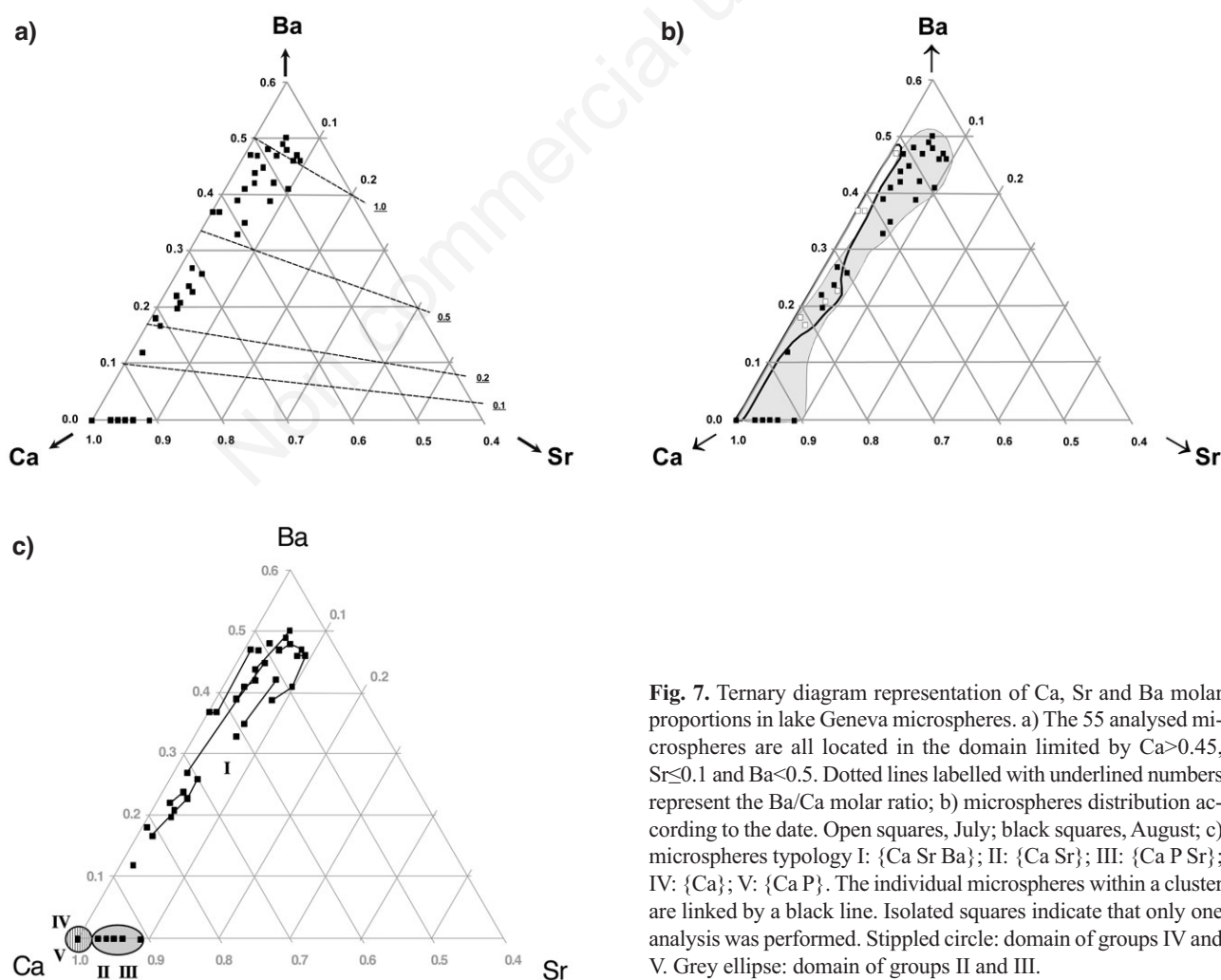
Fig. 7. Ternary diagram representation of Ca, Sr and Ba molar proportions in lake Geneva microspheres. a) The 55 analysed microspheres are all located in the domain limited by Ca>0.45, Sr≤0.1 and Ba<0.5. Dotted lines labelled with underlined numbers represent the Ba/Ca molar ratio; b) microspheres distribution according to the date. Open squares, July; black squares, August; c) microspheres typology I: {Ca Sr Ba}; II: {Ca Sr}; III: {Ca P Sr}; IV: {Ca}; V: {Ca P}. The individual microspheres within a cluster are linked by a black line. Isolated squares indicate that only one analysis was performed. Stippled circle: domain of groups IV and V. Grey ellipse: domain of groups II and III.

category (Barthelemy, 2012; Jolyon, 2012). Its basic formula may be written as $(Ba,Sr)_6(Ca,Mn)_6Mg(CO_3)_{13}$, with Ba, Sr and manganese (Mn) varying in proportions. In the Magnet-Cove variety (Anthony *et al.,* 2012), the formula is $(Ba_{5.27}Sr_{0.73})Ca_{6.00}(Mg_{0.79}Ca_{0.12}Mn_{0.09})(CO_3)_{13}$ or simply $Ba_6Ca_6Mg(CO_3)_{13}$. The variability in composition of different species of benstonite is illustrated in Tab. 3 (from literature) and Tab. 4 (our samples).

In the absence of any significant amount of Mg and Ba, types II, III and IV chemical compositions could be those of an amorphous $CaCO_3$ analogous to vaterite with varying amounts of Sr. The molar Sr/Ca ratio in these types of microspheres is around 0.05 (Tab. 5), equal to that found by Lauchnor *et al.* (2013) in microbially induced Ca and Sr co-precipitates. This value lies in the miscibility region of the phase diagram of $Sr_xCa_{1-x}CO_3$ solids (Ruiz-Hernandez *et al.,* 2010). As already mentioned, in lake Constance this ratio – computed for well *crystallised* calcite – is only 0.0084 (Stabel *et al.,* 1991). For ostracod valves in lake Geneva, Sr/Ca never exceeds 0.0025 (Decrouy *et al.,* 2012). These comparisons seem to indicate a higher Sr sequestration potential for the processes producing microspheres.

The EDS analyses being of semi-quantitative nature, caution has to be exercised when comparing our microspheres' composition to that of *mineralogical* or lake Alchichica benstonite-like phase, the latter given as $(Sr_{1.0}Ba_{2.7}Mg_{1.4}Ca_{0.9})Ca_6 \cdot_0 Mg(CO_3)_{13}$ (Tab. 5, last column). Compared to synthetic benstonite (Tab. 4), lake Geneva microspheres may be higher in Ca (type I, max. Sr and min. Ba), and are always lower in Mg and Sr. All the formulas for *mineralogical* benstonite found in literature have in common an index very close to 6.0 for Ca. This is the case for some lake Geneva type I microspheres, but not for Alchichica granules (6.9). As regard to this and the rather imprecise definition of benstonite, we will consider the attribution of type I microspheres to this mineral phase as tentative only.

Some interesting trends emerge from the element ratios given in Tab. 5. First, the AEM molar ratios are not the same in water and in the microspheres; with respect to Ca, Mg is depressed in the precipitates whereas Sr (average 0.06 in precipitates *vs* 0.0054 in water) and especially Ba (0.30-0.60 *vs* 0.00012) are strongly enriched in the microspheres. The dominance of Sr in water (Sr/Ba=44.3) is inverted in type I microspheres (Sr/Ba=0.12). This Ba enrichment is similar to that existing (as barite) in desmids (Wilcock *et al.,* 1989) and marine bacteria (Gonzalez-Muñoz *et al.,* 2012). This could reflect the affinity of Ba for biota (Martin and Knauer, 1973; McGrath *et al.,* 1989).
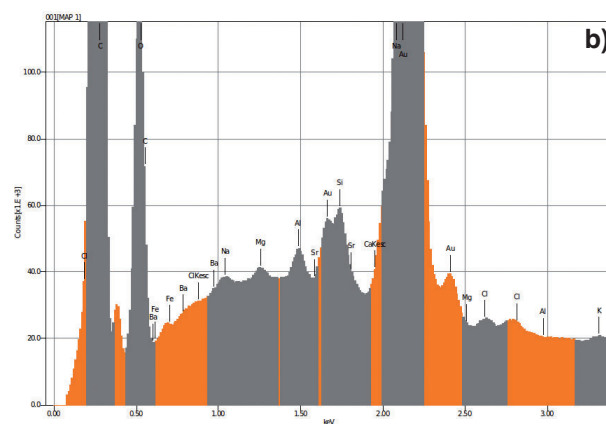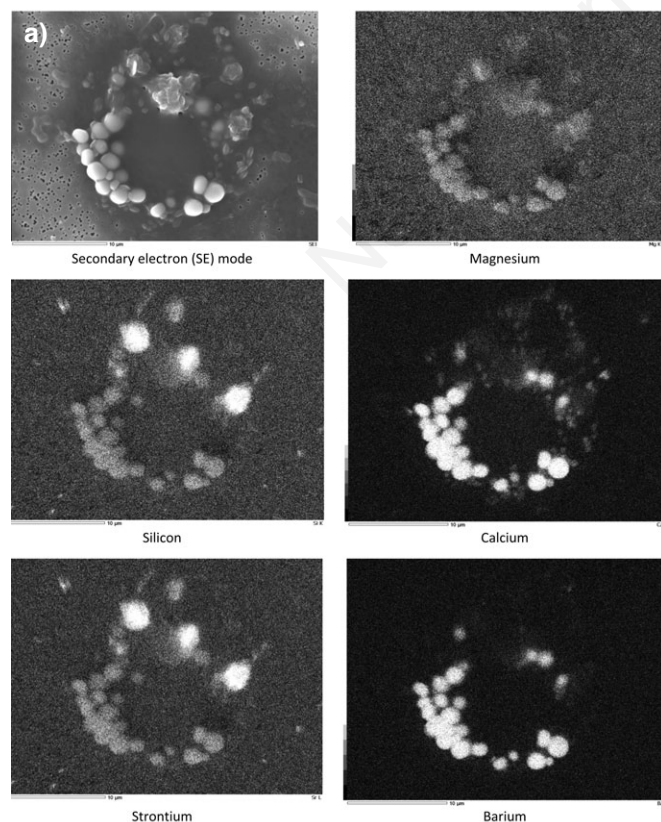
Fig. 8. a) Energy-dispersive X ray spectrometry (EDS) mapping of cluster *Sp2_4* (07.08.2012), embedded in mucilage. Scale bar: 10 μm. Apart from the microspheres, presence of siliceous particles and picoplanktonic cells (1 μm diameter, visible in secondary electron mode). Group IIA metals mineralisation is restricted to bright, >2 μm microspheres. Strontium map is confounded with silicon (spectral peak overlap). Notice the weaker magnesium signature, matching well the *Sp2_4 -001* point analysis (not shown); b) Extract of spectrum corresponding to the mapping of cluster *Sp2_4*. X-axis: energy in keV; Y-axis: counts × 10^3. Main peaks are shown in dark grey. Si *K* (1.73 keV) and Sr *L* (1.8 keV) peaks are very close.

Tab. 5. Selected element atom and molar ratios of water at 5 m depth, in microspheres and various species of benstonite-like phases.

Cation	Water 10.07.2012 5 m	Water 07.08.2012 5 m	Microspheres type I (average)	Microspheres type II (average)	Microspheres type III	$(Sr_{0.5}Ba_{5.5})^*$ theoretical 1	$(Ba_{4.5}Sr_{1.5})^*$ synthetic EDS	$(Ba_{2.7}Sr_{1.0}Mg_{1.4}Ca_{0.9})^*$ Couradeau *et al.* (2012)
Mg/Ca°	0.14	0.15	0.01	0.01	0.01	0.10	0.06	0.34
	0.23	0.25	0.02	0.01	0.02	0.17	0.11	0.56
Sr/Ca	0.012	0.012	0.15	0.11	0.12	0.55	0.54	0.15
	0.0053	0.0055	0.07	0.05	0.06	0.25	0.24	0.07
Ba/Ca	0.00041	0.00041	1.96	1.01		2.57	3.20	0.39
	0.00012	0.00012	0.62	0.29		0.75	0.93	0.11
Sr/Mg	0.081	0.078	9.81	22.7	8.56	5.41	8.41	0.45
	0.022	0.022	3.10	6.29	2.40	1.50	2.33	0.12
Sr/Ba	28.3	29.4	0.07			0.21	0.17	0.39
	44.3	46.1	0.12			0.33	0.26	0.61

EDS, energy dispersive X-ray spectrometry; Mg, magnesium; Ca, calcium; Sr, strontium; Ba, barium. *First row: variable cations, in addition to fixed Mg_1 Ca_6; °top: atom ratio; bottom: molar ratio.

An explanation for the differential enrichment of Sr and Ba in the microspheres could be traced in Rogerson *et al.* (2008), who found that ions other than Ca can be chelated into biofilm EPS, and that this process was highly selective in favour of those ions with small charge density.

Second, with respect to lake Alchichica AAEMC granules, microspheres in lake Geneva are much lower in Mg (Mg/Ca=0.02 *vs* 0.56) and much higher in Ba (Ba/Ca=0.30-0.60 *vs* 0.11). This reflects the highly alkaline character of lake Alchichica waters (Tab. 1, bottom row), with high Mg and low Ca, Sr and Ba concentrations.

CONCLUSIONS

Type I amorphous microspheres (0.6-3 μm diameter) containing Mg, Ca, Sr and Ba found in the epilimnion of lake Geneva in summer 2012 have been tentatively interpreted as a benstonite-like mineral phase. Types II, III and IV, without Ba and with variable Sr, could be ascribed to a vaterite-like phase, a precursor of calcite. All these types are characteristically precipitated within a mucilaginous matrix embedding picoplanktonic cells.

Type I AAEMC microspheres' chemical composition, determined semi-quantitatively by EDS, bears some analogy to that of cyanobacterial intracellular inclusions found in alkaline lake Alchichica (Mexico) microbialites. In lake Geneva, however, the microspheres are pelagic, seemingly extracellular, and contain less Mg but more Ba.

Discovered *a posteriori* in dried suspended matter deposited on filters, these precipitates could be studied only in a preliminary manner. In the context of the little-known Sr and Ba cycles in freshwater, their occurrence raises a series of questions, which will be dealt with in a dedicated study planned for 2013. Is the typology found in 2012 a permanent feature, and how can it be explained? What is the taxonomic attribution of the picoplanktonic cells spatially associated with microspheres within the mucilage? Precipitating in epilimnion, do the microspheres survive in hypolimnion, and possibly in the sediment? Finally, the internal structure and exact composition of the AAEMC precipitates (as carbonate or phosphate in type V?) and associated mucilage should be investigated with adequate tools in order to gain a proper understanding of this peculiar process of AEM sequestration.

REFERENCES

Acharya C, Joseph D, Apte SK, 2009. Uranium sequestration by a marine cyanobacterium, Synechococcus elongatus strain BDU/75042. Bioresource Technol. 100:2176-2181.

Addadi L, Raz S, Weiner S, 2003. Taking advantage of disorder:

amorphous calcium carbonate and its role in biomineralization. Adv. Mater. 15:959-970.

Alvarado Quiroz NG, Hung C-C, Santschi P, 2006. Binding of thorium (IV) to carboxylate, phosphate and sulfate functional groups from marine exopolymeric substances (EPS). Mar. Chem. 100:337-353.

Anneville O, Pelletier J-P, 2000. Recovery of Lake Geneva from eutrophication. Arch. Hydrobiol. 148:607-624.

Anneville O, Souissi S, Ibanez F, Ginot V, Druart JC, Angeli N, 2002. Temporal mapping of phytoplankton assemblages in Lake Geneva: annual and interannual changes in their patterns of succession. Limnol. Oceanogr. 47:1355-1366.

Anthony JW, Bideaux RA, Bladh KW, Nichols MC, 2012. Handbook of mineralogy. Mineralogical Society of America ed., Chantilly: 628 pp.

Ball JW, Nordstrom DK, 1991. User's manual for WATEQ4F, with revised thermodynamic data base and test cases for calculating speciation of major, trace, and redox elements in natural waters. Available from: http://wwwbrr.cr.usgs.gov/projects/GWC_chemtherm/pubs/wq4fdoc.pdf

Barthelemy D, 2012. Mineralogy database. Available from: http://webmineral.com/

Belykh OI, Sorokovikova EG, 2003. Autotrophic picoplankton in Lake Baikal: Abundance, dynamics, and distribution. Aquat. Ecosyst. Health 6:251-261.

Bock C, Krienitz L, Pröschold T, 2011. Taxonomic reassessment of the genus *Chlorella* (Trebouxiophyceae) using molecular signatures (barcodes), including description of seven new species. Fottea 11:293-312.

Brook AJ, 1980. Barium accumulation by desmids of the genus *Closterium* (Zygnemaphyceae). Brit. Phycol. J. 15:261-264.

Callieri C, 2010. Single cells and microcolonies of freshwater picocyanobacteria: a common ecology. J. Limnol. 69:257-277.

Callieri C, Caravati E, Morabito G, Oggioni A, 2006. The unicellular freshwater cyanobacterium Synechococcus and mixotrophic flagellates: evidence for a functional association in an oligotrophic, subalpine lake. Freshwater Biol. 51:263-273.

Callieri C, Piscia R, 2002. Photosynthetic efficiency and seasonality of autotrophic picoplankton in Lago Maggiore after its recovery. Freswater Biol. 47:941-956.

Callieri C, Stockner JC, 2002. Freshwater autotrophic picoplankton: a review. J. Limnol. 61:1-14.

CIPEL, 2011. General conclusions on the state of Lake Geneva in 2010. Commission Internationale pour la Protection du Léman ed., Nyon.

Couradeau E, Benzerara K, Gérard E, Moreira D, Bernard S, Brown Jr GE, López-García P, 2012. An early-branching microbialite cyanobacterium forms intracellular carbonates. Science 336:459-462

Decho AW, Visscher PT, Reid RP, 2005. Production and cycling of natural microbial exopolymers (EPS) within a marine stromatolite. Palaeogeogr. Palaeocl. 219:71-86.

Decrouy L, Vennemann TV, Ariztegui D, 2012. Mg/Ca and Sr/Ca of ostracod valves from living species of Lake Geneva. Chem. Geol. 314-317:45-56.

Dittrich M, Kurz P, Wehrli B, 2004. The role of autotrophic picocyanobacteria in calcite precipitation in an oligotrophic lake. Geomicrobiol. J. 21:45-53.

Dittrich M, Obst M, 2004. Are picoplankton responsible for calcite precipitation in lakes? Ambio 33:559-564.

Dittrich M, Sibler S, 2006. Influence of H$^+$ and calcium ions on surface functional groups of *Synechococcus* PCC 7942 cells. Langmuir 22:5435-5442.

Dittrich M, Sibler S, 2010. Calcium carbonate precipitation by cyanobacterial polysaccharides, p. 51-63. In: H.M. Pedley and M. Rogerson (eds.), Tufas and speleothems: unravelling the microbial and physical controls. Geological Society of London Publ.

Dupraz C, Reid RP, Braissant O, Decho AW, Norman RS, Visscher PT, 2009. Processes of carbonate precipitation in modern microbial mats. Earth-Sci. Rev. 96:141-162.

Fahnenstiel GL, Carrick HJ, Rogers CE, Sicko-Goad L, 1991. Red fluorescing phototrophic picoplankton in the Laurentian Great Lakes: what are they and what are they doing? Int. Rev. Hydrobiol. 76:603-616.

Finlay BJ, Hetherington NB, Davison W, 1983. Active biological participation in lacustrine barium chemistry. Geochim. Cosmochim. Ac. 47:1325-1329.

Gallina N, Anneville O, Beniston M, 2011. Impacts of extreme air temperatures on cyanobacteria in five deep peri-alpine lakes. J. Limnol. 70:186-196.

Glass-Haller L, 2010. Microbial and geochemical characterization of a contaminated freshwater ecosystem (the case of Vidy Bay, Lake Geneva, Switzerland). University of Geneva ed., Geneva: 186 pp.

Gonzalez-Muñoz MT, Martinez-Ruiz F, Morcillo F, Martin-Ramos JD, Paytan A, 2012. Precipitation of baryte by marine bacteria: a possible mechanism for marine barite formation. Geology 40:675-678.

Gower L, 2008. Biomimetic model systems for investigating the amorphous precursor pathway and its role in biomineralization. Chem. Rev. 108:4551-4627.

Groleau A, Sarazin G, Vinçon-Leite B, Tassin B, Quiblier-Llobéras C, 2000. Tracing calcite precipitation with specific conductance in a hard water alpine lake (Lake Bourget). Water Res. 43:4151-4160.

Hernández Mariné M, Clavero E, Roldán M, 2004. Microscopy methods applied to research on cyanobacteria. Limnetica 23:179-185.

Hood WC, Steidl PF, 1973. Synthesis of benstonite at room temperature. Am. Mineral. 58:341-343.

Hood WC, Steidl PF, Tschopp DG, 1974. Precipitation of norsethite at room temperature. Am. Mineral. 59:471-474.

Jansson C, Northen T, 2010. Calcyfying cyanobacteria. The potential of biomineralization for carbon capture and storage. Curr. Opin. Biotech. 21:1-7.

Jaquet J-M, Favarger P-Y, Peter A, Vernet J-P, 1983. [Premières données sur la matière en suspension dans le Léman]. [Book in French]. Institut Forel, University of Geneva ed., Geneva: 83 pp. Available from: http://archive-ouverte.unige.ch/vital/access/manager/Repository/unige:27100

Jaquet J-M, Nembrini G, Garcia J, Vernet J-P, 1982. The manganese cycle in Lac Léman (Switzerland): the role of *Metallogenium*. Hydrobiologia 91-92:323-340.

Jeandel C, Tachikawa K, Bory A, Dehairs F, 2000. Biogenic barium in suspended and trapped material as a tracer of export production in the tropical NE Atlantic (EUMELI sites). Mar. Chem. 71:125-142.

Jolyon R, 2012. Mindat.org, the mineral and locality database. Available from: http://www.mindat.org

Kelts K, Hsu KJ, 1978. Freshwater carbonate precipitation, p. 295-323. In A. Lerman (ed.), Lakes: chemistry, geology, physics. Springer-Verlag.

Konhauser K, Riding R, 2012. Bacterial biomineralization, p. 105-130. In: A.H. Knoll, D.E. Canfield and K.O. Konhauser (eds.), Fundamentals of geobiology. Blackwell Publ.

Krejci MR, Wassermann B, Finney L, McNulty I, Legnini D, Vogt S, Joester D, 2011. Selectivity of biomineralization of barium and strontium. J. Struct. Biol. 176:192-202.

Lauchnor EG, Schulz LN, Bugni S, Mitchell AC, Cunningham AB, Gerlach R, 2013. Bacterially induced calcium carbonate precipitation and strontium coprecipitation in a porous media flow system. Environ. Sci. Technol. 47:1557-1564.

Lazarotto J, Klein A, 2012. Physical-chemical changes in the waters of Lake Geneva. Available from: http://www.cipel. org/wp-content/uploads/2012/11/Evolution-physico-chim-ique.pdf

Lee BD, Apel WA, Walton MR, 2006. Calcium carbonate formation by *Synechococcus* sp. strain PCC 8806 and *Synechococcus* sp. strain PCC 8807. Bioresource Technol. 97:2427-2434.

Lynn DH, 2010. The ciliated protozoa: characterization, classification, and guide to the literature. Springer, Amsterdam: 605 pp.

Martin JH, Knauer GA, 1973. The elemental composition of plankton. Geochim. Cosmochim. Ac. 37:1639-1653.

McGrath M, Davison W, Hamilton-Taylor J, 1989. Biogeochemistry of barium and strontium in a softwater lake. Sci. Total Environ. 87/88:287-295.

Mori Y, Enomae T, Isogai A, 2009. Preparation of pure vaterite by simple mechanical mixing of two aqueous salt solutions. Mater. Sci. Eng. C29:1409-1414.

Parkhurst DL, Appelo CAJ, 1999. User's guide to PHREEQC (version 2): a computer program for speciation, batch reaction, one-dimensional transport, and inverse geochemical calculations. US Department of the Interior ed., denver: 309 pp. Available from: ftp://brrftp.cr.usgs.gov/pub/dlpark/ geochem/unix/phreeqc/manual.pdf

Pereira S, Zille A, Micheletti E, Moradas-Ferreira P, De Philippis R, Tamagnini P, 2009. Complexity of cyanobacterial exopolysaccharides : composition, structures, inducing factors and putative genes involved in their biosynthesis and assembly. FEMS Microbiol. Rev. 33:917-941.

Personnic S, Domaizon I, Dorrigo U, Berdjeb L, Jacquet S, 2009. Seasonal and spatial variability of virio-, bacterio-, and picoplanktonic abundance in three perialpine lakes. Hydrobiologia 627:99-116.

Plée K, Ariztegui D, Martini R, Davaud E, 2008. Unravelling the microbial role in ooid formation – results of an *in situ* experiment in modern freshwater Lake Geneva in Switzerland. Geobiology 6:341-350.

Rogerson M, Pedley HM, Wadhawan JD, Middleton R, 2008. New insights into biological influence on the geochemistry

of freshwater carbonate deposits. Geochim. Cosmochim. Ac. 72:4976-4987.

Ruiz-Hernandez SE, Grau-Crespo R, Ruiz-Salcador AR, De Leuw NH, 2010. Thermochemistry of strontium incorporation in aragonite from atomistic simulations. Geochim. Cosmochim. Ac. 74:1320-1328.

Sanchez-Moral S, Luque L, Cañaveras JC, Laiz L, Jurado V, Hermosin B, Saiz-Jimenez C, 2004. Bioinduced barium precipitation in St. Callixtus and Domitilla catacombs. Ann. Microbiol. 54:1-12.

Schultze-Lam S, Beveridge TJ, 1994. Nucleation of celestite and strontianite on a cyanobacterial S-Layer. Appl. Environ. Microb. 60:447-453.

Sondi I, Matijevic E, 2003. Homogenous precipitation by enzyme-catalyzed reactions. 2. Strontium and Barium carbonates. Chem. Mater. 15:1322-1326.

Stabel H-H, 1986. Calcite precipitation in Lake Constance. Limnol. Oceanogr. 31:1081-1093.

Stabel H-H, 1989. Coupling of strontium and calcium cycles in Lake Constance. Hydrobiologia 176-177:323-329.

Stabel H-H, Kleiner J, Merkel P, Sinemus HW, 1991. [Stoffkreislaüfe ausgewählter Spurenelemente im Bodensee]. [Article in German]. Vom Wasser 76:73-91.

Stabel H-H, Küchler-Krischun J, Kleiner J, Merkel P, 1986. Removal of strontium by coprecipitation in Lake Constance. Naturwissenschaften 73:551-553.

Sugiayma M, Hori T, Kihara S, Matsui M, 1992. A geochemical study on the specific distribution of barium in Lake Biwa, Japan. Geochim. Cosmochim. Ac. 56:597-605.

Sun D-M, Wu Q-S, Ding Y-P, 2006. A novel method for crystal control: synthesis and design of strontium carbonate with different morphologies by supported liquid membrane. Sol. St. Phen. 39:544-549.

Tadonleke RD, 2012. Primary production and chlorophyll a biomass in Lake Geneva. Campagne 2011:78-84.

Tien C-J, 2002. Biosorption of metal ions by freshwater algae with different surface characteristics. Process Biochem. 38:605-613.

Watanabe K, Imase M, Sasaki K, Ohmura N, Saiki H, Tanaka H, 2006. Composition of the sheath produced by the green alga *Chlorella sorokiniana*. Lett. Appl. Microbiol. 42:538-543.

Wilcock JR, Perry CC, Williams RJP, Brook AJ, 1989. Biological minerals formed from strontium and barium sulphates. II. Crystallography and control of mineral morphology in desmids. P. Roy. Soc. Lond. B Bio. 238:203-221.

Winder M, 2009. Photosynthetic picoplankton dynamics in Lake Tahoe: temporal and spatial niche partitioning among prokariotic and eukaryotic cells. J. Plankton Res. 31:1307-1320.

Wu Q-S, Sun D-M, Liu H-J, Ding Y-P, 2004. Abnormal polymorph conversion of calcium carbonate and nano-self assembly of vaterite by a supported liquid membrane system. Cryst. Growth Des. 4:717-720.
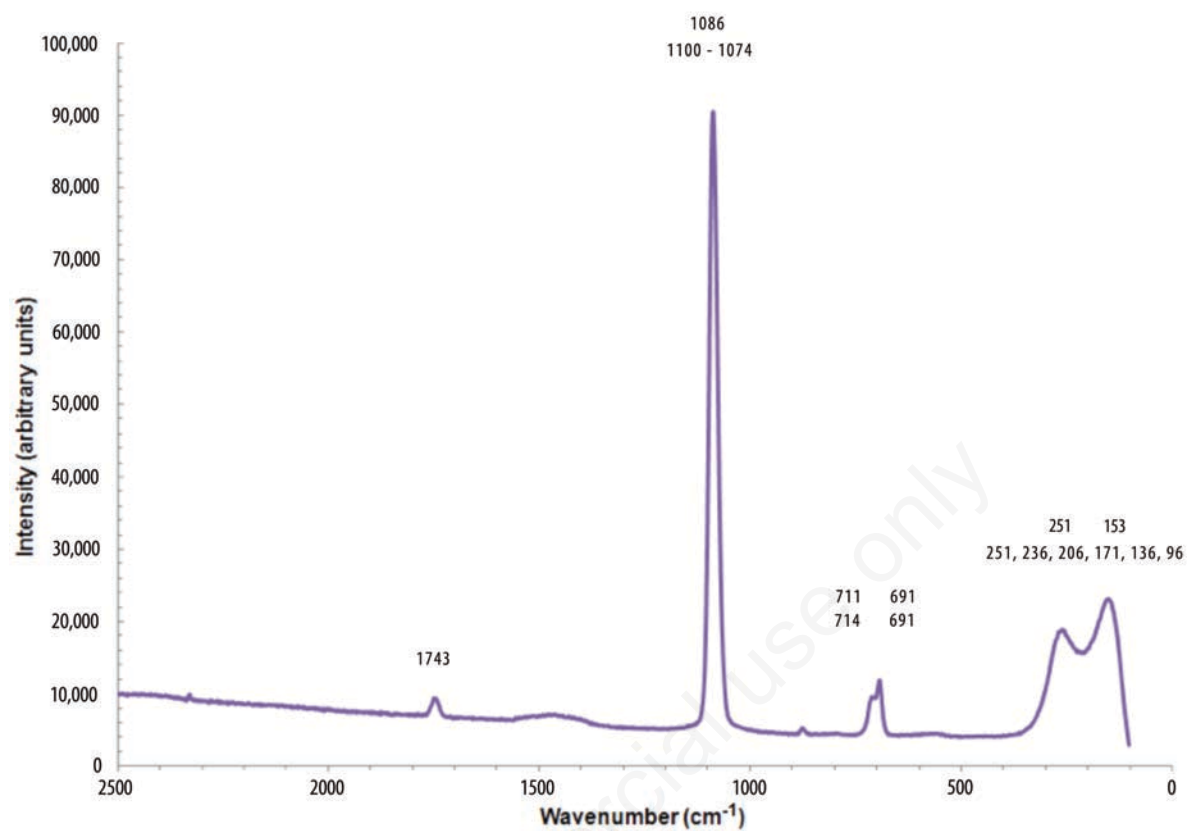
Supplementary Figures.
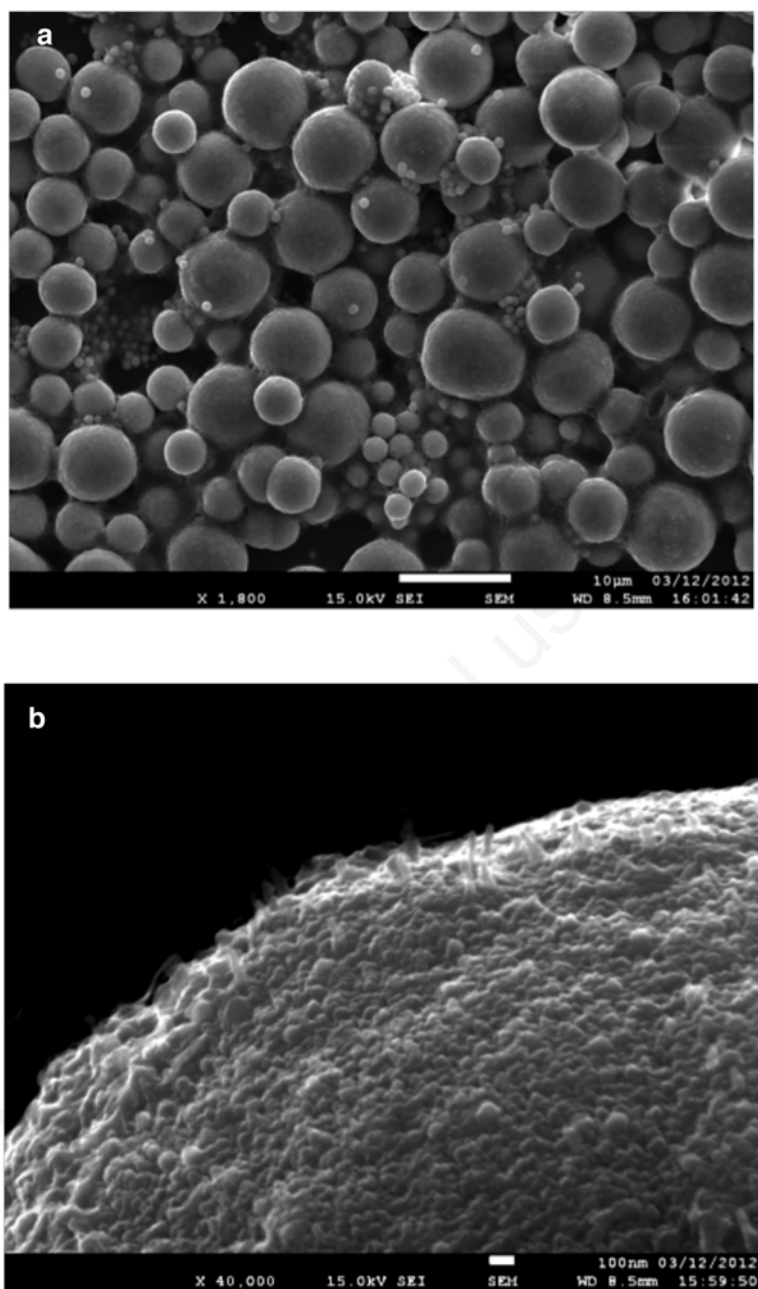
Supplementary Fig. 1. a) Spherical concretions of synthetic benstonite Mg (Ba$_{4.5}$ Sr$_{1.5}$) Ca$_6$ (CO$_3$)$_{13}$, aged 3 days. Scale bar: 10 µm; b) close-up on a concretion surface. Scale bar: 100 nm. The concretion consists of individual, spherical (diameter <100 nm), or needle-shaped nanoparticles.
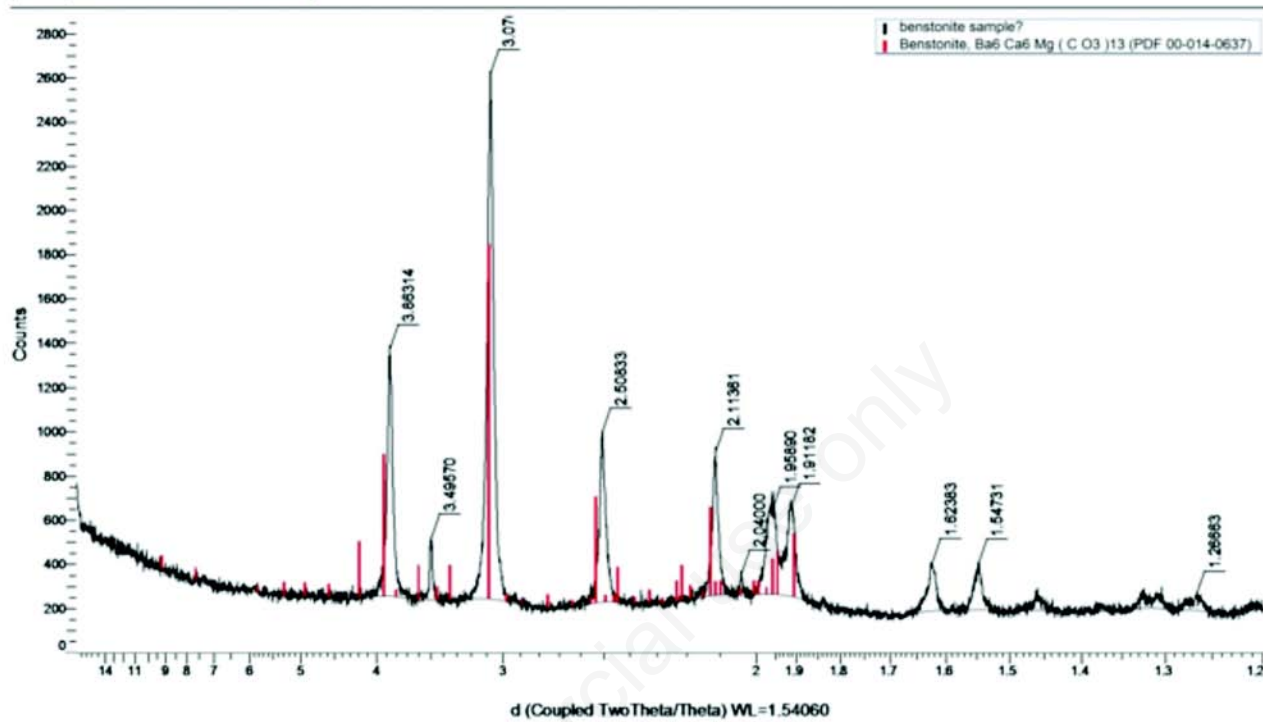
Supplementary Fig. 2. X-ray diffraction diagram of synthetic benstonite (black), with standard [Mg Ca$_6$ Ba$_6$ (CO$_3$)$_{13}$].

Supplementary Fig. 3. Raman spectrum of synthetic benstonite. Wavenumber of main peaks is compared to those of $Ca_7 Ba_6 (CO_3)_{13}$.

Conference paper

Bruno Thien, Agathe Martignier, Jean-Michel Jaquet and Montserrat Filella*

Linking environmental observations and solid solution thermodynamic modeling: the case of Ba- and Sr-rich micropearls in Lake Geneva

Abstract: Intracellular inclusions of amorphous Ba- and Sr-rich calcium carbonates – referred to as "micropearls"– have recently been detected in Lake Geneva. These micropearls are formed under conditions of pronounced Ba and Sr undersaturation in the lake waters. Their formation can be explained by the ability of certain microorganisms to preconcentrate these trace elements in tandem with a non-equilibrium solid-solution growing mechanism.

Keywords: amorphous carbonate; barium; biomineralisation; calcium; growth entrapment; ISSP-17; lake water; solid solution; strontium; uptake kinetic effect.

Introduction

Intracellular inclusions of amorphous Ba- and Sr-rich calcium carbonates – referred to as "micropearls" – have recently been detected in Lake Geneva [1]. Initially, they were thought to exist as agglomerates inside an organic matrix but it was subsequently discovered that they are in fact intracellular mineral inclusions in unicellular phytoplankters. Scanning electron microscope (SEM) images and energy dispersive X-ray spectroscopy (EDXS) analyses have revealed two distinct types of micropearls, distinguished mainly by their chemical composition: Sr-rich and Ba-rich ones with the Ba-rich type also containing minor amounts of Sr. Micropearls always appear in clusters, embedded in the organism's cell (Fig. 1a and b). Clusters can contain ~10–200 micropearls (diameter: 0.2–3 μm). The unicellular alga *Tetraselmis cf. cordiformis*, the organism where Sr-micropearls was detected, has a diameter of 15 μm and the micropearls contain up to 25 mol% $SrCO_3$. The organisms which contain Ba-micropearls are, as yet, unidentified biflagellate eukaryotes. The associated micropearls can contain up to 97 mol% $BaCO_3$ with a maximum of 10 mol% $SrCO_3$ (Fig. 1 in Sup Info file). They range from 7 to 20 μm in size. The micropearls in the smaller organisms (7–10 μm) contain more Ba than those in the larger ones (20 μm).

Considering the low concentration of Ba and Sr in Lake Geneva waters, the formation of micropearls requires strong preconcentration inside the cells. This might be complemented by a solid solution formation-linked mechanism. A solid solution is a mixture of two crystalline solids that coexist as a new crystalline solid. Its solubility is usually lower than that of the two pure phases. Thermodynamic concepts have already

---

---

*Corresponding author: Montserrat Filella, Institute F.-A. Forel, University of Geneva, 1205 Geneva, Switzerland, e-mail: Montserrat.Filella@unige.ch
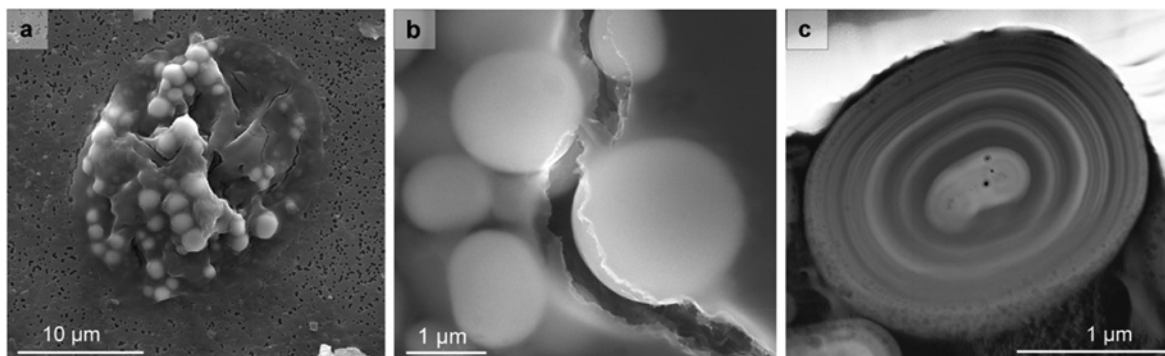Bruno Thien: Laboratory for Waste Management, Paul Scherrer Institute, 5232 Villigen, Switzerland; and Fluid and Mineral Resources Group, ETH, 8092 Zürich, Switzerland
Agathe Martignier and Jean-Michel Jaquet: Department of Earth Sciences, University of Geneva, 1205 Geneva, Switzerland

Fig. 1: Barium-rich micropearls. (a and b) Scanning electron microscopy-secondary electron images (SEM-SEI) of Ba-rich micropearls, still embedded in the dried organic matter of the unicellular organism which produces them. (c) Transmission electron microscopy high angle annular dark field (TEM HAADF) image of a focused ion beam (FIB)-cut section of a Ba-rich micropearl showing oscillatory zoning. The bright material at the top is the protective Pt cover and the dark material at the bottom, organic material. The bright zonations have a higher Ba content than dark ones. Black holes in the middle of the micropearl are due to beam damage. Experimental details in [1].

been successfully applied to account for equilibrium of trace elements between microorganisms and water [2, 3]. In this study, we test whether solid solution-based modeling provides an insight on the formation of the observed micropearls.

Some theoretical background

The distribution of a trace element Tr (relative to the host component Hc) between a mineral and an aqueous solution can be described by a fractionation coefficient, $\Delta_{Tr/Hc}$:

$$\Delta_{Tr/Hc} = \frac{\{Tr/Hc\}_{mineral}}{\{Tr/Hc\}_{solution}} \tag{1}$$

where $\{Tr/Hc\}$ are molar concentration or activity ratios. $\Delta_{Tr/Hc}$ can be experimentally measured (e.g. [4]) or derived from theoretical calculations (e.g. [5]). It has been shown that the higher the host mineral growth rate is, the more $\Delta_{Tr/Hc}$ deviates from the equilibrium value (e.g. [6]). This effect has been theoretically explained by Watson [7] with the "growth entrapment model" that postulates that a growing mineral has a tendency to take the composition of its surface layer. It implies that the measured $\Delta_{Tr/Hc}$ can be higher or lower than the value measured at equilibrium and that the measurement of $\Delta_{Tr/Hc}$ at equilibrium requires a very low growth rate of the host mineral. An alternative model has been proposed by DePaolo [8]. This model gives quantitatively similar results but the mechanisms are different: precipitation and re-dissolution kinetics. The deviation of $\Delta_{Tr/Hc}$ from the equilibrium value has been called the uptake kinetic effect and can be implemented in geochemical modeling codes [9]. This is the approach considered in this study. Heberling and co-workers offer a different concept called "thermodynamic adsorption/entrapment" [10] where the deviation from the equilibrium is due to different thermodynamic properties between the bulk mineral and the surface layers.

Methods

The incorporation of a trace element in a host mineral can be described by an aqueous – solid solution with two end-members, for instance $HcCO_3$ and $TrCO_3$ in the case of carbonates, with the composition of the mineral varying between these two limits. In this study, we considered aqueous – solid solutions with carbonates having a rhombohedral structure (RH) like calcite and an orthorhombic structure (OR) like aragonite.

The geochemical modeling package GEM-Selektor v.3 [11, 12] makes it possible to calculate the mineral composition as a function of the aqueous solution composition. To do so, the thermodynamic properties of the two end-members and the interaction coefficient of the aqueous-solid solution (W_G), which accounts for its non-ideality [13], must both be known. The non-ideality implies that $\Delta_{Tr/Hc}$ may vary either as a function of the solution composition or that some compositions of the aqueous – solid solutions may be metastable.

The chemical thermodynamic system was set up for Ba, C, Ca, H, O, Sr, and charge. Overall charge neutrality was assumed. The thermodynamic parameters of aqueous species, gasses and minerals come from the GEM-Selektor variant of the Nagra-PSI data base [14], except those for rhombohedral (RH) $SrCO_3$ and $BaCO_3$ which come from [15]. They are shown in Table 1 of the Sup Info file. Aqueous activity coefficients were calculated using the extended Debbye–Hückel equation (common ion size parameter of 0.372 nm and the third parameter b_g of 0.064 as for NaCl electrolyte were used). All the calculations have been performed at 25 °C because most of the data are available at this temperature.

The interaction parameters, W_G, were taken from the literature if available. When only an experimental value of $\Delta_{Tr/Ca}$ supposed to be at equilibrium is known, the corresponding W_G can be recalculated by using GEM-Selektor. The interaction parameters of the different aqueous – solid solutions used in this study are summarized in Table 1 of the Sup Info file. The Ca–Sr carbonate system has been investigated in detail by Kulik and co-workers [13]. They derived W_G values from theoretical considerations. For the calcite – $SrCO_3$(RH) solid solution, we recalculated $\Delta_{Sr/Ca}$ and it exactly coincides with the value by Tesoriero and Pankow [16]. For the aragonite – $SrCO_3$(OR) (strontianite) solid solution, no relevant experimental data were available for comparison. There is scant data for the Ca–Ba carbonate system. For calcite – $BaCO_3$(RH), $\Delta_{Ba/Ca}$ has been measured: 0.012 [16] and 0.016 [17]. We therefore considered an average value of 0.014 and derived the value of the interaction parameter. No such studies exist for the aragonite – $BaCO_3$(OR) (witherite) solid solution. $\Delta_{Ba/Ca}$ have been measured for sea-carbonates [18] but the high values of $\Delta_{Sr/Ca}$ obtained in the study suggest a high uptake kinetic effect. Therefore those values are not at equilibrium and cannot be considered to establish W_G. Wang and Xu [5] performed theoretical calculations in order to establish equilibrium $\Delta_{Tr/Ca}$ in carbonates. Although their results were not consistent with experimental observations for Sr in calcite, they were for Ba in calcite and Sr in aragonite. Since no better values are available, we considered this study for the value of $\Delta_{Ba/Ca}$ at equilibrium in the aragonite – witherite solid solution.

It should be mentioned that the carbonates in the phytoplankton are amorphous [1] whereas the studies cited concern well-crystallized carbonates. Values of distribution coefficients in amorphous carbonates (as is the case for thermodynamic data) are quasi non-existent in the literature but it has been shown that amorphous calcium carbonate is a precursor of crystalline carbonate and that a continuum exists between these two stages [19]. In addition, Politi et al. [20] showed that the amorphous precursor phase of calcite in sea urchin embryos exhibit a short-range order (i.e. a non-random distribution) similar to calcite. This is why this study considers the values for crystallized carbonates, on the assumption that they are not much different from amorphous ones [21].

Results and discussion

Composition of the carbonates

In Lake Geneva waters, Sr and Ba concentrations are much lower than Ca ones and well below the saturation values of their carbonates (Fig. 2 in Sup Info file). In comparison, the carbonate micropearls found in the phytoplankton contain significant amounts of both elements. Calculation of $\Delta_{Tr/Ca}$ considering the micropearls and lake water concentrations gives values ranging from 10.5 to 27863 (Table 1). Published $\Delta_{Sr/Ca}$ and $\Delta_{Ba/Ca}$ values for Ca carbonates range from 0.02 to 1.25 and 0.003 to 3 [4, 18], respectively. Observed variations are function of temperature, pH and mineral growth rate. Thus the carbonates in the phytoplankton contain higher concentrations of these trace elements than it is possible to incorporate directly from lake water.

Table 1: Molar ratios and fractionation coefficients Δ.

	Molar ratios		Δ Referred to lake water		Δ Referred to MO internal solution	
	Sr/Ca	Ba/Ca	$\Delta_{Sr/Ca}$	$\Delta_{Ba/Ca}$	$\Delta_{Sr/Ca}$	$\Delta_{Ba/Ca}$
Lake water[a]	4.65×10^{-3}	1.17×10^{-4}				
Solution inside MO	1.23	1.36				
Ca–Sr micropearls	0.075	–	16.1	–	0.061	–
Ca–Sr–Ba micropearls (smaller diameter)	0.087	3.26	18.7	27,863	0.071	2.40
Ca–Sr–Ba micropearls (larger diameter)	0.049	0.59	10.5	5043	0.040	0.43

[a]Average Lake Geneva waters (2012–2014). Values at the GE3 station. See Fig. 2 in Sup Info file.

Molar ratios were measured, except those for the solution inside the microorganisms (MO) that were calculated according to the hypothesis explained in the text. Δ were recalculated, for both lake water and solution inside the MO.

Enrichment in trace elements inside the microorganisms

For micropearls to form, phytoplankters must concentrate Ba, Sr and Ca inside the cell. Although the actual mechanism is not known, it is a plausible hypothesis that these hard-acid type elements are concentrated as they would be if complexed by carboxylate groups, which are the most common complexing groups in carbohydrates. By considering the equilibrium constant of acetate with Ca, Ba and Sr (values in Table 3 of Sup Info file), we calculated a possible composition of the aqueous solution inside the microorganisms (Table 1). It is important to note that such calculations do not provide absolute concentrations of the elements, but only concentration ratios. By considering that the carbonates grow from this solution, the corresponding $\Delta_{Tr/Ca}$ can be recalculated. The values obtained are given in Table 1. They fall exactly in the range given in the literature. Although it is worth pointing out that it is not yet known whether the micropearls are contained in the cell cytoplasm or in specific compartments (i.e. vacuoles), this has no impact on what follows.

Aqueous – solid solution and uptake kinetics

The next step is to investigate whether the measured composition of the micropearls and their composition calculated from the estimated composition of the internal cell solution are in accordance with the theory of aqueous solid solutions.

An important point, usually neglected in the calculation of fractionation coefficients at equilibrium when applying solid solution theory, is that they can vary as a function of the composition of the solution and/or the solid [22]. All literature Δ values discussed above correspond to a situation where {Tr}<<{Ca}. In our case, this condition does not apply inside the cells and, thus, we took it into account when calculating the theoretical values of $\Delta_{Tr/Ca}$ related to the micropearls (i.e. by considering the possible composition of the aqueous solution inside the microorganisms). The results (Table 2) indicate that the variation of $\Delta_{Tr/Ca}$ as a function of the solution composition is negligible for calcite-like structure aqueous – solid solutions, but becomes significant in aragonite-like structure aqueous – solid solutions. More details about the calculations

Table 2: Equilibrium fractionation coefficients of the different aqueous – solid solutions considered in this study.

Systems	$\Delta_{Tr/Ca}$ eq. lake water	$\Delta_{Tr/Ca}$ eq. MO water
Calcite – SrCO$_3$(RH)	0.021	0.025
Aragonite – SrCO$_3$(OR) (strontianite)	0.50	129
Calcite – BaCO$_3$(RH)	0.014	0.015
Aragonite – BaCO$_3$(OR) (witherite)	0.14	14

(RH) means rhombohedral structure (i.e. calcite-like structure), and OR means orthorhombic structure (i.e. aragonite-like structure).
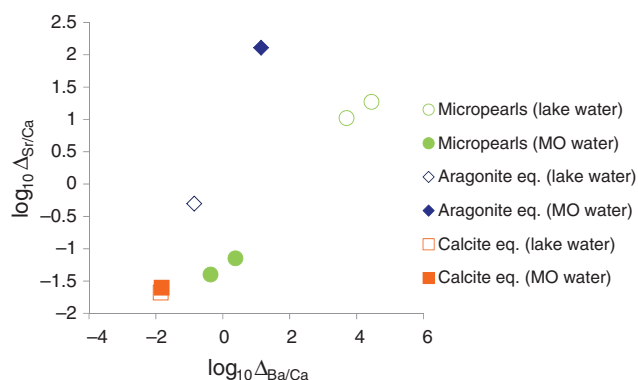
Fig. 2: Fractionation coefficients of the Ba–Sr–Ca micropearls, calculated by using the lake water composition and the estimated water composition inside the microorganisms (MO). Comparison with equilibrium values of calcite and aragonite.

along with their visualizations are given in Fig. 3 of Sup Info file. Although the calculated $\Delta_{Tr/Ca}$ values (Table 1) in the micropearls differ from the equilibrium values (Table 2), in calcite-like structures they remain within the same order of magnitude, while in aragonite-like structures the differences are very large. Therefore, these results clearly point to micropearls having calcite-like structures only.

The difference between $\Delta_{Sr/Ca}$ at equilibrium and $\Delta_{Sr/Ca}$ calculated in the micropearls can be explained by the uptake kinetic effect mentioned previously. When such a difference exists, an enrichment factor (i.e. the ratio between the measured value and the equilibrium value) can be calculated. It has been experimentally observed that $\Delta_{Sr/Ca}$ increases with the growth rate in the calcite – $SrCO_3(RH)$ solid solution with a maximum enrichment factor value around 6 [6, 16]. A similar effect has been observed for calcite – $BaCO_3(RH)$ solid solution with a maximum enrichment factor of 10 [16]. No such studies exist for the aragonite systems but enrichment factors of 2.3 for aragonite – strontianite and 15.5 for aragonite – witherite solid solutions in seawater can be estimated from measured $\Delta_{Sr/Ca} = 1.17$ and $\Delta_{Ba/Ca} = 2.17$ values for aragonite in seawater [18] and the assumption that Sr/Ca ratio in seawater is similar to that of Lake Geneva (i.e. equilibrium values of $\Delta_{Sr/Ca}$ for diluted systems given on Table 2 can be used).

Based on equilibrium $\Delta_{Tr/Ca}$ (Table 2) and estimated $\Delta_{Tr/Ca}$ (Table 1), the enrichment in the micropearls can be calculated. Let us first consider the calcite-like structures. The enrichment ranges between 1.6 and 2.8 for Sr; and between 29 and 160 for Ba. The values of 29 and 160 look too high when compared with the enrichment factor of 10 for Ba in calcite mentioned above, but it has been shown that, at very high growth rates, the enrichment can be higher than measured values of the enrichment factor based on sorption [23]. When considering an aragonite-like structure, the enrichment is always lower than one (i.e. depletion instead of enrichment) whereas the data of Gaetani and Cohen [18] might suggest that Sr is enriched rather than depleted in aragonite. Thus, we can again conclude that the micropearls consist of a calcite-like structure. Proper alignment of the Ca–Ba–Sr micropearls with equilibrium calcite in Fig. 2 reinforces the hypothesis of a calcite-like structure of the micropearls. Moreover, the correlation between the enrichment in Sr and in Ba suggests that the same enrichment mechanism occurs. These conclusions are fully in line with the experimental observations [1].

Are results valid at temperatures other than 25 °C?

The microorganisms form in the photic zone of the lake, where the temperature reaches 25 °C in summer, but can drop to as low as 4 °C in winter (Fig. 4 in Sup. Info). However, as mentioned above, we considered a temperature of 25 °C for this study and, thus, the results obtained are only valid for the carbonates formed at 25 °C unless the potential impact of lower temperatures is clarified. In fact, $\Delta_{Tr/Ca}$ decreases with an increase of temperature for Sr and Ba in aragonite [18, 24] and for Sr in calcite [25]. There is no data available for Ba in calcite but there is no reason why it should not follow the same behavior as Sr. The data reported in these

studies point to a maximum increase of $\Delta_{Tr/Ca}$ from 25 °C to 5 °C of 1.8 (at a similar growth rate). So, even if some of the microorganisms form at temperatures below 25 °C, this has no impact on the conclusions drawn in this study.

Effect of organism size on micropearl composition

The Ba-micropearls observed in the smaller organisms are more enriched in Sr and Ba than those formed in the larger ones. The reasons behind the existence of two different-sized organisms (i.e. different stages of their growing cycle versus different taxa) are outside the scope of this study. It can be mentioned however that the hypothesis of different growing stages is unlikely because, in this case, more than two sizes would be observed. On the other hand, and irrespective of the reasons behind the existence of organisms of two sizes, the effect of organism size on the micropearl composition is of interest.

This could be nicely explained by the interlinkage between precipitation rates and trace element solution concentrations in the frame of the solid solution approach: when considering a closed medium, the internal solution in the smaller microorganisms should get depleted in Ca sooner than in the bigger ones, and this would trigger a decrease in the micropearl precipitation rate (i.e. a decrease of the saturation index of the carbonates). Thus, the micropearls would automatically be less concentrated in Sr and Ba. Interestingly, even if the Ca depletion was not sufficient to trigger a significant decrease in the precipitation rate, the depletion of the solution in Sr and Ba would in any case lead to less enriched micropearls. And yet we observe that the micropearls in the small microorganisms are nonetheless enriched in Sr and Ba! In fact, the space inside the microorganisms is probably not a closed medium. If the microorganisms concentrate the elements from the lake water, it is reasonable to assume a capacity to reload the depleted solution. It has been observed [1] that the internal structure of the micropearls is not uniform but is constituted of several layers, suggesting the existence of depletion/reloading cycles (Fig. 1c). Such a mechanism is certainly not instantaneous but rather subject to a certain kinetic rate. In such a case, the capacity of the microorganism to bring the elements inside depends on the surface area of the cell membrane. The higher the surface/volume ratio is, the faster the replenishment process. By assuming a spherical shape of the space inside the microorganisms, the surface/volume ratio is equal to 3/r where r is the radius. Therefore, the smaller the microorganism (or the vacuole), the lower the depletion of the solution inside and the more enriched the micropearls will be.

The time scale of formation of micropearls

The time necessary to precipitate the carbonate micropearls can be estimated by using a kinetic equation (e.g. [26]) but it requires the saturation index of the mineral to be calculated. This is not possible as we cannot measure the composition of the solution inside the cells. Therefore, other methods need to be used to estimate the precipitation rate. For instance, $\Delta_{Sr/Ca}$ can be used because $\Delta_{Sr/Ca}$ in calcite increases as a function of the growth rate and, thus, a given value of $\Delta_{Sr/Ca}$ should correspond to a certain value of the growth rate. However, different studies report significant variations of $\Delta_{Sr/Ca}$ for a similar growth rate [9]. We use here the experimental data of Tang and co-workers [25] to estimate micropearl growth rates because their average pH values are in line with those of the lake (ca. 8). The recalculated growth rates corresponding to the $\Delta_{Sr/Ca}$ values under consideration are given in Table 3. If the size of the micropearls ranges between 0.3 and 2.5 µm, their potential growth time would then be between 0.6 and 72 days.

Since $\Delta_{Ba/Ca}$ decreases with the temperature and larger microorganisms form micropearls which are less concentrated in Ba, it would be tempting to formulate the hypothesis that micropearls in the larger microorganisms form at higher temperatures than in the smaller ones. Such an hypothesis would imply a growth time of micropearls of 1.6–13 days at 5 °C and of 9–72 days at 25 °C. This hypothesis is supported by the experimental observation that higher numbers of smaller microorganisms have been observed in winter than in summer [1]. However, processes in nature are probably more complex than this hypothesis suggests because bigger

Table 3: Micropearl linear growth rates, V, in nm s^{-1} recalculated from the data in [25].

$\Delta_{Sr/Ca}$	V at 5 °C	V at 25 °C
0.040	2×10^{-4}	2×10^{-4}
0.071	1.1×10^{-3}	2.8×10^{-3}

and smaller organisms have also been observed simultaneously in summer. Thus, other physico-chemical temperature-dependent factors such as higher content of dissolved CO_2 in cold water (which favors the precipitation of carbonates) or the Arrhenius effect (the higher the temperature, the faster the carbonate precipitation rate) very probably play a variable and simultaneous role. Finally, it should also not be forgotten that temperature has a direct effect on the presence and life cycle of the microorganisms, irrespective of the formation of micropearls.

Conclusions

Amorphous calcium carbonate micropearls growing inside phytoplanktonic microorganisms in Lake Geneva exhibit very high concentrations of Sr and Ba compared to the lake water. Such extreme enrichment can be explained by the probable pre-accumulation of those elements in the internal solution inside the microorganisms combined with a growth entrapment effect. On the basis of our solid solution thermodynamic modeling, we can conclude that the micropearls have a calcite-like structure and estimate a formation time of the order of a few days. Our results also provide an insight into the reasons why the micropearls in the smaller microorganisms are more enriched in Sr and Ba than those in the larger ones. This study shows that physico-chemical modeling provides a useful explanatory tool for understanding observed complex natural phenomena.

References

[1]   A. Martignier, M. Pacton, M. Filella, J.-M. Jaquet, F. Barja, K. Pollok, F. Langenhorst, S. Lavigne, P. Guagliardo, M. R. Kilburn, C. Thomas, R. Martini, D. Ariztegui. *Geobiology* **15**, 240 (2017).

[2]   J. M. Fein, C. J. Daughney, N. Yee, T. A. Davis. *Geochim. Cosmochim. Acta* **61**, 3319 (1997).

[3]   D. A. Fowle, J. B. Fein. *Geochim. Cosmochim. Acta* **63**, 3059 (1999).

[4]   E. Curti. *Appl. Geochem.* **14**, 433 (1999).

[5]   Y. Wang, H. Xu. *Geochim. Cosmochim. Acta* **65**, 1529 (2001).

[6]   R. B. Lorens. *Geochim. Cosmochim. Acta* **45**, 553 (1981).

[7]   E. B. Watson. *Geochim. Cosmochim. Acta* **68**, 1473 (2004).

[8]   D. J. DePaolo. *Geochim. Cosmochim. Acta* **75**, 1039 (2011).

[9]   B. M. J. Thien, D. A Kulik, E. Curti. *Appl. Geochem.* **41**, 135 (2014).

[10] F. Heberling, V. L. Vinograd, R. Polly, J. D. Gale, S. Heck, J. Rothe, D. Bosbach, H. Geckeis, B. Winkler. *Geochim. Cosmochim. Acta* **134**, 16 (2014).

[11] T. Wagner, D. A. Kulik, F. F. Hingerl, S. V. Dmytrieva. *Can. Mineral.* **50**, 1173 (2012).

[12] D. A. Kulik, T. Wagner, S. V. Dmytrieva, G. Kosakowski, F. F. Hingerl, K. V. Chudnenko, U. Berner. *Computat. Geosci.* **17**, 1 (2013).

[13] D. A. Kulik, V. L. Vinograd, N. Paulsen, B. Winkler. *Phys. Chem. Earth A/B/C* **35**, 217 (2010).

[14] W. Hummel, U. Berner, E. Curti, F. J. Pearson, T. Thoenen. Technical Report 02-16, Nagra/PSI Chemical Thermodynamic Data Base 01/01, Universal Publishers, Parkland, Florida (2002).

[15] D. A. Sverjensky. *Geochim. Cosmochim. Acta* **48**, 1127 (1984).

[16] A. J. Tesoriero, J. K. Pankow. *Geochim. Cosmochim. Acta* **60**, 1053 (1996).
[17] J. D. Rimstidt, A. Balog, J. Webb. *Geochim. Cosmochim. Acta* **62**, 1851 (1998).
[18] G. A. Gaetani, A. L. Cohen. *Geochim. Cosmochim. Acta* **70**, 4617 (2006).
[19] C. Rodriguez-Navarro, K. Kudłacz, Ö. Cizerc, E. Ruiz-Agudo. *Cryst. Eng. Comm.* **17**, 58 (2015).
[20] Y. Politi, Y. Levi-Kalisman, S. Raz, F. Wilt, L. Addadi, S. Weiner, I. Sagi. *Adv. Funct. Mater.* **16**, 1289 (2006).
[21] N. Cam, T. Georgelin, M. Jaber, J-F. Lambert, K. Benzerara. *Geochim. Cosmochim. Acta* **161**, 36 (2015).
[22] M. Prieto, F. Heberling, R. M. Rodriguez-Galan, F. Brandt. *Prog. Cryst. Growth Ch.* **62**, 29 (2016).
[23] R. I. Gabitov, E. B. Watson. *Geochem. Geophys. Geosyst.* **7**, 12 (2006).
[24] M. Dietzel, N. Gussone, A. Eisenhauer. *Chem. Geol.* **203**, 139 (2004).
[25] J. Tang, S. J. Köhler, M. Dietzel. *Geochim. Cosmochim. Acta* **72**, 3718 (2008).
[26] M. Wolthers, G. Nehrke, J. P. Gustafsson, P. Van Cappellen. *Geochim. Cosmochim. Acta* **77**, 121 (2012).